

BEHAVIOR OF AXIALLY LOADED DRILLED SHAFTS IN BEAUMONT CLAY

PART THREE - FIELD TESTS

by

Michael W. O'Neill
Lymon C. Reese

Research Report Number 89-8

Soil Properties as Related to Load Transfer
Characteristics of Drilled Shafts

Research Project 3-5-65-89

conducted for

The Texas Highway Department

in cooperation with the
U. S. Department of Transportation
Federal Highway Administration

by the

CENTER FOR HIGHWAY RESEARCH
THE UNIVERSITY OF TEXAS AT AUSTIN

December, 1970

The opinions, findings, and conclusions expressed in this publication are those of the authors and not necessarily those of the Federal Highway Administration.

PREFACE

This report is the eighth in a series of reports from Research Project 3-5-65-89 of the Cooperative Highway Research Program. The principal aim of the report is to describe the results of axial load tests of full-scale, instrumented drilled shafts in the Beaumont Clay formation in Houston, Texas. The tests were conducted to measure side and base stresses in cylindrical and underreamed shafts, constructed by both wet and dry procedures. The distribution of shear stresses along the sides of the shafts was measured to provide an insight into the mechanism affecting the load transfer behavior of drilled shafts in clay. Maximum side shear stresses and base capacities have been correlated with the undrained shear strength of the soil as indicated by laboratory procedures and with results of Texas Highway Department cone penetration tests.

The report is issued in five separately bound parts:

Part One - "State of the Art" describes the historical development of drilled shafts, describes construction procedures, presents the mechanics of shaft behavior, outlines current methods of design, and presents a summary of the results of field tests reported in the technical literature.

Part Two - "Site Investigation and Test Shaft Instrumentation" gives details of the geotechnical investigation of the test site, describes the test shafts and anchorage systems, describes the various instrumentation

systems, and presents results of monitoring the instrumentation under no-load conditions.

Part Three - "Field Tests" describes the field test procedures and presents the detailed results of the tests.

Part Four - "Design Influences and Conclusions" presents criteria, obtained through the field tests and from the literature review, for designing drilled shafts in Beaumont Clay.

Part Five - "Appendices" gives supporting data and details not contained in the main body of Parts One through Four.

It is not intended that the reader read the entire report in order to obtain information on any particular subject. The report was separated into the various Parts, any of which can be consulted for specific details, for this reason. It is expected that most readers will desire to consult only Part Four, which briefly summarizes Parts One through Three, and then concisely presents design criteria for axially loaded drilled shafts in Beaumont Clay. The Chapters are numbered continuously from Part One through Part Five. Although some cross-referencing exists, the various Parts are written to be as independent as possible. The reference list is contained in Part Four.

This report is the manifestation of the efforts of many individuals. The technical contributions of Dr. Walter R. Barker, Mr. Harold H. Dalrymple, Mr. James N. Anagnos, Mr. Frederick E. Koch, and Mr. Olen L. Hudson merit special recognition. Mr. James Holmes skillfully made the drawings. Miss Mary Kern proficiently prepared the final copy. Thanks

are also due to Miss Pamela Terwelp, Miss Cheryl Johnson, and Mrs. Eddie B. Hudepohl for their assistance in preparing the report. The authors also acknowledge the valuable assistance and advice given by Mr. Horace Hoy, Mr. H. D. Butler, and Mr. Gaston Berthelot, all of the Texas Highway Department, and by the maintenance personnel of District 12.

Michael W. O'Neill

Lymon C. Reese

December 1970

This page replaces an intentionally blank page in the original.

-- CTR Library Digitization Team

LIST OF REPORTS

Report No. 89-1, "Field Testing of Drilled Shafts to Develop Design Methods," by Lymon C. Reese and W. Ronald Hudson, describes the overall approach to the design of drilled shafts based on a series of field and laboratory investigations.

Report No. 89-2, "Measurements of Lateral Earth Pressure in Drilled Shafts," by Lymon C. Reese, J. Crozier Brown, and H. H. Dalrymple, describes the development and evaluation of pressure gages to measure lateral-earth pressures on the drilled shaft.

Report No. 89-3, "Studies of Shearing Resistance Between Cement Mortar and Soil," by John W. Chuang and Lymon C. Reese, describes the overall approach to the design of drilled shafts based on field and laboratory investigations.

Report No. 89-4, "The Nuclear Method of Soil-Moisture Determination at Depth," by Clarence J. Ehlers, Lymon C. Reese, and James N. Anagnos, describes the use of nuclear equipment for measuring the variations of moisture content at the drilled shaft test sites.

Report No. 89-5, "Load Distribution for a Drilled Shaft in Clay Shale," by Vasant N. Vijayvergiya, W. Ronald Hudson, and Lymon C. Reese, describes the development of instrumentation capable of measuring axial load distribution along a drilled shaft, the development, with the aid of full-scale load testing, of a technique of analysis of observed data, and the correlation of observed data with the Texas Highway Department cone penetration test.

Report No. 89-6, "Instrumentation for Measurement of Axial Load In Drilled Shafts," by Walter R. Barker and Lymon C. Reese, describes the development and performance of various instrumentation systems used to measure the axial load distribution in field tests of full-scale drilled shafts.

Report No. 89-7, "The Determination of Soil Properties In Situ," by David B. Campbell and W. Ronald Hudson, describes the use of the Menard Pressure-meter, the Texas Highway Department cone penetrometer, and The University of Texas in situ device in estimating soil properties in situ and estimating load transfer values obtained from drilled shaft tests.

Report No. 89-8, "Behavior of Axially Loaded Drilled Shafts in Beaumont Clay," by Michael W. O'Neill and Lymon C. Reese, describes the results of axial load tests of instrumented drilled shafts having varying geometry and differing methods of installation and presents a tentative design procedure for drilled shafts in Beaumont Clay.

This page replaces an intentionally blank page in the original.

-- CTR Library Digitization Team

ABSTRACT

A drilled shaft is a foundation element formed by boring a cylindrical hole into the soil and backfilling the hole with concrete. The recent increase in the utilization of drilled shafts as foundations for major structures has created a need for systematic investigations of their behavior. One such investigation, in which four full-sized drilled shafts of varying geometries were loaded axially to failure, was conducted at a site in the stiff, fissured Beaumont Clay in Houston, Texas. The test shafts were constructed by both wet and dry procedures. They were fully instrumented for measurement of the distribution of axial load, thereby permitting a calculation of the distribution of developed side resistance and of base resistance.

Prior to and during the field tests, a careful site investigation was conducted, and a shear strength profile was developed based on unconsolidated, undrained triaxial test results and Texas Highway Department cone penetrometer soundings. The maximum side shear stresses developed during the load tests were compared to the shear strength profile and penetrometer results in order to arrive at shear strength reduction factors that could be relied upon in predicting design values for side friction.

The side shear stresses were observed to vary considerably from the tops of the shafts to the bottoms, generally being quite small at both ends. Overall, the shafts that were installed in dry boreholes developed an average maximum side shear stress of about one-half of the shear

strength of the clay. The single shaft installed in a processed borehole developed an average of only about one-third of the shear strength of the clay along its sides.

The load measurements indicated that bearing capacity equations used for ultimate base resistance for piles in clay were valid for both belled and cylindrical test shafts.

After the tests were completed, soil adjacent to the walls of three of the shafts was sampled in an attempt to determine the nature of the mechanism of shear strength reduction in soil immediately adjacent to the sides of drilled shafts. In the shafts installed in dry boreholes, some soil softening due to an increase in moisture content occurred, particularly near the bases. This softening, produced by water from the setting concrete, accounted for some, but not all of the measured strength reduction. Other reasons for shear strength reduction are reasoned to be the effects of remolding and opening of fissures as the boreholes were drilled and mechanical base-side interference. Samples taken adjacent to the shaft installed in a processed hole revealed pockets of trapped drilling mud between the sides of the borehole and the wall of the shaft.

Based upon the field study and a comprehensive review of related research conducted in similar soil formations, a tentative design procedure is suggested. That procedure includes criteria for providing an adequate factor of safety against plunging failure and for limiting immediate settlement at working load to an acceptable value.

KEY WORDS: piles, bored piles, drilled shafts, soil mechanics, undrained shear tests, cohesive soils, cone penetrometer, instrumentation, field tests, design criteria

SUMMARY

The purpose of this report is to describe the results of field tests of full-sized, instrumented drilled shafts in the Beaumont Clay formation. Drilled shafts with varying base geometry, length, and method of installation were load tested to obtain measurements of the distribution of axial load with depth and of base load-settlement characteristics in order to develop design criteria.

Pertinent soil parameters were obtained by various standard procedures, including the unconsolidated, undrained triaxial test and the T.H.D. cone penetrometer test to provide a basis for the correlation of test results.

The test shafts were observed to develop considerable resistance in side friction. Furthermore, side resistance was observed to develop much sooner than base resistance, with the result that side resistance predominated over base resistance at design load. The shafts installed in dry boreholes mobilized an average of one-half of the shear strength of the soil in side friction, while the side frictional stresses in the shaft installed in a processed borehole were significantly smaller. An investigation showed that the shafts installed in the dry were well-formed and bonded securely to the soil composing the borehole walls, while the shaft installed in a processed hole contained pockets of drilling mud between the concrete and natural soil. Based upon these observations, the numerical test results, and field tests of other investigators in similar soil formations, a tentative design procedure incorporating side resistance is formulated.

This page replaces an intentionally blank page in the original.

-- CTR Library Digitization Team

IMPLEMENTATION STATEMENT

The study indicated that considerable load was resisted in side friction in axially loaded drilled shafts in stiff clay with both straight sides and underreams, installed in dry boreholes and in boreholes processed with drilling mud. The possibility that considerably smaller frictional resistance occurs in shafts installed in processed holes was observed, however. The test results generally agree with those of other investigators in similar soils.

Measured side shear and base capacities were correlated with standard soil strength tests. It appears that side friction can be reliably estimated for shafts in dry boreholes, and to some extent for shafts installed in processed holes, from laboratory soil tests or from penetrometer soundings. Therefore, a new design procedure for drilled shafts is suggested that incorporates side friction, a resistance component heretofore omitted from consideration. The incorporation of side friction in the design of drilled shafts will undoubtedly result in considerable monetary savings in bridge foundation construction.

The suggested general design parameters are, of necessity, somewhat conservative, because of the limited number of tests that were conducted and because field testing was limited to short-term loading in one specific soil formation. Further savings can be realized by extending the research into long-term testing, into testing in other soil formations, and into reevaluating construction techniques for installation of shafts in processed boreholes. Such research would provide a better definition of the design parameters in all situations and would therefore permit the design of drilled shafts to be more rational and less conservative.

This page replaces an intentionally blank page in the original.

-- CTR Library Digitization Team

CONTENTS

	<u>Page</u>
PART ONE - STATE OF THE ART	
PREFACE.	iii
LIST OF REPORTS.	vii
ABSTRACT	ix
SUMMARY.	xi
IMPLEMENTATION STATEMENT	xiii
NOMENCLATURE	xxiii
CHAPTER I, INTRODUCTION.	1
Description of the Drilled Shaft	2
History of the Development of Drilled Shafts and Drilling Equipment	5
Scope of Study	12
CHAPTER II, CONSTRUCTION PROCEDURES.	15
Excavation Techniques.	15
Dry Method	16
Wet Method	22
Reinforcement.	28
Concrete	30
Typical Drilled Shaft Construction Problems.	31
Extraneous Water in the Borehole	32
Rising Steel	32
Necking.	33
Separation	33
Miscellaneous Problems	35
Correction of Deficiencies Caused by Poor Construction	37

	<u>Page</u>
Effect of Construction Method on Behavior Under Load.	38
Comparison of Drilled Shafts and Driven Piles	39
CHAPTER III, MECHANICS OF DRILLED SHAFT BEHAVIOR.	41
Removal of Applied Load by Soil Surrounding Stem.	41
Resistance of Soil Beneath Base	49
Mathematical Synthesis of Behavior.	55
Discrete Element Method Requiring Load Transfer Curves as Input.	55
Discrete Element Method Employing Mindlin's Solution.	56
Finite Element Method	57
CHAPTER IV, CURRENT METHODS OF DESIGN AND ANALYSIS.	59
General Design Concepts	59
Prediction of Allowable Compressive Load on an Isolated Drilled Shaft	60
Semiempirical Procedures.	60
Rational Procedures	61
Load Tests.	75
Prediction of the Settlement of a Single Drilled Shaft.	83
Immediate Settlement.	84
Load Tests.	84
Nondimensional Load-Settlement Relationships.	84
Approximate Methods Based on Theory of Elasticity	85
Analytical Methods for Synthesis of Complete Behavior	92
Long-Term Settlement.	92
Design of Drilled Shafts in Expansive Soils	98
Negative Side Resistance.	100
Lateral Load.	101
Uplift Capacity	102

	<u>Page</u>
Concrete Deterioration.	102
Behavior of Groups of Axially Loaded Drilled Shafts	103
Group With Rigid Cap.	105
Groups in Sand.	105
Groups in Clay.	107
Group With Flexible Cap	110
Other Considerations.	113
CHAPTER V, PREVIOUS FIELD STUDIES	115
Correlation of Field Test Results With Soil Properties.	122
Studies in London Clay.	127
Studies in Texas Soils.	137
Other Studies	141
Tests in Sands and Silts.	145
Summary	146
PART TWO - SITE INVESTIGATION AND TEST SHAFT INSTRUMENTATION	
PREFACE	iii
LIST OF REPORTS	vii
ABSTRACT.	ix
SUMMARY	xi
IMPLEMENTATION STATEMENT.	xiii
NOMENCLATURE.	xxiii
CHAPTER VI, SCOPE AND OBJECTIVES OF PRESENT FIELD STUDY	149
CHAPTER VII, GEOTECHNICAL CONDITIONS.	157
Geological Description of Beaumont Clay	157

	<u>Page</u>
Soil Profile at SH225 Test Site	159
Strength Tests.	166
UU Triaxial and Unconfined Compression Tests (Single Step Shear - U.T.)	169
UU Triaxial Compression Tests (Multiple Phase Shear - T.H.D.)	191
Direct Shear.	197
T.H.D. Penetrometer	198
Pocket Penetrometer	200
Comparison of Results of Strength Tests	200
Mortar Migration Studies.	205
Consolidation Tests	236
CHAPTER VIII, FIELD INSTALLATION PROCEDURES	243
Installation Schedule	243
Reaction System	251
Test Shaft Construction	253
S1.	254
S2.	255
S3.	257
S4.	259
Concrete Control.	260
CHAPTER IX, TEST SHAFT INSTRUMENTATION.	261
Method of Obtaining Load Distribution Information from Instrumentation.	261
Previous Attempts at Measurement of Axial Load Distribution in Driven Piles and Drilled Shafts.	263
Load Measurement Procedures Used in Present Study	269
Instrumentation Systems Used in Tests	273
Mustran System.	274

	<u>Page</u>
Concrete Embedment Gage System.	289
Bottomhole Load Cell.	298
Strain Rods	307
Hydraulic Pressure Cell	313
Weldable Gages.	314
Thermocouples	315
Overall Instrumentation	315
Site Instrumentation.	315
CHAPTER X, NO-LOAD PERFORMANCE OF TEST SHAFTS	327
Performance of Mustran Cells.	327
Performance of Embedment Gages.	335
Strain Rods	341
Bottomhole Load Cell.	341
Thermocouples	343
PART THREE - FIELD TESTS	
PREFACE	iii
LIST OF REPORTS	vii
ABSTRACT.	ix
SUMMARY	xi
IMPLEMENTATION STATEMENT.	xiii
NOMENCLATURE.	xxiii
CHAPTER XI, FIELD TEST PROCEDURES	345
Loading System.	345
Jack-Pressure Errors.	348
Settlement Measurement.	352
Data Acquisition.	353

	<u>Page</u>
General Test Procedures	359
Description of Individual Tests	359
S1, Test No. 1 (S1T1)	360
S1, Test No. 2 (S1T2)	360
S1, Test No. 3 (S1T3)	360
S2, Test No. 1 (S2T1)	360
S2, Test No. 2 (S2T2)	360
S3, Test No. 1 (S3T1)	360
S4, Test No. 1 (S4T1)	361
S4, Test No. 2 (S4T2)	361
S4, Test No. 3 (S4T3)	361
CHAPTER XII, TEST RESULTS	363
Test Shaft No. 1.	364
S1T1.	364
S1T2.	377
S1T3.	378
Test Shaft No. 2.	386
S2T1.	386
S2T2.	400
Test Shaft No. 3.	411
S3T1L1.	412
S3T1L2.	419
S3T1L3.	422
Test Shaft No. 4.	429
S4T1.	429
S4T2.	438
S4T3.	452
Comparison of Test Results.	459
Field Inspection and Moisture Migration Studies	493
Visual Inspection of Test Shafts.	493
Field Moisture Migration Study.	499

	<u>Page</u>
Significance of Test Results	520
PART FOUR - DESIGN INFERENCES AND CONCLUSIONS	
PREFACE	iii
LIST OF REPORTS	vii
ABSTRACT	ix
SUMMARY	xi
IMPLEMENTATION STATEMENT	xiii
NOMENCLATURE	xxiii
CHAPTER XIII, DESIGN INFERENCES OF THE FIELD TESTS	527
Review of Field Research	527
Site Description	527
Instrumentation	529
Loading Arrangement.	529
Data Interpretation.	530
Design Categories.	531
Safe Design Against Plunging Failure	533
Calculation of Plunging Load	535
Calculation of Safe Design Load.	540
Calculation of Settlement at Design Load	541
Concrete	544
Example Design Problems	545
Example Problem No. 1	545
Example Problem No. 2	550
Implementation of Design Procedures	553
CHAPTER XIV, CONCLUSIONS AND RECOMMENDATIONS	554
REFERENCES	559

PART FIVE - APPENDICES

PREFACE	iii
LIST OF REPORTS	vii
ABSTRACT	ix
SUMMARY	xi
IMPLEMENTATION STATEMENT	xiii
NOMENCLATURE	xxiii
APPENDIX A. DRILLING REPORTS	573
APPENDIX B. HYDROMETER RESULTS	587
APPENDIX C. TABULATION OF RESULTS OF UNCONFINED, DIRECT SHEAR, PENETROMETER, AND U.T. TRIAXIAL TESTS	591
APPENDIX D. MORTAR MIGRATION TEST RESULTS	605
APPENDIX E. VOID RATIO VERSUS EFFECTIVE PRESSURE CURVES	629
APPENDIX F. FIELD NOTES	635
APPENDIX G. CONCRETE REST RESULTS	647
APPENDIX H. MUSTRAN CELL CALIBRATION DATA	653
APPENDIX I. CONVERSION FACTORS FOR MUSTRAN CELLS	659
APPENDIX J. OUTPUT OF INSTRUMENTATION DURING LOAD TESTS	665
APPENDIX K. INDIVIDUAL AND AVERAGE GAGE RESPONSE CURVES, S1T1, S2T1, S3T1L1, S4T1	757
THE AUTHORS	775

NOMENCLATURE

<u>Symbol</u>	<u>Definition</u>
A_B	area of base
A_c	transformed cross-sectional area of stem (including effects of reinforcing steel)
A_S	peripheral area of stem
A'_S	nominal peripheral area of the stem excluding sections at the top and bottom, each equal in height to twice the stem diameter
B	diameter of loaded area
\bar{B}	width of group of piles or shafts
C'	change in void ratio for increment of applied load
C_c	compression index
C_e	expansion index
c'	effective cohesion
c_{base}	average undrained cohesion of clay beneath base of shaft
c_{mean}	average undrained soil cohesion for fissured soil
c_{sides}	average undrained cohesion of clay along sides of shaft
c_u	undrained cohesion
c_v	coefficient of consolidation
D_r	relative density
d	diameter of shaft or pile
d_{stem}	diameter of stem
E_c	Young's modulus of concrete

<u>Symbol</u>	<u>Definition</u>
E_o	slope of initial tangent to nonlinear soil stress-strain curve; circuit output
$\frac{E_o}{c_u}$	ratio of E_o to half of maximum indicated undrained stress difference of clay
$e_{\text{corrected}}$	void ratio at beginning of loading increment of consolidation test corrected for elastic compression of consolidation apparatus
e_i	indicated void ratio at beginning of loading increment in consolidation test
e_o	void ratio of soil under overburden pressure, p_o
e'_o	void ratio after load increased to preconsolidation pressure, then decreased to overburden pressure in consolidation test
e_{50}	void ratio corresponding to t_{50}
e_{100}	void ratio corresponding to t_{100}
F.S.	factor of safety at working load
f_1, f_2	base shape factors
H	thickness of compressible layer
h	depth of base of shaft
I_ρ	settlement influence coefficient
K	gage factor
K_o	coefficient of lateral earth pressure, or the ratio of horizontal effective stress to vertical effective stress
L	unit length along shaft
L_s	length of stem

<u>Symbol</u>	<u>Definition</u>
l	length of shaft or pile
N	number of blows per foot for T.H.D. penetrometer
N_c, N_q, N_γ	bearing capacity factors
N_q^*	bearing capacity factor for sands
NMC	natural moisture content
P_i	point at center of i^{th} layer at which consolidation settlement is computed
p	factor relating penetrometer results to maximum unit side resistance
Δp	increment of applied pressure causing consolidation
p'	factor relating penetrometer results to unit base capacity
P_c	preconsolidation pressure
P_i	i^{th} point on load transfer or load distribution curve
P_o	overburden pressure, or initial effective vertical pressure at the center of the compressible layer
$Q(z)$	function relating load in the shaft to depth
Q_B	total amount of load taken by the base
Q_S	total amount of load removed by the sides in shear
Q_T	applied load
$(Q_B)_{\text{ult}}$	ultimate base load
$(Q_S)_{\text{ult}}$	ultimate side load
$(Q_T)_{\text{ult}}$	ultimate load at top of pile or shaft
q	contact pressure
$(q_B)_{\text{ult}}$	unit ultimate bearing stress on the base

<u>Symbol</u>	<u>Definition</u>
$(q_S)_{ult}$	unit ultimate side resistance
$(q_B)_{ult, net}$	net unit ultimate bearing stress on the base
r	stem radius
S	mean shear strength of clay soil
S_r	degree of saturation
S_0	shear strength of soil before softening
S_1	shear strength of soil after softening
$S1, S2, S3, S4$	abbreviations for Test Shaft No. 1, Test Shaft No. 2, Test Shaft No. 3, Test Shaft No. 4
$SlT1, etc.$	abbreviation for "Test No. 1 on Test Shaft No. 1," etc.
s	shear stress, spacing between piles in a group
T_z	tensile force at depth z
t_{50}	time required to develop 50 per cent of primary consolidation (logarithm of time plot)
t_{100}	time required to develop 100 per cent of primary consolidation (logarithm of time plot)
v	applied voltage
w	downward movement, moisture content
w_T	downward displacement of the butt
$w_{\bar{z}}$	downward displacement at depth \bar{z}
z	depth coordinate
\bar{z}	generic depth
α	shear strength reduction factor
α_{avg}	average shear strength reduction factor over a specified length of shaft

<u>Symbol</u>	<u>Definition</u>
α_{\min}	minimum shear strength reduction factor from a laboratory test series
α_{peak}	α_{avg} corresponding to peak side load
α_{ult}	α_{avg} corresponding to ultimate load
α_z	shear strength reduction factor at depth z
α_1	ratio of shear strength of soil around shaft after placing concrete to that existing before placing concrete
α_{11}	that part of α_1 due to softening because of migration of water from concrete into soil
α_{12}	that part of α_1 due to the shear strength reduction not accompanied by moisture migration (remolding, opening of surface fissures)
α_{13}	that part of α_1 due to surface effects and base-side mechanical interference
α_2	adhesion coefficient
$\bar{\alpha}$	average shear strength reduction factor over entire stem excluding top and bottom two diameters
β	settlement correlation coefficient, settlement interaction factor
γ'	effective unit of weight of soil
δ	angle of friction between the soil and concrete
δ_s	elastic compression of stem
ϵ	strain, general
$\epsilon_{\text{circuit}}$	circuit strain
ϵ_1	axial strain in triaxial or unconfined compression test
$\epsilon_{1\text{steel}}$	strain in steel in longitudinal direction

<u>Symbol</u>	<u>Definition</u>
$\epsilon_{2_{\text{steel}}}$	strain in steel in transverse direction
ϵ_{50}	strain corresponding to one-half of the principal stress difference at failure
μv	abbreviation for microvolts
ν	Poisson's ratio
ξ	settlement ratio
ρ_B	average settlement beneath loaded area
ρ_c	total compression of compressible layer
σ	normal stress
σ'_v	vertical effective stress in the soil adjacent to the shaft
σ_Δ	principal stress difference in a triaxial or unconfined compression test
σ_1	maximum principal stress
σ_3	minimum principal stress
ϕ	angle of internal friction
$\phi' (= \phi_d)$	effective angle of internal friction
ϕ_u	undrained angle of internal friction
ψ	additional shear strength reduction factor for shafts installed in a processed hole
ω	bearing capacity reduction factor for fissured clay

CHAPTER XI
FIELD TEST PROCEDURES

The four instrumented test shafts described in Part Two were load tested in order to measure their load transfer characteristics. The procedures and the load tests are described in this chapter.

Loading System

All four test shafts were loaded with hydraulic rams which were jacked against the reaction systems described in Chapter VIII. Bayou Industries' 500-ton-capacity double-acting jacks were employed. Single jacks were used on S1, S3, and for Tests 2 and 3 on S4. Two jacks acting in tandem and with a common pressure supply were used in all other tests.

To promote uniform stress distribution at the calibration levels and to prevent cracking of the concrete at the top of the shafts, load was applied through 18-inch by 30-inch by 1 3/4-inch mild steel load distribution plates, which were centered on the shafts and carefully leveled. A capping compound was placed between the concrete and the loading plates to facilitate leveling and to prevent cracking. The jacks were centered on the protruding portion of each test shaft. Slight eccentricities in placing the formwork for the protruding sections were thereby reflected in small, but insignificant, eccentricities in applied load.

Plywood blocks were placed between the jack pistons and the loading boxes to act as seats for the piston heads. Flat steel shims were used between the plywood and loading box where necessary.

Hydraulic pressure was applied to the jacks through an SC Hydraulic Engineering Corporation Model 10-600 hydraulic pump, pictured in Fig. 11.1.

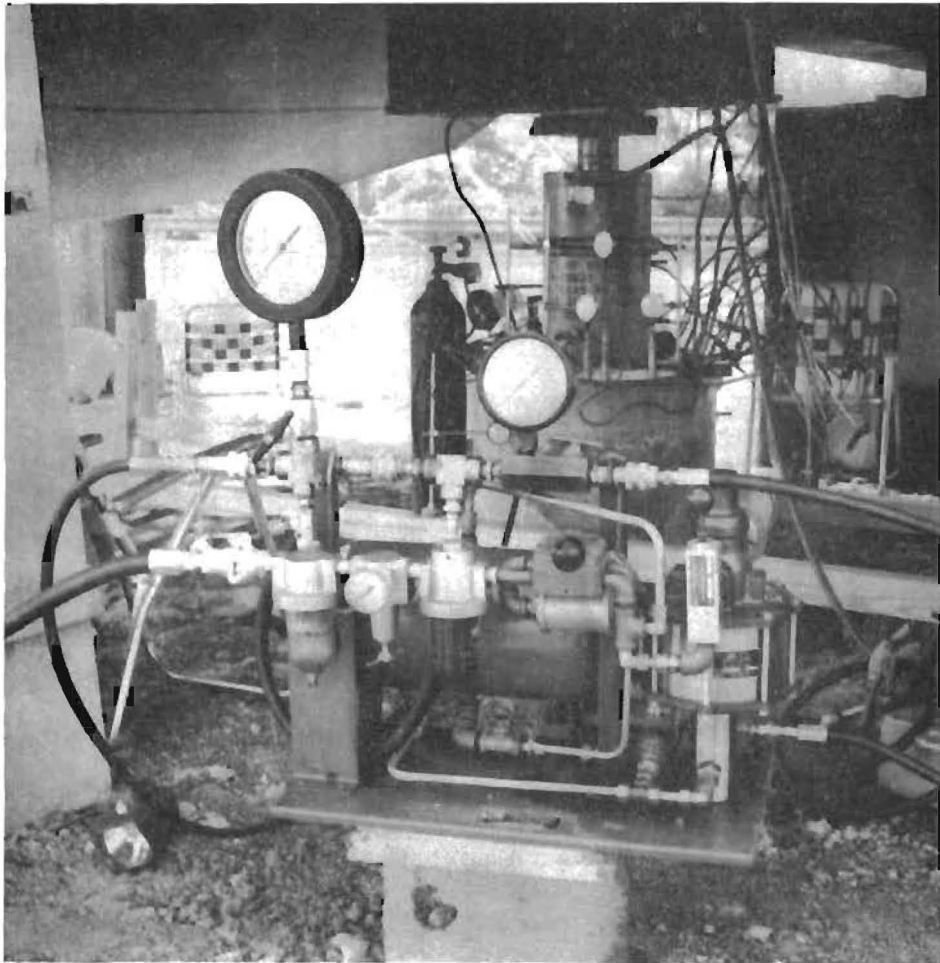


Fig. 11.1. Hydraulic Pump

The pump was air-operated, requiring an air pressure of 90 psi to pressurize the hydraulic fluid to 20,000 psi. Air pressure was supplied by a portable gasoline-powered compressor, which was capable of delivering 125 cubic feet of air per minute at 100 psi.

The hydraulic pump, which was controlled by one man, allowed precise regulation of the load at all times. Furthermore, it permitted load increments to be applied in a few seconds, and it provided the necessary discharge to allow the shaft to be plunged completely at failure. The pump also furnished an easy means for loading to achieve a constant rate of penetration.

A manual pump was used in the second load test on S4, which was conducted at sustained load, because the air compressor used had been unreliable when operated for prolonged periods of time.

The magnitude of the load delivered to the butt of the shaft was measured by metering the pressure in the hydraulic lines. Pressure-load relationships for the jacks, acting individually and in tandem, were found from calibration tests in the laboratory, which were conducted at intervals during the test program. Pressure metering in the field tests was achieved by using two Bourdon gages, one low range (0 to 5,000 psi) and one high range (0 to 20,000 psi), and a BLH GP 20,000 psi-capacity electrical pressure transducer, which was the primary pressure measuring device. Values of applied load could be resolved to the nearest tenth of a ton using the electrical pressure transducer with one jack in the system and to the nearest fifth of a ton when tandem jacks were employed.

The Bourdon gages were the only pressure measuring devices used in the first test on S1. Thereafter, they were used as a backup to the transducer and to provide the pump operator with a visual indication of

the value of the load, since the transducer was connected directly to the data acquisition unit, which displayed and recorded voltage values instead of values of pressure or load.

The low-range Bourdon gage could resolve only about one ton with a single jack in the system and two tons with tandem jacks. Resolution was about one-fourth as good for the high-range gage. Consequently, the load was read from the low-range gage whenever the jack pressure was less than 5,000 psi. To improve the ability of the pump operator to apply more accurate increments of load, the pressure transducer was taken off the data acquisition system in the tests on S4 and wired directly to a strain indicator. In this way, the pump operator was able to read and record manually the magnitude of the applied load directly with the high resolution afforded by the pressure transducer.

A schematic drawing of the entire loading system is shown in Fig. 11.2.

Jack-Pressure Errors

The reliability of measuring loads through jack pressures is sometimes questionable because of the presence of piston friction. With the relatively rigid reaction system utilized in the tests and the care taken in leveling the loading plate and the loading box for each shaft, no significant eccentric loads on the jack pistons are thought to have occurred. In addition, the jacks were well designed, with a tight fit between the pistons and seals. The pistons were lubricated before each test and were protected from the weather between tests by enclosing each shaft head, together with in-place jacks, within a small portable shed. When the jacks were not in use, the pistons were fully retracted. Jack friction is, therefore, reasoned to be small, and consequently, loads obtained by measuring hydraulic fluid pressure are reasonably accurate.

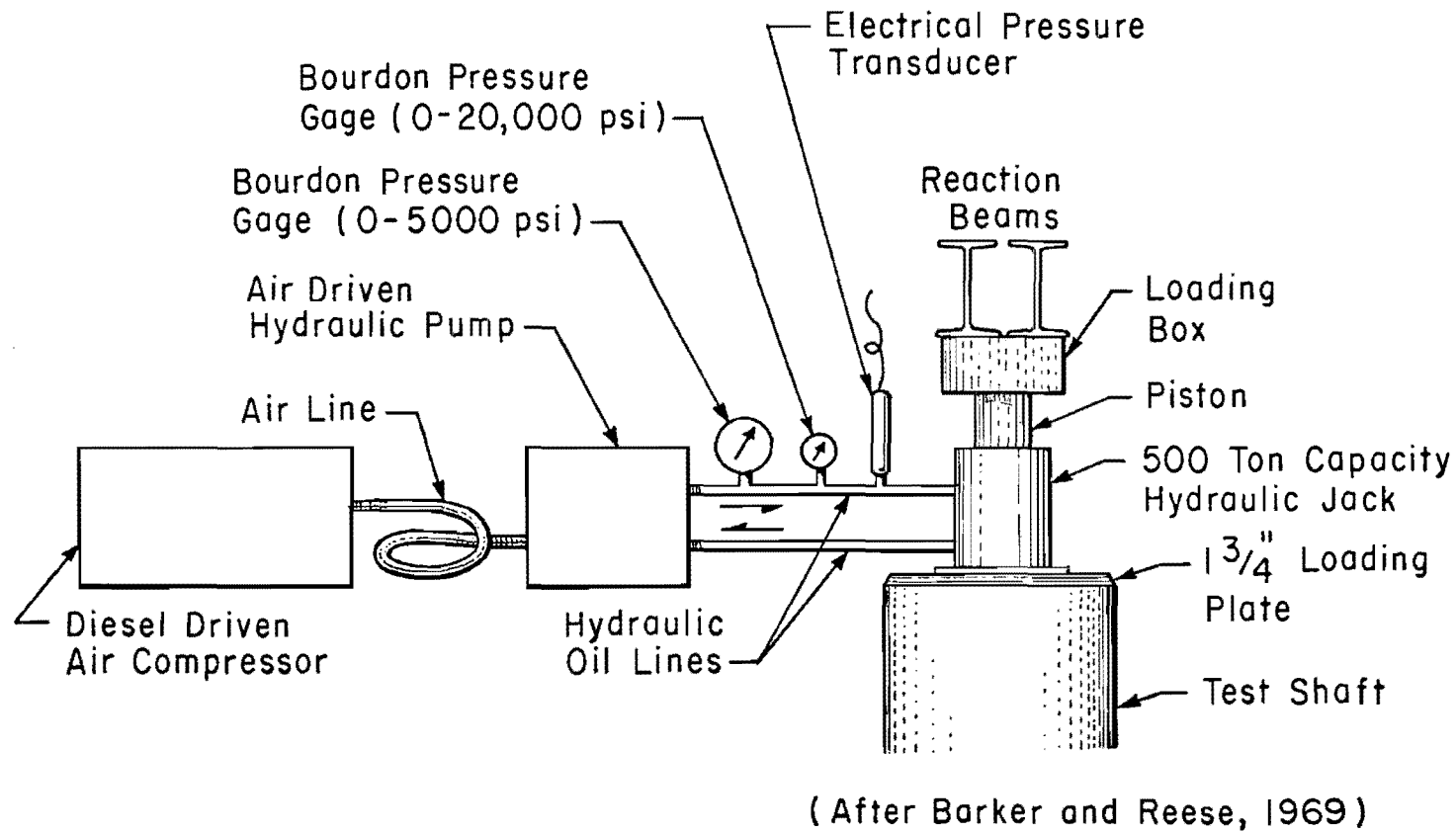
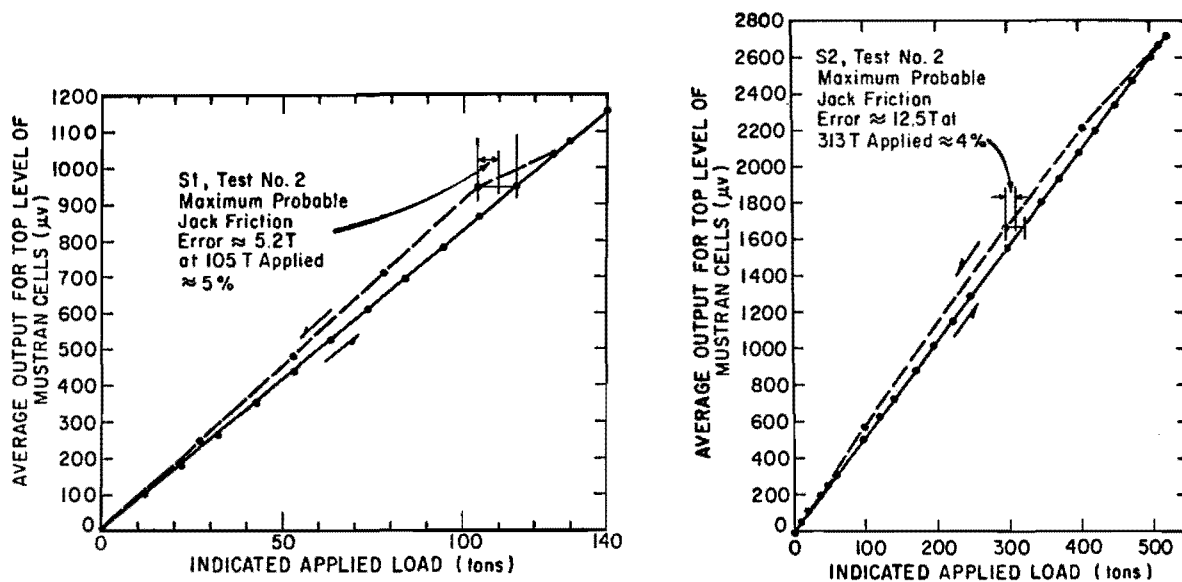


Fig. 11.2. Schematic Diagram of Loading System

Attempts were made to evaluate errors in the indicated load caused by jack friction by plotting jack pressure (or indicated load) against the average output of the calibration cells at the top of the shaft for increasing and decreasing loads for each test. The resulting relationship usually exhibited a small hysteresis, which is assumed to be due entirely to jack friction. (A part of the hysteresis effect, ignored in estimating jack pressure errors, is undoubtedly caused by the concrete in which the calibration cells were embedded.) The pressure range corresponding to half the maximum width of the hysteresis loop is then equal to or greater than the maximum error in the indicated applied load. In general, the maximum error so calculated was less than two per cent of the indicated load (overestimations of true load during increasing load) for all but two tests: S1, Test No. 2; and S2, Test No. 2. Maximum errors approaching five per cent were obtained in those tests. Typical hysteresis curves are given in Fig. 11.3.

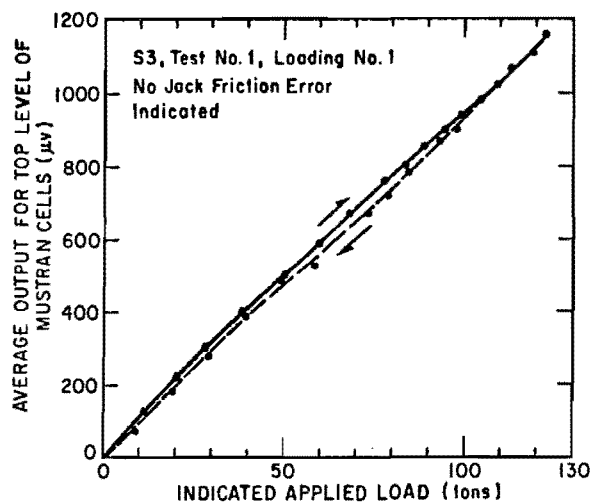
To gather information concerning jack pressure errors unaffected by concrete hysteresis, an electrical load cell was placed between the piston and the loading box for the third test on S4, and a direct load-jack pressure relationship was obtained for field conditions. The load cell indicated a maximum error in load measured by the pressure transducer of about four per cent. This test is discussed further in Chapter XII.

In retrospect, the errors introduced by measuring jack pressures were tolerably small in this study. However, inclusion of a load cell between the piston and loading box eliminates the uncertain effect of jack friction. The development of an accurate load cell designed specifically for use in drilled shaft testing would be desirable. Such a



a. Shaft 1, Test 2

b. Shaft 2, Test 2



c. Shaft 3, Test 1, Loading 1

Fig. 11.3. Jack Pressure Error Curves

load cell, which must have a small height, a high capacity, and a low sensitivity to eccentric loads, would be essential for incorporation in tests of instrumented shafts conducted by personnel not experienced in field testing of drilled shafts.

The values of applied loads reported in connection with the test results in Chapter XII are those values indicated by measuring the jack pressure. No estimated corrections for jack friction have been included.

Settlement Measurement

Butt settlement was measured by two dial indicators (settlement gages) mounted on reference beams located on opposite sides of the test shaft. The indicator stems were supported on flat stages affixed to the sides of the test shaft approximately one foot above the ground surface. The reference beams were twenty-foot-long timber four-by-fours anchored by pairs of wooden stakes at their ends. Timber beams were used in preference to steel beams because temperature and vibration effects were smaller. As the shaft and stages moved downward under load, the reference beams remained stationary, and the settlement was registered on the dial indicators, which had a 0.001-inch least count and a two-inch travel. When the settlement exceeded two inches, spacer blocks were placed between the stages and the indicator stems to allow further deflections to be measured.

Settlement gages were placed in pairs to check nonuniform settlement. However, the gages tracked each other very closely in all tests, thereby verifying that settlement of the butt was essentially uniform in every test.

Direct-current-powered linear variable differential transformers (LVDT's) were used to supplement the dial indicators in two tests. The LVDT output and pressure transducer output were used to drive an x-y plotter to obtain an instantaneous load-settlement graph, which was of value of the test director in determining the proximity to failure of the test shaft. Although the LVDT readings agreed closely with the settlement gage readings, some electrical drift was observed, resulting in small errors in plotted settlement. On occasions when LVDT's were not used, manual plots of load versus settlement were made as the test progressed. When LVDT's were not used, an engineer's level was used to measure settlements to provide a backup to the settlement gages.

A photograph of the butt of S2 just prior to the first load test is shown in Fig. 11.4. The loading jacks, reference beams, settlement gages, telltale gages, and pyrometer are clearly shown. Figure 11.5 gives a larger view of the test arrangement, including the loading jack, pump, reference beams, level, small reaction frame, and tarpaulin. The shaft shown is S1. An overall view of the entire test site is shown in Fig. 11.6, taken just prior to the first load test on S2.

Data Acquisition

During the majority of the load tests, data from the Mustran cells, embedment gages, bottomhole load cell, and pressure transducer were acquired digitally with a Honeywell Model 620 Data Logging System. The system, which is a portable modular unit, pictured in Fig. 11.7, was usually placed physically inside a van adjacent to the test site; consequently, it was protected from the sun and wind. An air conditioning unit



Fig. 11.4. Butt of Shaft 2 Prior to Load Test



Fig. 11.5. Test Arrangement, Shaft 1



Fig. 11.6. Overall View of SH225 Test Site



Fig. 11.7. Data Logging System

in the van provided acceptably low ambient temperatures (below 90°F) during tests conducted in hot weather, thereby improving the operation of the system. To minimize resistance changes in the electrical leads between the shaft and the system, the leads were sheltered from direct sunlight on sunny days by the large tarpaulin that covered the test site.

The operation of the data logging system is shown schematically in Fig. 11.8. Each electrical gage to be read was connected to a balancing circuit. This connection was made directly with the gage leads in S1 and S2 and through the manifold plugboards in S3 and S4. The entire measuring system was continuously powered by a three-kilowatt portable generator. The voltage to each circuit was controlled by an electronic power supply, which provided six volts d.c. with a 0.01 per cent regulation to all Mustran, embedment gage, and pressure transducer circuits. Twenty-four volts d.c. was provided for the bottomhole load cell circuit. Each circuit was initially balanced with a potentiometer, which was a part of the balancing circuit shown in Fig. 11.8.

Each data circuit was connected to one of the 40 input channels of a data scanner in the system. Data from all of the 40 channels was automatically read and recorded in a preset sequence. When a set of readings was desired, an external command caused the scanner to step to the first channel. The signal from that channel was fed into a preamplifier, which scaled the signal to the proper level to be read by a digital voltmeter. The voltmeter sampled the preamplified signal and converted the voltage (gage output) to a decimal number, which was sent to the printer module. The gage output voltage was then printed on paper tape, and a step command was sent to the scanner to advance to the next channel. This

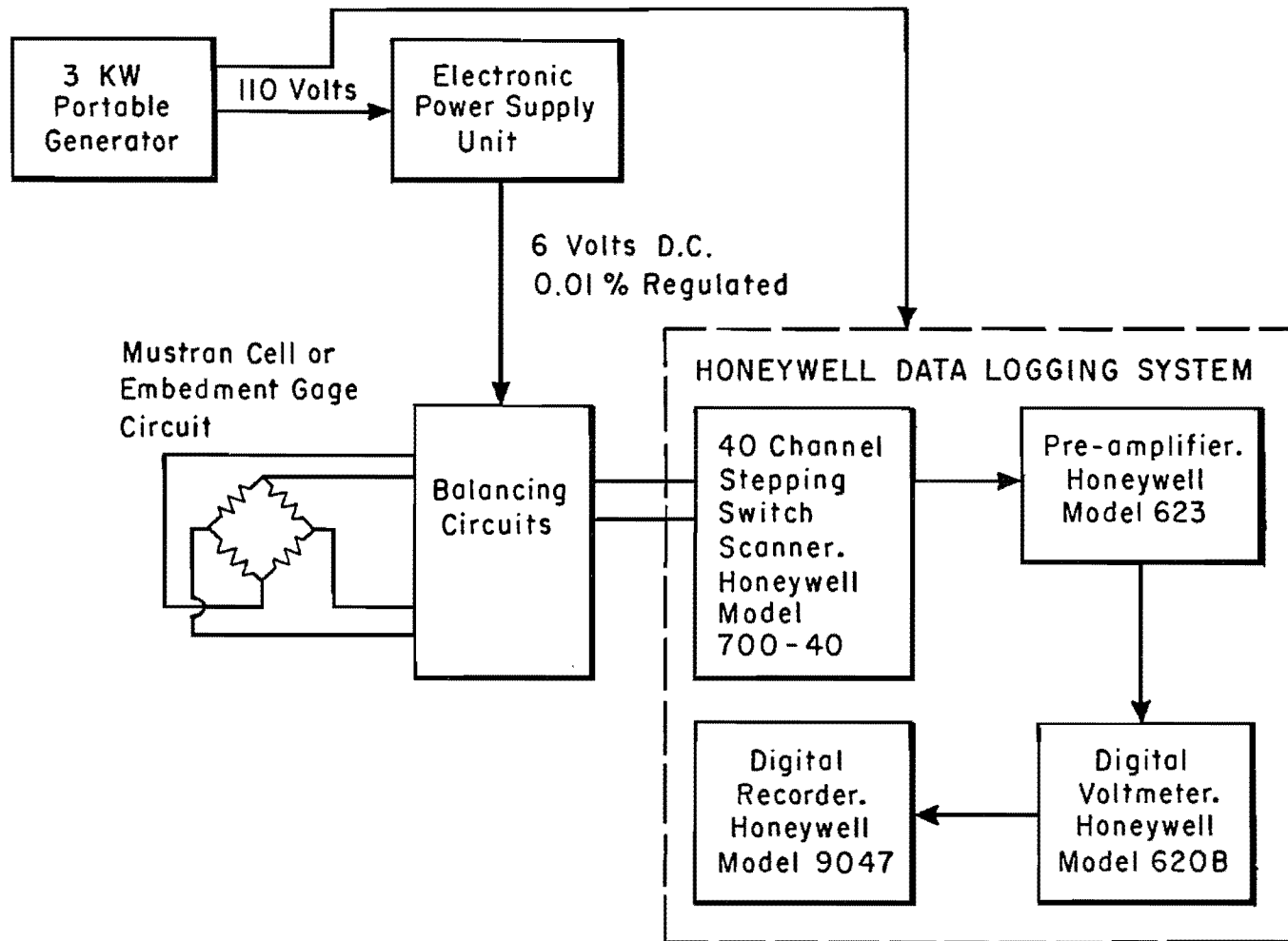


Fig. 11.8. Diagram of Honeywell Data Logging System

process was repeated until all gages were read. Using this procedure, gages were read at the rate of about one per second. At the end of a test, a complete printed record of all gage readings was thus available. The readings were taken off the paper output tape manually and punched on computer cards for automatic data reduction.

The logging system required continuous powering of the gages for its operation. As mentioned previously, continuous powering did not cause electrical drift in the Mustran cells, but it did cause drift in the embedment gages. However, under the circumstances, embedment gage drift was acceptable, since the Mustran cells made up the primary instrumentation system. Moreover, it was decided that the fast-scan advantage afforded by the Honeywell system outweighed the disadvantage of embedment gage drift. Prior to each load test, all circuits were powered for several hours until embedment gage drift corrections could be established or until drift was minimized.

For the scale used in the tests (1 microvolt resolution), the system has a quoted accuracy of about ± 2 microvolts, which translates to about ± 0.6 tons for the Type 1 Mustran cells and ± 1.2 tons for the Type 2 Mustran cells for the shafts tested.

Problems were encountered with the printer module during the first test on S4, necessitating manual stepping and recording of voltage output, which is displayed visually on the front panel of the digital voltmeter. The digital voltmeter module malfunctioned during the test on S3. In that test, a separate digital voltmeter (Hewlett Packard Model 3440A) with a resolution of ± 5 microvolts was connected to the scanner. The scanner was stepped manually and the voltmeter output was recorded manually.

The data logging system was not used in the second test on S4, which was a sustained load test. Since minimizing reading time was not important, gage output was obtained with a strain indicator.

General Test Procedures

Each load test began as soon as drift readings had been completed. The QL procedure, described in Chapter IV, was followed in all but portions of two tests. Once failure had been achieved in the test on S3, the shaft was plunged at a constant rate of penetration. In the second test on S4, sub-failure sustained loads were held for several hours. Otherwise, the usual procedure was as follows: load increments of five or ten tons were applied to the butt every 2 1/2 minutes. Thirty seconds after load application, the settlement gages were manually read and the electrical gages were scanned. Readings were again taken just prior to the application of the next increment of load. Test results reported in Chapter XII are all based upon the second set of readings. Load increments were applied until the shaft plunged (settled at a uniform rate without application of additional load). Afterwards, load was removed in decrements of 10 to 20 per cent of the ultimate capacity every 2 1/2 minutes. Settlement gages and electrical circuits were read during rebound. They were also monitored periodically for about thirty minutes after all load had been removed.

Description of Individual Tests

The following paragraphs explain the purpose of each load test and departures from the usual testing procedure. Plunging failure was achieved in every test. Nine tests were conducted in the chronological order listed below. The date of each test is given in Table 8.2.

S1, Test No. 1 (S1T1). This test was conducted by the QL procedure to determine the load transfer characteristics of S1 under virgin loading.

S1, Test No. 2 (S1T2). This test was conducted by the QL procedure directly after the conclusion of S1T1 to determine the capacity of S1 upon immediate reloading.

S1, Test No. 3 (S1T3). This test was conducted by the QL procedure 3 1/2 months after S1T2 to measure the load transfer characteristics of S1 upon delayed reloading. Load was applied in increments of approximately 15 tons.

S2, Test No. 1 (S2T1). S2T1 was performed to observe the load transfer characteristics of S2 under virgin loading. The QL procedure was followed, except that loading increments were increased to 25 tons after shear failure had occurred along the sides of the stem.

S2, Test No. 2 (S2T2). Following the same test procedure as for S2T1, S2T2 was conducted 3 1/2 months after S2T1 to determine the load transfer characteristics of S2 upon delayed reloading.

S3, Test No. 1 (S3T1). S3T1 was the only load test conducted on S3. The test was carried out in three loading phases, designated S3T1L1, S3T1L2, and S3T1L3. In S3T1L1, the load transfer characteristics of the shaft under virgin loading were determined, using the QL procedure. Once side failure occurred, the shaft was pushed downward under a constant rate of penetration of 0.1 inches per minute until the full travel of the jack piston had been reached, and the load was then released. The CRP portion of S3T1L1 was performed to obtain an indication of the limit of the shear capacity of the sides under large displacement. As soon as several inches of shim could be placed between the piston and the loading

box, S3T1L2 was performed. It was conducted in the same manner as S3T1L1. The principal purpose of this loading phase was to push the shaft downward to seat the base against the bottom of the pre-formed cavity. Once S3T1L2 was concluded, additional shims were placed, and the shaft was loaded again using the QL procedure (S3T1L3). This final loading was conducted to determine the base capacity of S3 and to observe the effects of end bearing on load transfer near the base. The entire test required approximately five hours.

S4, Test No. 1 (S4T1). This test was performed, following the QL procedure, for the purpose of obtaining the load transfer characteristics of S4 under virgin loading.

S4, Test No. 2 (S4T2). S4T2 was conducted about two weeks after S4T1. The applied load was increased to approximately 70 per cent of the failure load observed in S4T1, following the QL procedure. That load was then maintained for 17 hours in order to observe whether any redistribution of the load (load shedding) occurred along the shaft. The applied load was then increased to about 80 per cent of the previous failure load, and load distribution measurements were made for an additional 5 1/2 hours. The shaft was then plunged by continuous application of load from a hand pump.

S4, Test No. 3 (S4T3). The irregular shape of S4 caused the method of top level calibration, used in the other three test shafts to be unusable for S4. Following S4T2, soil was excavated from around S4 to a depth of 24 feet, exposing the top seven levels of Mustran cells. S4T3 was then conducted to give individual load-output curves for each of these levels, to be applied as direct calibrations in the reduction of

data from S4T1 and S4T2. S4T3, which was conducted by the QL method, was also performed to evaluate further the errors in indicated load due to jack friction and to obtain a direct indication of the approximate load which had been transferred in the top 24 feet of the shaft in the first two tests.

CHAPTER XII

TEST RESULTS

Following the completion of each load test described in the previous chapter, data from the various instrumentation systems were processed by electronic computer. Reduction of data was accomplished with the use of a program similar to program DARES, described by Barker and Reese (1970). The automated data reduction process consisted essentially of the following steps, as described in Chapter IX:

1. Computation of the equation of the in-shaft calibration curve from the response of the top level of gages.
2. Computation of discrete values of load remaining in the shaft at each instrumentation level for each value of applied load.
3. Computation of the equation of the third, fourth, or fifth degree polynomial least-squares, load-distribution regression line corresponding to each value of applied load.
4. Tabulation of the load-settlement relationships for both the butt and base.
5. Computation of the load transfer relationships from the load distribution equations at specified depths.

Computer output, containing an echo print of the raw test data and computed discrete values of load at each gage level, is given in Appendix J for every test except S1T2 and S4T3.

Shaft compression, base settlement, and load transfer relationships were obtained from the load distribution curves by procedures discussed

in Chapter III. The shear strength profile, to which developed shear stresses are referred for the determination of shear strength reduction factors, is the curve designated "UT triaxial" in Chapter VII.

Results from each individual test are presented in the following sections. That presentation is followed by a comparison of the various aspects of behavior of the four test shafts, tabulations of values of parameters having design implications, a discussion of observations made upon uncovering two of the shafts and sampling next to the stem on a third, and an overall interpretation of the significance of the test results. Figure 6.2, from Part Two, is included again on the following page to provide the reader with a brief review of the soil and test shaft profiles. The reader is referred to Part Two for complete descriptions of the test shafts, soil conditions, and instrumentation.

Test Shaft No. 1

S1T1. For the purposes of this study, the ultimate capacity, or failure load, of each test shaft is defined as the butt load at plunging failure. The ultimate capacity for S1T1, conducted between 0600 and 0800, August 29, 1968, was 140 tons. The load-settlement relationship obtained for this test is given in Fig. 12.1. In addition to the total load-settlement curve, the side and base components are also indicated in the figure. Base, side, and total load have been plotted as functions of mean settlement, which is nearly equal to the settlement measured at the butt. Base settlement was found from a numerical form of Eq. 3.1 using \bar{z} as the shaft length. The base load corresponding to each plotted value of mean settlement was obtained from the base load indicated by

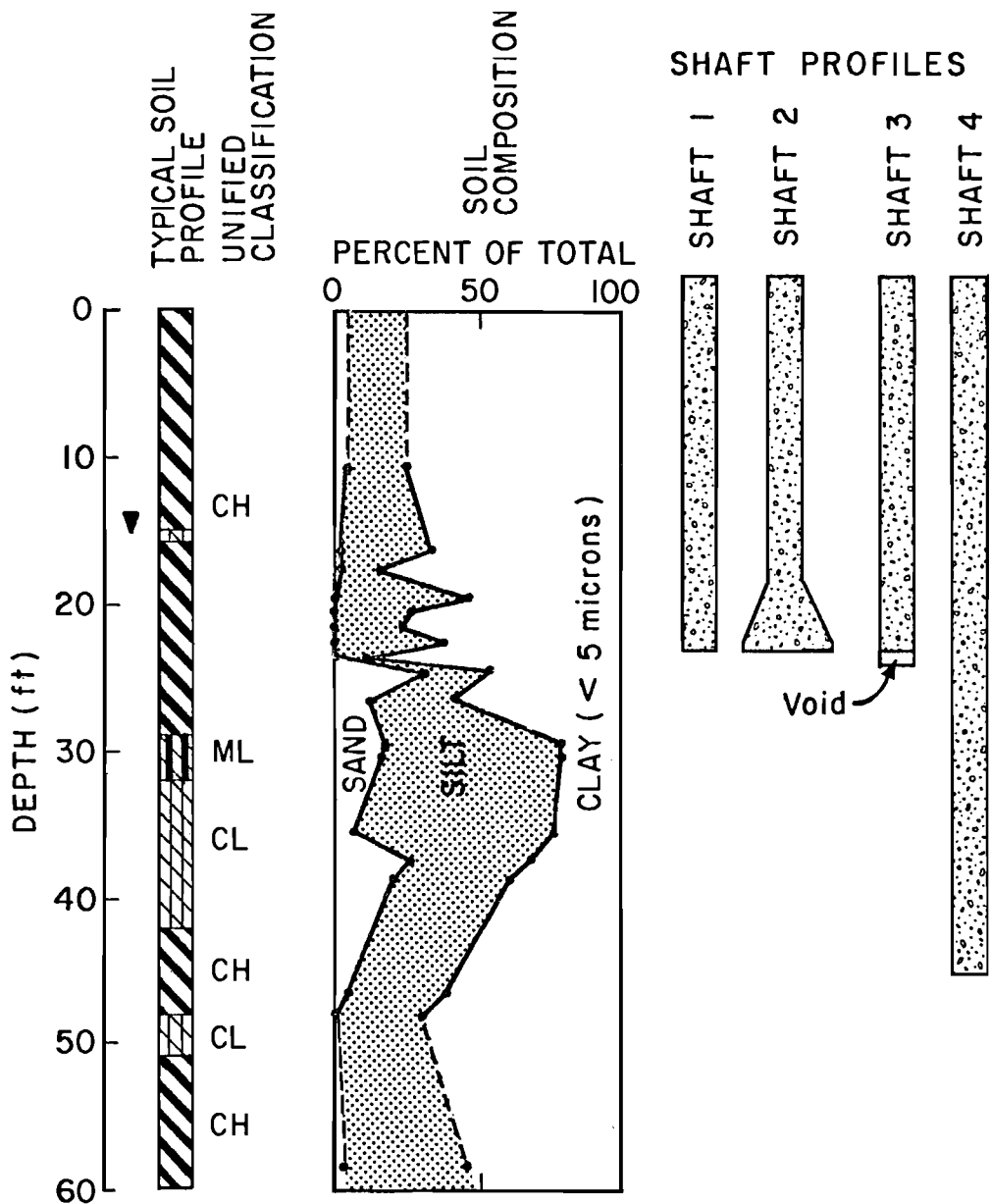


Fig. 6.2. Profiles of Soil Composition and Test Shafts, SH225 Test Site

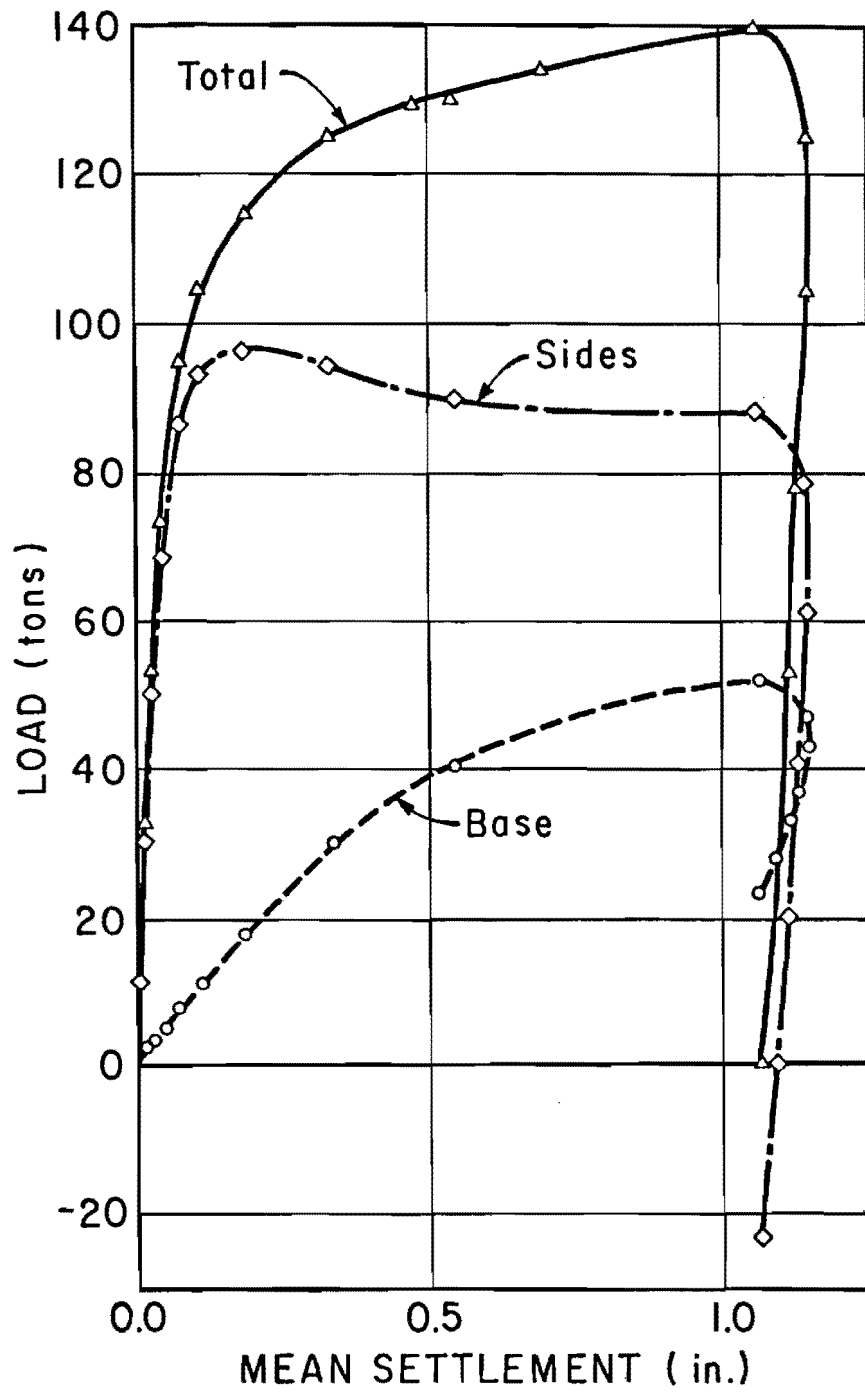


Fig. 12.1. Load-Settlement Curves for S1T1

the appropriate load-distribution curve; the corresponding side load was then determined by subtraction.

Several important features are evident in Fig. 12.1. First, the side load-settlement relationship was dominant over that of the base, especially in the early stages of loading. Second, both the side and base load-settlement relationships were nearly linear up to one-half of the respective peak component reactions. Third, a settlement of about 0.2 inches was required to mobilize completely the strength of the soil along the sides of the stem, while a settlement of more than one inch was required to mobilize the strength at the base. Fourth, the total rebound was about 0.09 inches after removal of the load. Finally, it is apparent that some load shedding occurred after the peak side reaction was achieved.

Individual gage response diagrams, in which gage responses are plotted against applied load for the loading phase, are given in Appendix K. The shapes of the average reading-versus-load curves are typical of the cell response in the stem of a drilled shaft. That is, the relationships are initially linear, followed by an upturn in the curve which indicates that side failure is occurring above the level represented. The curves for individual Mustran cells indicate some eccentricity in the load (shown by differing cell responses in two cells at the same level), which is seen to increase as side shear failure progressed. Individual cell responses at the 15-foot level were divergent, an effect apparently induced by a small collar that formed in the silty soil at that level (discussed later in this chapter). The Mustran cells at the 21-foot level indicate an eccentric base failure.

Several embedment gages were excluded from the load distribution calculations because of low resistance to ground or because of excess no-load drift. Only results from those gages used in data reduction are shown in Appendix K.

The curve showing the response of the bottomhole load cell, Fig. 12.2, illustrates the manner in which load reached the base of the shaft and how base load was relieved as the applied load was removed. The linearity of the initial portion of the curve, side shear failure (upturn of curve), and load shedding (slight reverse curvature) are apparent from the shape of the loading phase of the curve.

The loads at various depths were obtained directly from the in-shaft calibration curves for Mustran and embedment systems (except for the bottomhole cell, for which the laboratory calibration curve was used). Fourth degree regression curves appeared visually to provide the best fit for the load distribution data and were, therefore, used. Load distribution curves for several values of applied load are shown together with discrete values of indicated load in Fig. 12.3. Mustran and embedment system data have been given equal weight in generating the load distribution curves. Scatter in the data was small until side resistance failure occurred, at which time scatter increased significantly. This phenomenon was observed in the tests on all of the shafts at the SH225 test site. The load distribution curves corresponding to smaller applied loads, therefore, give more accurate representations of true load distribution than those for higher applied load. The slopes of the load distribution curves are highest near the midheight of the shaft, indicating greatest load transfer at that depth.

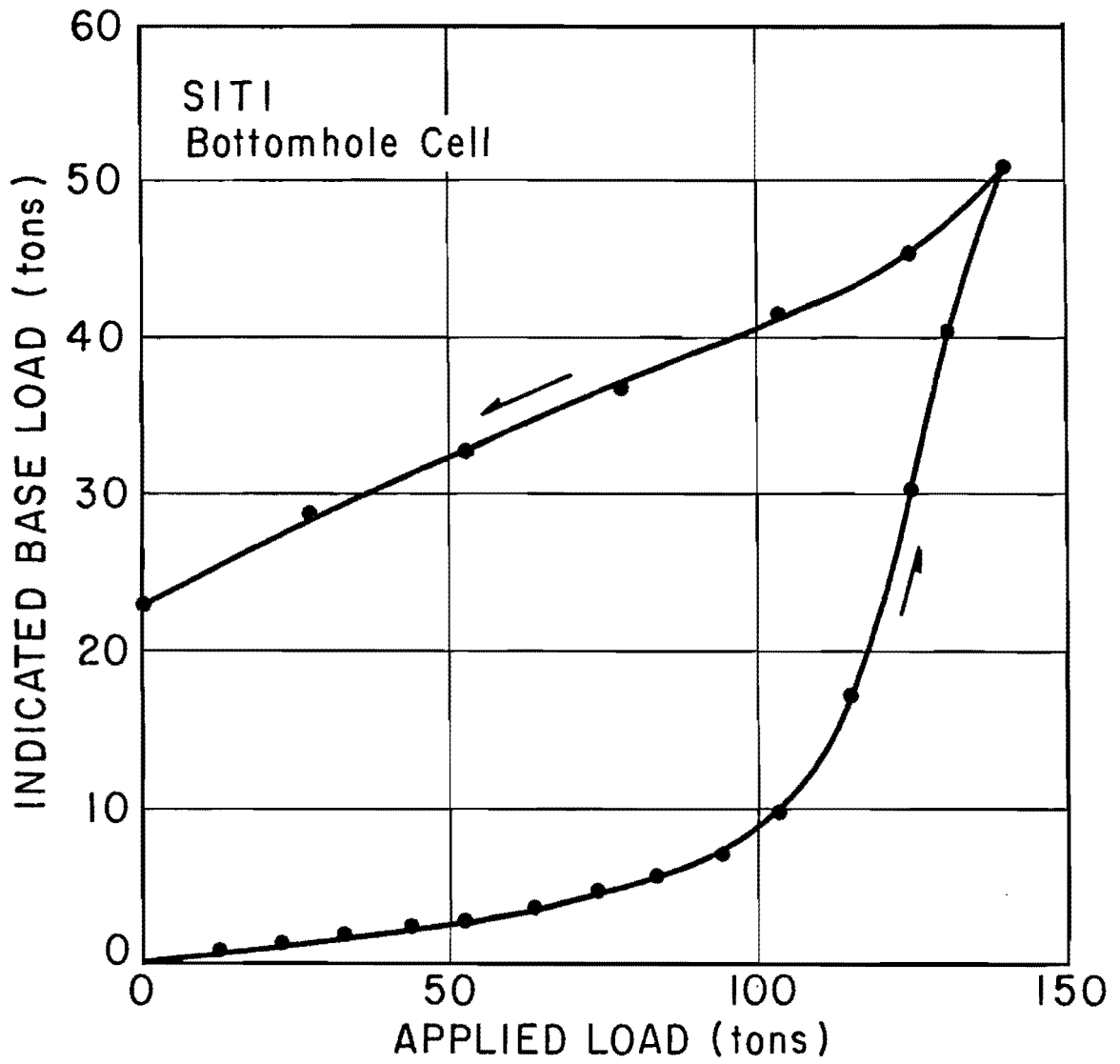


Fig. 12.2. Bottomhole Load Cell Response Curve for S1T1

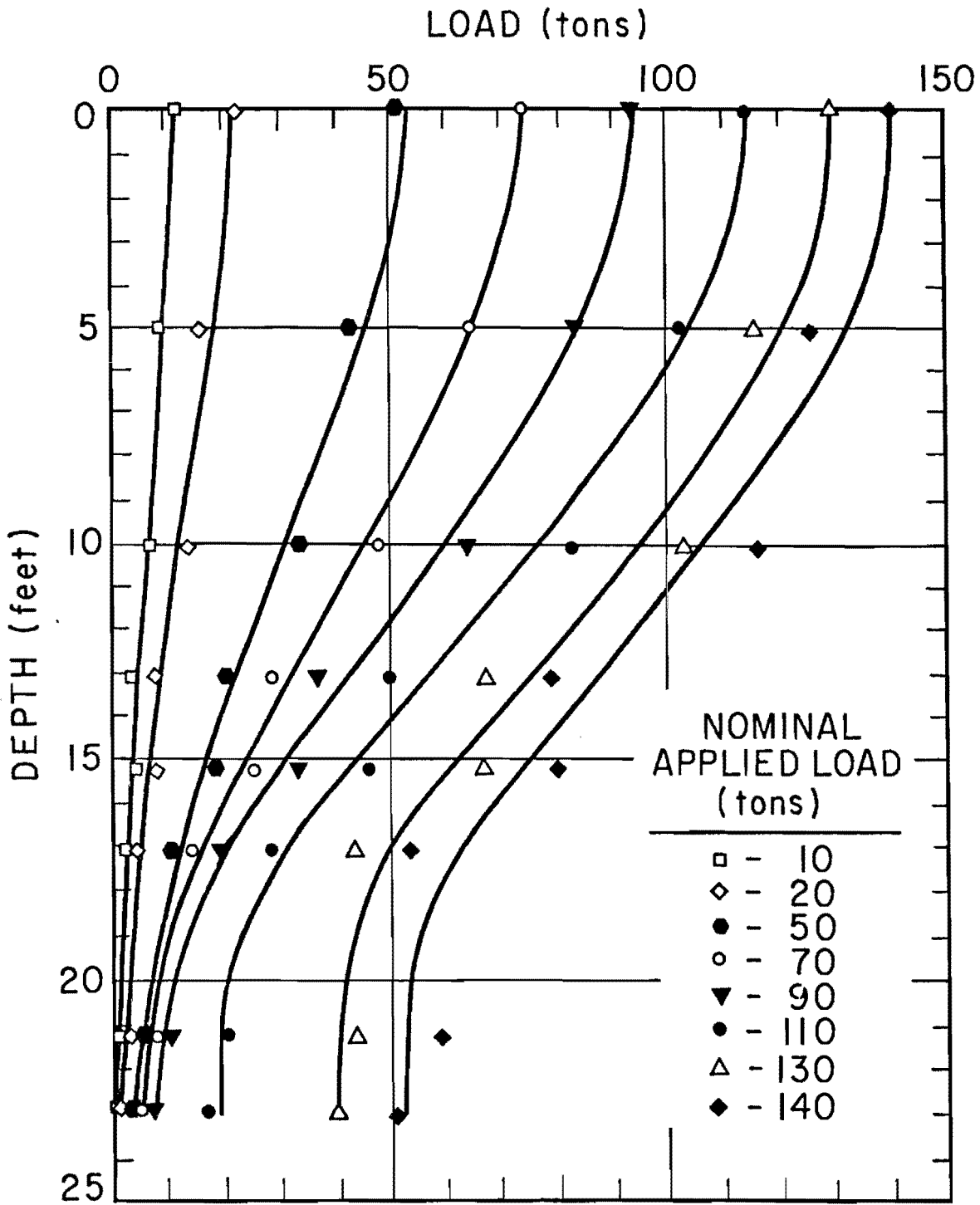


Fig. 12.3. Load Distribution Curves for S1T1

Load transfer curves are perhaps the best way of illustrating the manner in which the soil around the stem behaved during the test. Such curves were developed for S1T1 at several depths as shown in Fig. 12.4. Load transfer curves were routinely generated for depths of 50 inches (4.1 feet), 100 inches (8.3 feet), 150 inches (12.5 feet), 175 inches (14.6 feet), 200 inches (16.7 feet), 225 inches (18.8 feet), and 250 inches (20.8 feet) for all tests. In S1T1, the load transfer curves were derived from the regression curves in Fig. 12.3 and reflect, to a degree, the mathematical properties of the polynomials used to fit the load distribution data. They are, however, believed to be accurate estimates of the true load transfer relationships. The shaft diameter was assumed to be 30 inches when calculating load transfer from the load distribution curves. From Fig. 12.4 it is again observed, rather vividly, that the load transfer was greatest between the 12- and 15-foot levels, where a peak shear stress of about 0.9 tsf was developed. Less load transfer appeared near the surface and near the base. These phenomena will be discussed later. From the positions of the peaks of the load transfer curves, side shear failure is observed to progress from the base and surface (failure at lowest displacement) toward the mid-height of the shaft (failure at largest displacement). Peak stress was developed at the 4.1-foot level at a displacement of 0.12 inches, at the 20.8-foot level at 0.07 inches, and at the 14.6-foot level at 0.25 inches.

Another way to illustrate soil behavior is to plot the shear stress distribution along the shaft at various magnitudes of applied load. A family of such curves is shown in Fig. 12.5a along with the shear strength

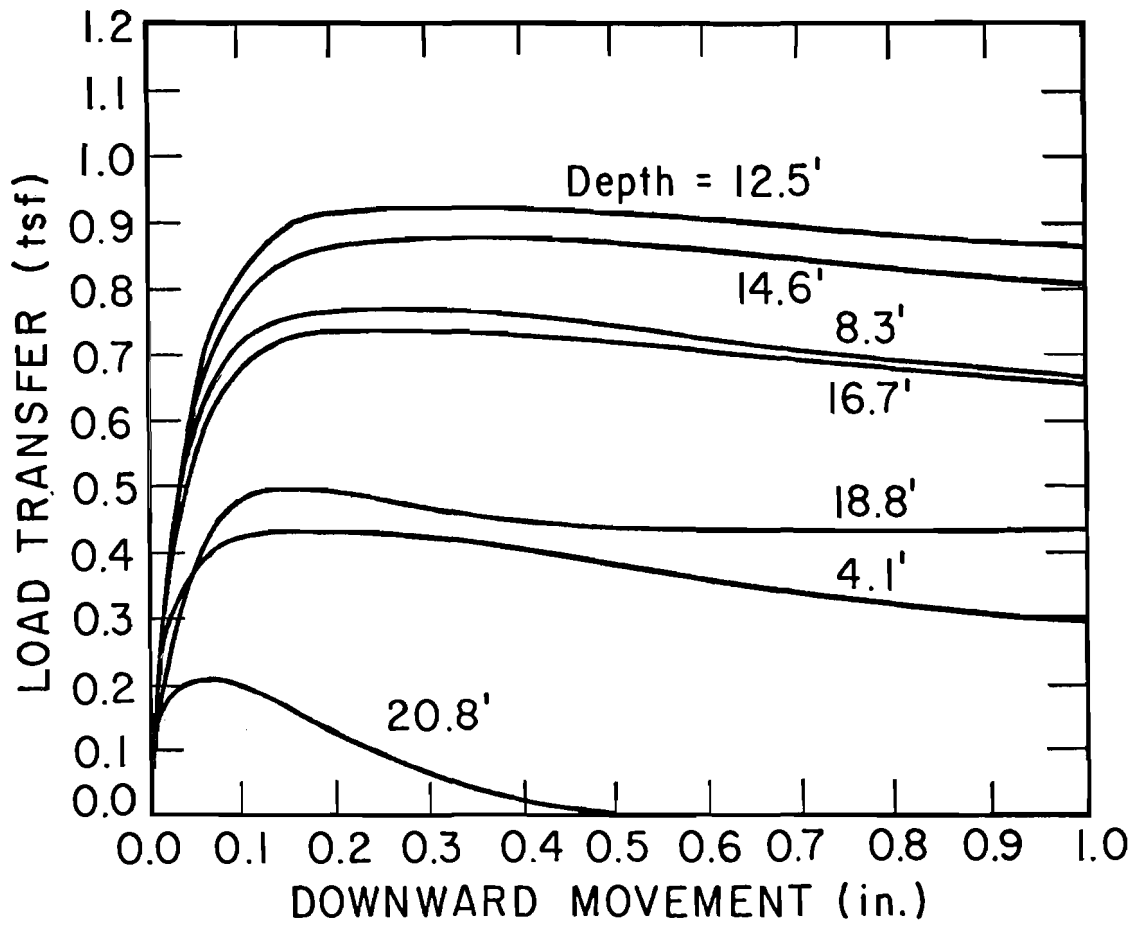


Fig. 12.4. Load Transfer Curves for S1T1

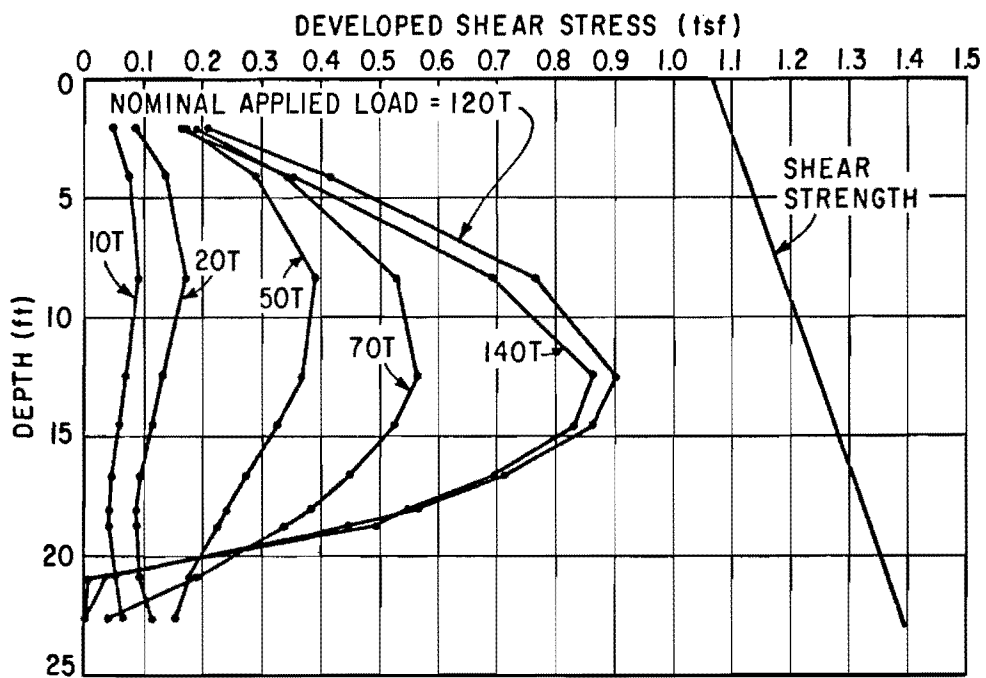


Fig. 12.5a. Distribution of Developed Shear Stresses for S1T1

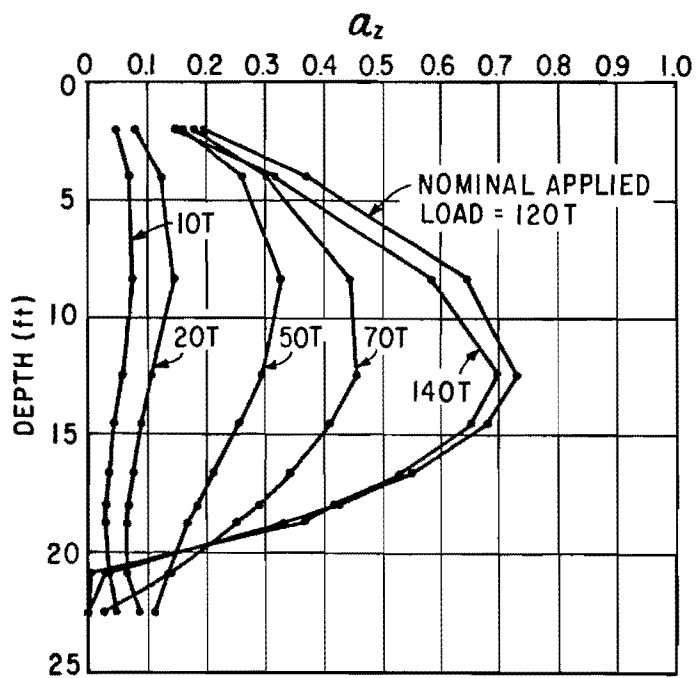


Fig. 12.5b. α_z Versus Depth for S1T1

profile indicated by the UT triaxial tests (see Chapter VII) for the top 23 feet of Layer I. Figure 12.5b has been produced by dividing the developed shear stress at each level by the appropriate value of shear strength for that level. The ratio of developed shear stress to shear strength (normalized developed shear stress) is denoted α_z . The curve corresponding to a nominal applied load of 120 tons corresponds to the peak load transfer. That curve shows the variation of the peak shear strength reduction factor with depth. The average value of the shear strength reduction factor, α_{avg} , at peak load transfer was 0.44, although a variation from 0.0 at the base to a maximum of about 0.7 near the middle was observed. By the time plunging failure was achieved, α_{avg} had dropped to 0.40.

Again, the shapes of the curves shown in Figs. 12.5a and b are influenced somewhat by the properties of the load distribution regression polynomials, but the curves are thought to be good representations of the true shear stress distributions.

Fifteen minutes after the load was removed, considerable load remained in the shaft, as illustrated in Fig. 12.6. Such a residual load distribution might approximate the initial stress distribution in a driven pile of the same dimensions as Test Shaft No. 1. It is felt that such residual load dissipates considerably with time, as evidenced in Fig. 10.3.

Results from telltales and the Gloetzl cell were unusable. Concrete strains were too small to permit reliable telltale operation. The Gloetzl cell did not function properly, giving a severe underregistration of stress.

Very little load transfer was indicated near the surface and near the base. Decreased load transfer in the top two or three diameters possibly can be attributed to surface effects, including that of surface soil

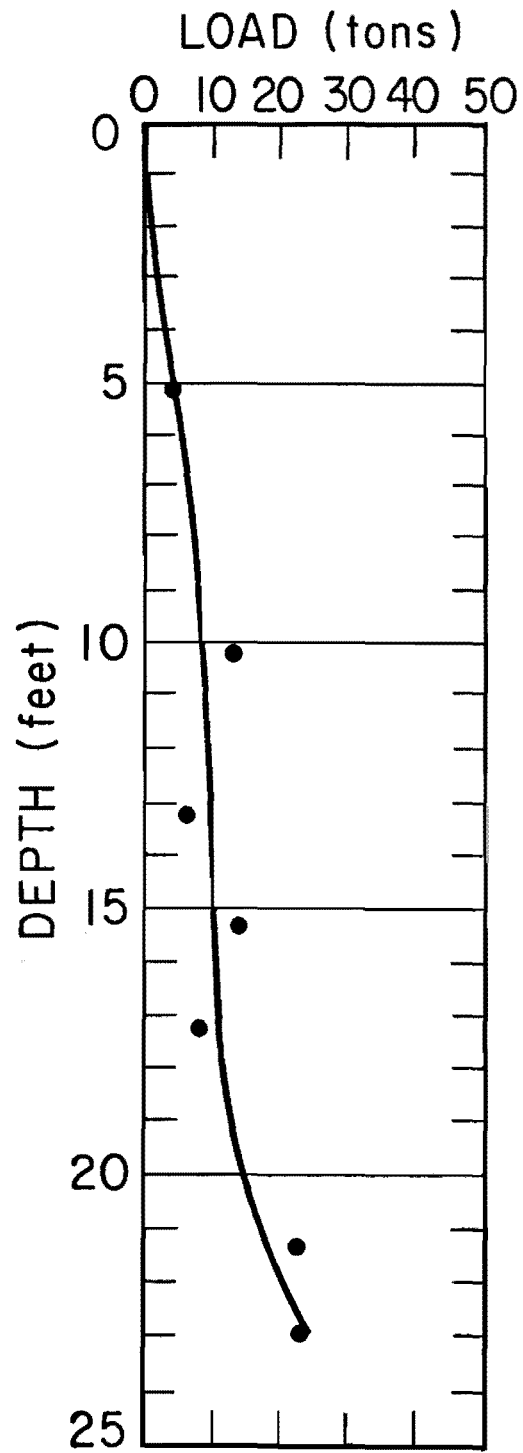


Fig. 12.6. Distribution of Load in Shaft Immediately After S1T1

shrinkage, although the latter effect was probably small, since the ground around the top of the shaft was damp at the time of testing. No-load monitoring reported in Chapter X showed that the concrete in the top of a shaft can also shrink with the passage of time, possibly contributing to the small load transfer in the top few feet.

The explanation for the near absence of load transfer in the bottom two diameters is not completely clear. However, some information pertinent to this question was obtained when Test Shaft No. 1 was exposed and moisture content profiles were taken in the soil adjacent to the shaft at several depths about one year after S1T1 (described later). An increase in moisture content of 2 to 8 per cent was observed to occur in the soil near the shaft below a depth of 18 feet, while no such moisture content increase was observed above a depth of 18 feet. According to Eq. 7.1, an increase in moisture content of 8 per cent reduces the remolded shear strength of Beaumont Clay by about half; undisturbed strength would presumably be reduced by a somewhat smaller amount. Hence, excess soil softening probably accounted for part, but not all, of the loss of load transfer near the base. The source of the excess moisture is believed to be the extraneous water present in the borehole at the time of casting. It is further thought that excess mixing water not required for concrete hydration could have migrated down the shaft after the concrete set up, increasing the moisture supply to the soil around the base. Further softening could have occurred because of the small oil leak in the bottomhole cell, but no evidence of oil was found in the soil around the base when the shaft was exposed and removed.

The configuration of the load transfer curve for a depth of 20.8 feet in Fig. 12.4 suggests that another effect, in addition to soil softening, caused the loss of load transfer. The small peak load transfer of only about 0.2 tsf cannot be explained by a moisture content increase in the order of only 8 per cent. The sharp decrease in load transfer beyond the peak at the 20.8 foot level suggests that removal of vertical support from soil surrounding the bottom of the shaft, brought about by the downward displacement of the base, produced an effect analogous to that discussed in Chapter IV in relation to decrease of load transfer for shafts in sand. First, less relative movement between the soil and shaft is expected in the area of the base because of the general downward movement of the mass of soil around the base as the base is forced downward. Second, reduction in effective vertical pressure in the clay around the base due to base displacement can cause a reduction in the residual strength of the soil. [If soil near the base of a drilled shaft is even slightly compressible, Ellison (1968) has shown that tension zones can be produced in the soil around the base.] Such a mechanical base-side interference effect, in addition to soil softening, appeared to cause reduced load transfer near the base for S1T1.

S1T2. The ultimate capacity for S1T2, conducted about one hour after S1T1, was again 140 tons. Thus, no reduction in total load capacity occurred upon immediate reloading of Test Shaft No. 1, although the ultimate base capacity indicated by the bottomhole cell increased to 59 tons (compared to 52 tons for S1T1), implying a reduction in ultimate side capacity in comparison to S1T1. The total load-settlement curve was nearly identical to that obtained in S1T1. No load distribution data were

processed because of uncertainties in establishing drift corrections for the embedment gages.

S1T3. The ultimate capacity obtained in S1T3, conducted between 1600 and 1800 on December 10, 1968, 3 1/2 months after S1T1 and S1T2, was 135 tons. The total, base, and side load-settlement relationships, derived in a manner similar to that described for S1T1, are shown in Fig. 12.7. The bottomhole cell was inoperative at the time of testing, so the base load was estimated by extrapolating the load distribution curves defined by the Mustran and embedment systems to the depth of the base. The maximum load so obtained (assuming no residual load present in the shaft at the beginning of the test) was 60 tons, implying a corresponding side resistance of 75 tons, or an α_{avg} of 0.34. No load shedding was in evidence in S1T3.

The load-settlement curves are initially "stiffer" than the corresponding curves for S1T1. Part of this effect may be due to the larger applied load increment used in S1T3. No pronounced knee appears in the side load-settlement curve, but full side shear was developed at a mean settlement of 0.25 inches. The total rebound was 0.12 inches.

Load distribution curves for various values of applied load, and the measured loads from which they were obtained, are shown in Fig. 12.8. The same gages and same in-shaft calibration procedure were used for subsurface load measurement as in S1T1, except that the bottomhole cell and the level of embedment bridges at 13 feet drifted excessively under continuous no-load powering prior to S1T3, and were excluded from consideration. Fourth degree polynomials were used in fitting the load distribution data for S1T3. The same general shape is evident in S1T3 as in

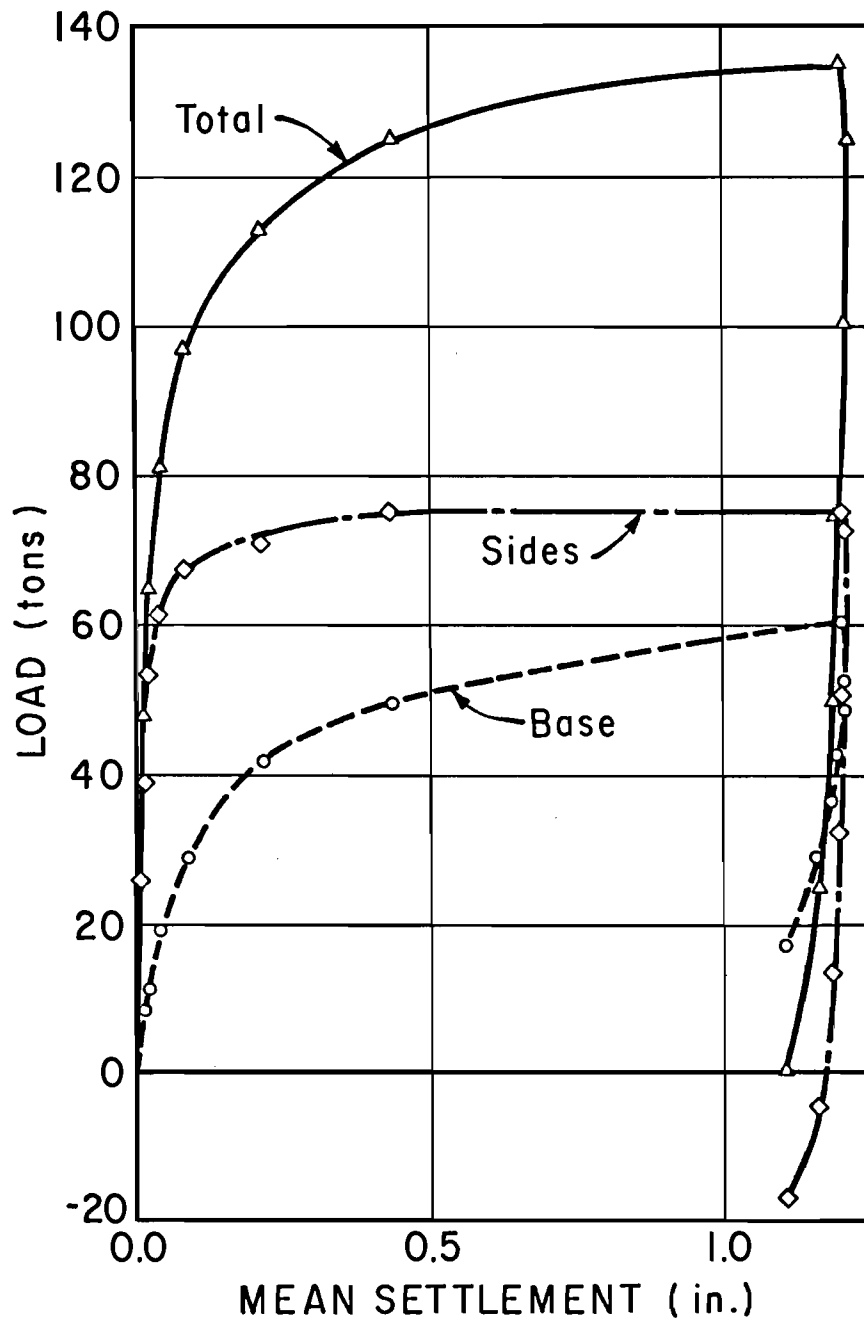


Fig. 12.7. Load-Settlement Curves for S1T3

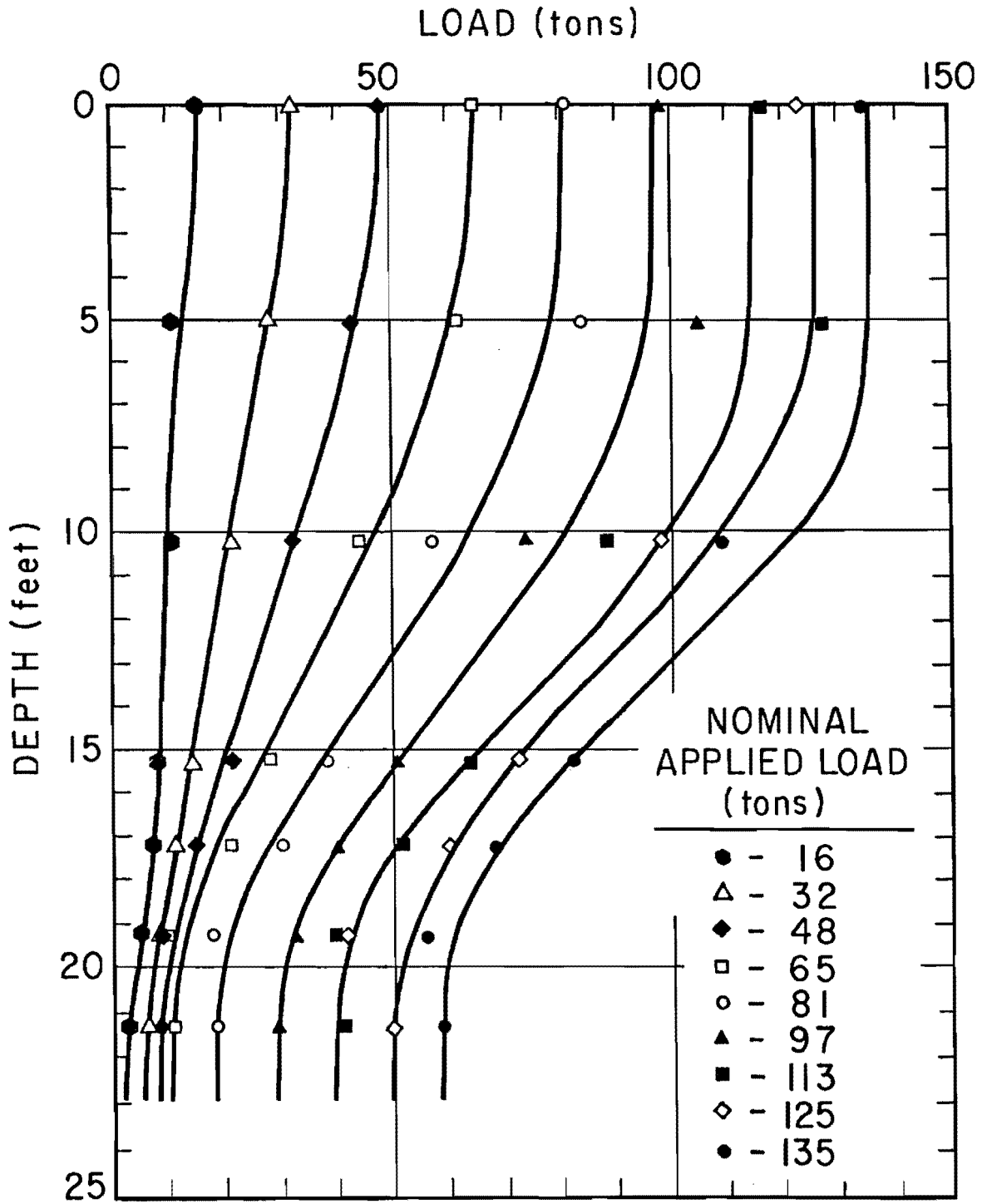


Fig. 12.8. Load Distribution Curves for S1T3

SlT1, although less load transfer was measured near the top and bottom of the shaft in SlT3.

A family of load transfer curves is shown in Fig. 12.9. Again, shear failure appeared to progress from the top and bottom toward the center of the shaft. The soil near the base (20.8 feet) was quite "brittle" in its reaction to load, although some load transfer was measured, indicating some redevelopment of adhesion between the soil and shaft at that depth since SlT1.

Figures 12.10a and b show the variation of developed shear stress and α_z , respectively, with depth. The maximum shear stress development occurred at a lower level in SlT3 than in SlT1, and the peak α_z was slightly greater in SlT3. The surface soil was quite dry when SlT3 was conducted and had shrunk away from the top of the shaft; hence, very little load transfer was developed in the upper five feet of the shaft.

The load distribution behavior of Test Shaft No. 1 during reloading is compared with that during virgin loading at two values of nominal applied load (50 tons and 110 tons) in Fig. 12.11, which illustrates the reduced load transfer in reloading. Load transfer curves for SlT1 and SlT3 for depths of 8.3 feet and 16.7 feet are superimposed to compare the development of load transfer at these levels in the two tests in Figs. 12.12a and b, respectively. The reason for the increased indicated maximum load transfer at the 16.7-foot level in SlT3 is not clear. However, the small increase may have been caused by a small collar in the shaft, discovered just above the 16.7-foot level during excavation of the shaft. The collar may have produced a wedge effect in the silty clay around the 15-foot level upon reloading, thereby causing an increase in load transfer just below the midheight of the shaft.

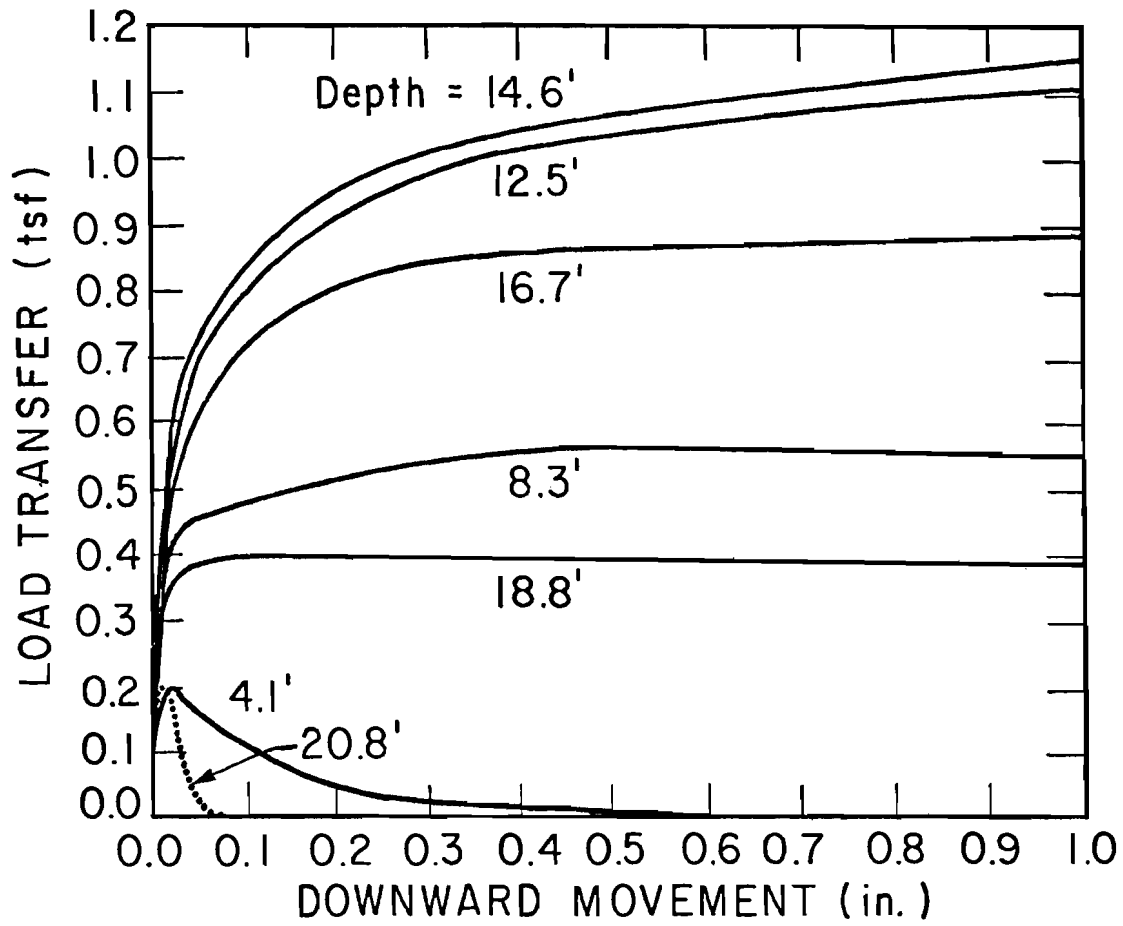


Fig. 12.9. Load Transfer Curves for S1T3

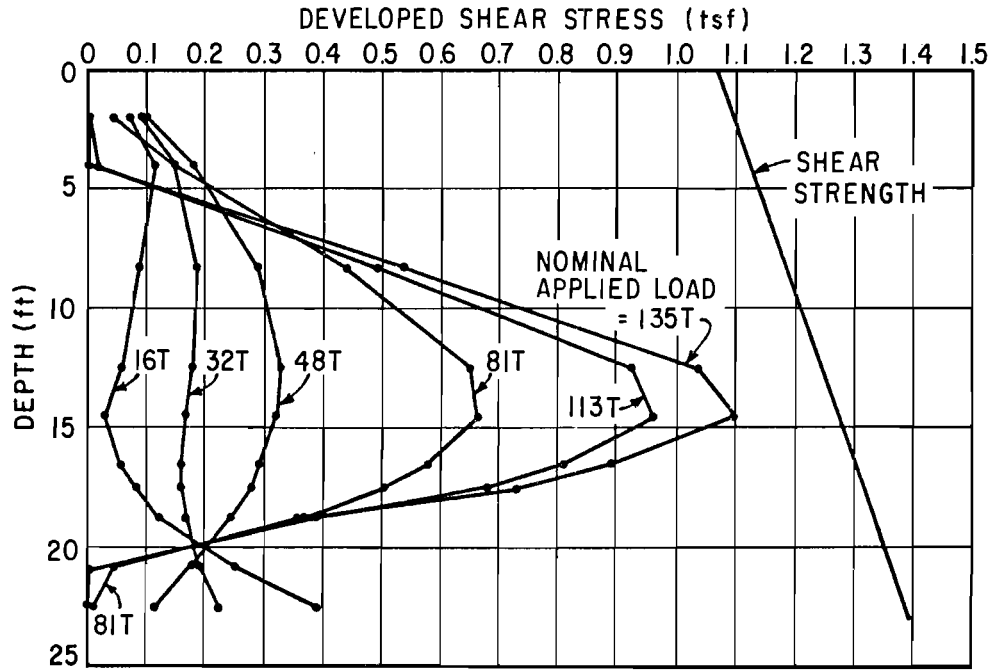


Fig. 12.10a. Distribution of Developed Shear Stresses for S1T3

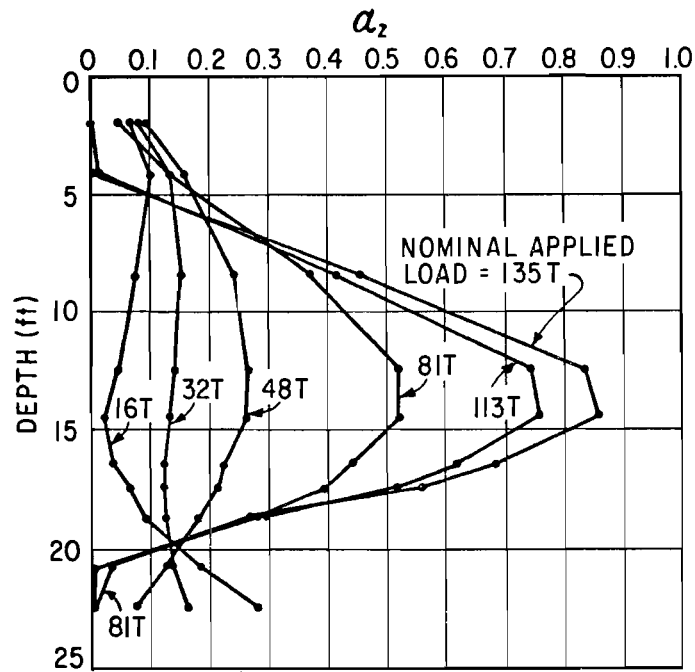


Fig. 12.10b. α_z Versus Depth for S1T3

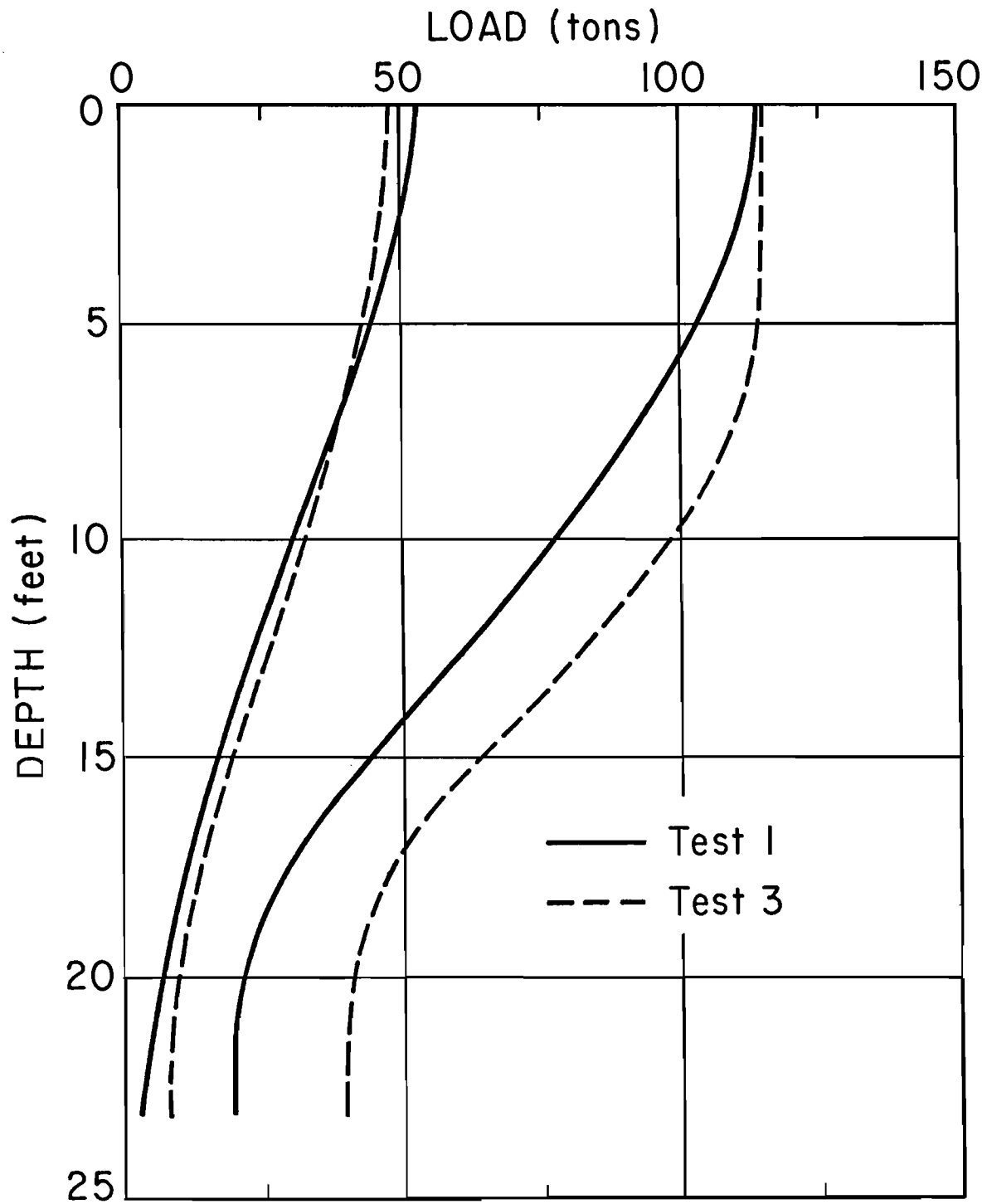


Fig. 12.11. Comparisons of Load Distribution for S1T1 and S1T3

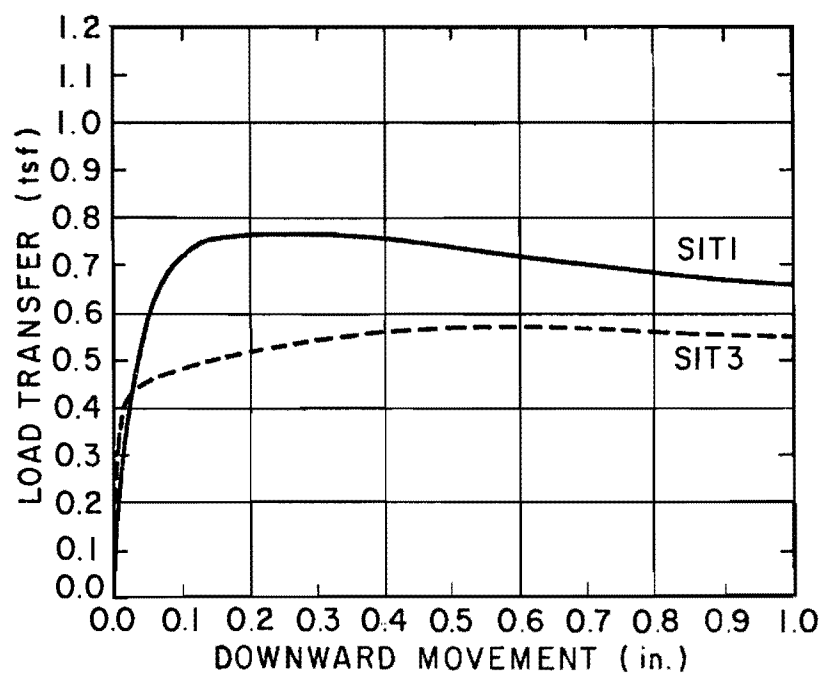


Fig. 12.12a. Comparison of Load Transfer Behavior at a Depth of 8.3 Feet for SIT1 and SIT3

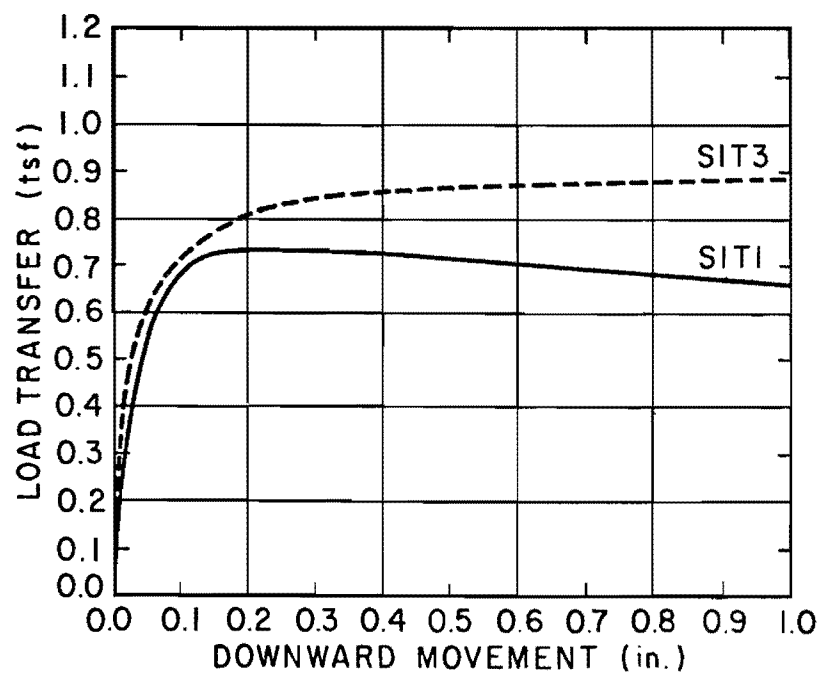


Fig. 12.12b. Comparison of Load Transfer Behavior at a Depth of 16.7 Feet for SIT1 and SIT3

In summary, the overall effect of reloading was to reduce the peak average shear strength reduction factor, α_{avg} , from 0.44 obtained initially to 0.34 in the third test (corresponding to a total gross downward displacement of about 2.5 inches), to increase the base capacity from 52 tons to 60 tons, and to cause the load transfer and base load-settlement curves to have a higher initial slope.

Test Shaft No. 2

S2T1. The first load test on Test Shaft No. 2 was conducted between 1600 and 1800 on March 4, 1969. The ultimate total capacity was 537 tons, while the peak base and side reactions were 447 tons and 92 tons, respectively. Load-mean settlement (average of settlement at butt and top of bell) relationships are given in Fig. 12.13. Side reaction was again dominant for lower loads, but the base reaction became dominant above an applied load of 180 tons. Peak side reaction was essentially realized at a displacement of 0.15 inches, while a displacement of 2.85 inches was required for full mobilization of base resistance. A rebound of 0.77 inches occurred after removing the load.

Individual Mustran cell response curves for the loading phase of the test are shown in Appendix K. The response curves indicate some eccentricity in the applied load, which was provided by tandem jacks. Once side failure began to occur, the individual response curves at each level began to show considerable divergence, indicating that the bell was picking up load eccentrically. From the reactions of the level of cells at 17 feet, 2 inches, the resultant base reaction force apparently shifted from the center of the base of the bell toward the Grid North Kern point as the bell picked up significant load.

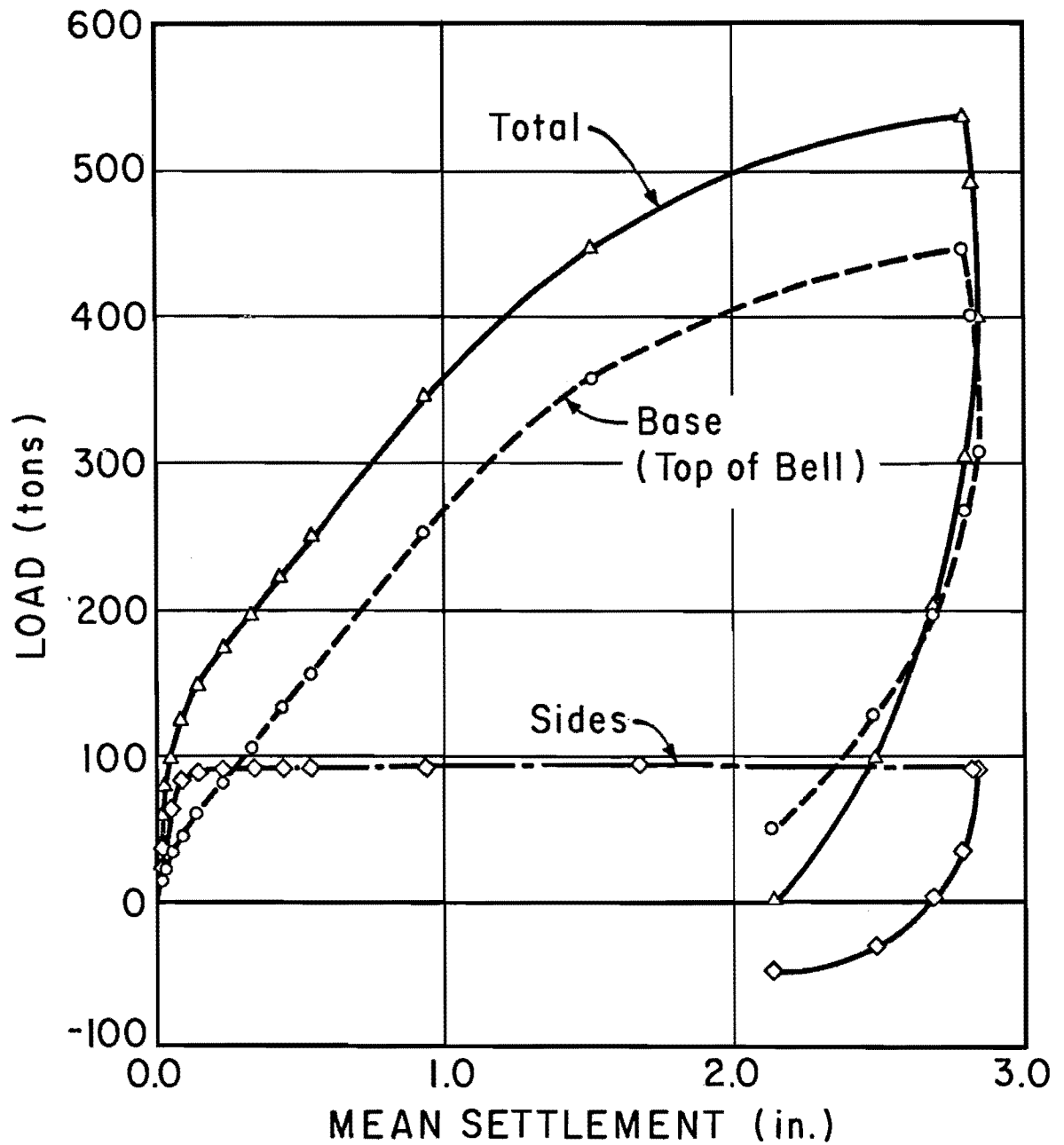


Fig. 12.13. Load-Settlement Curves for S2T1

Because of the large difference between side and total capacities, significant segments of the response curves were generated under essentially constant side shear, between applied loads of about 250 and 450 tons, as can be observed in Fig. K.5. Since the various curves are almost perfectly linear in that range, it would appear that the exact increment of applied load was reaching each level of cells. In other words, a nearly constant shearing resistance was achieved along the sides with neither load shedding nor load transfer increase apparently occurring beyond a displacement of 0.3 inches. Since the slope of the average response curves differed somewhat, it appeared that the top-level calibration procedure might not give the most accurate load distribution information. The discrepancies in response are thought to be due principally to the practice of placing three cells at a level, but with the cells on a given side of the shaft being staggered in plan location, and to the large bending moment that developed as the bell picked up load. The high moment evidently caused the cells at one level to respond slightly differently than those at another level, at which the cells were oriented differently in plan. Furthermore, stress concentrations in the stem just above the bell caused by the abrupt change in cross section could have influenced the response of the bottom level of Mustran cells. For these reasons, the slopes of the average response curves between applied loads of 250 and 450 tons (Fig. K.5) were taken to be the direct calibration constants for the respective levels. That is, load in the shaft at each level was obtained for all values of applied load by multiplying the cell output by the slope of the appropriate response curve, between 250 and 450 tons, from Fig. K.5.

Load distribution relationships obtained from a top-level calibration (standard method) and individual-level calibration are compared in Fig. 12.14 for a third degree polynomial least-squares fit for two values of applied load. The two methods give reasonably consistent results at low loads (curves on left), but they diverge somewhat, particularly near the bell, at higher loads (curves on right). It is seen that the fitting procedure using least-squares actually yields a reverse curve near the bell in the top-level calibration method, which is a physical impossibility.

Referring again to the load-settlement relationships (Fig. 12.13), the base loads were obtained by extrapolating the load-distribution curves determined from the individual level calibration procedure to a depth of 18.5 feet (top of the bell), and the corresponding side loads were then computed by subtraction. The loads at the top and base of the bell were assumed to be equal. The base load-settlement relationship was linear up to a base load of about 250 tons, except for a slight initial nonlinear portion thought to be caused by the breakdown of adhesion between the top of the concrete bell and the soil and by side shear on the six-inch cylindrical section at the bottom of the bell. Once the bell was displaced downward slightly (0.1 to 0.2 inches), the nonlinearity disappeared until the soil beneath the base began to fail. The side load-settlement relationship was essentially linear up to a load of about two-thirds of its ultimate value.

Load distribution relationships are shown in Fig. 12.15. Third degree least-squares polynomials were used, since they appeared to provide the best fit. Only the Mustran system was used to define these relationships, although loads indicated by the embedment bridges at the 4- and 14-foot

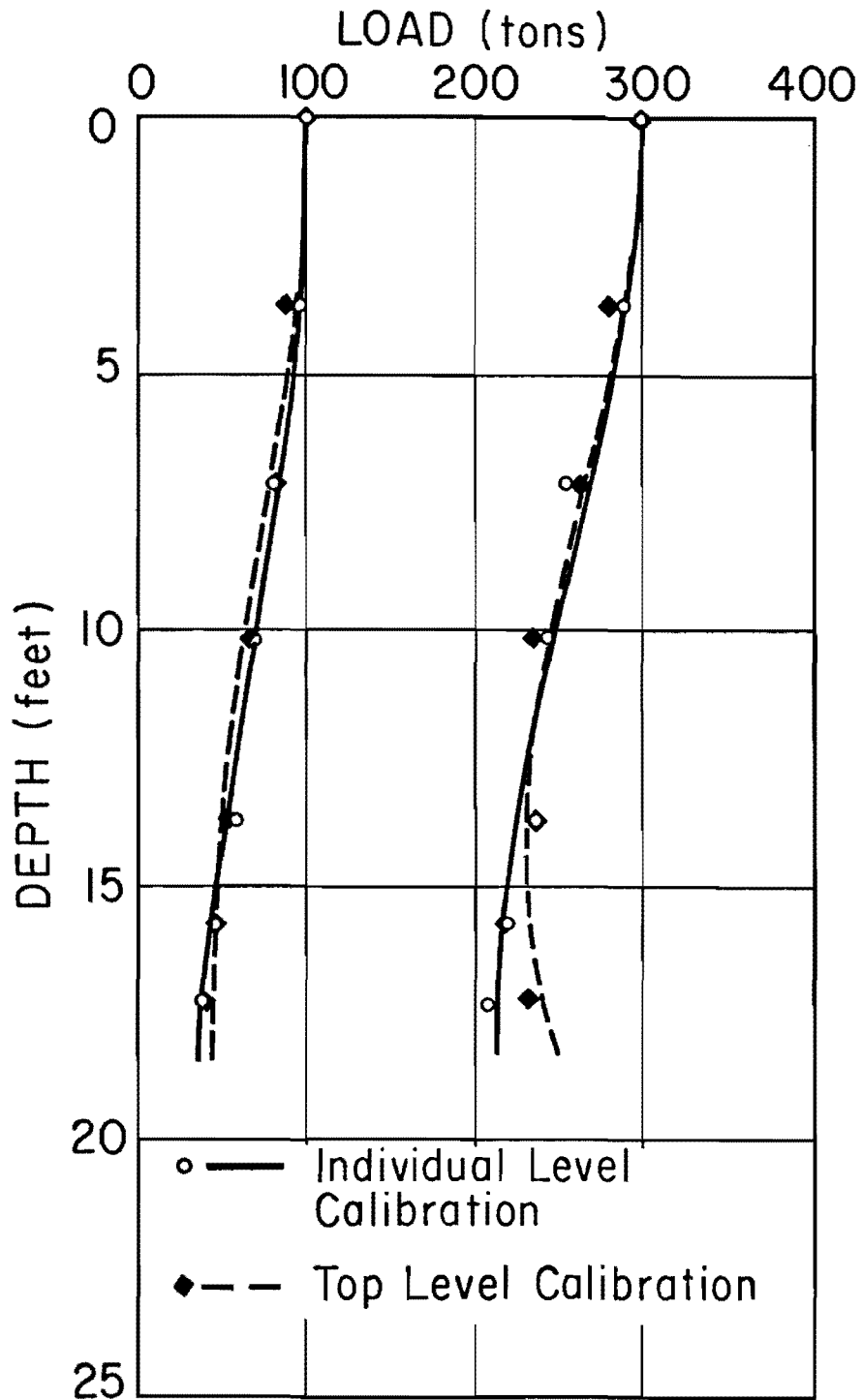


Fig. 12.14. Comparisons of Computed Load Distribution for S2T1 Using Both Top-Level and Individual-Level Calibration

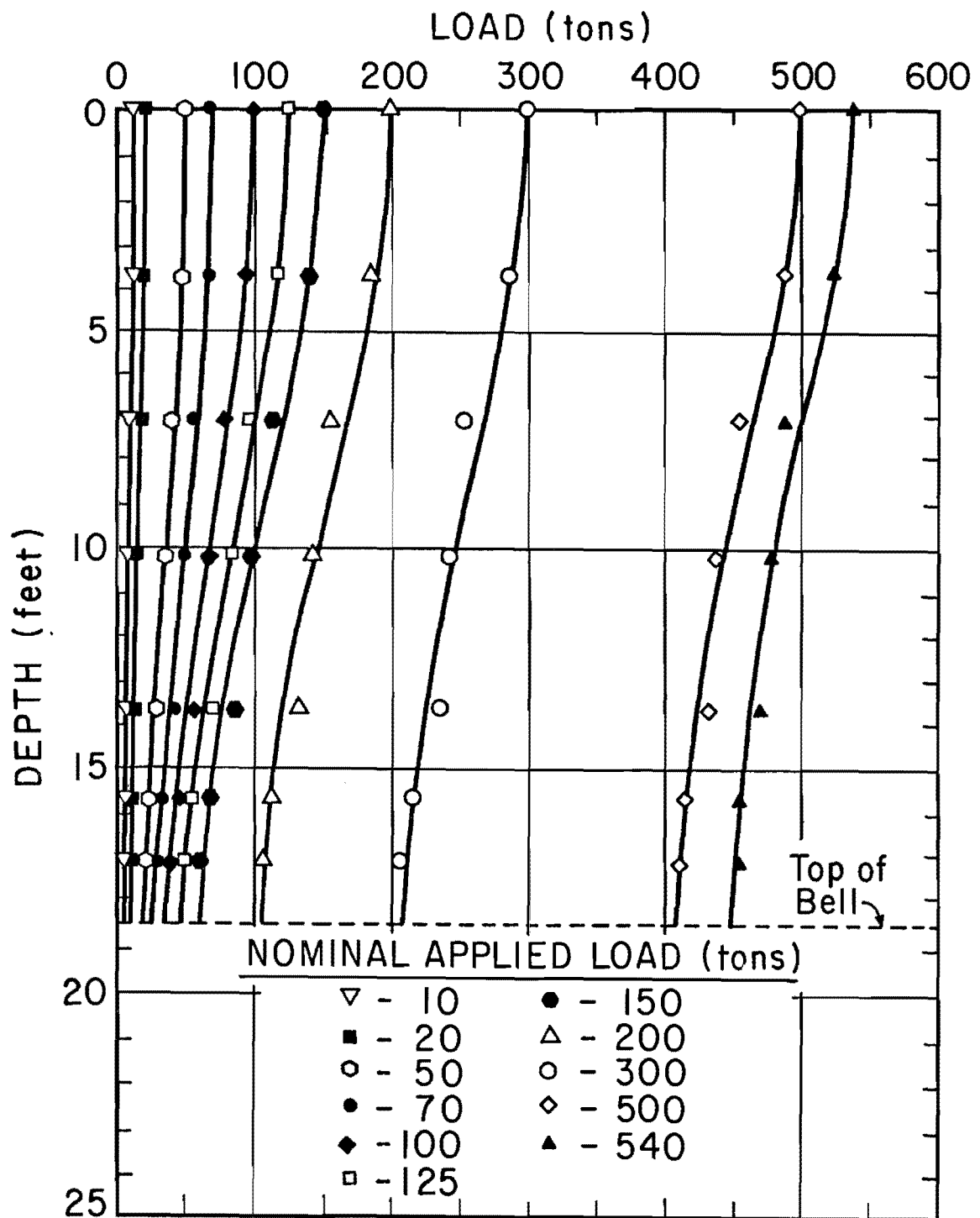


Fig. 12.15. Load Distribution Curves for S2T1

levels differed from the average of those indicated by the Mustran cells at the same levels by no more than seven per cent after appropriate drift corrections were made. Values of measured load are shown in Fig. 12.15. The scatter again increased markedly after side shear failure occurred.

Load transfer curves for S2T1 are shown in Fig. 12.16. As in the tests on Shaft No. 1, they are somewhat influenced by the exact curve-fitting procedure for obtaining load distribution relationships, but they are thought to be a reasonably faithful representation of the true load transfer relationships.

Load transfer was again greatest near the midheight of the stem, as illustrated in Figs. 12.17a and b, which give shear stress and α_z variations with depth. The peak value of α_z was about 0.8 at a depth of 8.3 feet, but α_z decreased sharply in value below 8.3 feet at peak load transfer (250 tons applied load in Figs. 12.17a and b) to zero just above the base.

The reduction in load transfer capability below the midheight of the stem appears to be caused more by mechanical interference by the base than by excess softening of the borehole walls near the bottom of the stem, particularly since the borehole was completely dry at the time concrete was placed.

The average peak shear strength reduction factor for S2T1 was 0.53. The bearing capacity factor N_c was 8.9 with respect to the average shear strength for a distance of two base diameters beneath the base.

For reasons mentioned in Chapter IX, the results of the telltales were quantitatively invalid. The pair of telltales located in the bell, however, demonstrated quite vividly the eccentric failure that occurred

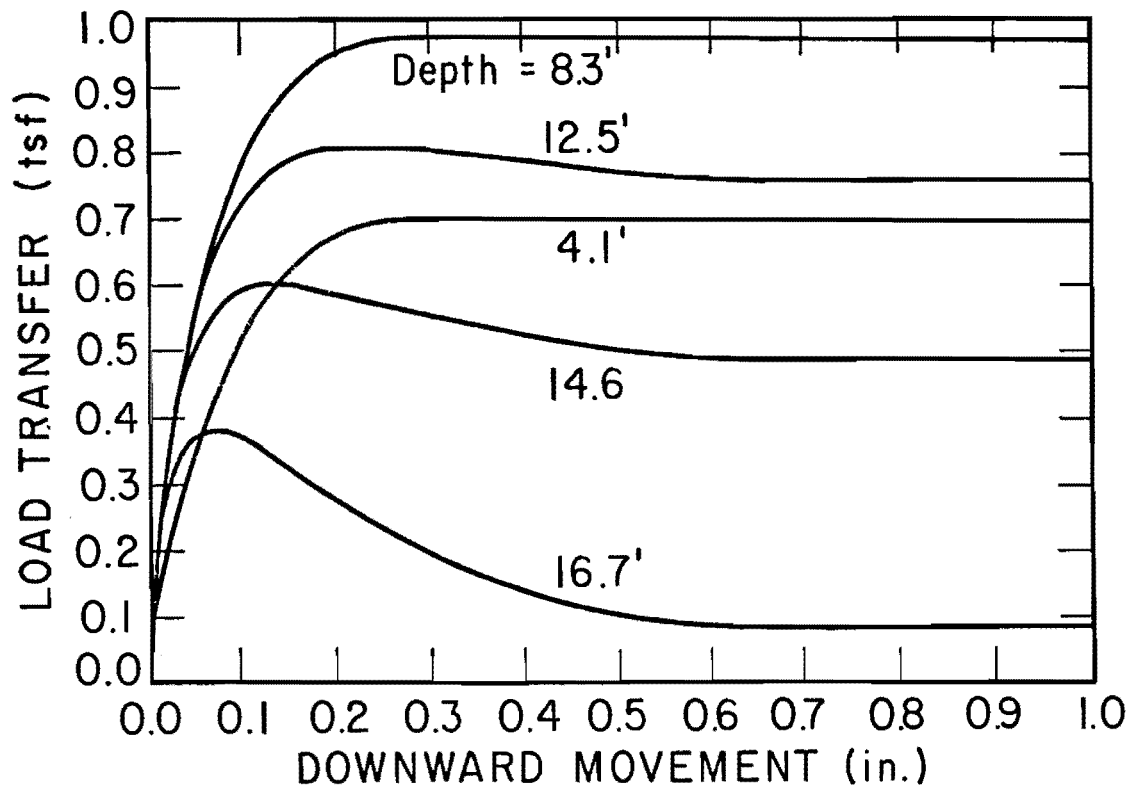


Fig. 12.16. Load Transfer Curves for S2T1

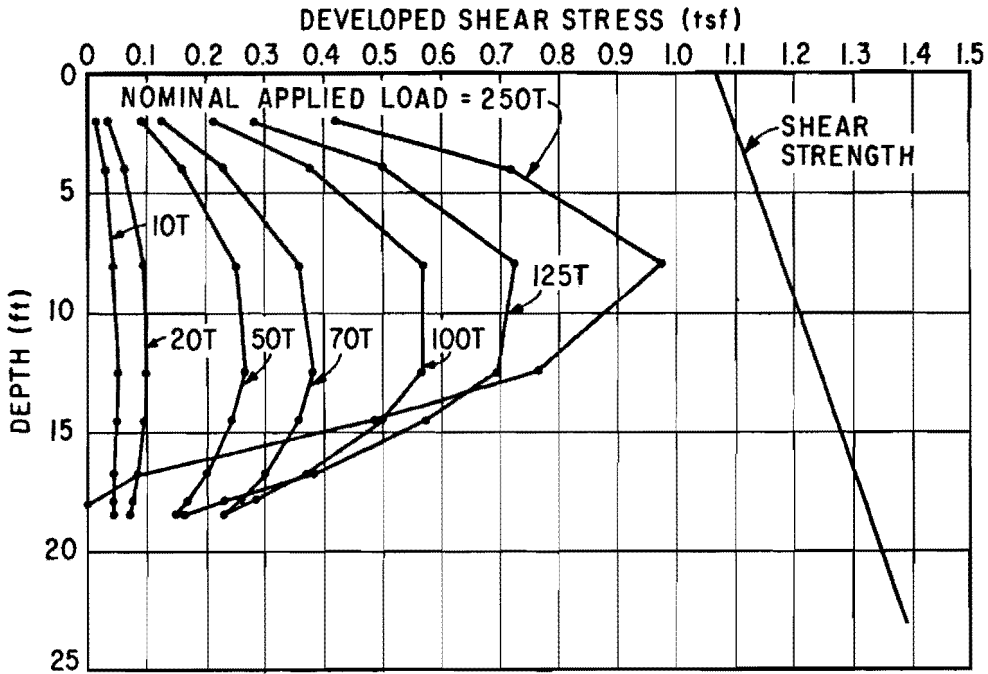


Fig. 12.17a. Distribution of Developed Shear Stresses for S2T1

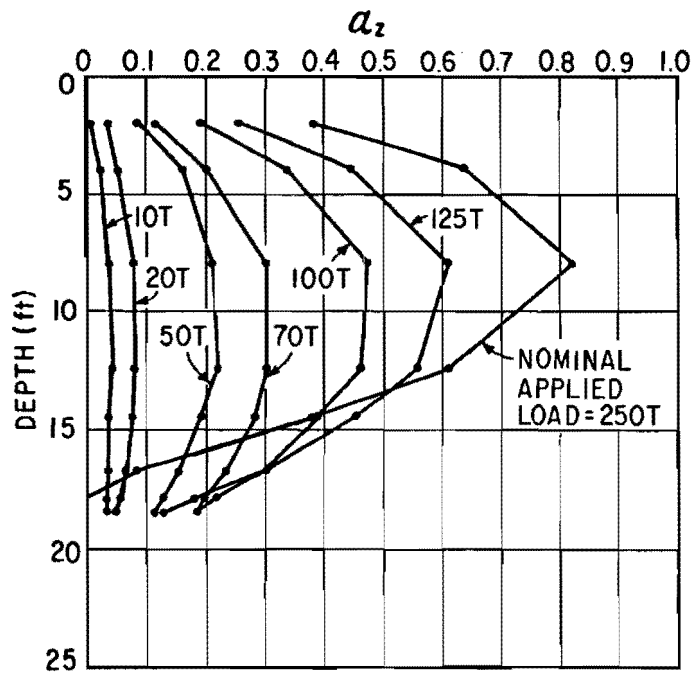


Fig. 12.17b. α_z Versus Depth for S2T1

(Fig. 12.18). Qualitatively, the telltales responded much like the electrical gages: initial linear response, increased sensitivity between 100 and 200 tons as the sides failed, and, finally, nearly linear response as constantly increasing elastic compression occurred in the stem and bell. The lower level of telltales (placed near the bottom of the bell) indicated a total stem and bell compression (below ground) of about 0.048 inches at 500 tons applied load, while a value of 0.047 inches was inferred in the stem alone at the same value of applied load by the electrical Mustran cells. (The value of 0.056 shown in Fig. 12.18 includes compression of the protruding portion of the shaft.)

Load distribution was computed from telltale data by plotting compression in the shaft between the ground level and each telltale level versus depth and passing a smooth curve through the points so defined. The compression at a given level was obtained by taking the average reading of the pair of telltales at that level. This procedure is illustrated in Fig. 12.19. Since the load at the surface is known, the slope of the telltale compression curve is also known; hence, the top slope was taken as a boundary condition in establishing the best compression curve for each value of applied load. The telltale data are uncorrected for temperature changes, which were only one or two degrees during the period of the test. Values of load present at various depths were then obtained from the slopes of the compression curves and elastic properties of the stem.

Shaft compression indicated by telltales and by electrical gages are compared in Fig. 12.20, and corresponding load distribution curves are shown in Fig. 12.21. Load distribution was not defined very accurately

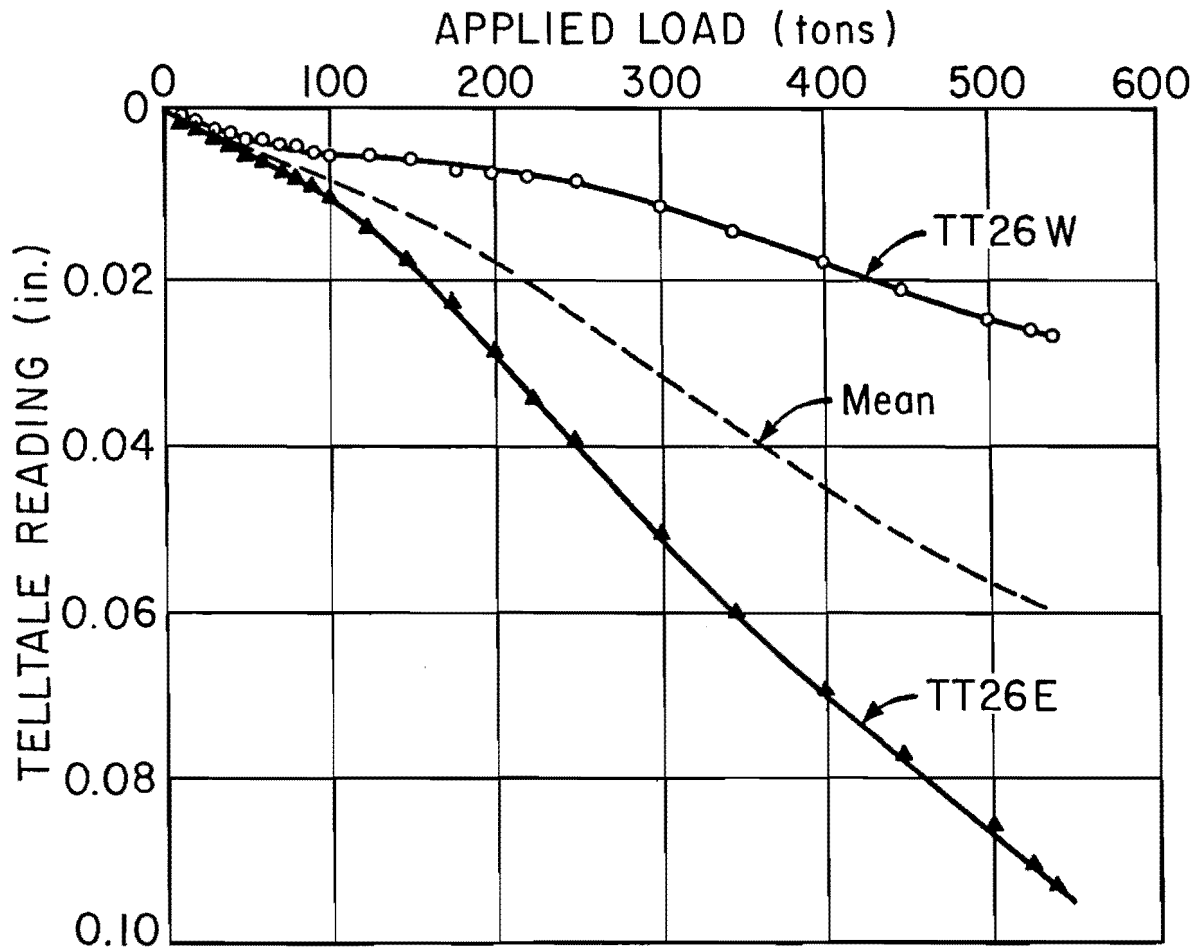


Fig. 12.18. Telltale Reading Versus Applied Load for TT26E and TT26W, S2T1

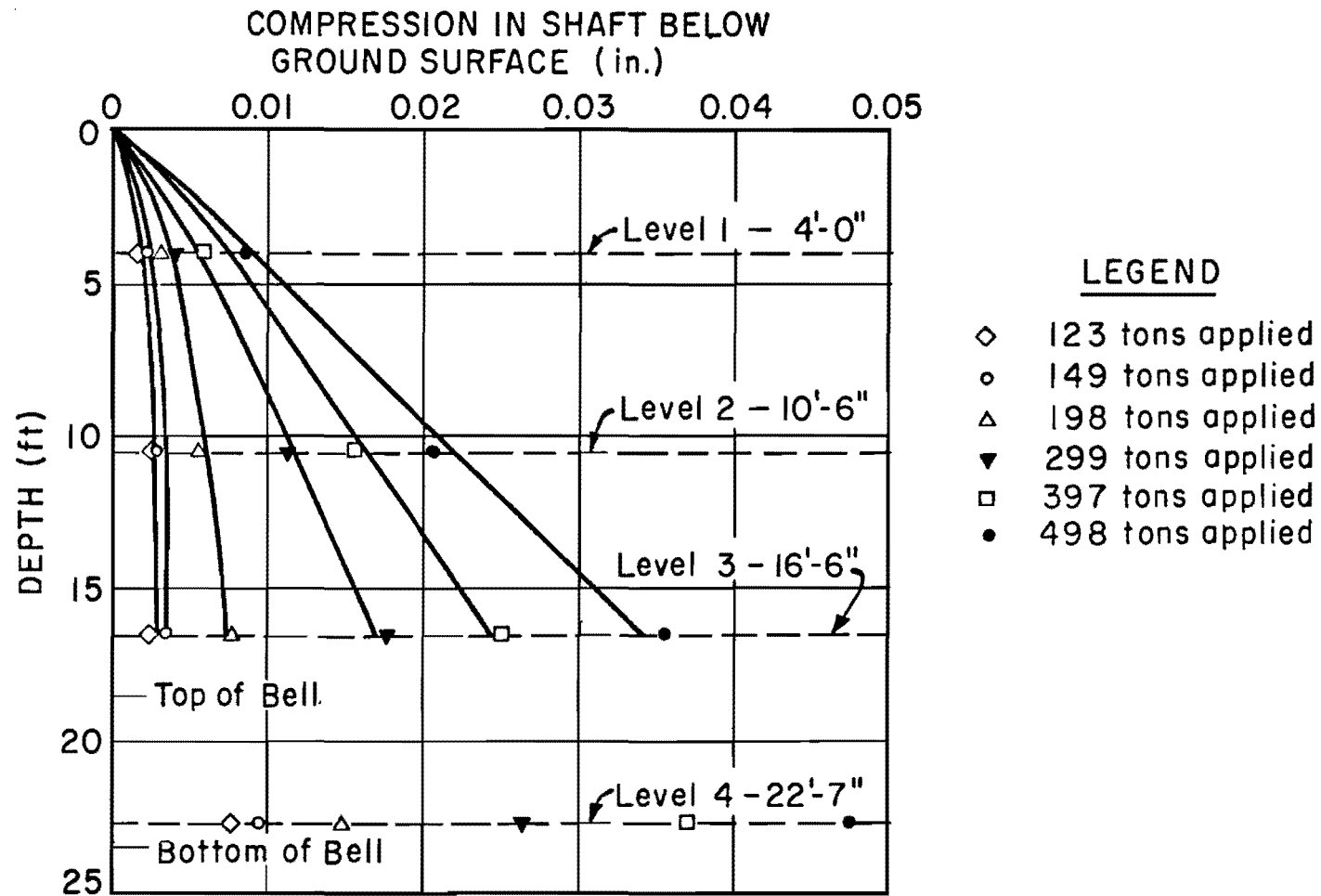


Fig. 12.19. Compression in Shaft as Indicated by Telltales, S2T1

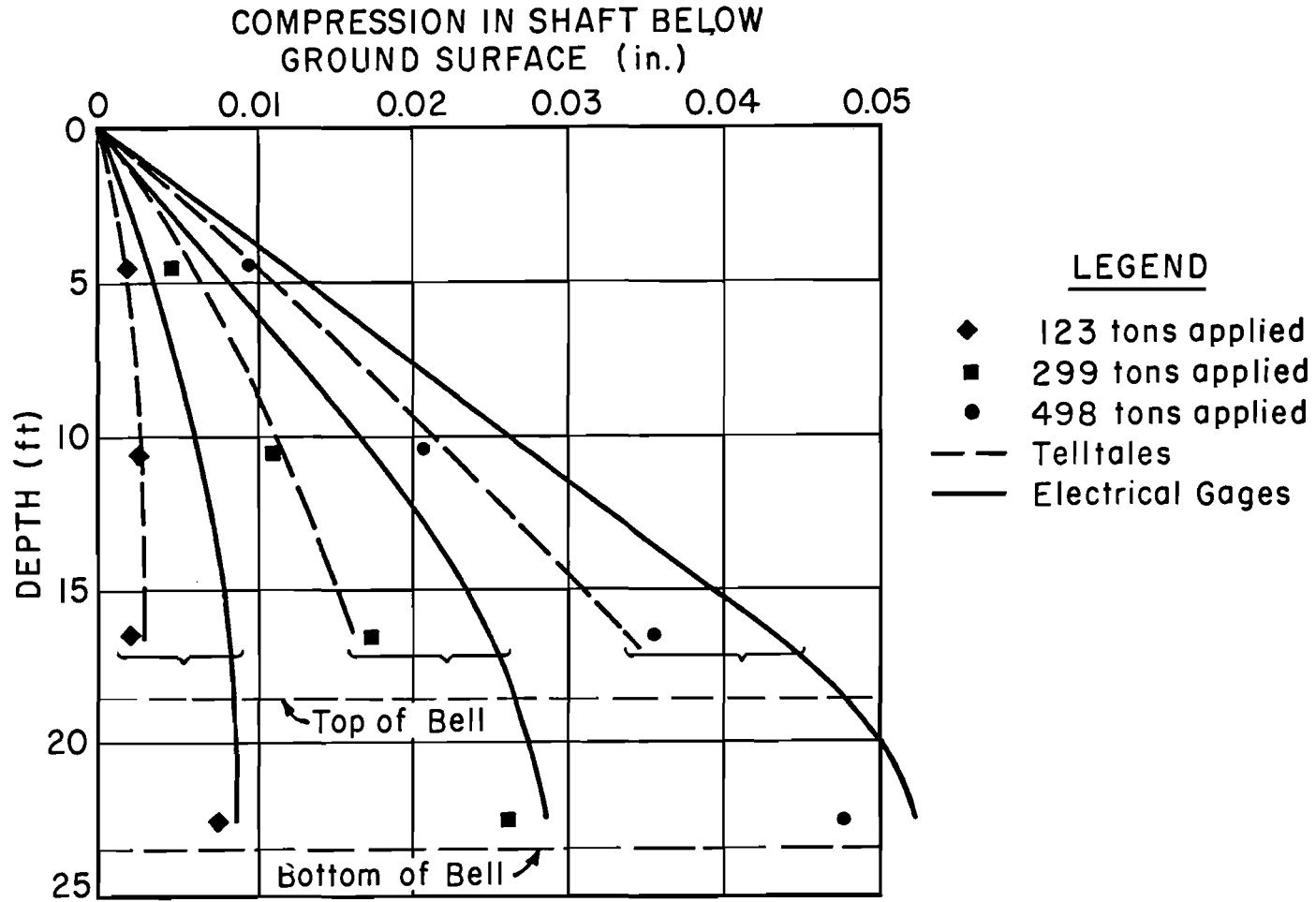


Fig. 12.20. Comparison of Compression in Shaft Indicated by Telltales and by Electrical Instrumentation, S2T1

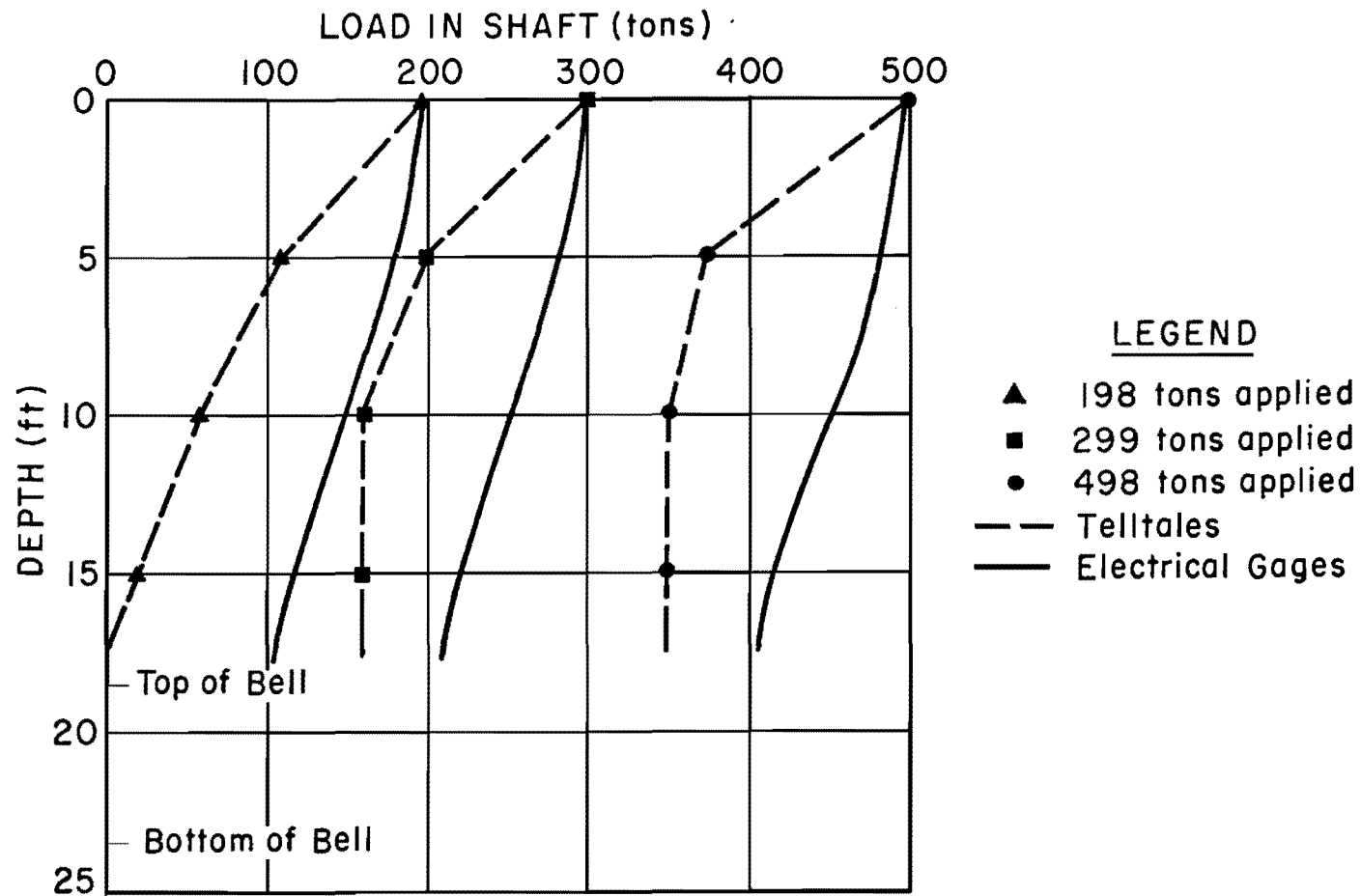


Fig. 12.21. Comparison of Load Distribution Indicated by Telltales and by Electrical Instrumentation, S2T1

by the telltales. Because of binding, the telltales indicated a greater degree of load transfer than is believed to have actually occurred.

As in S1T1, considerable compressive load remained in the shaft after all butt load was removed. The distribution of residual load is given in Fig. 12.22. A residual compressive load of approximately 50 tons was indicated at the top of the bell.

One important result of S2T1 is the fact that Test Shaft No. 2 required a large gross settlement to mobilize a resistance equal to a reasonable working load. For instance, for an applied working load of 215 tons (factor of safety of 2.5 with respect to plunging failure), the gross settlement was 0.4 inches, since much of the resistance appeared in end bearing. A gross settlement of only about 0.15 inches was required to mobilize full side shear. Hence, at the working load value defined above, the sides would be in a "failed" condition.

S2T2. The second load test on Test Shaft No. 2 was conducted between 1500 and 1700 on June 18, 1969, 3 1/2 months after the initial test of Shaft No. 2. The ultimate total capacity was 521 tons. Load-settlement relationships are given in Fig. 12.23. For purpose of calculating developed base and side loads, no residual loads were assumed to exist in the shaft at the time of S2T2. Base and side loads were determined as described for S2T1. As in S2T1, no load transfer was assumed to occur along the roof and sides of the bell; thus, the load at the top of the bell was assumed to be that present at the base.

Considerably less total side load was developed in S2T2 than in S2T1 (43 tons versus 92 tons), implying that the large displacement of the shaft relative to the soil produced in S2T1 had significantly reduced

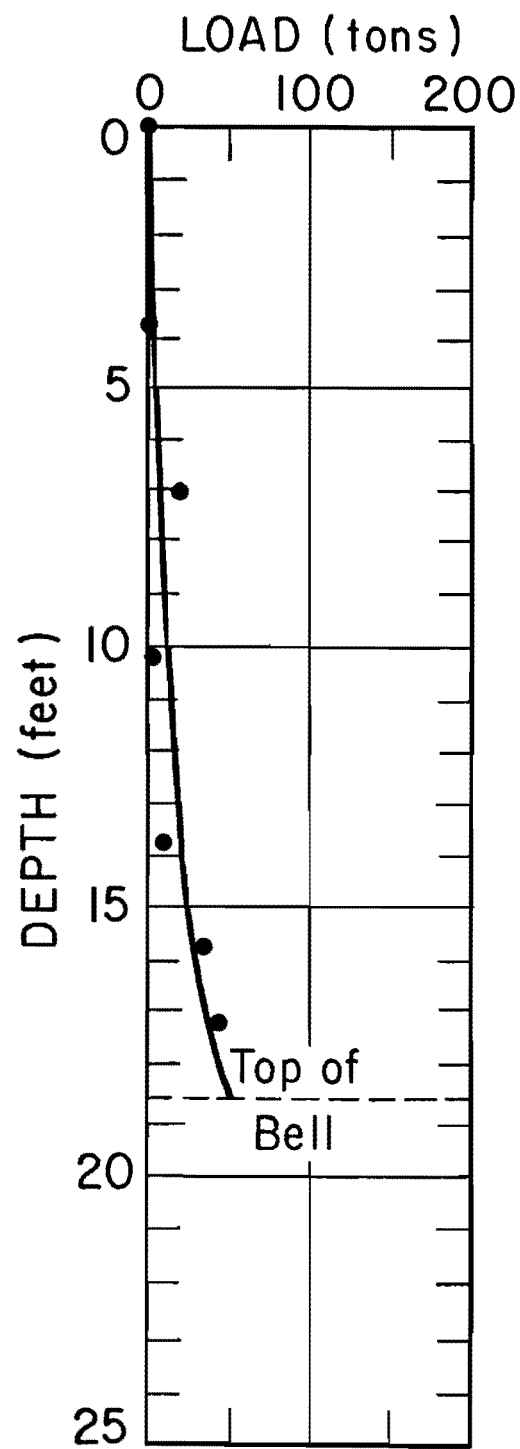


Fig. 12.22. Distribution of Load in Shaft Immediately After S2T1

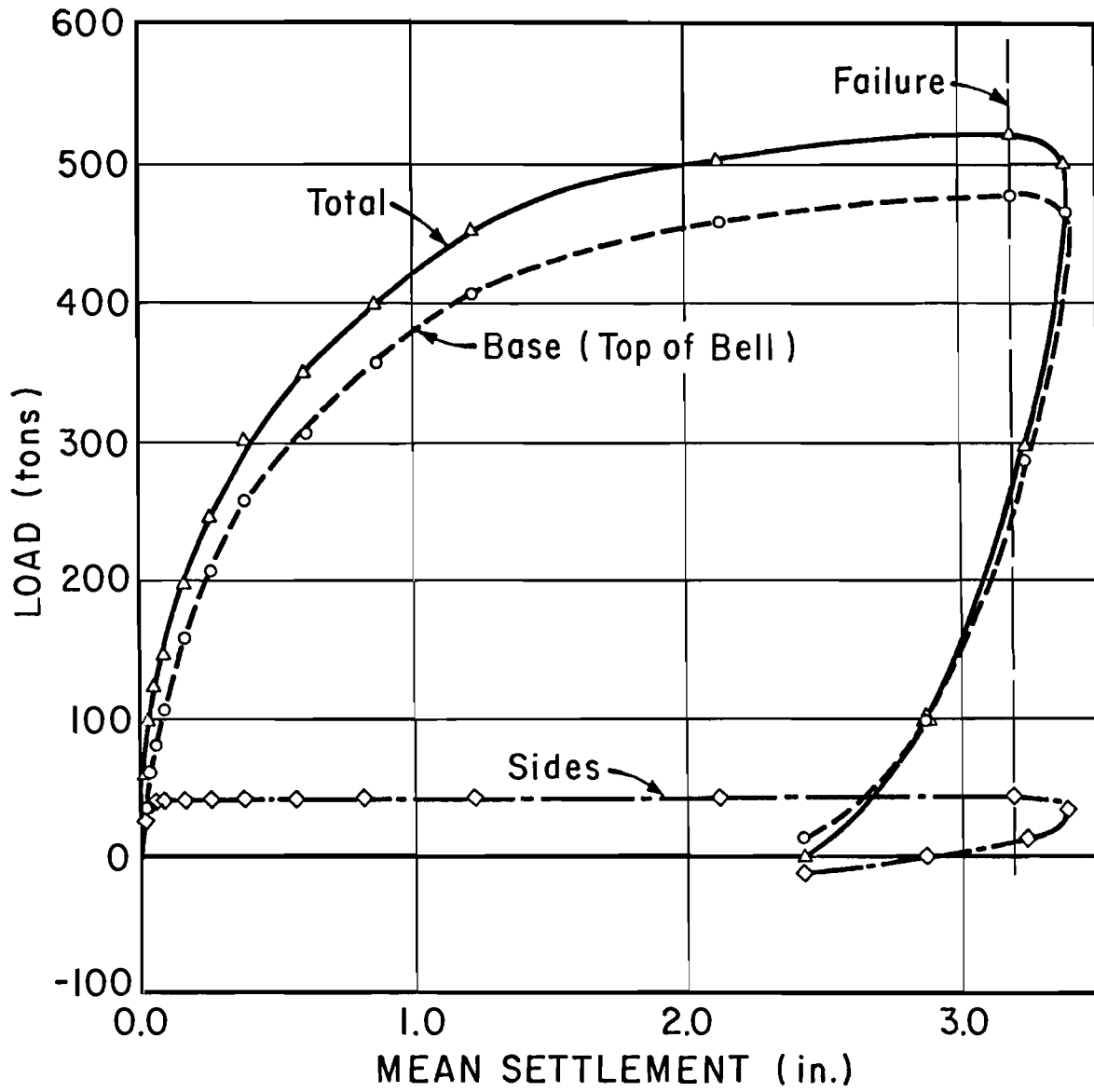


Fig. 12.23. Load-Settlement Curves for S2T2

the available side resistance. Maximum side resistance was developed at a gross settlement of only about 0.10 inches, compared with about 0.15 inches in S2T1. Maximum base load of 478 tons was developed at a displacement of about 3.1 inches (refer to beginning of S2T2; approximately 5.2 inches total settlement since beginning of S2T1). Both side and base load-settlement relationships exhibited stiffer behavior under reloading in S2T2 than occurred in the initial loading to failure in S2T1.

Several possible causes for the reduction of load transfer capability between S2T1 and S2T2 exist. First, the added displacement produced in S2T2 may have caused the shear strength of the soil surrounding the stem to approach a residual value, which was not achieved in S2T1. Second, the presence of an existing upward-directed load from the base remaining after S2T1 induced long-term shear stresses in the soil around the stem, which may have produced structural changes in the soil. Third, in conjunction with the second point, the residual shear stresses against the soil surrounding the stem following S2T1 could have produced an inward migration of porewater if the soil at the site had a negative A-parameter. [The A-parameter for the soil at the test site was not determined, but the study conducted by Al-Layla (1970) indicates that Beaumont Clay does not have a negative A-parameter, thereby inferring that the third possibility is a remote one.] Fourth, the shearing disturbance caused by S2T1 could have opened fissures in the soil around the stem, allowing groundwater to migrate toward the walls of the stem and further soften the supporting soil. Fifth, the possibility exists that a cavity was temporarily created above the roof of the bell after S2T1. With time, the soil could have crept downward to fill the cavity, possibly causing

fissures to open in the soil for several feet above the bell, consequently weakening the soil along the sides of the stem. Sixth, the test site was much drier for S2T2 than for S2T1. Therefore, adhesion between the soil and shaft may not have been as good in S2T2 in the top few feet of the stem.

It was not possible to ascertain which of the above possibilities caused the loss of load transfer, or whether other factors may have been active. A rather complex combination of these effects is, however, the most likely explanation.

The load distribution relationships, again obtained with a third degree least-squares polynomial, are shown in Fig. 12.24. Values of load in the shaft were calculated using the individual level technique explained for S2T1.

Load transfer curves at several levels are given in Fig. 12.25. The maximum load transfer of 0.57 tsf was developed at a depth of 8.3 feet. As in S2T1, a marked decrease in load transfer was observed below the 8.3-foot level. No load transfer whatever was developed in the bottom five feet of the stem beyond a displacement of 0.25 inches.

Variations of developed shear stress and α_z at several values of applied load are presented in Figs. 12.26a and b, respectively. The curves for 250 tons represent both "peak" and "ultimate" relationships. Load shedding occurred in the bottom five feet of the stem, as evidenced by the reduction in developed shear stress in the bottom part of the shaft above an applied load of 70 tons. Such load transfer reduction is again thought to be caused by mechanical interference from the base, such as

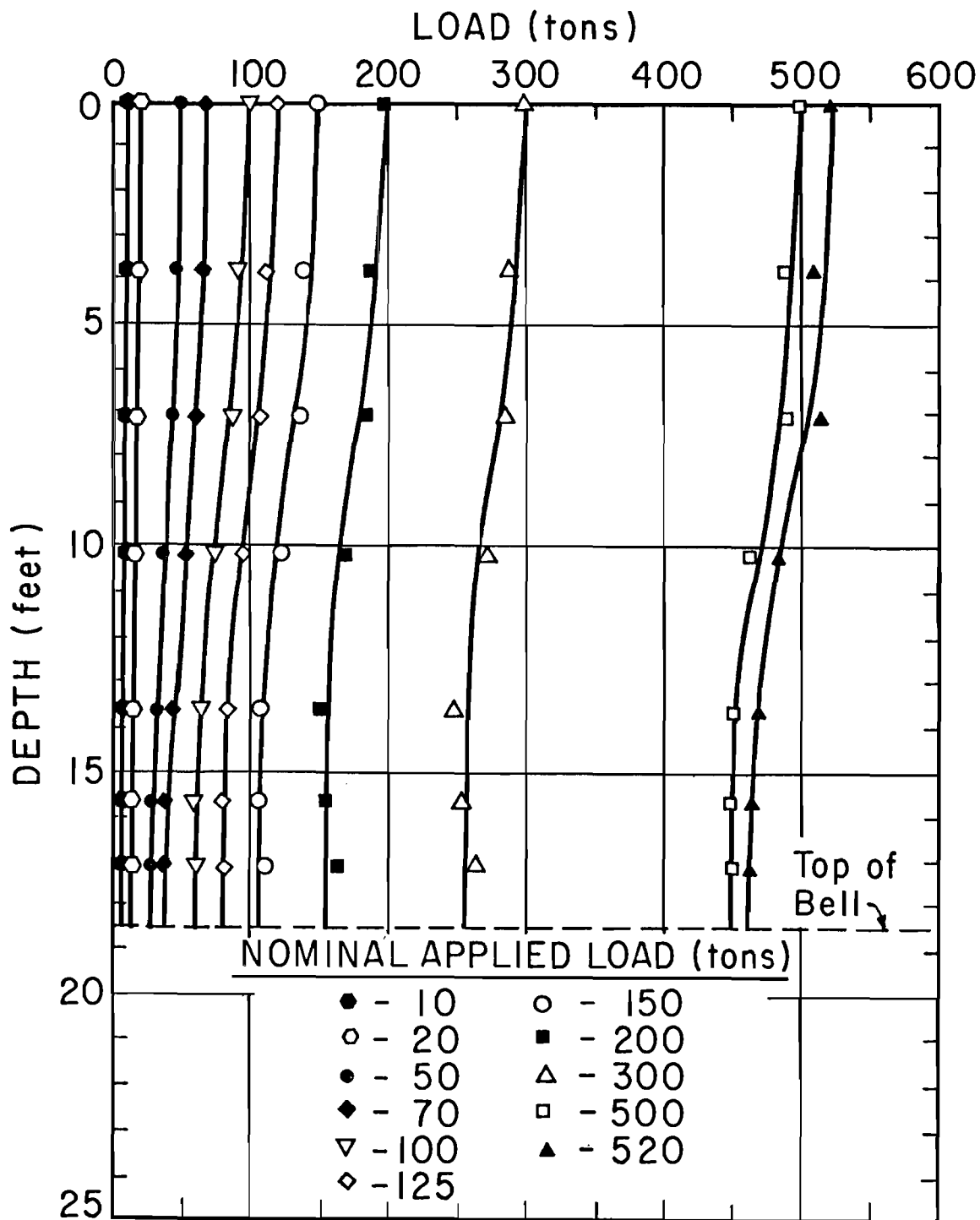


Fig. 12.24. Load Distribution Curves for S2T2

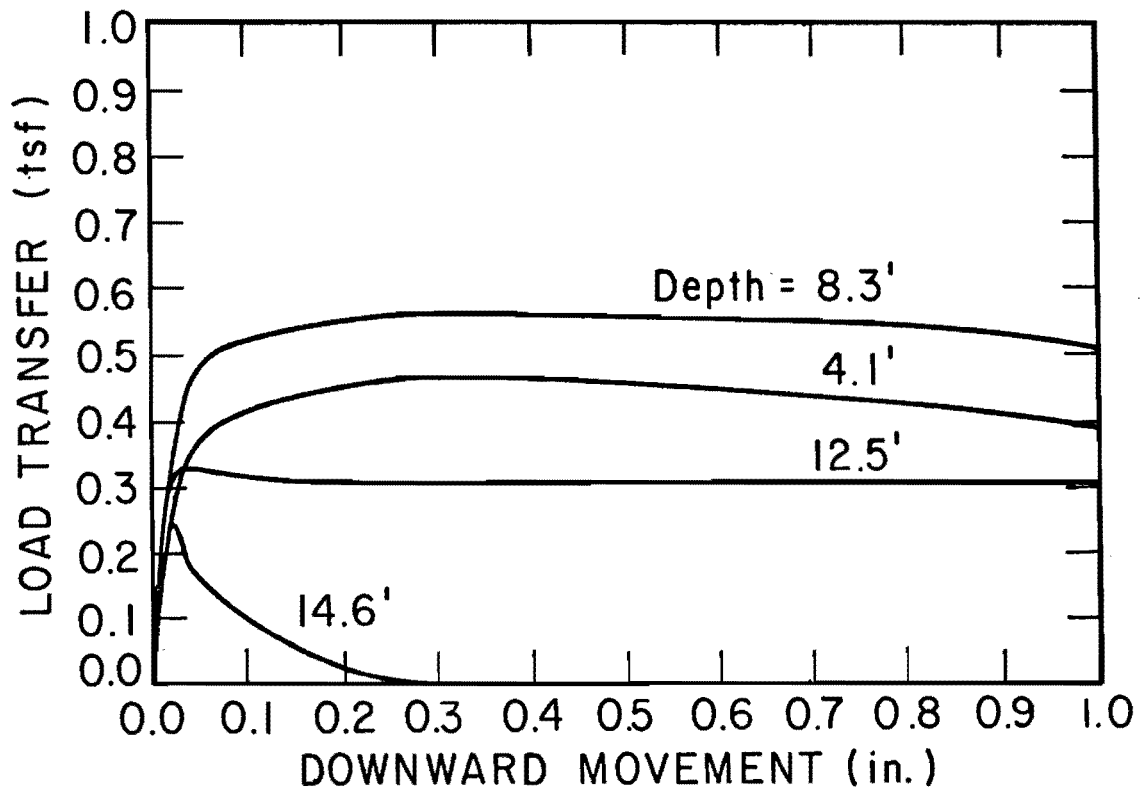


Fig. 12.25. Load Transfer Curves for S2T2

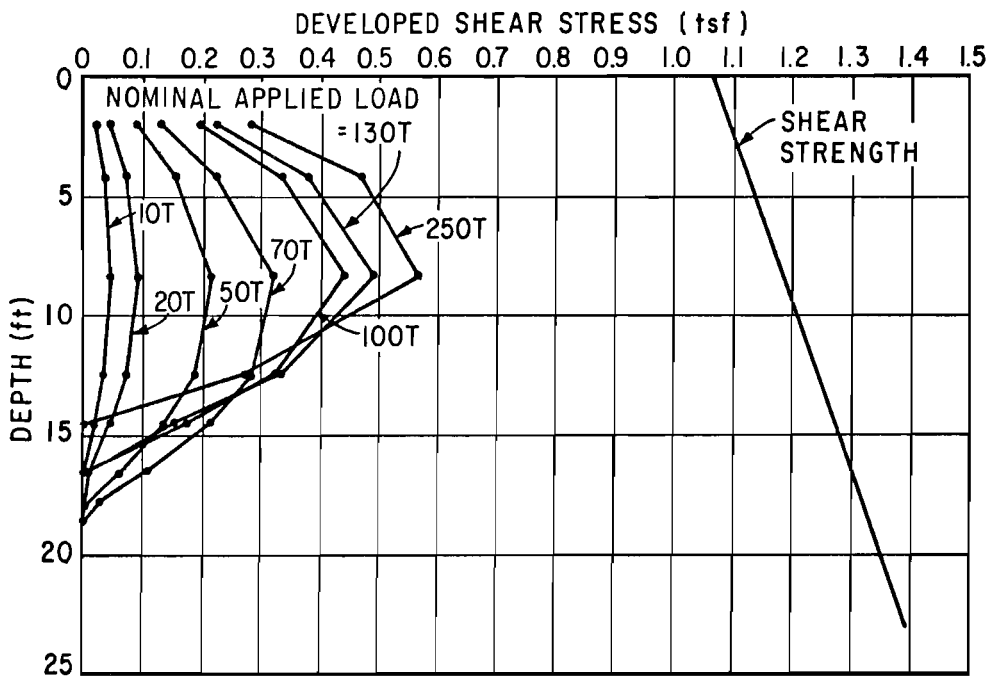


Fig. 12.26a. Distribution of Developed Shear Stresses for S2T2

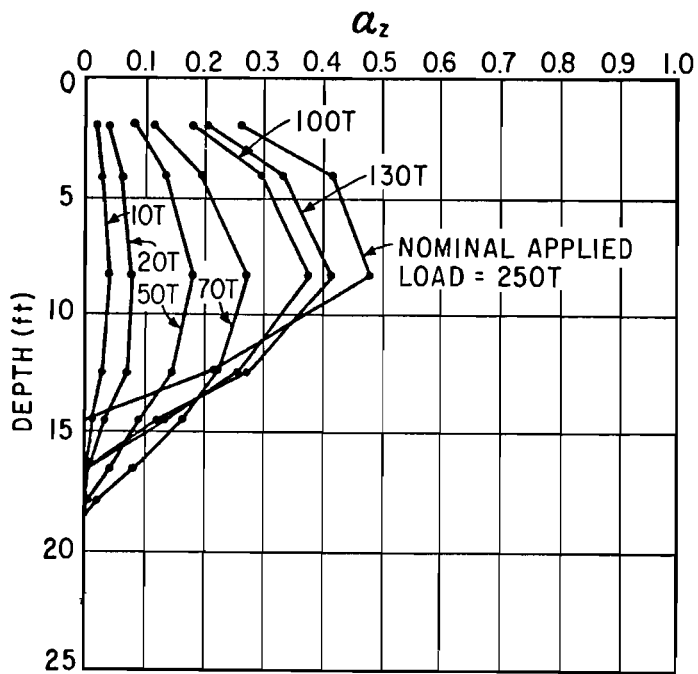


Fig. 12.26b. α_z Versus Depth for S2T2

described for S1T1. The overall average shear strength reduction factor for the stem, α_{avg} , was 0.25.

The behavior of Test Shaft No. 2 during S2T1 is compared with that during S2T2 in Figs. 12.27 and 12.28. Load distribution relationships at applied loads of 100 and 300 tons are shown in Fig. 12.27. Load transfer curves for depths of 8.3 feet and 14.6 feet are given in Figs. 12.28a and b, respectively. These figures graphically illustrate the diminished capacity for load transfer at all depths for S2T2. Because of the relatively short length of stem in Test Shaft No. 2, it cannot be determined whether the primary mechanism causing load transfer reduction upon reloading is associated with previously-mentioned factors involving the presence of the bell, in which case the reduction in load transfer would be confined to a localized zone in the stem above the bell, or whether the reduction is associated mainly with the large prior displacement of the shaft, in which case the reduction would be general throughout the length of the stem. Figures 12.27 and 12.28 suggest that the reduction occurs throughout the length of the stem, but that it is more pronounced near the bell.

After completion of S2T2, the indicated residual base load was only about 12 tons, compared with 50 tons after S2T1.

Telltales were read during S2T2, but the performance of the telltales, as in S2T1, was rather poor. The telltales overestimated load transfer by about the same amount indicated in S2T1.

The Mustran cells in Test Shaft No. 1, which was located about 14.5 feet from Shaft No. 2, were monitored as S2T2 was conducted in order to gain some insight into the way in which loaded shafts might influence

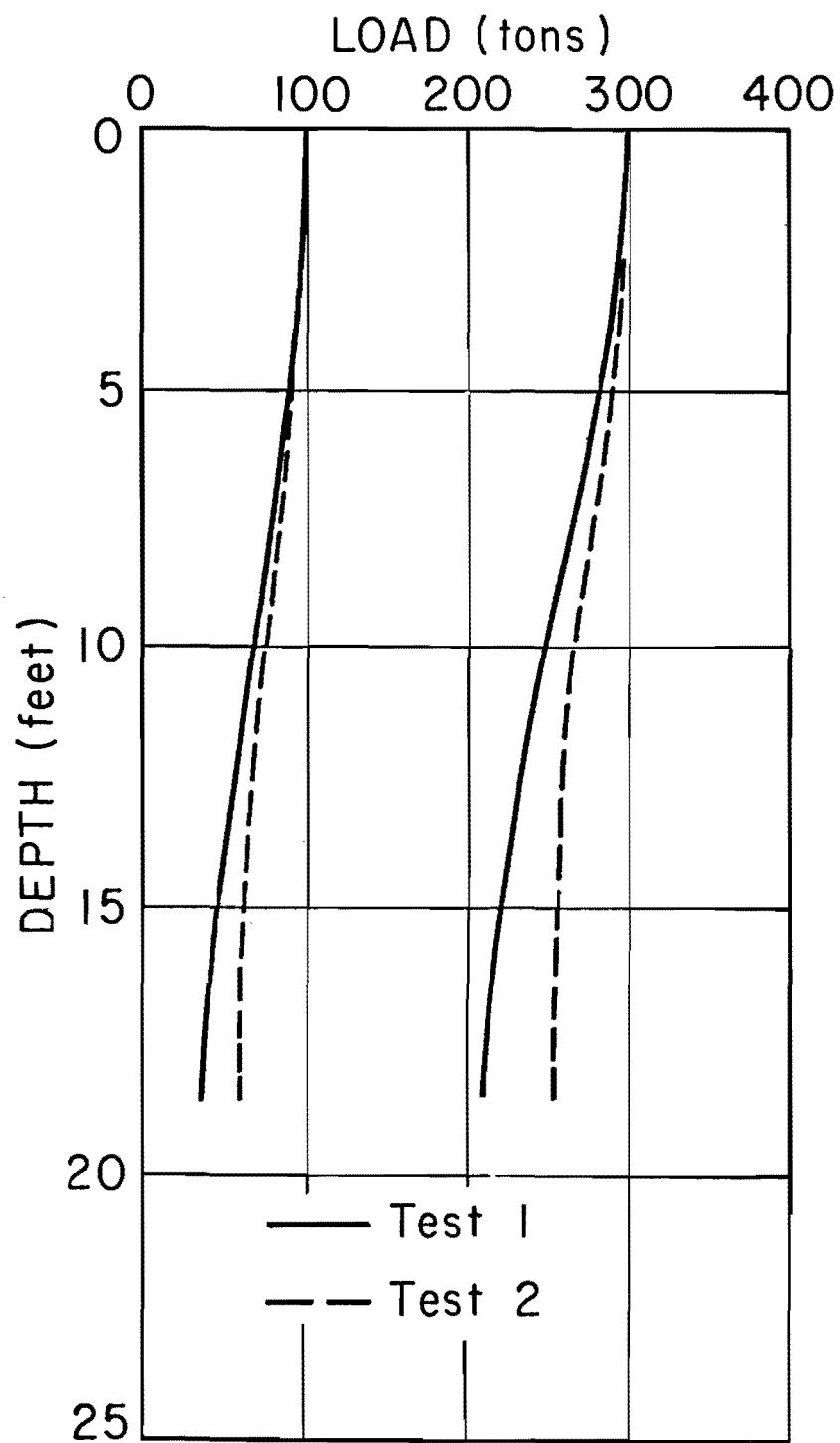


Fig. 12.27. Comparison of Load Distribution for S2T1 and S2T2

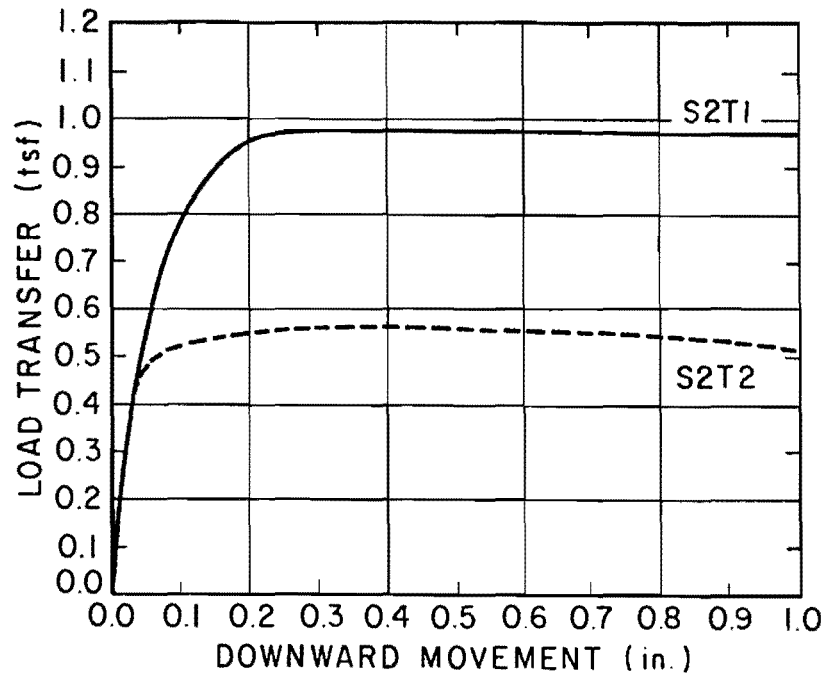


Fig. 12.28a. Comparison of Load Transfer Behavior at a Depth of 8.3 Feet for S2T1 and S2T2

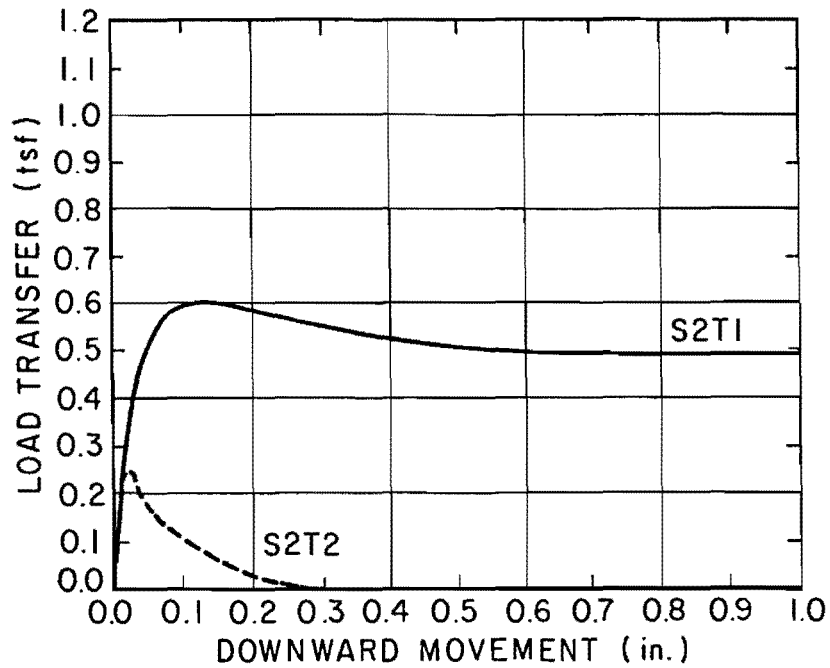


Fig. 12.28b. Comparison of Load Transfer Behavior at a Depth of 14.6 Feet for S2T1 and S2T2

other shafts in a group. The results of this experiment were somewhat erratic. No significant changes in cell output occurred in Shaft No. 1 until after side failure occurred in S2T2, but the cells did indicate that a small compressive load of about five tons developed on the base of Shaft No. 1 as complete base failure was approached in S2T2.

Test Shaft No. 3

Only one test was conducted on Test Shaft No. 3. That test involved pushing the shaft through a distance of 14 inches. Since the allowable travel on the jack piston was only about six inches, the test was conducted in three stages, or loadings, designated S3T1L1, S3T1L2, and S3T1L3. After each of the first two loadings, the shaft was unloaded, and spacers were placed between the piston and loading box to permit the shaft to be pushed farther.

The primary purpose of the test, conducted from 1100 to 1630 on October 3, 1969, was to determine the immediate residual side shear capacity of a shaft in Beaumont Clay at large displacement. Once the base became seated at the bottom of the one-foot cavity that had been formed beneath the base, the shaft was loaded with the intent of determining the bearing capacity of the base. Furthermore, it was hoped to acquire direct evidence concerning the effect of base movement on side shear capacity, which could be accomplished by observing changes in the load distribution curves as the base became seated and picked up load.

The shaft was loaded by the QL procedure until plunging failure occurred. Thereafter, downward movement was maintained by the CRP method, using a rate of penetration of 0.1 inches per minute. S3T1L1 continued

until a gross settlement of 5 1/2 inches was reached. S3T1L2 was conducted entirely under CRP and continued until the base became seated at a settlement of about 11 inches. The expected displacement for initiation of base loading was 12 inches. Evidently, however, some heave had occurred in the cavity, or concrete had penetrated beneath the base plate, causing slightly premature loading of the base. Finally, S3T1L3 was conducted by the QL procedure.

S3T1L1. The peak capacity was 121 tons (all in side resistance), which occurred at a displacement of 0.45 inches, as shown in Fig. 12.29. After failure occurred, a pronounced reduction in side resistance appeared, until the side load-settlement curve became asymptotic to a resistance of 64 tons at a displacement of 5 1/2 inches. These values of side resistance correspond to values of α_{avg} of 0.54 and 0.29, respectively. Almost no rebound occurred upon removal of load.

The average and individual Mustran cell response curves for the initial loading phase are given in Appendix K. Water had collected in the cavity beneath the base; however, the vent tube provided pressure relief. Figure K.7 shows a small increase in load on the base due to the static pressure of the water in the vent tube. The value of indicated base load due to the water pressure has been subtracted from the applied load in computing side resistances at failure and during CRP loading.

The family of average response curves in Fig. K.7 exhibits the characteristic that each response curve becomes horizontal as shear failure occurs below the level it represents. The response of the individual cells at the top level (Depth = 0') represented in Fig. K.8 indicates some eccentricity in the applied load, which was provided by a single jack.

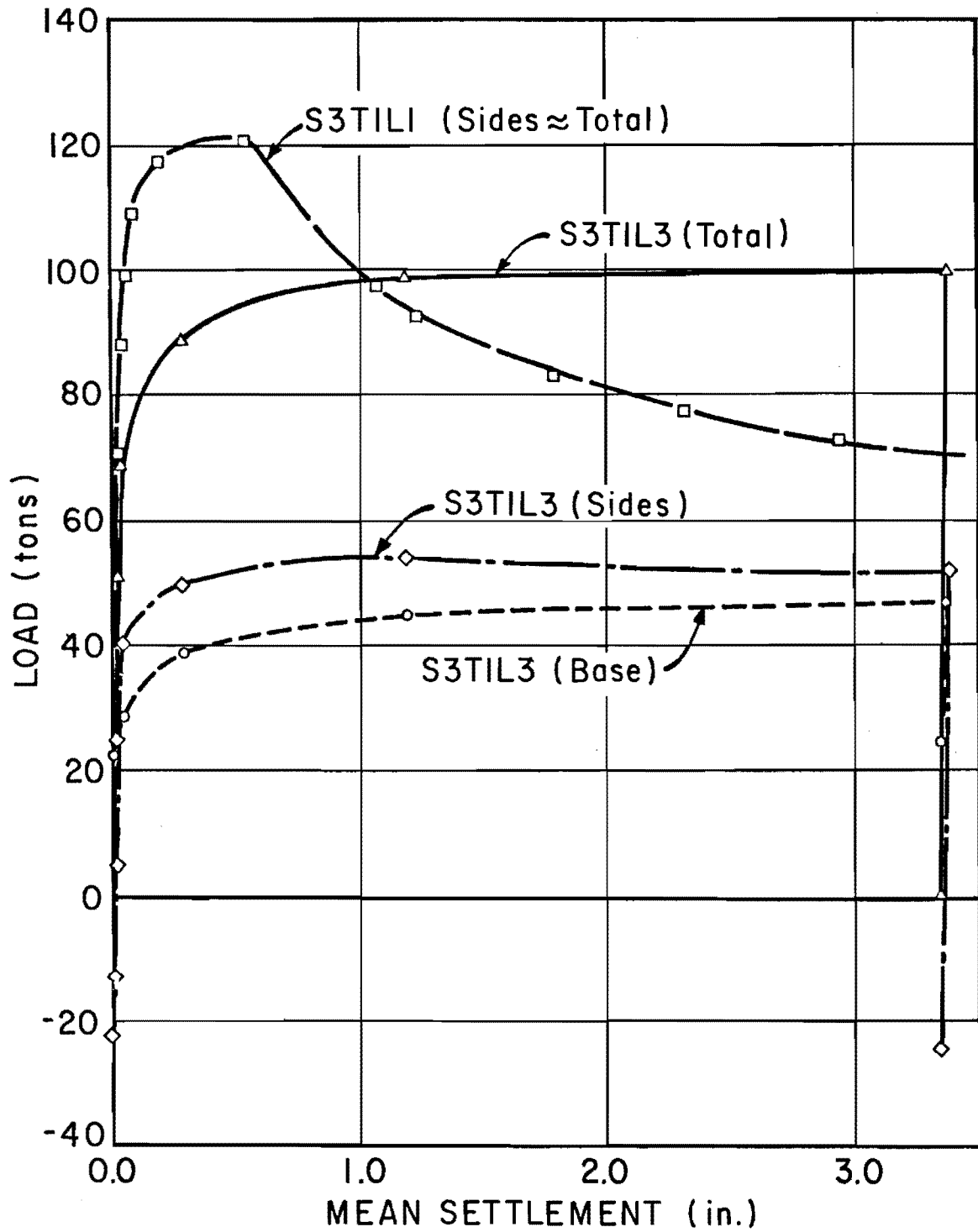


Fig. 12.29. Load-Settlement Curves for S3T1

Load distribution curves for the QL phase of the test are given in Fig. 12.30. Loads at each level were determined by the top-level calibration procedure described previously. Less data scatter was observed from S3T1L1 than from previous tests. Fourth degree polynomials were used to fit the data. Except for high loads, the load distribution curves are observed to be nearly linear below a depth of about five feet.

There is, however, some reverse curvature in the load distribution curves near the bottom of the shaft at high loads, which indicates a reduction in load transfer despite the fact that the base was not yet interacting with the soil beneath the shaft. Several months after the test, an access hole was bored beside Test Shaft No. 3. The hole was entered, and radial moisture content profiles were obtained to examine the phenomenon of mortar and moisture migration in the field, as described later. An increase in moisture content of 4 to 8 per cent above the natural moisture content was observed in the soil directly adjacent to the walls of the shaft from depths of 18 to 21 feet. (No moisture content increase was found from 21 to 23 feet, but the acetone used to dissolve the styrofoam pad had penetrated the soil in that depth interval, possibly causing the soil to dry rapidly before moisture content determination could be properly made.) As with Test Shaft No. 1, the magnitude of moisture content increase which was observed suggests a remolded shear strength decrease of about fifty per cent and a resultant decrease in the shear strength reduction factor from the value occurring in regions where no significant softening took place. It is of interest to restate the fact that the borehole for Test Shaft No. 3 was completely dry when concrete was placed. The source of the moisture supply necessary to

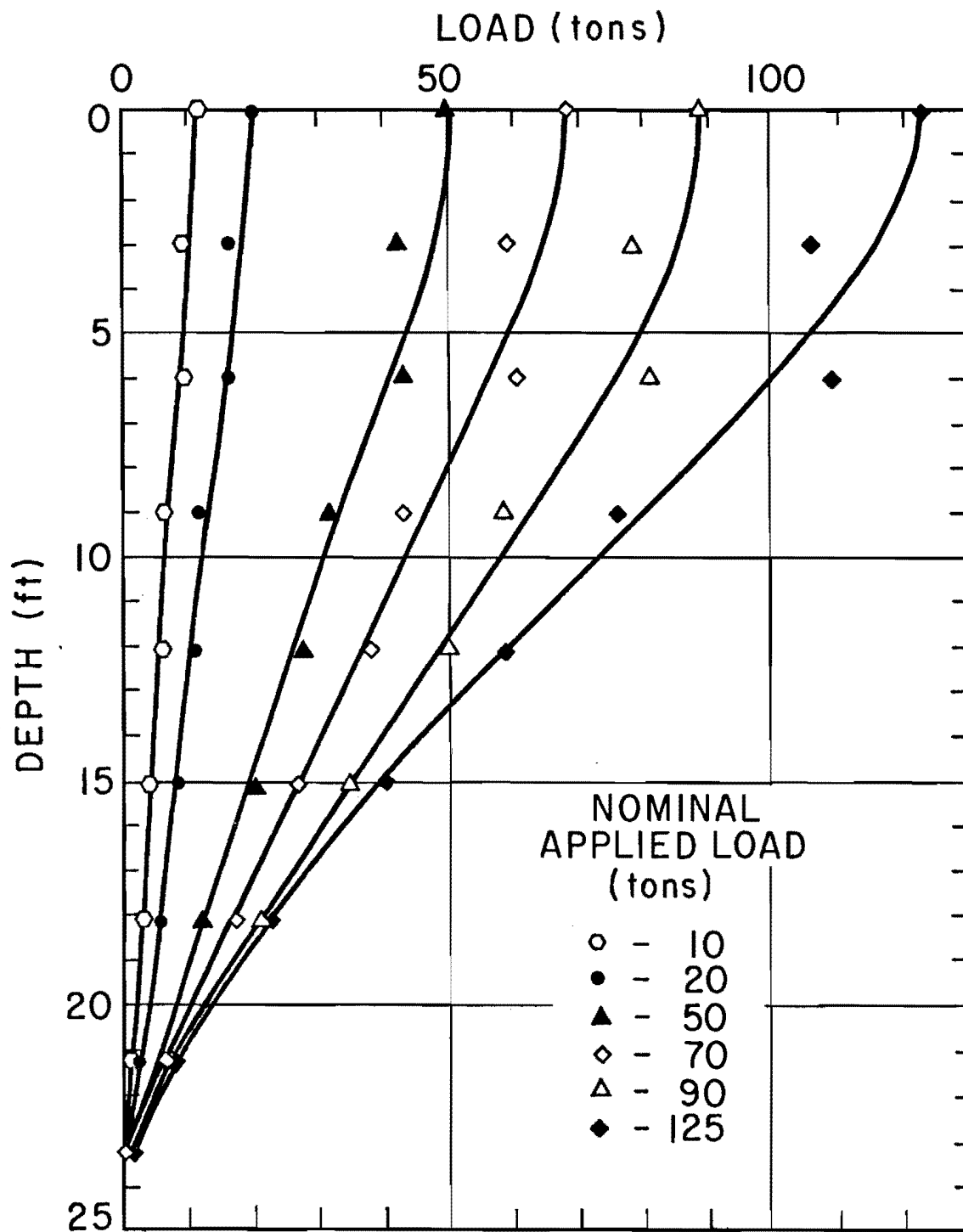


Fig. 12.30. Load Distribution Curves for QL Phase of S3T1L1

cause the observed moisture content increase in the soil near the base presumably was the concrete shaft itself. Evidently, either a downward migration of excess mixing water occurred after set-up, causing a concentration of excess moisture in the bottom few feet of the concrete, or the shaft acted as a wick, drawing water which had collected in the cavity into the bottom of the shaft. No-load monitoring (Chapter X, Fig. 10.1) indicated that the greatest vertical extension in the concrete occurred near the bottom of the shaft, possibly implying that the concrete was swelling there as a result of pooling of moisture. However, the lack of base restraint could have produced the same result. Hence, no-load monitor data could not provide conclusive evidence concerning the phenomenon of moisture concentration in the concrete near the bottom of the shaft.

The distribution of load during the CRP portion of S3T1L1 is shown in Fig. 12.31. The scatter of the data was much more pronounced during this phase of the test, conceivably because small irregularities along the side were causing local moments to be produced. The majority of load transfer reduction during the CRP phase apparently occurred between 10 and 18 feet. The small indicated base load is due to the pressure of the water in the vent tube.

Several load transfer curves developed during the QL phase of S3T1L1 are shown in Fig. 12.32. Apparently, side shear failure progressed from bottom to top, since the load transfer curves representing the greatest depth indicate failure at the smallest displacement. The greatest developed shear stress was about 0.9 tsf in the 8- to 12-foot depth interval. The load transfer relationships near the base have a pronounced

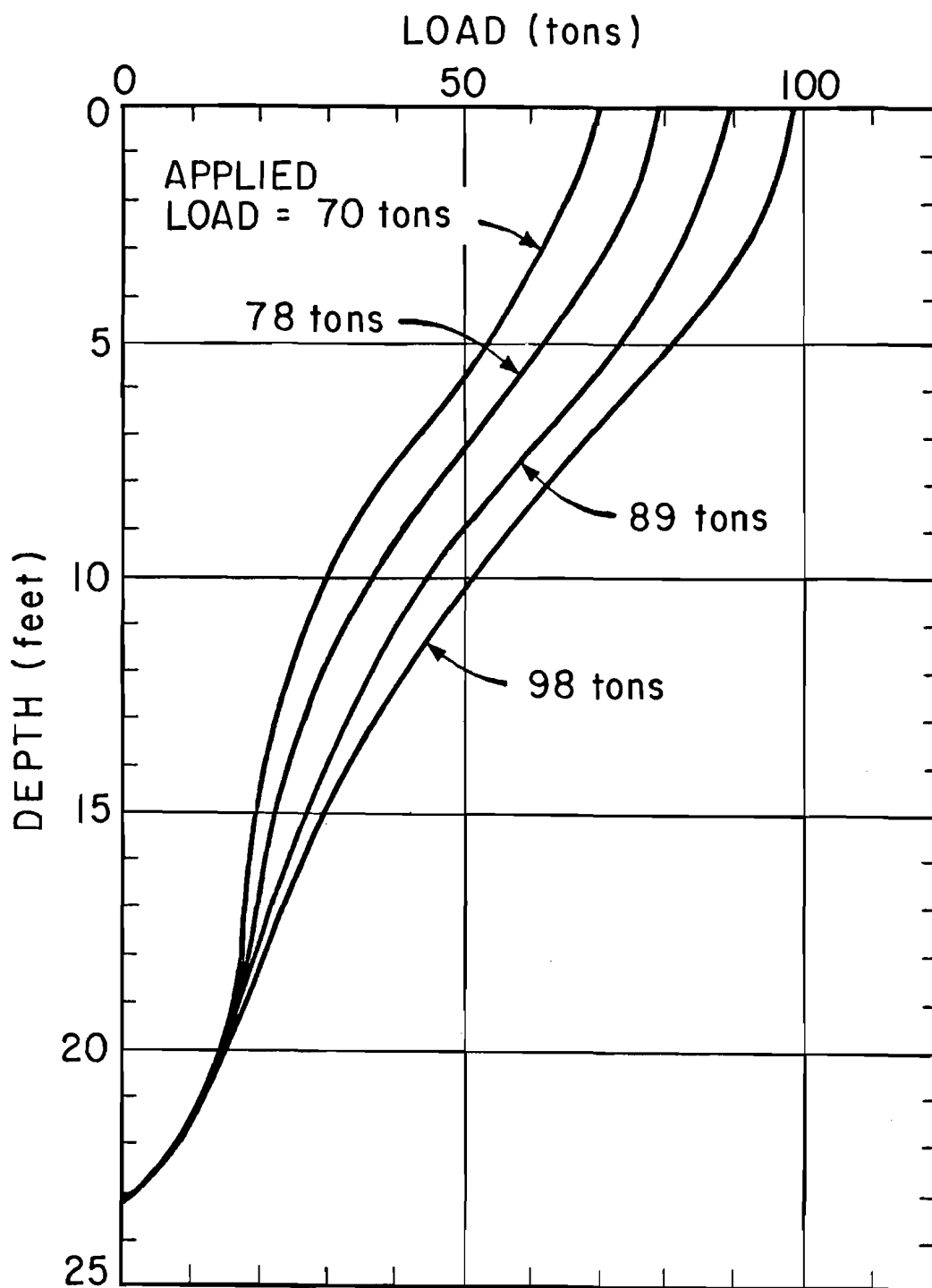


Fig. 12.31. Load Distribution Curves for CRP Phase of S3T1L1

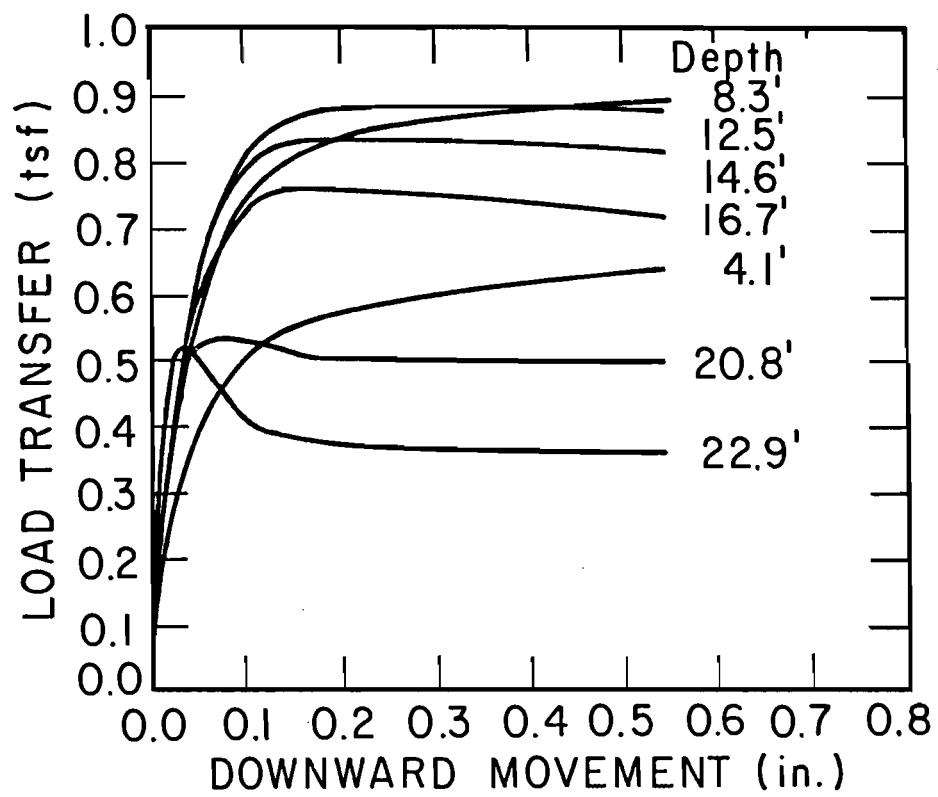


Fig. 12.32. Load Transfer Curves for S3T1L1

peak, as did those near the base in Test Shaft Nos. 1 and 2, but the residual resistance remained high in S3T1L1.

Curves showing developed shear stress and α_z versus depth for the QL phase are given in Figs. 12.33a and b, respectively. The shapes of the curves are similar to those obtained in the tests on Test Shaft Nos. 1 and 2, but without the extreme reduction of load transfer near the bottom. The maximum shear strength reduction factor was 0.75, occurring near the middle of the shaft. The peak α factor at the base was 0.5, which occurred under applied loads of 70 to 90 tons. That value had decreased to 0.36 by the time complete side failure occurred.

By way of comparison, Test Shaft No. 1 produced a peak side resistance of 97 tons compared with 121 tons in S3T1L1, with the principal difference being the magnitude of shear stress developed in the bottom few feet of the shafts. Evidently, the absence of base-side interaction in S3T1L1 and, perhaps, increased softening in the soil adjacent to the bottom sections of Test Shaft No. 1 contributed significantly to the difference in peak side resistance.

The indicated residual compressive load remaining in the shaft at the conclusion of S3T1L1, shown in Fig. 12.34, was insignificant.

The improved embedment gage circuit, located just below the surface (see Chapter IX), performed well during S3T1L1. A concrete modulus of 6.5×10^6 psi was indicated from the readings, assuming a Poisson's ratio of 0.15 for the concrete, compared to 6.4×10^6 psi measured in cylinder tests.

S3T1L2. The shaft was pushed an additional 5 1/2 inches during the second loading. At the end of the loading, significant load had been

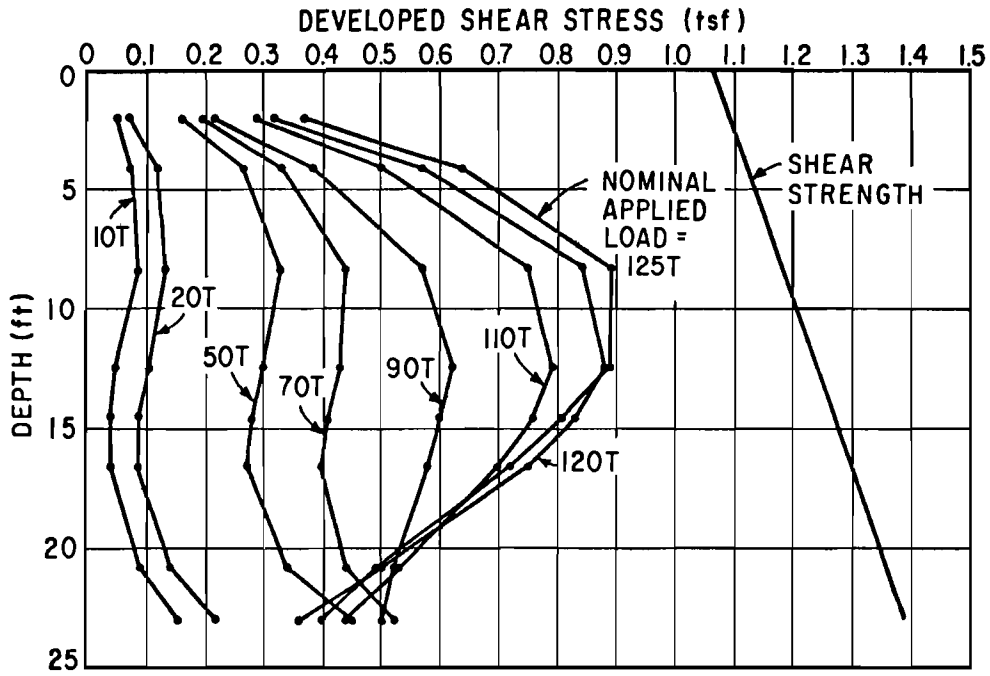


Fig. 12.33a. Distribution of Developed Shear Stresses for S3T1L1

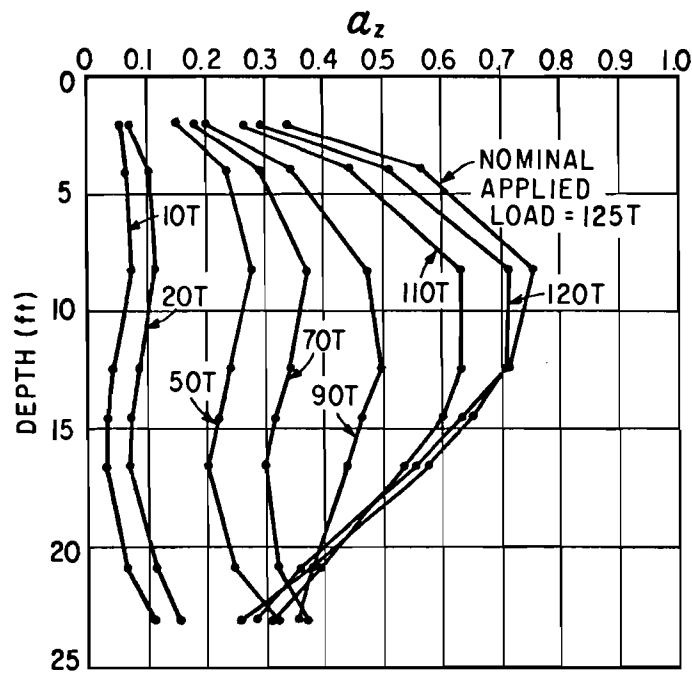


Fig. 12.33b. α_z Versus Depth for S3T1L1

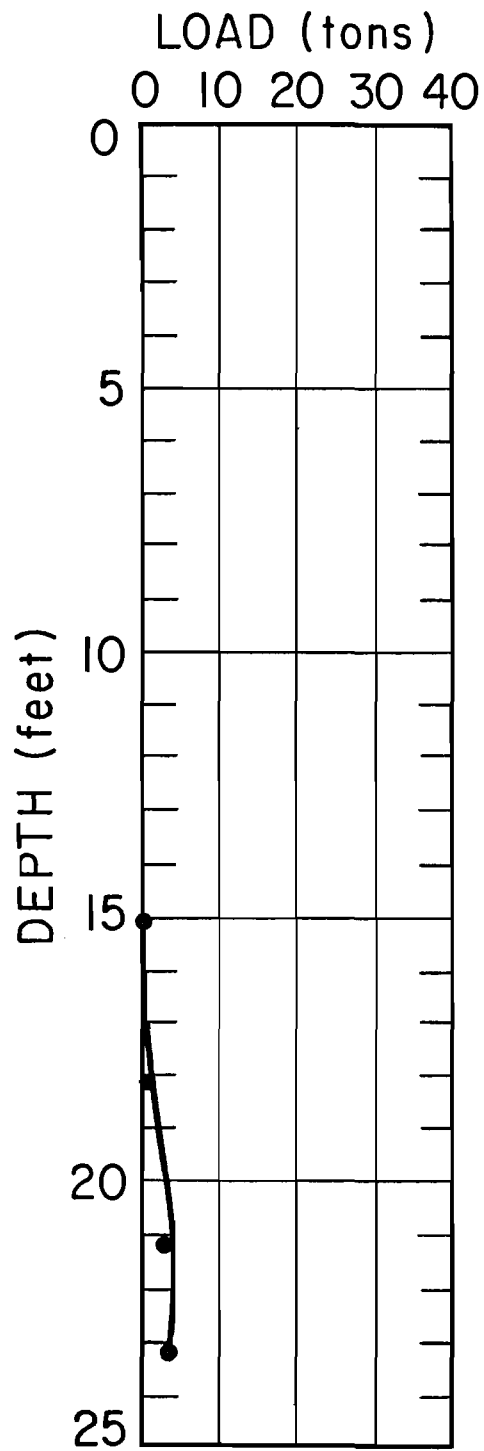


Fig. 12.34. Distribution of Load in Shaft Immediately After S3T1L1

registered at the base. The distribution of load in the shaft after butt load was removed is shown in Fig. 12.35.

S3T1L3. The third loading began immediately after the second loading phase was completed. The residual loads existing in the shaft after the second loading (Fig. 12.35) were assumed to be present at the beginning of S3T1L3. Loads based upon zero-applied-load readings taken just prior to S3T1L3 were added to the residual loads at each level to obtain the real load distribution at any stage during the third loading.

The load-settlement relationships are shown in Fig. 12.29, which also gives the load-settlement curve for S3T1L1. The mean settlement shown for S3T1L3 is the added settlement, or settlement since the beginning of the third loading. The peak side resistance was 54 tons. This load corresponds to an average shear strength reduction factor of 0.24, compared to the residual value of 0.29 found in S3T1L1. The ultimate base load, which occurred at an added displacement of three inches, was 48 tons, indicating a bearing capacity factor, N_c , of 8.7, even after softening of the soil had occurred due to water accumulation in the cavity. Very little decrease in side resistance was measured between added displacements of one and three inches.

Figure 12.36 shows the load distribution relationships for S3T1L3, obtained again from fourth degree least-squares polynomials. Surprisingly, an increase in load transfer is indicated near the base at higher loads, suggesting, if anything, that base interference increases the shear capacity of the shaft near the base. It is believed, however, that this increased load transfer was a false indication that could have been caused by wedging of a thin ring of concrete between the sides of the

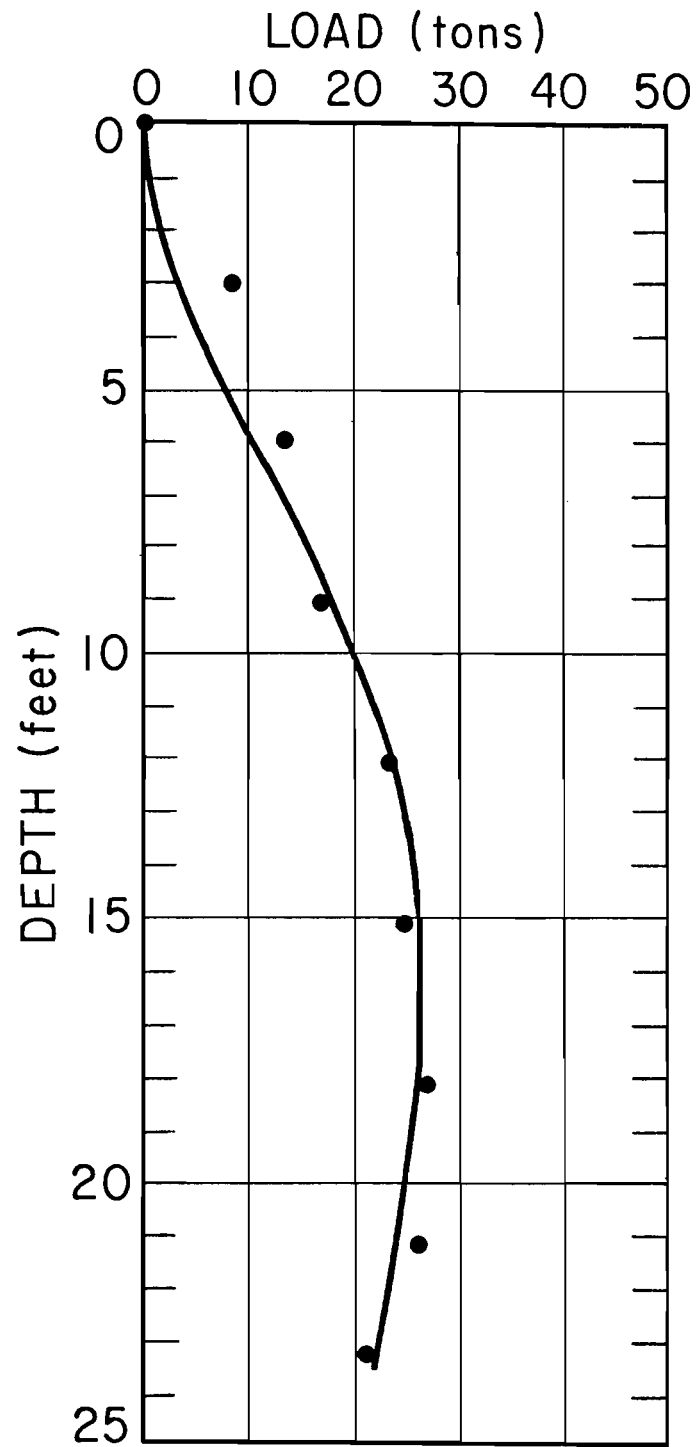


Fig. 12.35. Distribution of Load in Shaft Immediately After S3T1L2

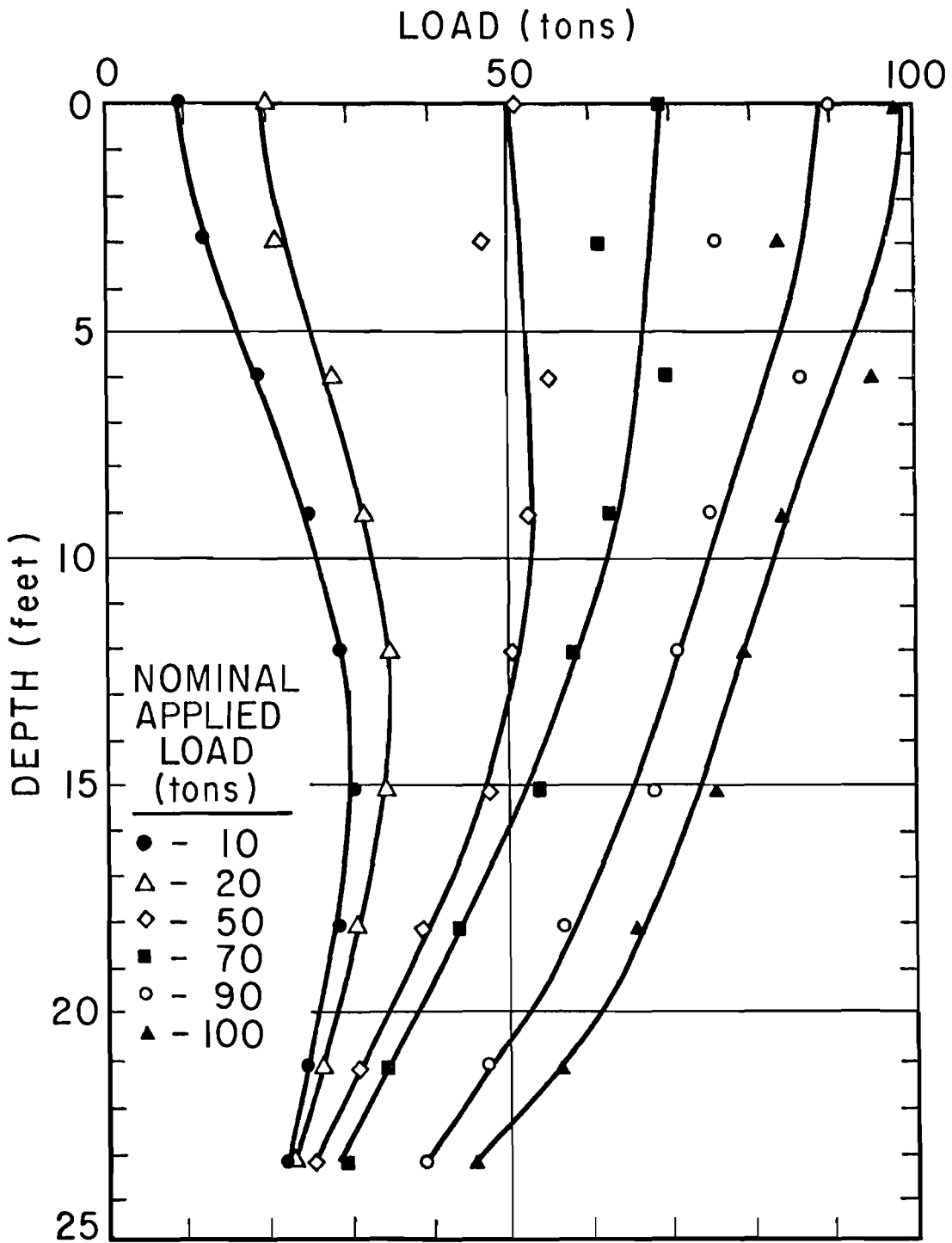


Fig. 12.36. Load Distribution Curves for S3T1L3 Including Residual Loads from S3T1L2

lower part of the shaft and the soil, thus enhancing load transfer. Such a ring of concrete may have spilled into the space between the styrofoam pad and borehole wall during casting. Another possible cause of the indicated increased load transfer is underregistration of the Mustran cells at the bottom level due to faulty embedment. The bottom lips of those cells were bolted to the quarter-inch-thick plate that formed the bottom of the shaft. The plate was not set in the concrete; hence, the bottom lips of the bottom set of Mustran cells were not actually embedded.

The load transfer curves for S3T1L3 are shown in Fig. 12.37. With the residual loads included, the load transfer at each level was initially negative (upward-directed shear stresses on soil). The gradually-increasing load transfer at the 20.8-foot level beyond a settlement of 0.2 inches suggests that the bottom level of Mustran cells was under-registering, since a wedging action or increased shear capacity due to base interference should have resulted in a gradual leveling-off in the load transfer relationship at that level. The maximum load transfer along most of the length of the shaft was about 500 psf.

Developed shear stress and α_z variations are shown in Figs. 12.38a and b, respectively. These curves again reflect the presence of the residual compressive forces at the beginning of the loading.

Comparisons of the behavior of Test Shaft No. 3 during the first and third loadings are best seen in the load transfer curves. Two such comparisons, for depths of 12.5 and 16.7 feet, are given in Fig. 12.39. The diminished shear resistance in the third loading, as well as a decreased movement to mobilize that resistance, are evident.

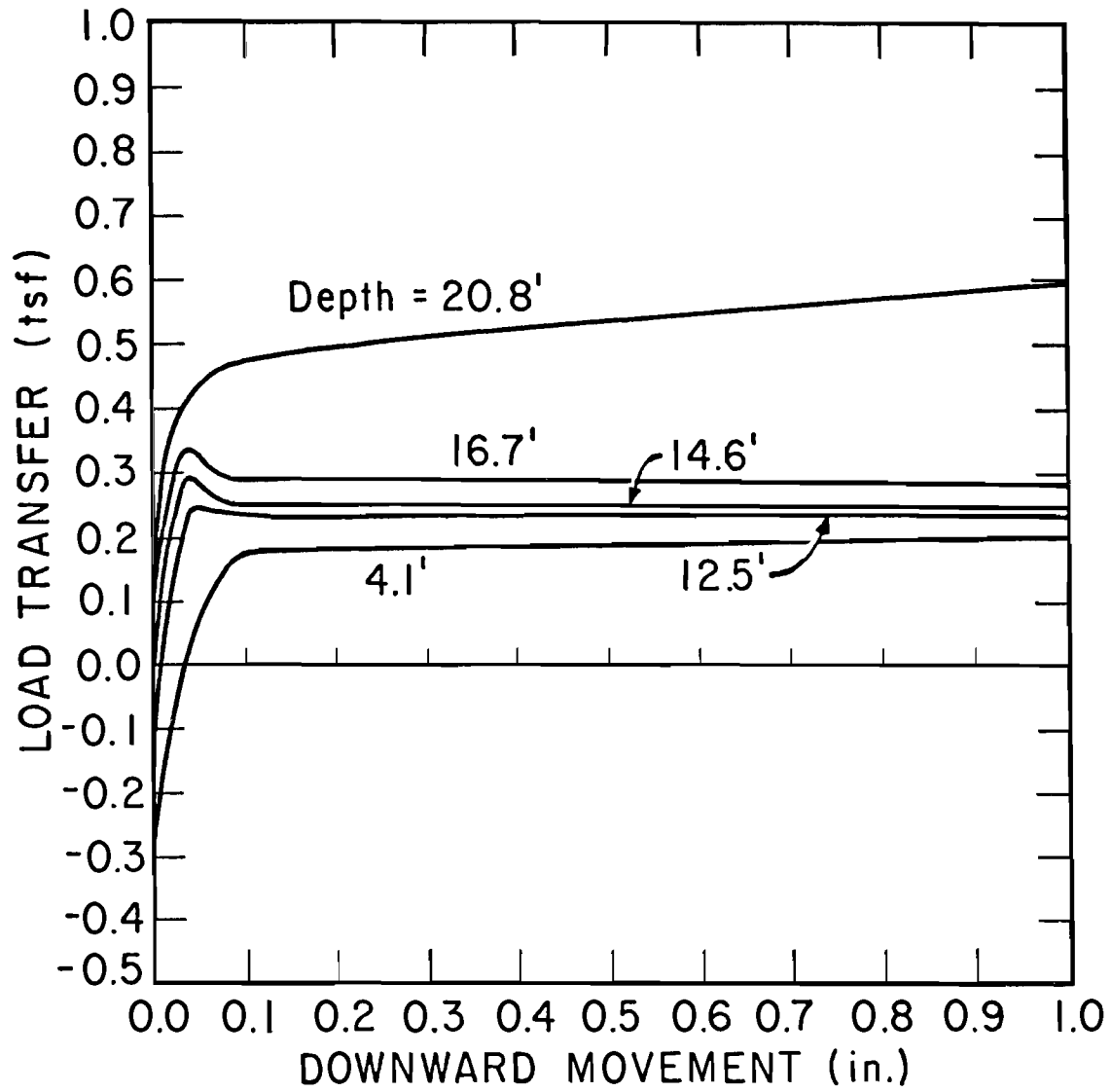


Fig. 12.37. Load Transfer Curves for S3T1L3 Including Residual Stresses from S3T1L2

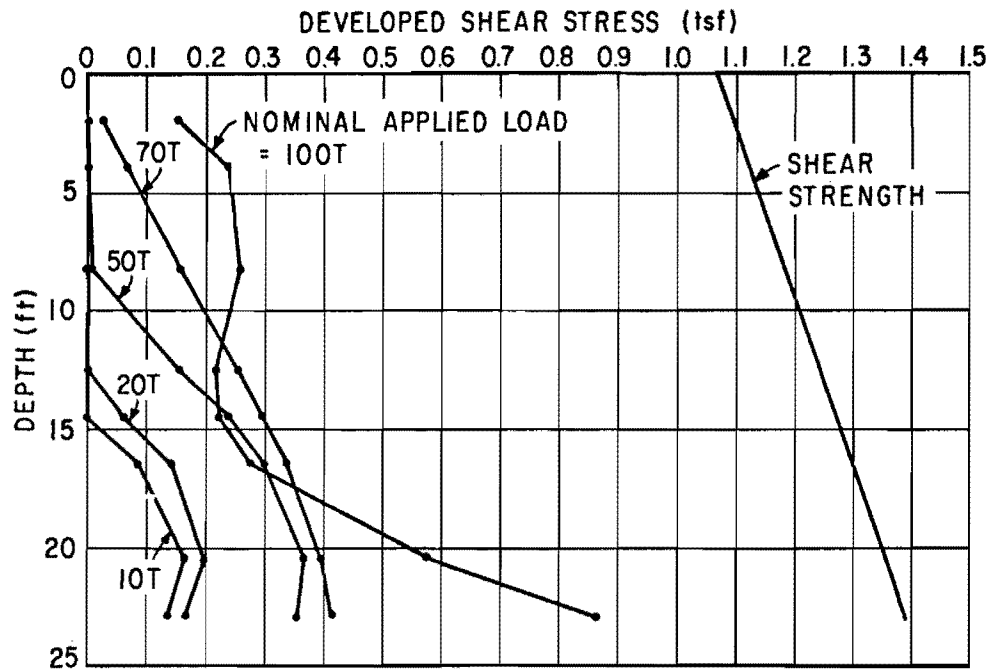


Fig. 12.38a. Distribution of Developed Shear Stresses for S3T1L3

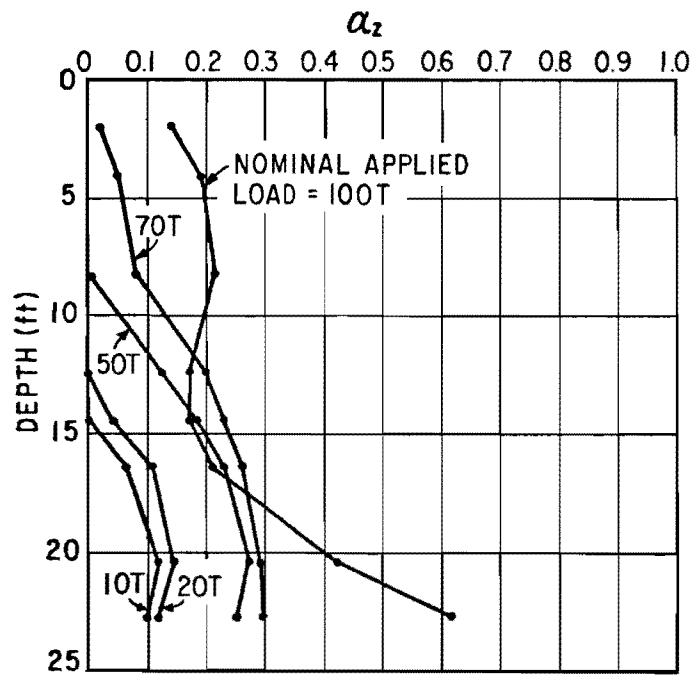


Fig. 12.38b. α_z Versus Depth for S3T1L3

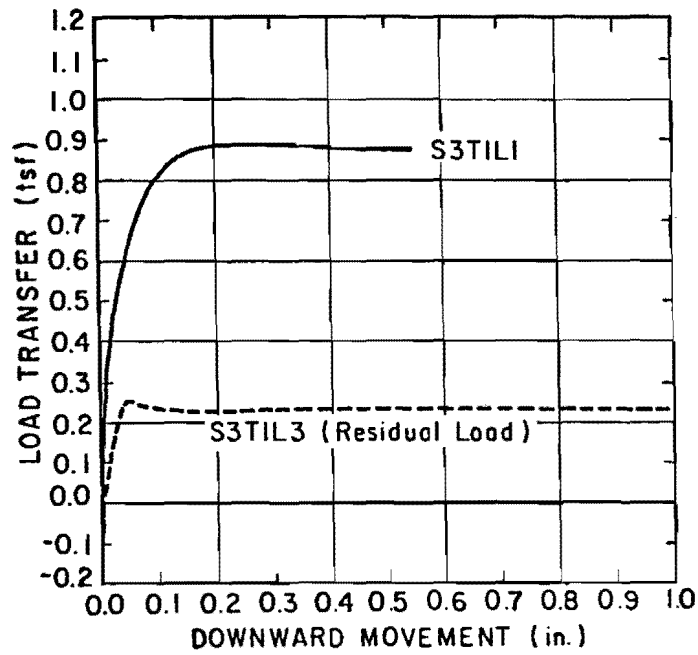


Fig. 12.39a. Comparison of Load Transfer Behavior at a Depth of 12.5 Feet for S3TIL1 and S3TIL3

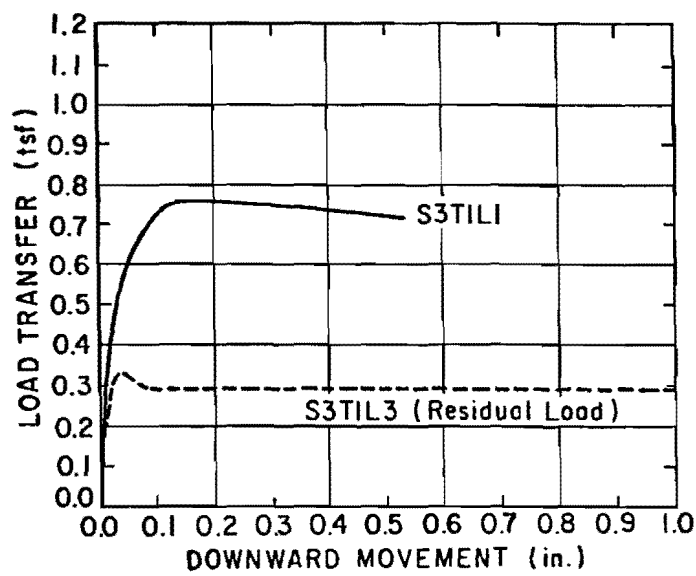


Fig. 12.39b. Comparison of Load Transfer Behavior at a Depth of 16.7 Feet for S3TIL1 and S3TIL3

Test Shaft No. 4

S4T1. The first load test was conducted on Test Shaft No. 4 between 1030 and 1330 on December 4, 1969, using the QL procedure. Test Shaft No. 4, which was 45 feet deep, had been installed on July 9, 1969, in a hole processed to a depth of 40 feet with bentonite, soil cuttings, and water. The final five feet had been drilled in the dry. A small surface collar had developed during installation. That collar, which was about two feet deep, was trimmed off flush with the body of the stem with air hammers prior to S4T1.

It had been hoped to conduct the first load test on Test Shaft No. 4 two to three months after casting, in order to permit the results to be compared directly with those of the three shafts installed in the dry, each of which had been tested initially within that time interval. Testing within two to three months would have eliminated time between casting and testing as a test parameter. Delays in setting the reaction frame unfortunately prevented S4T1 from being conducted at the desired time; however, it is felt that delayed testing did not materially effect the behavior of Test Shaft No. 4.

The total capacity of S4T1 was 321 tons. Side, base, and total load-settlement relationships are given in Fig. 12.40. It is seen that the peak side resistance was 194 tons, achieved at 0.3 inches mean settlement, while the ultimate side resistance was 179 tons. The peak value corresponds to an average shear strength reduction factor of 0.38, and the ultimate value to a factor of 0.35. The ultimate base capacity of 142 tons occurred at a settlement of 1.8 inches. Base load was calculated from the load distribution data, as before. A total rebound of 0.11 inches was recorded.

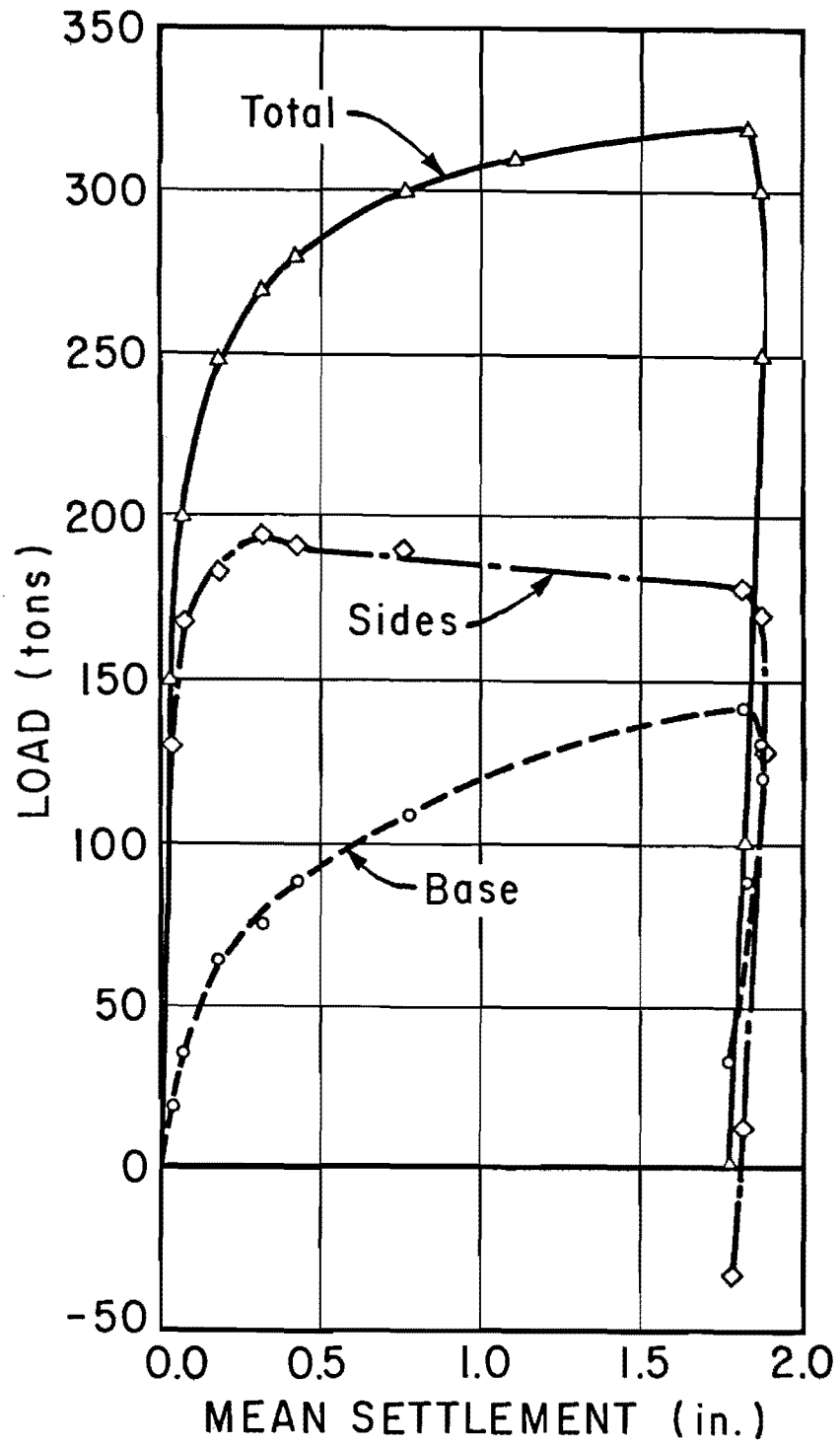


Fig. 12.40. Load-Settlement Curves for S4T1

As in all previous initial loadings, the side load-settlement behavior was dominant over that of the base at small settlements. However, the base picked up load at a relatively higher rate in S4T1 than in S1T1, presumably because of the stiffer soil present at the 45-foot depth. The side load-settlement relationship was linear to about two-thirds of the peak load, while the base load-settlement curve was linear to only about one-third of the ultimate base load.

The individual Mustran cell responses are shown graphically for the loading phase of S4T1 in Appendix K. As shown in Fig. K.9, the levels of cells in the top half of the shaft behaved rather erratically, exemplified by the fact that initial response sensitivity did not appear to be controlled by the depth of the level. The initial response sensitivities of the levels of cells below 24 feet were inversely proportional to depth and decreased in rather uniform steps. These facts pointed to the conclusion that the shaft was irregularly shaped from the surface to a depth of about 20 to 25 feet. Furthermore, the extreme decrease in initial rate of response from that of the calibration level at all levels below the surface suggested that the shaft was generally larger than the nominal diameter of 30 inches, which was the diameter at the calibration level. Response curves from Fig. K.9 also imply that the shaft was overly enlarged at a depth of 4 feet, while possibly necked at a depth of 16 feet.

All of the suppositions expressed above were verified when the top 24 feet of the shaft was exposed by augering completely around the stem in April, 1970. Results of this excavation are discussed later. Because of the irregular shape of the shaft, the in-shaft calibration procedure

employed on other shafts could not be used on Test Shaft No. 4. Instead, the shaft was calibrated, in effect, by reloading the shaft with 24 feet freestanding after the excavation (S4T3). This procedure provided a direct, individual calibration constant for the pairs of cells at the 0-, 4-, 8-, 12-, 16-, and 20-foot levels. Those calibration constants, indicated by the initial tangents to the S4T3 response curves, were used directly in the reduction of load distribution data for the top 20 feet in S4T1 and S4T2. The average of the direct calibration constants for the first five levels below ground was then applied to the remaining seven levels in order to compute values of load in the remainder of the shaft. This technique carries the assumption that the average diameter of the shaft below 20 feet was the same as that above 20 feet. The direct calibration constant obtained in S4T3 for the 24-foot level was not used because it was felt that augering between the 20- and 24-foot levels may have been incomplete. Cell response graphs for the levels in the freestanding section are given in the discussion of S4T3.

It is felt that the method of calibration described above should be used whenever possible for instrumented processed shafts, which are likely to have a somewhat irregular shape.

Examination of individual response relationships in Fig. K.10 reveals that unexplained aberrations occurred in the data for the 8- and 12-foot levels, possibly resulting from the presence of the irregularities in the shaft or of drilling mud entrapped between the concrete and the soil. The smoother response curves for levels below 24 feet suggest a more uniform shape and more consistent soil-concrete bond in that zone.

As in previous test shafts, an eccentric base failure is implied from the response curves for the cells at a depth of 45 feet (Fig. K.10). No base-level underregistration problems, such as were indicated in S3T1L3, are believed to exist in Test Shaft No. 4 because the plate to which the bottom level of cells was bolted was securely and completely embedded in concrete.

The cells at the calibration level exhibited extreme scatter, as shown in Fig. K.10 (Depth = 0'). Considerable difficulty had been experienced in placing good quality concrete above the surface while constructing Test Shaft No. 4. Because the form for the protruding section had split as it was being placed, the concrete in the form could not be adequately consolidated. When the form was removed, considerable honeycombing was observed. In fact, part of cell 32W was visible through a void, indicating poor embedment. Although an attempt was made to patch the voids prior to S4T1, underregistration was still observed in cell 32W. Fortunately, the output from the top level was not required, since the direct calibration procedure explained earlier was used for data reduction.

The average output for the top level of Mustran cells was greater in S4T1 than in the tests on Shaft Nos. 1 and 3, which also contained Type 1 Mustran cells. The added sensitivity is presumed to be due to the extensive honeycombing in the concrete at the top level, which caused the effective modulus of the concrete to be less than that in Shaft Nos. 1 and 3.

The load distribution data for S4T1 are shown in Fig. 12.41. The points were fitted with fifth degree least-squares regression polynomials.

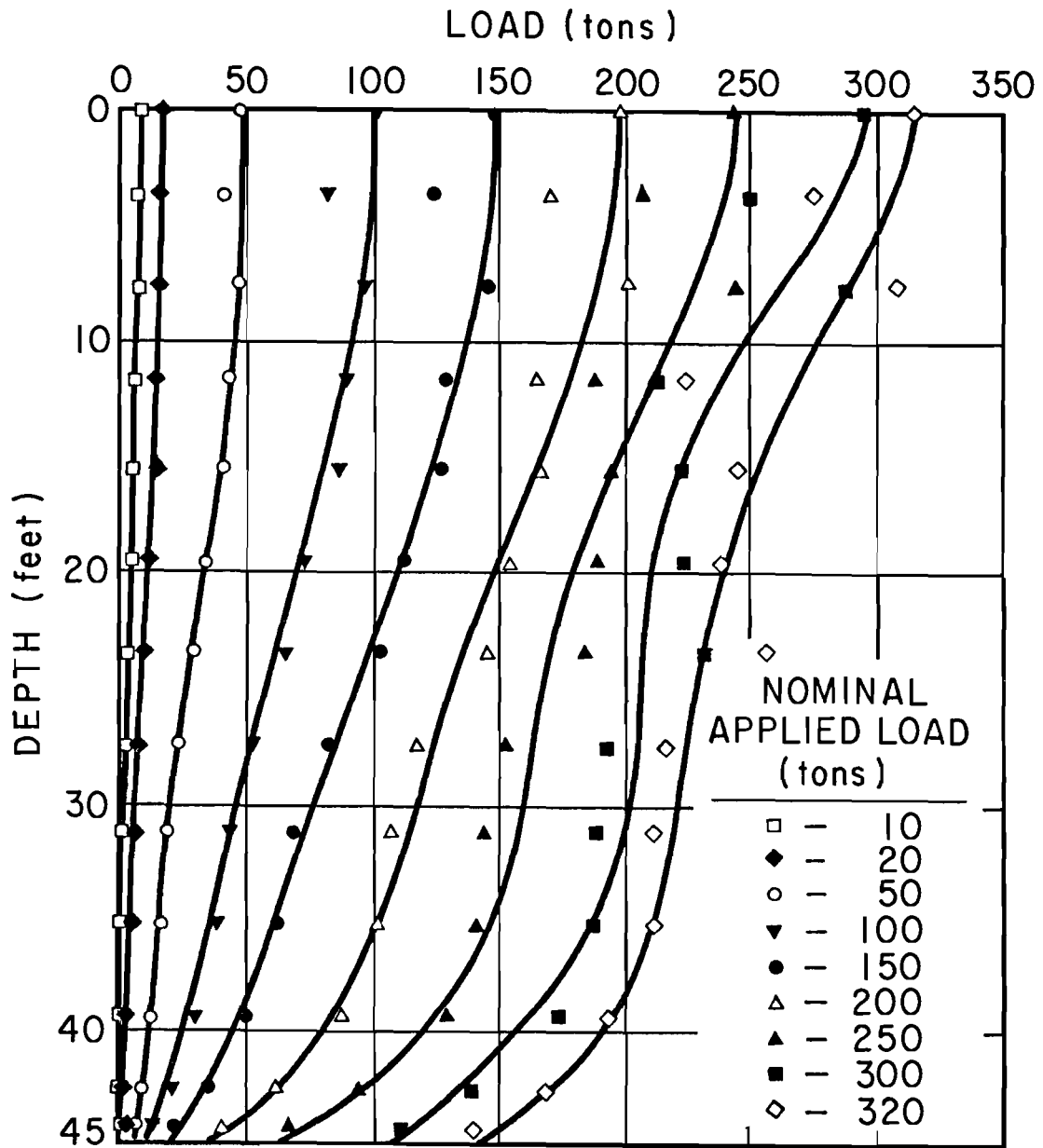


Fig. 12.41. Load Distribution Curves for S4T1

Even with the direct calibration constants from S4T3, data scatter was pronounced at high loads, possibly indicating considerable side bearing or wedging of collars or "knots" above 28 feet. As will be demonstrated later, considerably less load transfer occurred in the top 23 feet than occurred in the initial tests on the shafts drilled in the dry. However, load transfer was quite high in the bottom few feet of the shaft, which were drilled dry.

During the excavation around the top 24 feet, pockets of drilling mud up to six inches thick were found between depths of 6 and 18 feet. These pockets were easily distinguishable because the drilling mud, which had been mixed from bentonite and the gray-colored soil from Layer II, contrasted vividly with the red-colored natural soil. The pockets of mud were variable in extent and thickness.

Below the 18-foot level, the concrete at the soil-shaft interface was of very poor quality. It contained only coarse aggregate weakly bonded with a small amount of cement mortar. The thin layers of this poor concrete at the interface could be easily broken away from the better quality concrete farther from the interface.

These findings imply that a shaft constructed by the wet method outlined in Chapter II may not possess side resistance characteristics as good as those of shafts installed in the dry. Barker and Reese (1970), however, found no such evidence of entrapped drilling mud or poor quality interface concrete in a similar investigation of a test shaft installed at the HB&T test site (Fig. 6.1) using the same technique employed in installing Test Shaft No. 4. An explanation for drilling mud entrapment and poor interface concrete is offered by Barker and Reese (1970).

The variation in load transfer behavior along the shaft during S4T1 is shown in Fig. 12.42. (An average diameter of 32 inches was later measured in the exposed portion of the shaft. That diameter was used in conversion of load distribution data to load transfer relationships.) Again, the greatest unit load transfer was developed near the bottom of the shaft, where no drilling mud was used. No mechanical base-side interference is indicated, but that effect may have been overshadowed by the better adhesion that developed between the shaft and the soil in the bottom few feet.

The lowest load transfer is indicated in the depth range of 15 to 30 feet, roughly corresponding to the depths at which the entrapped mud and weak interface concrete were later found. A wedging effect, rather than shearing resistance, evidently occurred in the top ten feet, where the shaft was oversized (indicated by the relatively large displacements required to mobilize load transfer and continued increase in load transfer at large displacements at the 4.1- and 8.3-foot levels).

Initial failure occurred in the center portion of the shaft, where soil-concrete bond was weakest and where no wedging evidently took place. Peak shearing resistance was developed after a displacement of 0.04 inches at 30 feet (corresponding to the depth of Layer II described in Chapter VII). On the other hand, a displacement of 0.40 inches was required to develop the peak shearing resistance below 40 feet.

In the zone from 10 to 35 feet, the average indicated peak and ultimate load transfer was about 0.4 tsf. The average indicated peak load transfer in the 40- to 45-foot zone was 1.4 tsf, the highest load transfer measured in any of the tests at the SH225 test site.

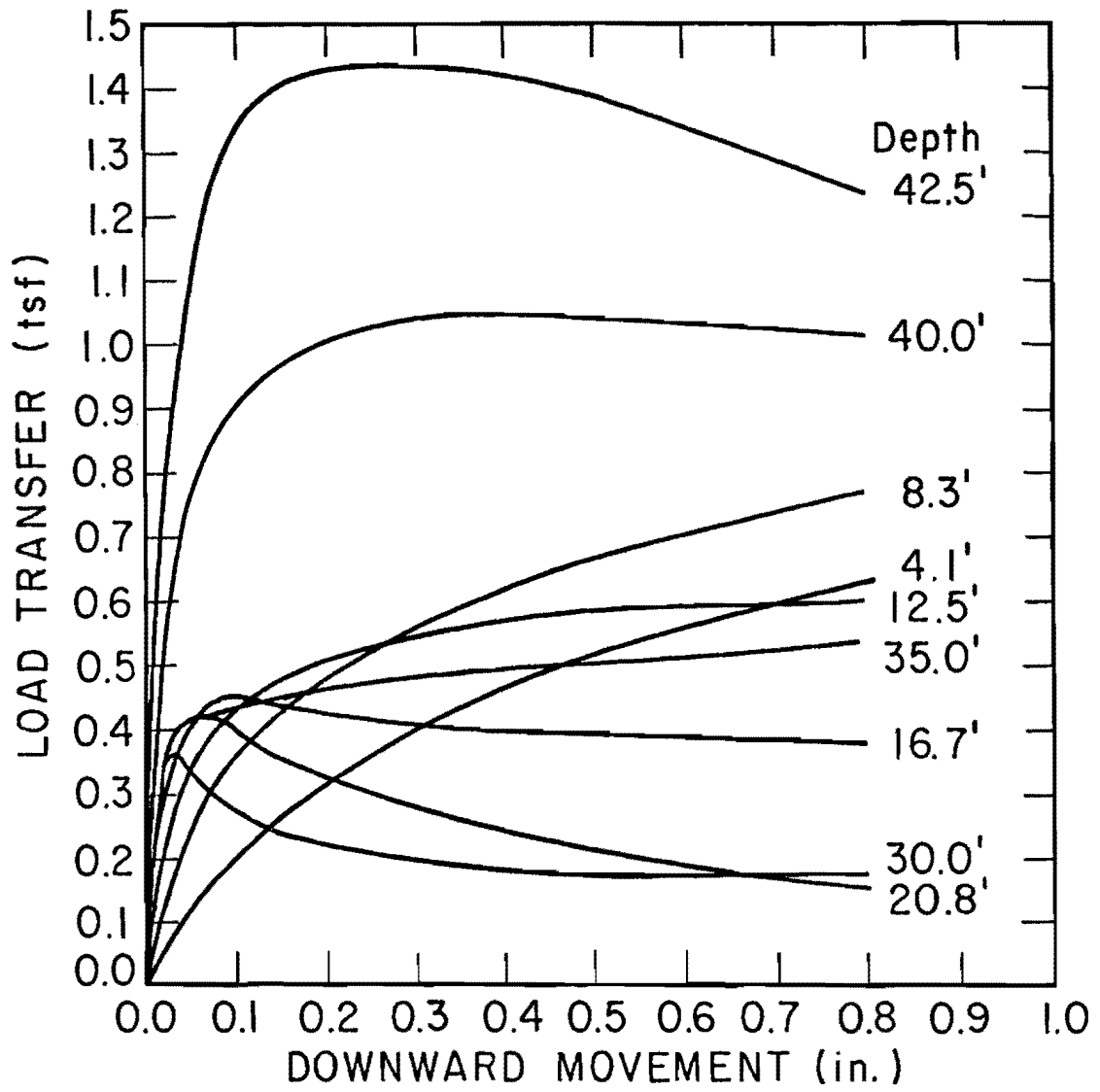


Fig. 12.42. Load Transfer Curves for S4T1

The distribution of developed shear stress and α_z at various stages of S4T1 are shown in Figs. 12.43a and b, respectively. It is observed that the distribution of maximum developed shear stress roughly follows the shear strength profile. There is a rather pronounced reduction in α_z from peak to ultimate in the 15- to 35-foot zone.

From Fig. 12.43b it is observed that the peak shear strength reduction factor for Layer II (waterbearing clayey silt) was in the order of 0.4, while the shear strength reduction factor at ultimate dropped to about 0.25. These values are approximate and are greatly influenced by the smoothing operation resulting from generation of a best-fit load distribution curve, since the layer is so thin.

The weldable gages (see Chapter IX) performed well, but the sensitivity was rather low. Weldable-gage data were excluded from consideration in calculating load distribution in the shaft.

S4T2. S4T2 was conducted between 1600 on December 16, 1969, and 1600 on December 17, 1969. The shaft was loaded in approximately 50-ton increments to 244 tons by the QL procedure. That load was held for 17 hours. The butt load was then increased to 270 tons, and the load was held for 5 1/2 hours. The load was then increased continuously until the shaft plunged at an applied load of 307 tons. Load-settlement relationships are given in Fig. 12.44.

The peak side resistance of 180 tons was obtained when the applied load of 244 tons was reached (settlement of 0.10 inches). This value corresponds to an average shear strength reduction factor of 0.35. About eight per cent of the peak side shear developed at that stage was shed to the base during the 17 hours that the applied load was maintained at

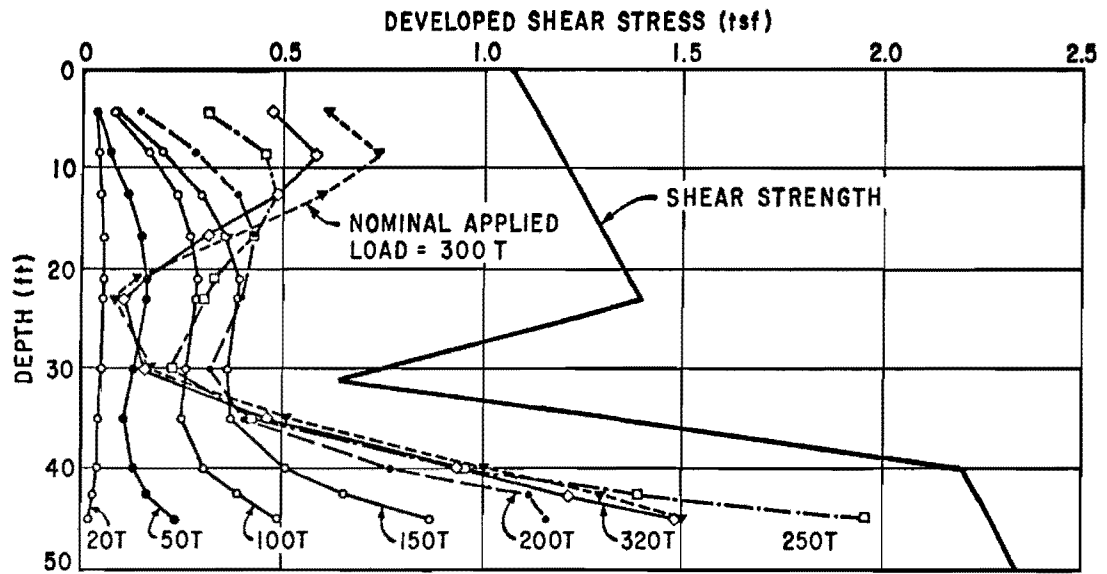


Fig. 12.43a. Distribution of Developed Shear Stresses for S4T1

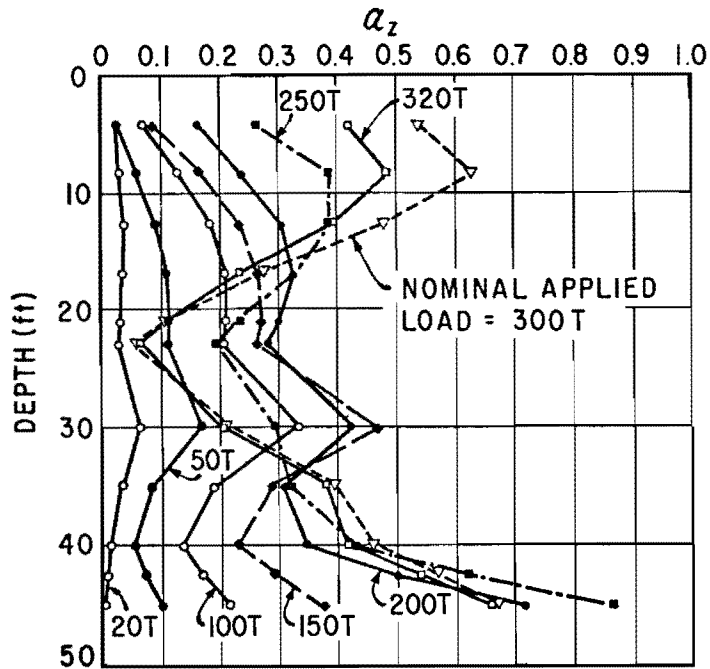


Fig. 12.43b. α_z Versus Depth for S4T1

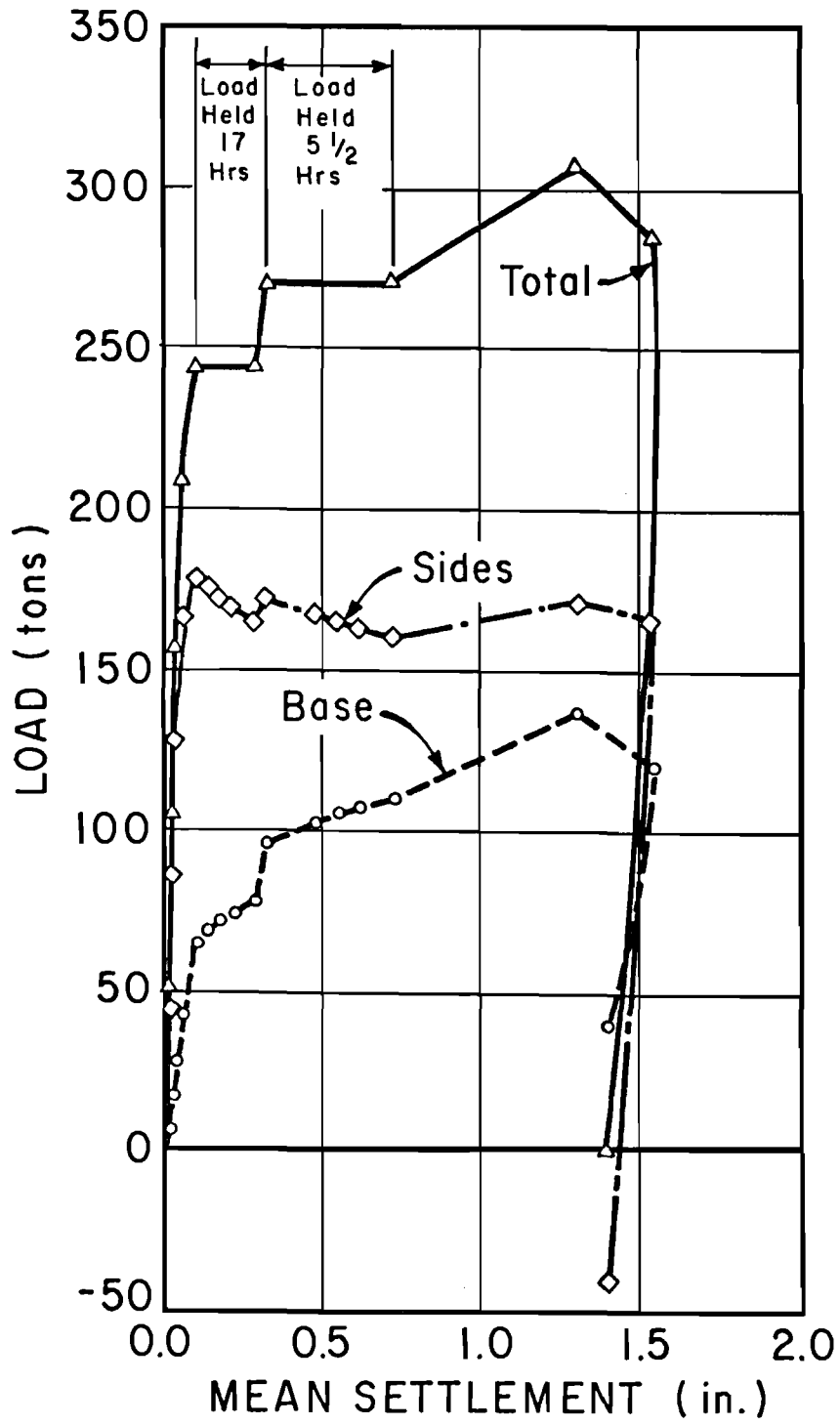


Fig. 12.44. Load-Settlement Curves for S4T2

244 tons. The side resistance increased momentarily as the butt load was increased from 244 to 270 tons, but it decreased again soon after 270 tons was reached. These phenomena are seen in the side load-settlement curve in Fig. 12.44.

The side resistance at plunging load was 165 tons, corresponding to an average shear strength reduction factor of 0.32. The maximum base load was 136 tons, which occurred at a settlement of about 1.3 inches (or a total settlement of about 3 inches since the beginning of testing of Test Shaft No. 4). No settlement gage readings were taken during the continuous loading between butt loads of 270 and 307 tons. Therefore, straight lines have been drawn for the portions of the load-settlement curves representing that interval of applied loads in Fig. 12.44.

The family of load distribution curves for S4T2 is shown in Fig. 12.45. The curves for 244 and 270 tons are those obtained immediately after load was attained. All curves were generated using fifth degree least-squares polynomials. The shaft was assumed to be free of residual loads at the beginning of S4T2 for purposes of computing load distribution and load transfer relationships. Loads were calculated using the same individual level calibration procedure explained for S4T1.

Load transfer curves developed through the end of the 244-ton maintained load period are given in Fig. 12.46. The peak load transfer in the depth interval of 10 to 35 feet was nearly constant at 0.4 to 0.5 tsf. Very little load shedding is in evidence in that interval. It appears from the load transfer curves that the greatest amount of load shedding during the maintained-load portion of the test occurred near the base of the shaft. As in S4T1, initial failure occurred in the zones

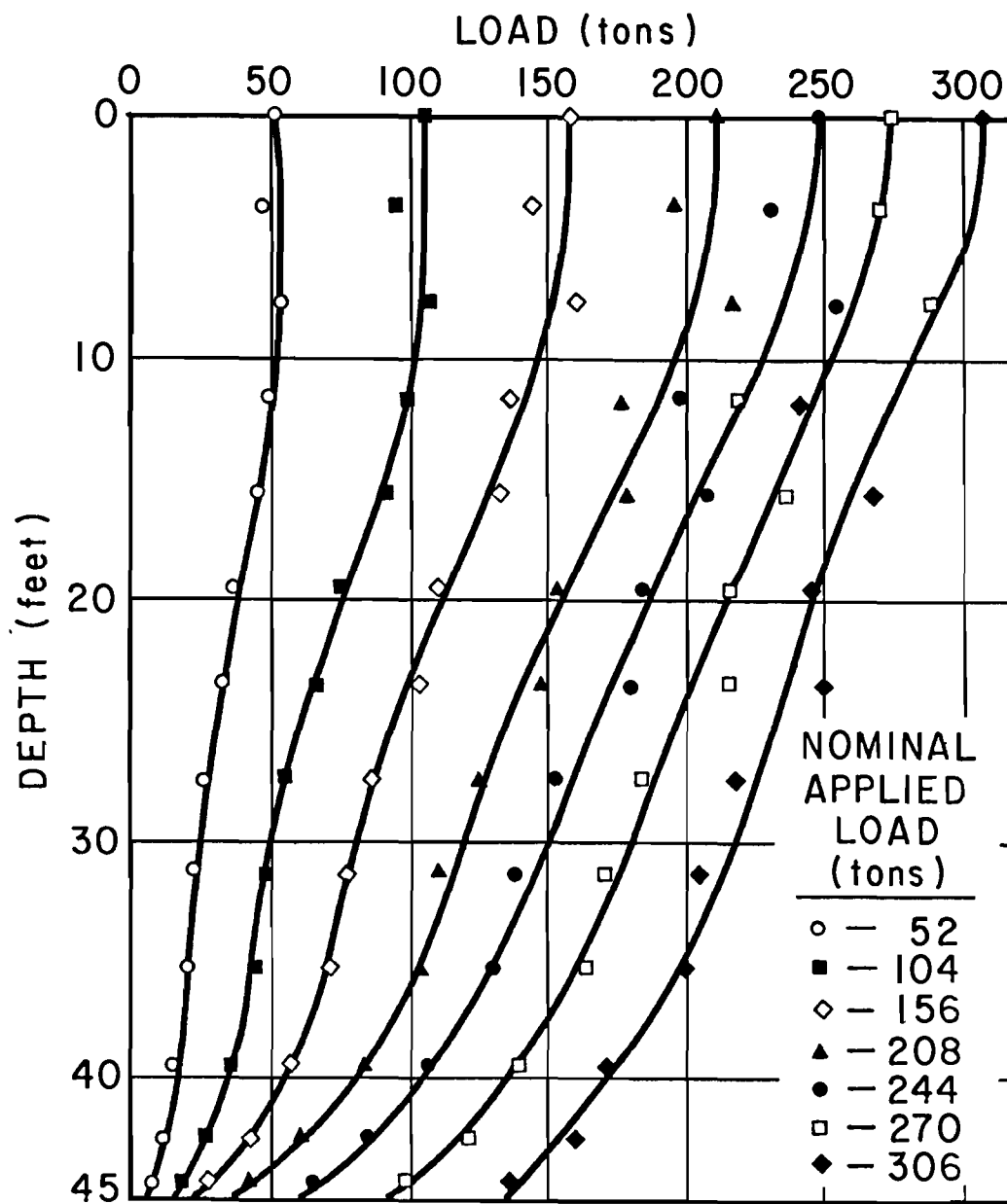


Fig. 12.45. Load Distribution Curves for S4T2

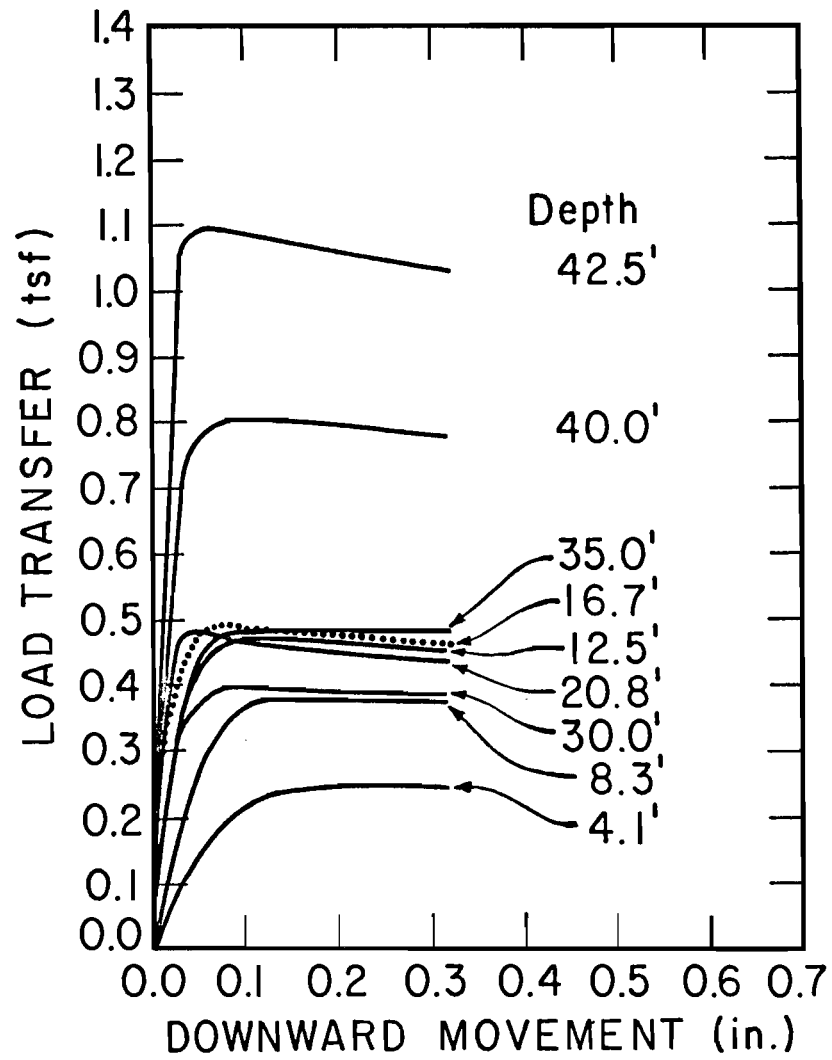


Fig. 12.46. Load Transfer Curves for S4T2

where bond between concrete and soil was weakest, near the center of the shaft. Wedging apparently continued near the top of the shaft.

Figures 12.47a and b give plots of developed shear stress and α_z versus depth at various stages of loading. The shapes of the curves are similar to those obtained for S4T1 at corresponding values of applied load, except that there appears to be less shear stress reduction beyond the peak in the middle of the shaft. The peak shear strength reduction factor in the clayey silt was about 0.45.

Some aspects of the behavior of Test Shaft No. 4 under sustained loading are now briefly presented. Figure 12.48 shows load distribution curves at the beginning and end of the two maintained-load phases of the test. These curves demonstrate the load shedding that occurred during sustained loading. Figure 12.49 indicates the time-rate of load shedding under an applied load of 244 tons. Most of the load shedding during the 244-ton maintained-load phase occurred in the first hour after load was attained. Figure 12.50 indicates the butt settlement versus time during the 244-ton maintained-load phase.

A comparison of load transfer behavior between S4T1 and S4T2 for four representative levels is given in Fig. 12.51. Less difference in load transfer behavior occurred upon reloading in Test Shaft No. 4 than in the other shafts. The greatest differences between S4T1 and S4T2 were at the 30-foot level, where no post-failure dropoff occurred in S4T2, and the 40-foot level, where the peak resistance was somewhat less in S4T2.

The shear strength reduction factors for both S4T1 and S4T2 may be broken down into the components acting on the part of the shaft drilled wet (above 40 feet) and the part drilled dry (below 40 feet). The results

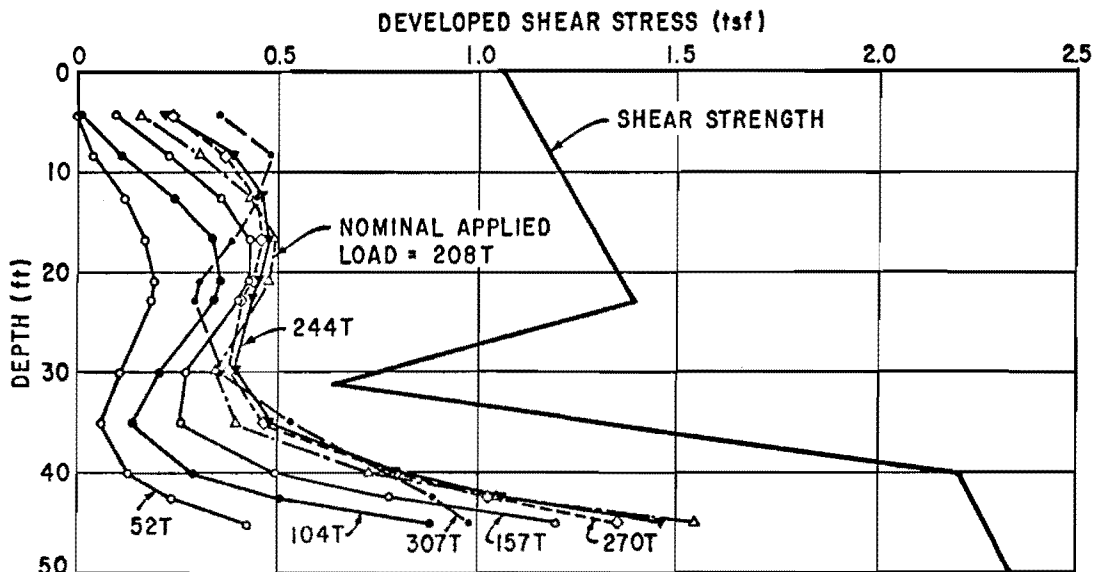


Fig. 12.47a. Distribution of Developed Shear Stresses for S4T2

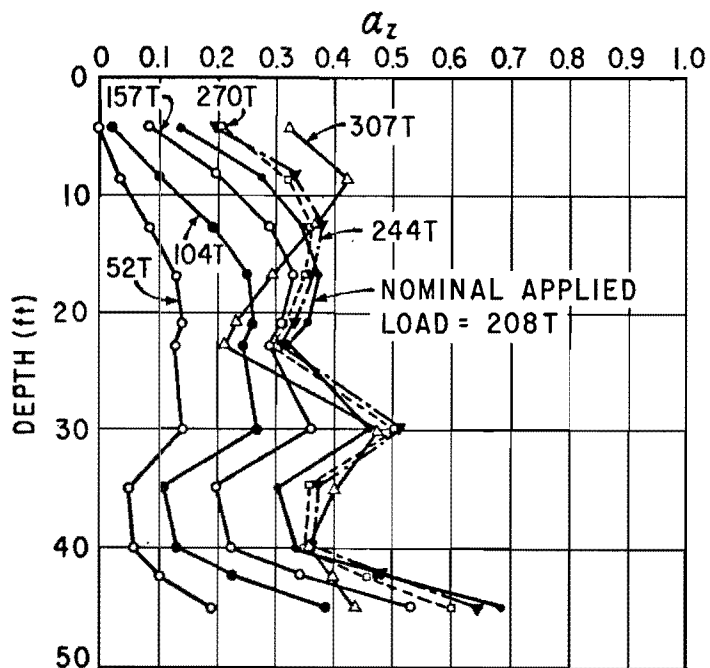


Fig. 12.47b. α_z Versus Depth for S4T2

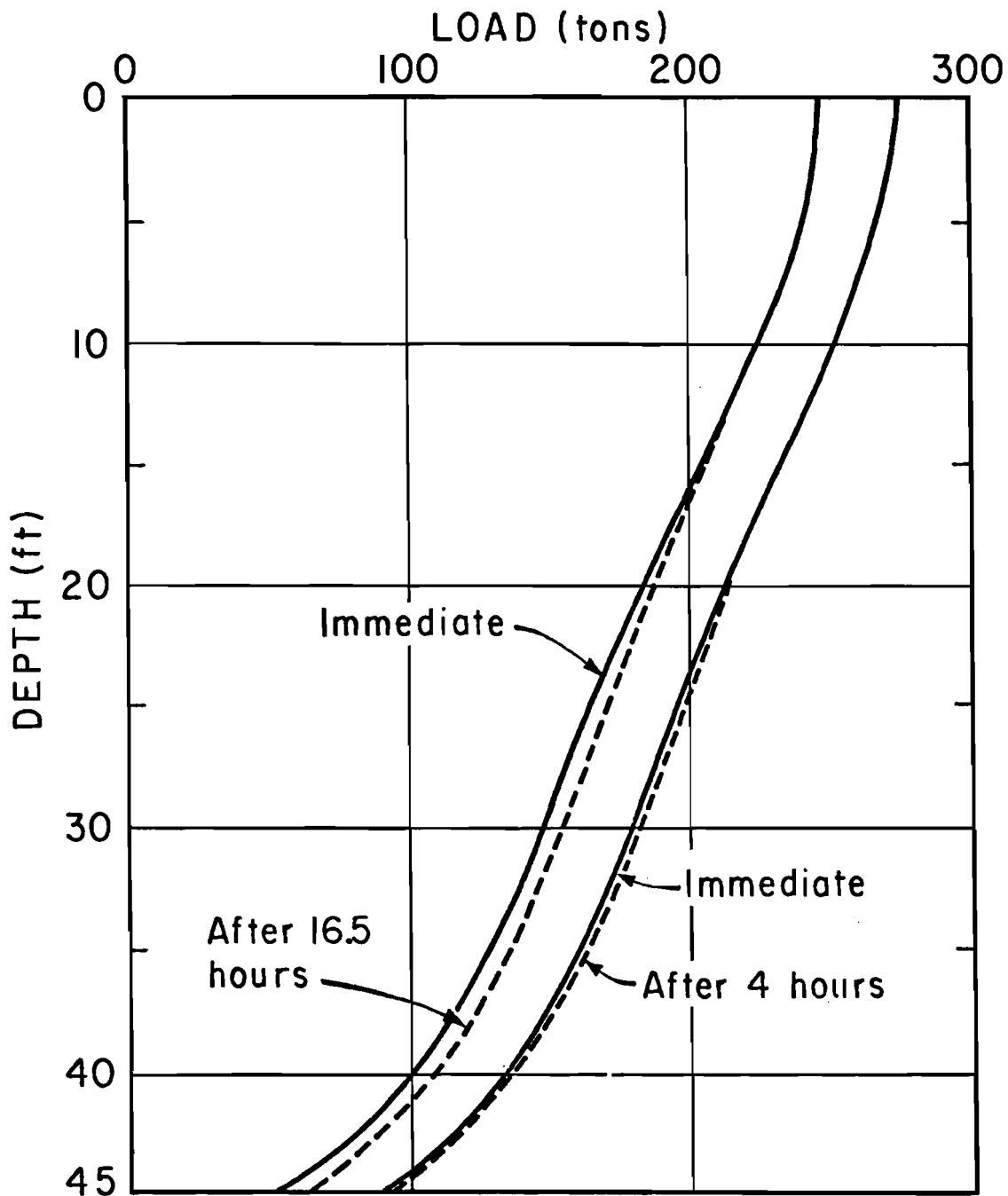


Fig. 12.48. Comparison of Load Distribution Curves Obtained Immediately After Loading and After the Passage of Several Hours, S4T2

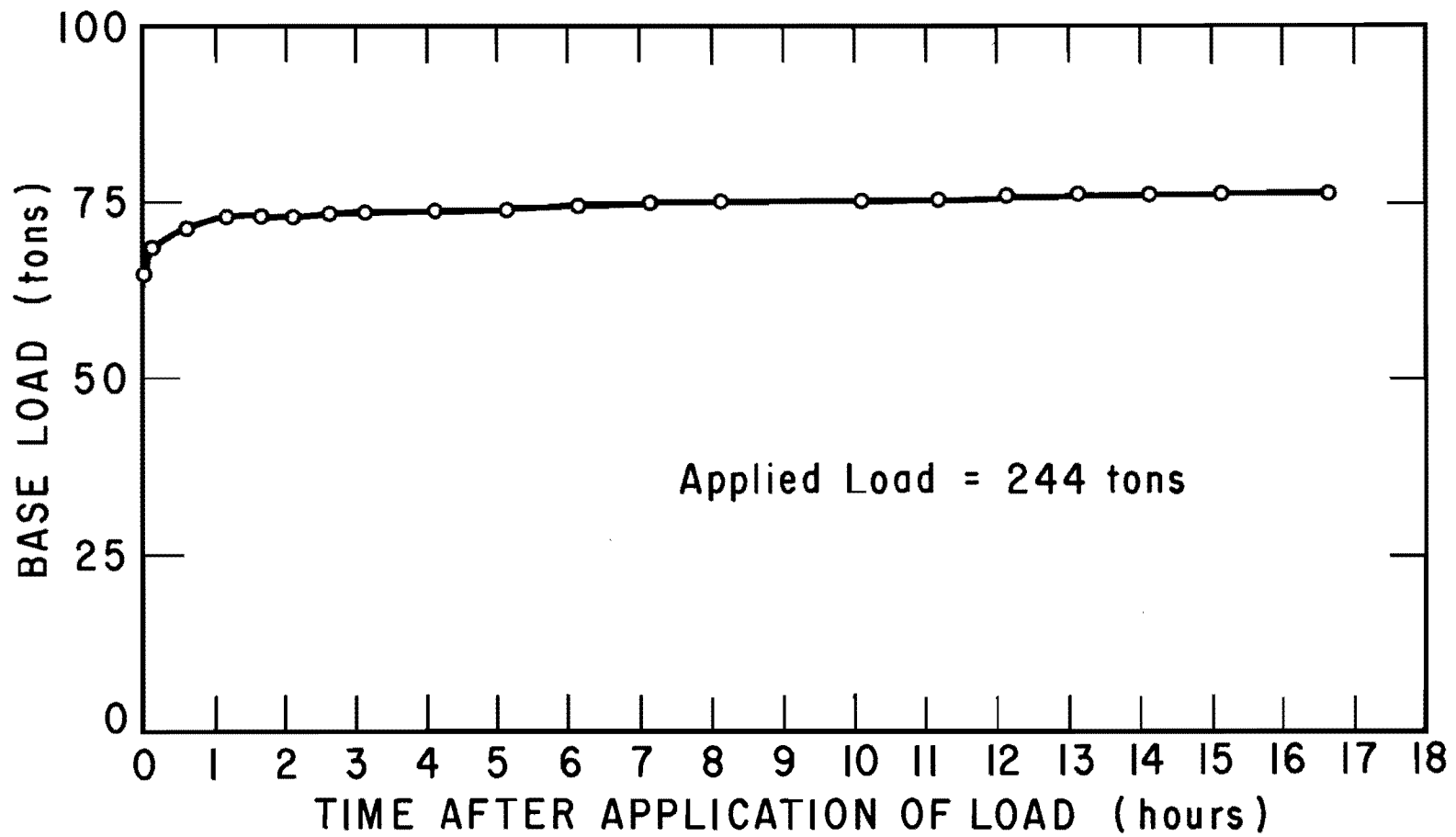


Fig. 12.49. Base Load Versus Time, S4T2, Applied Load of 244 Tons

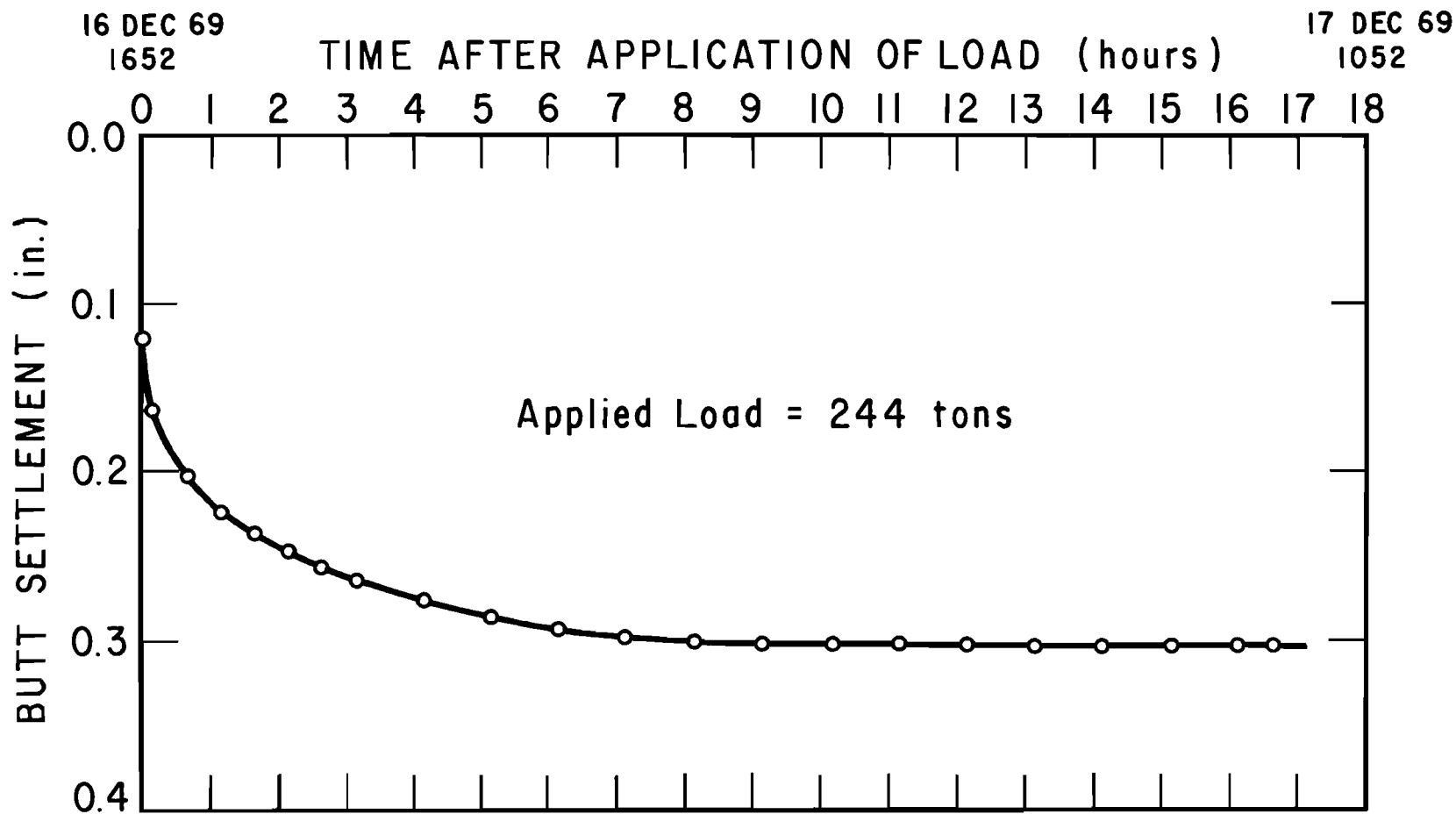
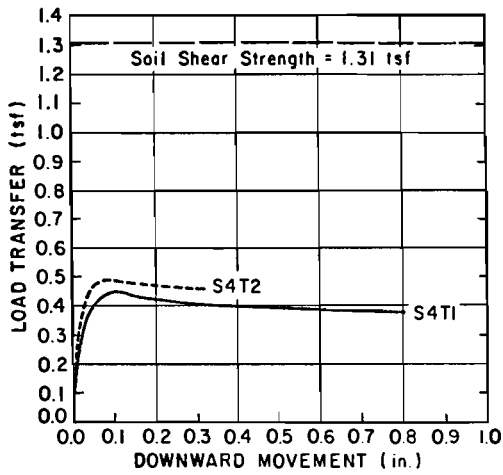
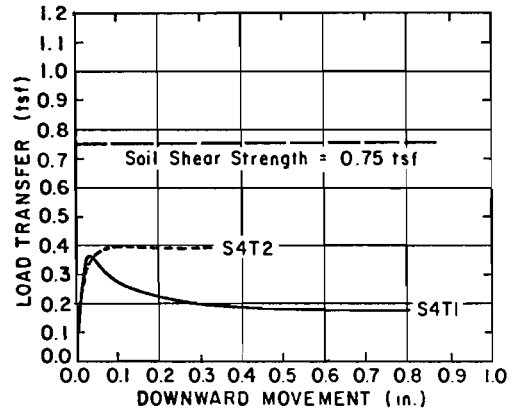


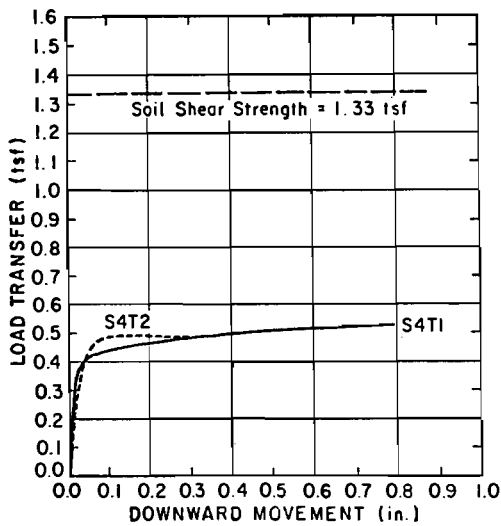
Fig. 12.50. Butt Settlement Versus Time, S4T2, Applied Load of 244 Tons



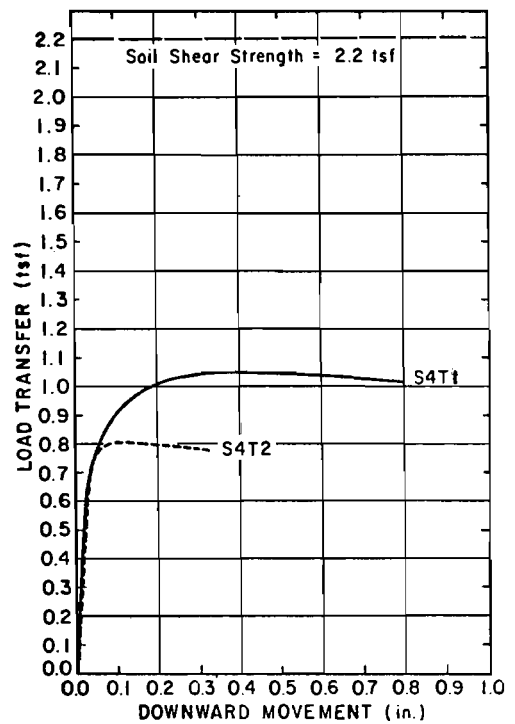
a. Depth: 16.7 Feet



b. Depth: 30 Feet



c. Depth: 35 Feet



d. Depth: 40 Feet

Fig. 12.51. Comparison of Load Transfer Behavior for S4T1 and S4T2

of such a delineation are shown in Table 12.1 for both peak and ultimate load transfer. If the assumption is made that the installation process is the only factor controlling load transfer behavior, it can be inferred from Table 12.1 that use of the wet drilling technique described in Chapter II can reduce the shear strength reduction factor by nearly half.

It is also of interest to note that the reported values for α_{avg} above 40 feet include the effects of wedging in the top few feet of the shaft, which was oversized. The amount of load removed by the wedging action can be estimated by examining the load transfer curves given in Fig. 12.42. Had no wedging occurred, the load transfer relationship for the 4.1- and 8.3-foot levels would have presumably peaked or become horizontal at a downward displacement of about 0.2 inches. If the tacit assumption is made that all resistance offered below a displacement of 0.2 inches was due to side friction and all resistance after a displacement of 0.2 inches was caused by collar bearing, the average maximum load transfer due only to side friction in the top ten feet was about 0.4 tsf. That value corresponds to a total maximum load transfer of about 33 tons in the top ten feet of the stem, compared to the approximately 48 tons actually measured.

Although this method of differentiating between load transfer due to shear and bearing is somewhat arbitrary, it does provide a rough estimation of the true load transfer due to shear only. If the 15 tons transferred in bearing in the top ten feet is subtracted from the 142 tons transferred above a depth of 40 feet, the peak and ultimate shear strength reduction factors both become 0.30 for that section of the shaft.

TABLE 12.1. SHEAR STRENGTH REDUCTION FACTORS ABOVE AND BELOW 40 FT.,

TEST SHAFT NO. 4

Test	Peak Load Transferred (tons)		Ultimate Load Transferred (tons)		Peak α_{avg}		Ult α_{avg}	
	Above 40'*	Below 40'**	Above 40'	Below 40'	Above 40'	Below 40'	Above 40'	Below 40'
S4T1	142	60	142	50	0.34	0.64	0.34	0.53
S4T2	138	46	131	37	0.33	0.49	0.31	0.39

* 422 tons maximum available from soil ($\alpha = 1$)

** 94 tons maximum available from soil ($\alpha = 1$)

It is also possible that the tabulated values for α below 40 feet are somewhat high. As discussed later, the measured bearing capacity factor N_c for the base of S4 was 12.6, instead of about 9 as measured for the other three shafts. One reason for a larger bearing capacity factor for S4 is an underestimation of shear strength for the soil in Layer IV, in which the bottom few feet of S4 was located. If the average shear strength of the soil in Layer IV were increased to such a value that the calculated value of N_c becomes equal to 9 for S4T1, the peak α factor for S4T1 below a depth of 40 feet is reduced from 0.64 to about 0.53.

S4T3. S4T3, the last axial load test at the SH225 test site, was conducted between 1100 and 1300 on June 17, 1970. Prior to the test, soil had been removed from around the top 24 feet of the stem. Considerable sloughing of soil into the void around the stem occurred between the time of excavation and S4T3, but the soil in the void was extremely loose and offered insignificant shearing resistance.

S4T3 was conducted to establish calibration constants for the top several levels of cells, as mentioned previously. The load was applied by a single jack and was somewhat eccentric. As the applied load was increased above 200 tons, some lateral movement of the freestanding portion of the shaft was visible. The load was increased until local failure of the loading box occurred at an applied load of 250 tons. The shaft had not plunged at that time, so no direct estimate of the amount of load transfer which had occurred in the top 24 feet in the first two tests was possible.

The load-settlement curve for S4T3 is shown in Fig. 12.52. All load was removed in one increment as soon as failure of the loading box was observed. Since S4T3 was not a test to failure, no load distribution data were reduced, and no base and side load-settlement graphs were obtained.

The average cell response as a function of applied load is shown for the top seven levels (in the freestanding part of the shaft) in Fig. 12.53. The initial slopes of those curves were used as calibration constants for data reduction in S4T1 and S4T2. The shaft was apparently unsymmetrical at the 12- and 16-foot levels, causing the pronounced curvature in the response relationships as bending increased.

Individual cell responses indicated that the applied load was eccentric from the beginning and that the eccentricity increased with applied load. Cells at the 24-foot level indicated that the shaft developed a horizontal tension crack at that depth as the loading box failed and the moment increased. (One cell showed a sudden increase in tension, while the cell on the opposite side of the shaft showed a corresponding increase in compression.) The large moments produced tension readings in cells at several levels above an applied load of 200 tons. No significant difference in cell sensitivity in tension and in compression was observed.

An additional objective of S4T3 was to gain some information concerning the errors involved in measuring applied loads by metering jack pressure. Therefore, applied load was measured directly with a load cell placed between the piston and the loading box as well as by the electrical pressure transducer in S4T3. A swivel-head leveling block was placed between the piston head and the load cell to protect the load cell in the

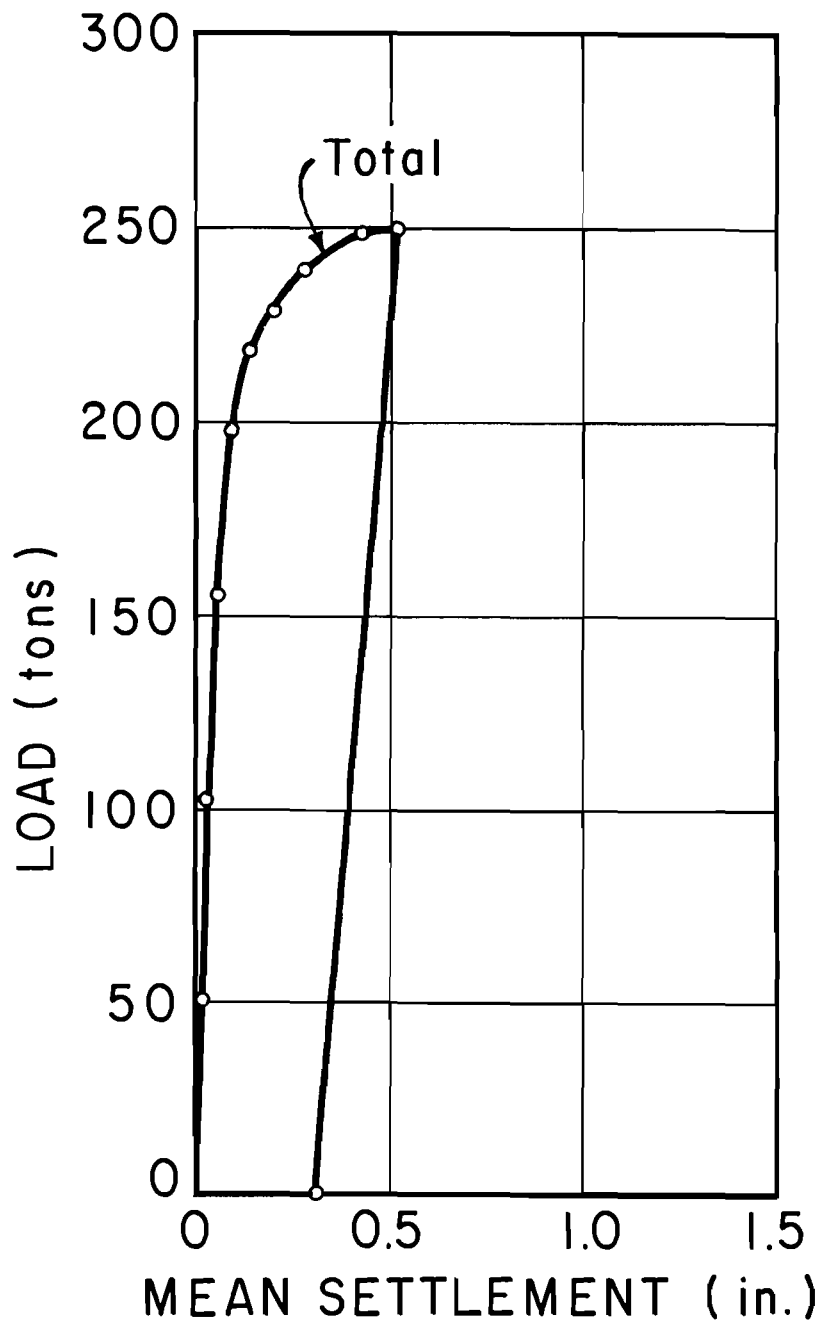


Fig. 12.52. Load-Settlement Curve for S4T2

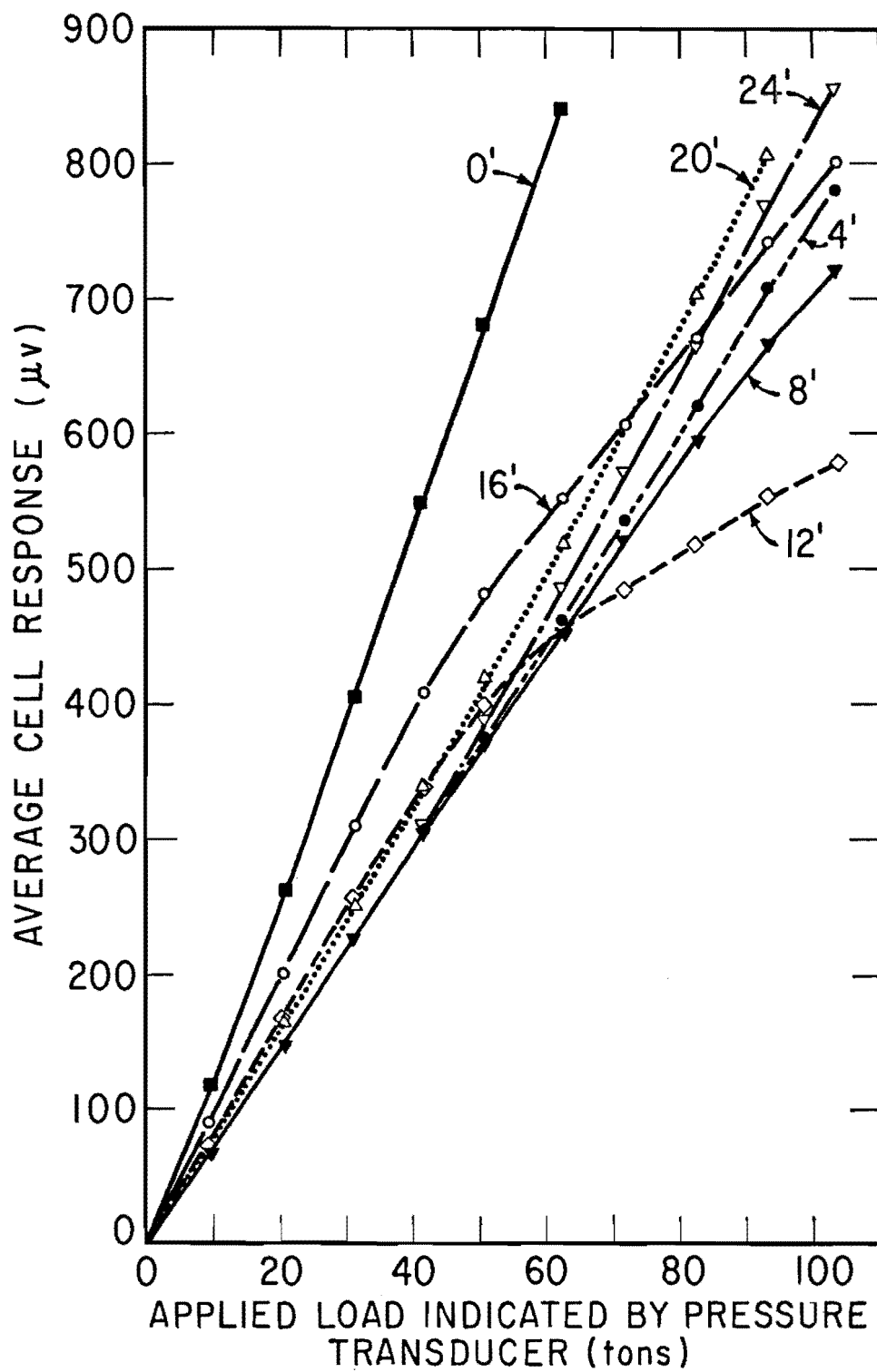


Fig. 12.53. Average Mustran Cell Response Curves for Top Seven Levels of Cells, S4T3

event that large eccentricity developed on the piston. The swivel-head block probably caused the piston friction to be somewhat lower than it would have been had the swivel head not been present (as was the case for all other tests at the SH225 test site). However, the amount of eccentricity in applied load for S4T3 was much greater than that for any other test at the SH225 site. Thus, the errors indicated by this test are assumed to be representative of the maximum expected error in the field test program due to jack friction. Rotation of the swivel-head block at high load, produced by unsymmetrical yielding of the loading box, caused S4T3 to be terminated prematurely. The load cell and swivel-head block, shown in Fig. 12.54, were rented from Bayou Industries Company, Channelview, Texas. Figure 12.54 also shows a spacer used to position the jack, since the distance between the loading box and butt had been increased because the large reaction beams and loading box that had been used for S4T2 had been replaced by the smaller beams and the light loading box that had been used for S3T1.

The results of the load calibration are shown in Fig. 12.55. Perfect correlation between pressure readings and load cell would have yielded a 45-degree line. The pressure transducer indicated loads about four per cent greater than did the load cell. It is expected, therefore, that butt loads reported for this test program are probably no more than four per cent too high, which is certainly within acceptable limits considering the other sources of error in the program, particularly the uncertainties in determining soil strength.

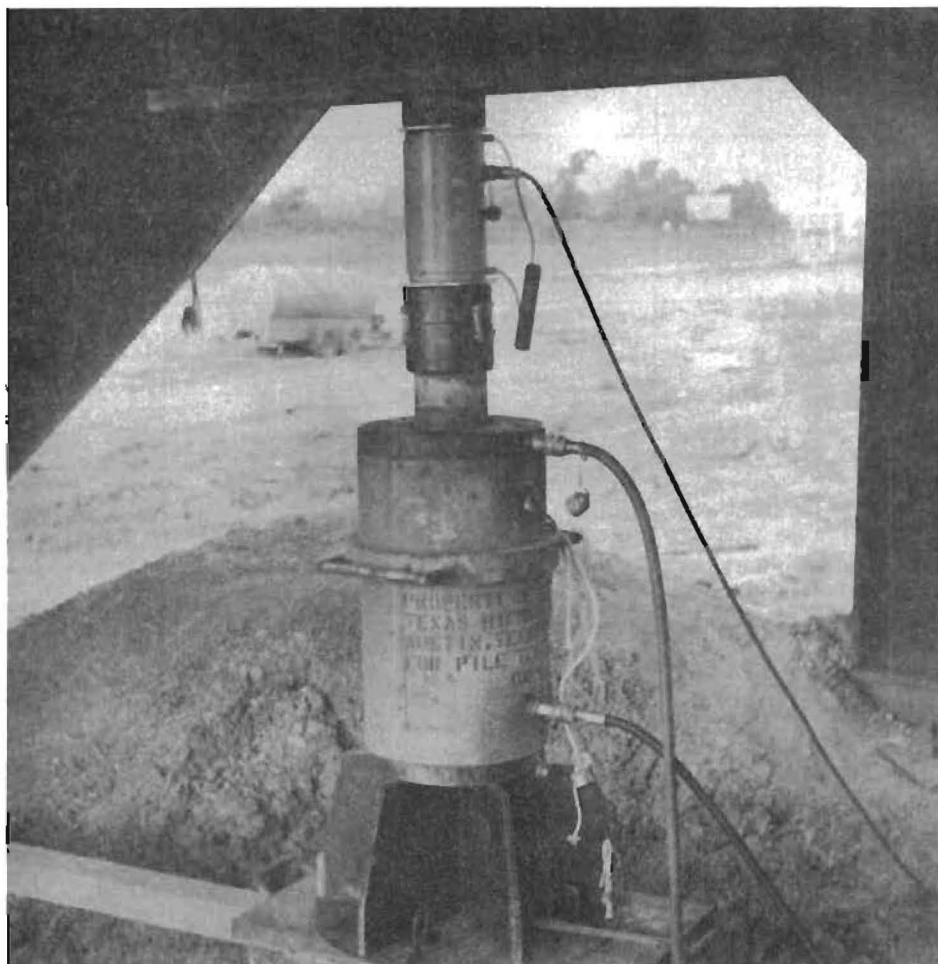


Fig. 12.54. Spacer, Hydraulic Jack, Swivel Head, Shim, and Loading Box, S4T3

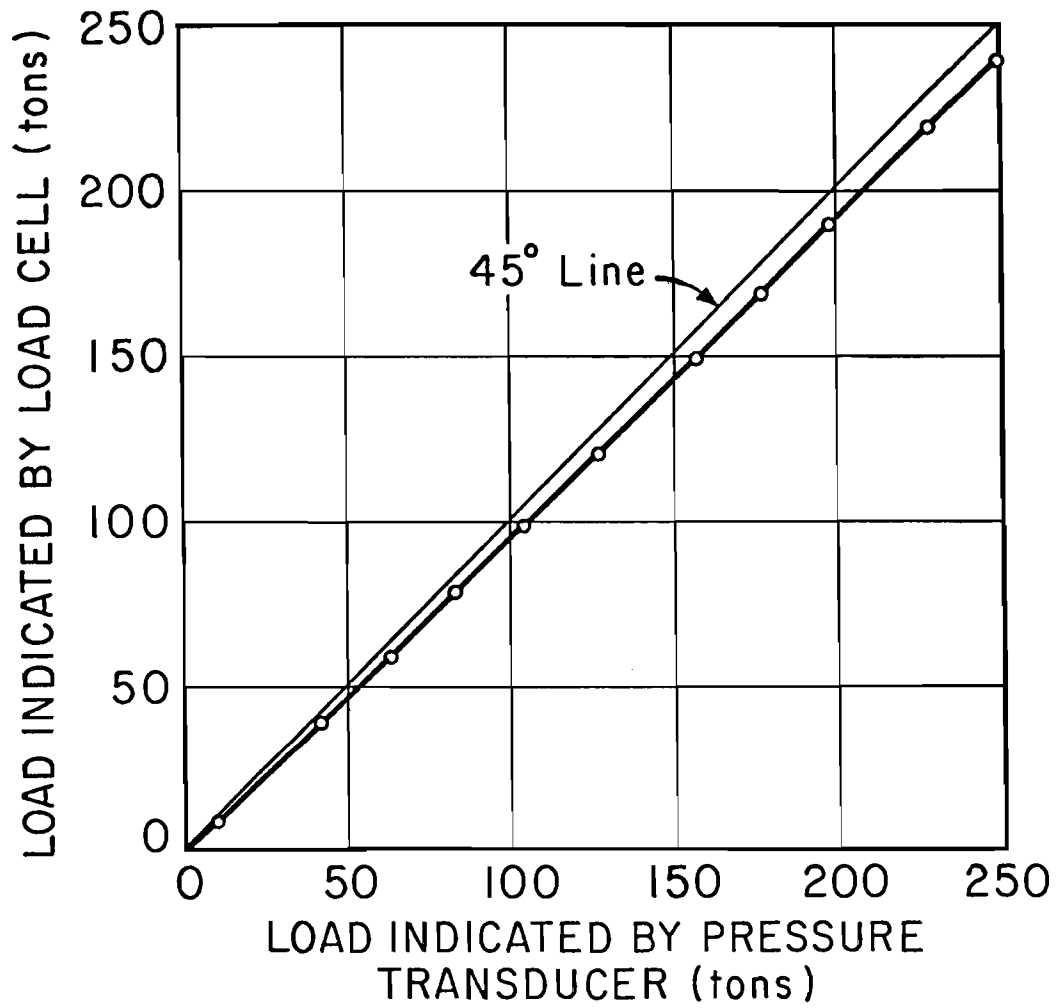


Fig. 12.55. Load Indicated by Load Cell Versus Load Indicated by Pressure Transducer, S4T3

Comparison of Test Results

Considerable information concerning the influence of various parameters on the behavior of the test shafts can be obtained by comparing the load test results that have just been presented individually for the four test shafts.

First, for purposes of reference, the butt load-settlement curves for the initial load tests discussed in the preceding section are superimposed in Fig. 12.56. The primary observation that such a comparison offers is the difference in load-settlement characteristics of straight and belled shafts and of straight shafts of differing geometries.

Useful information can be gained by contrasting the differences in side and base resistance among the test shafts. For example, Fig. 12.57 compares load distribution curves in the top 25 feet for two magnitudes of applied load. Less load has been transferred in S2T1 and S4T1 than in S1T1 and S3T1 because considerable load was picked up by the bell (S2T1) or by the lower part of the shaft (S4T1). A more significant load distribution comparison is made in Fig. 12.58, which displays curves developed at identical values of top displacement (0.045 inches), corresponding to about two-thirds of peak side resistance. If downward displacement were the only parameter affecting the development of load transfer, the shapes of the curves in Fig. 12.58 would be nearly identical, differing only in the value of applied load required to produce the prescribed displacement. However, the shapes differ appreciably near the bottoms of the stems of S1, S2, and S3, suggesting a base-side interaction effect. The slope of the load distribution curve for S4 is

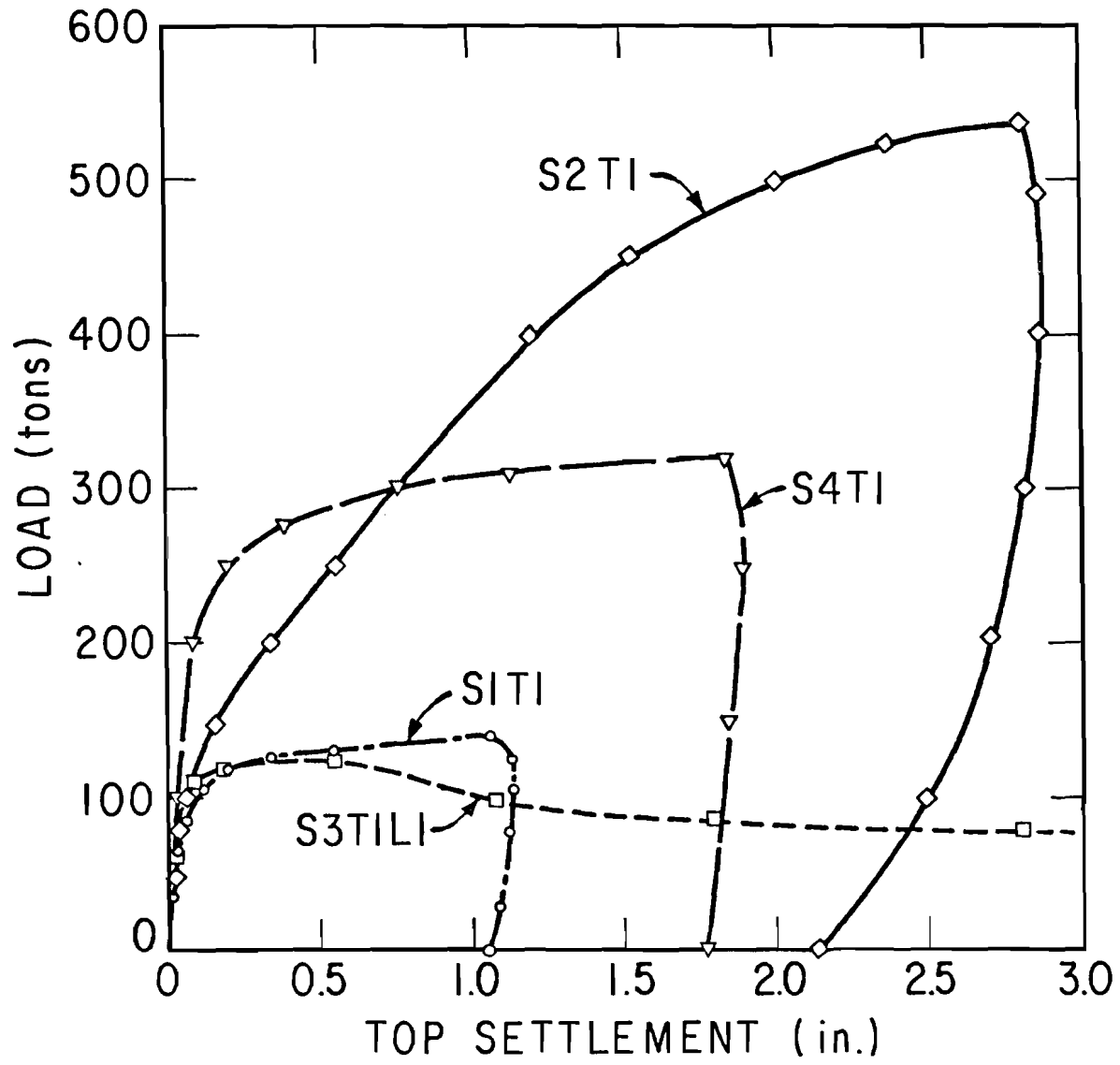


Fig. 12.56. Comparison of Load-Settlement Curves for Initial Load Tests

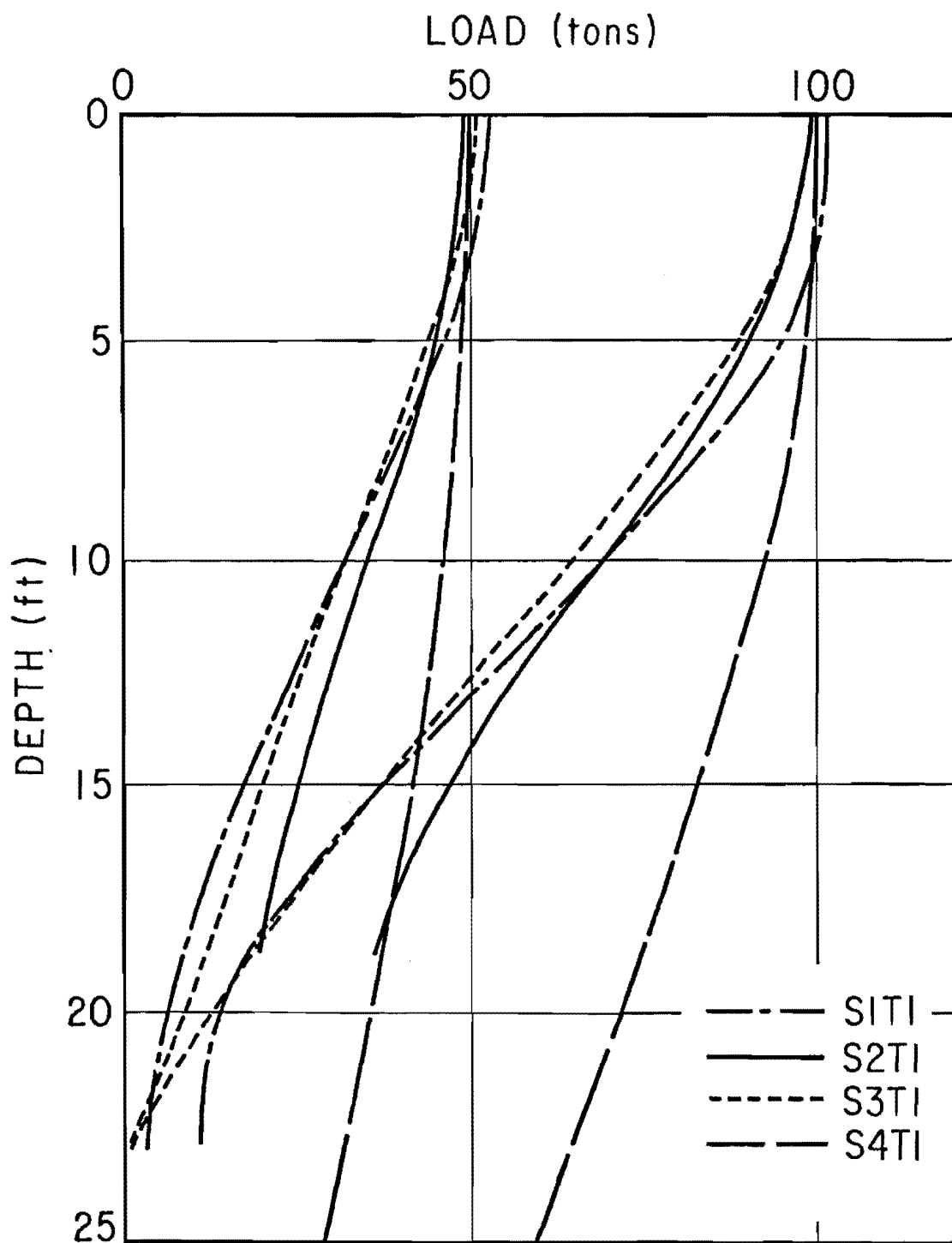


Fig. 12.57. Comparison of Load Distribution Curves at Two Magnitudes of Applied Load

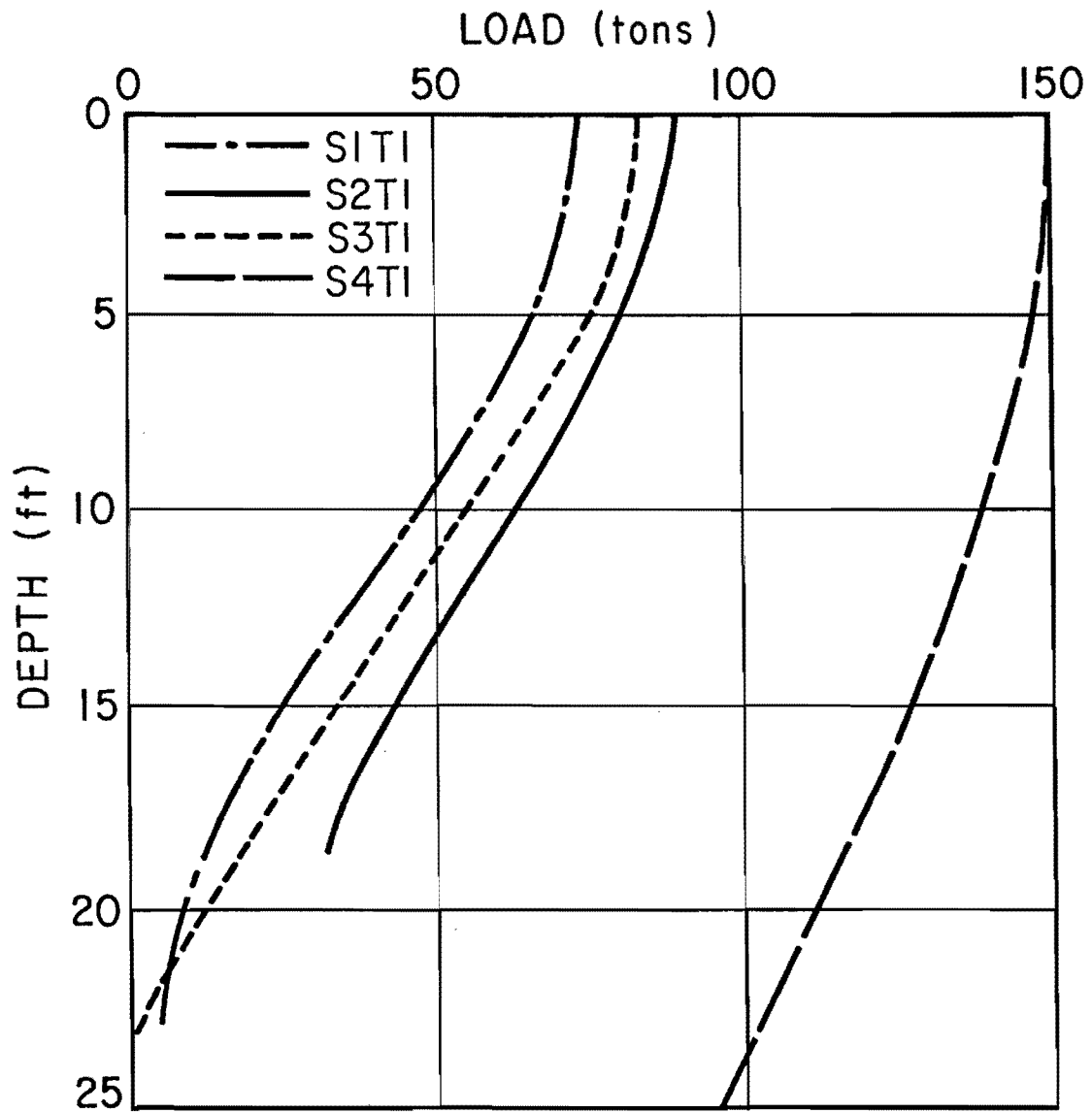


Fig. 12.58. Comparison of Load Distribution Curves at Butt Settlement of 0.045 Inches

considerably lower than those for the other three shafts, indicating considerable influence on development of side resistance from the drilling mud.

The load distribution curves near ultimate load are compared in Fig. 12.59. The curves have been normalized by translating every curve horizontally such that they originate from a common point (applied load of 130 tons). This translation was done to provide a direct visual comparison. In each case, the curve corresponding to the applied load just prior to ultimate was plotted, since the curve corresponding to ultimate load was not as precisely defined due to rapid redistribution of load. Figure 12.59 exhibits many of the same differences in shaft behavior as Fig. 12.58, which applies to shafts nearer working load. The losses in side shear capacity upon reloading are also in evidence for each shaft. The curve for S4T1 indicates a rather high load transfer near the surface because of bearing stresses against the collars and not because of high mobilized side shear stresses.

Dimensionless shear stress-versus-depth curves for the first load test on each of the four test shafts for a mean settlement of 0.045 inches are compared in Fig. 12.60. That figure clearly indicates that S4 was lagging behind in developing shearing resistance along its sides. It also shows the effect of load transfer reduction near the base in S1 and S2. Otherwise, the curves for S1, S2, and S3 are remarkably similar in the top 15 feet.

Figure 12.61 presents a similar comparison at peak developed side resistance. The curve predicted by the mortar migration study is superimposed on the stress-depth curves, indicating a rather poor

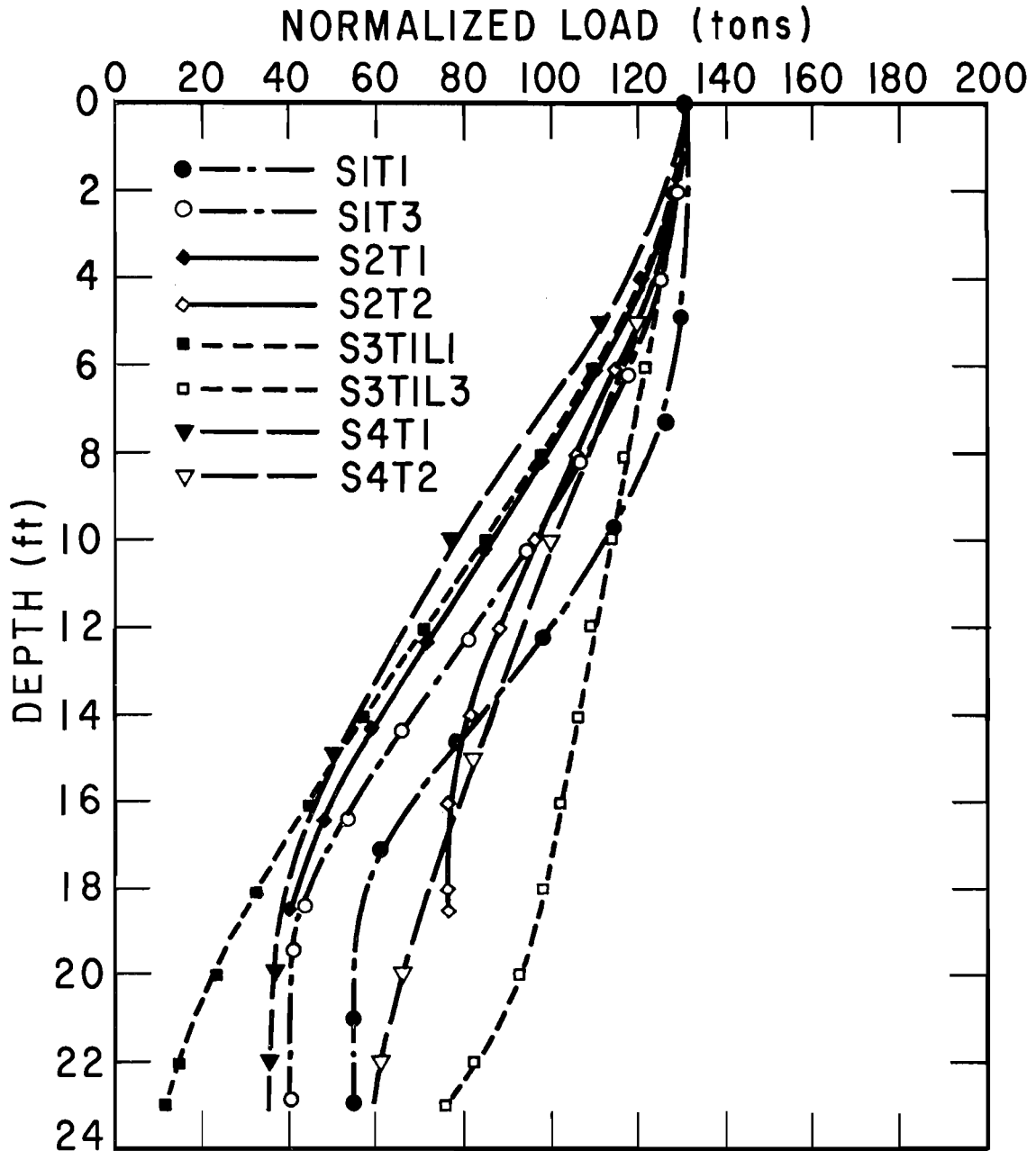


Fig. 12.59. Normalized Load Distribution Near Total Ultimate Capacity

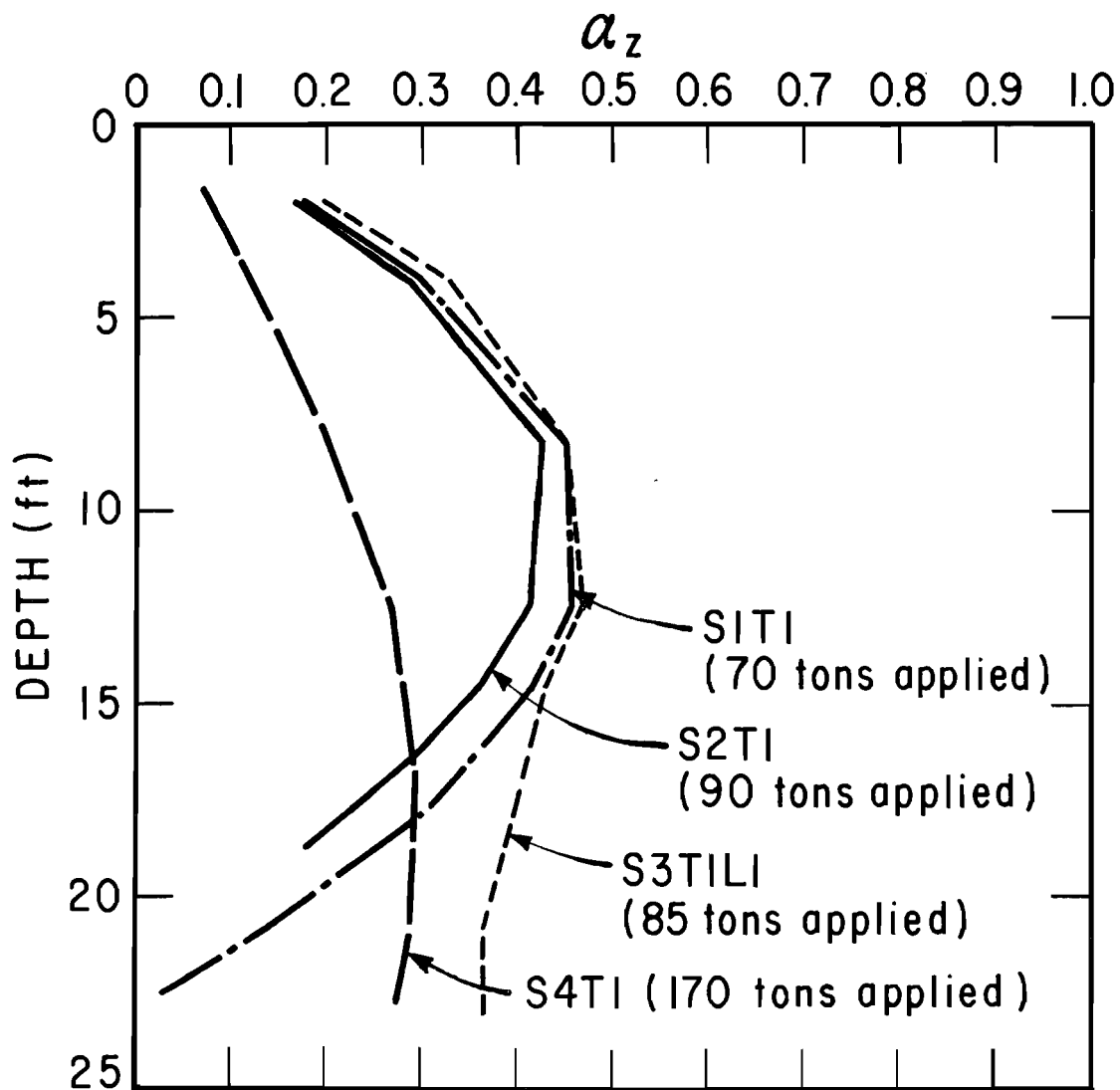


Fig. 12.60. α_z Versus Depth Curves at Butt Settlement of 0.045 Inches

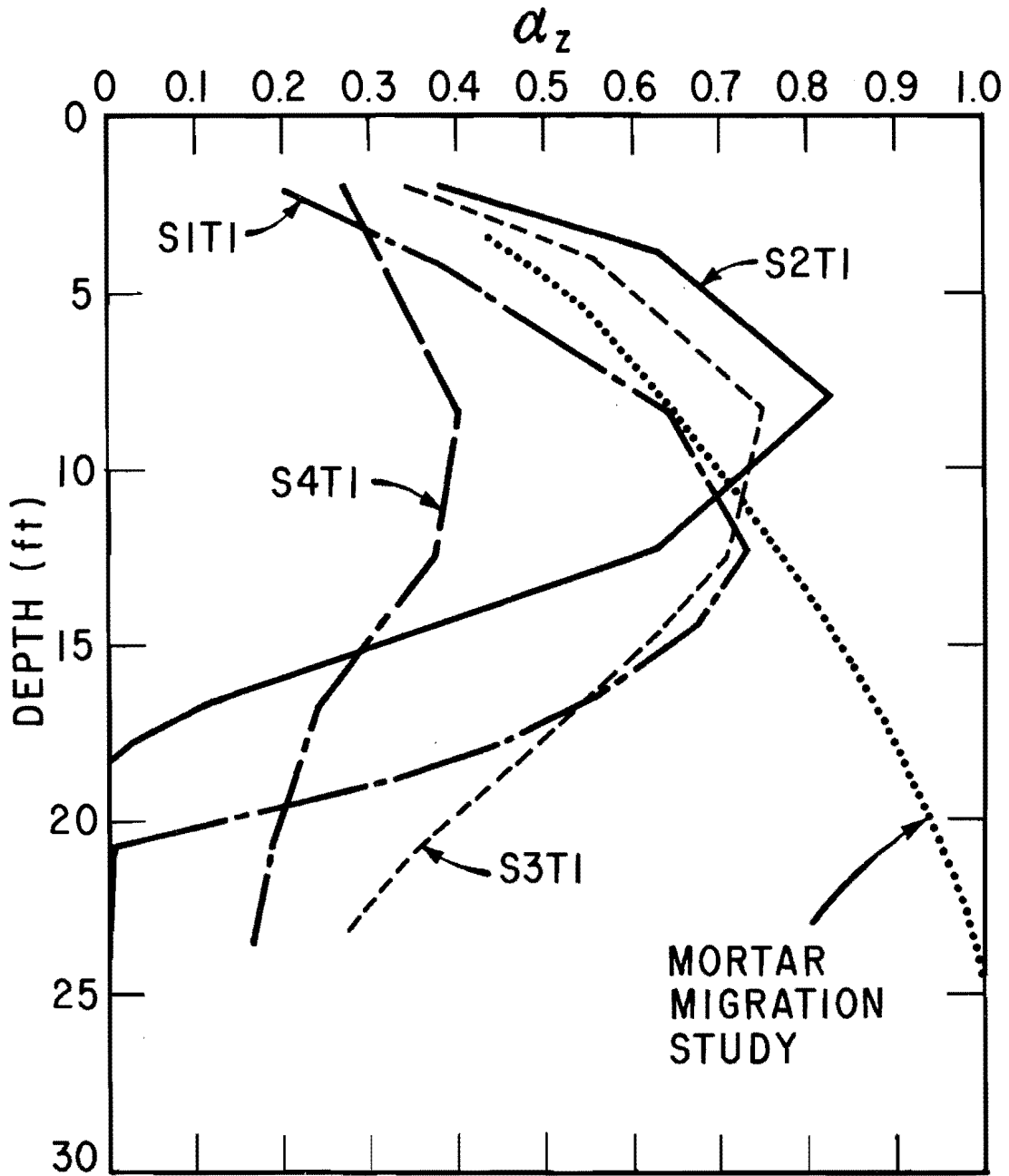


Fig. 12.61. α_z Versus Depth at Peak Side Resistance for Initial Load Tests

correlation with the shaft installed in a processed hole (S4) and correlating well with the shafts installed in the dry (S1, S2, S3) only in the top 12 feet, where, as described later, little change in moisture content in the soil adjacent to the shafts was found.

Another graphic illustration of the differences in behavior during initial loading can be found in the load transfer curve comparisons given in Figs. 12.62 through 12.65. Among the observations that can be made from these figures are:

1. The initial rate of development of load transfer with displacement is about equal, above a depth of about 20 feet, in the three shafts installed in the dry.
2. The initial rate of load transfer development for S4 (installed in a processed hole) is appreciably less than that for the other shafts at a depth of 8.3 feet due to the fact that side resistance was apparently being developed primarily in bearing against the collar which existed just above that level rather than in shear.
3. At levels where collars did not develop in S4 (for example, 14.6', 16.7'), the ultimate load transfer was considerably smaller than in S1 and S3.
4. A sharp post-peak decrease in load transfer appeared near the bases of S1 and S2 (20.8' and 16.7', respectively). A much smaller decrease appeared in S3, which had a void beneath the base.
5. Below a depth of 8.3 feet, the rate of load transfer development with displacement was smaller for S2 than for S1 and

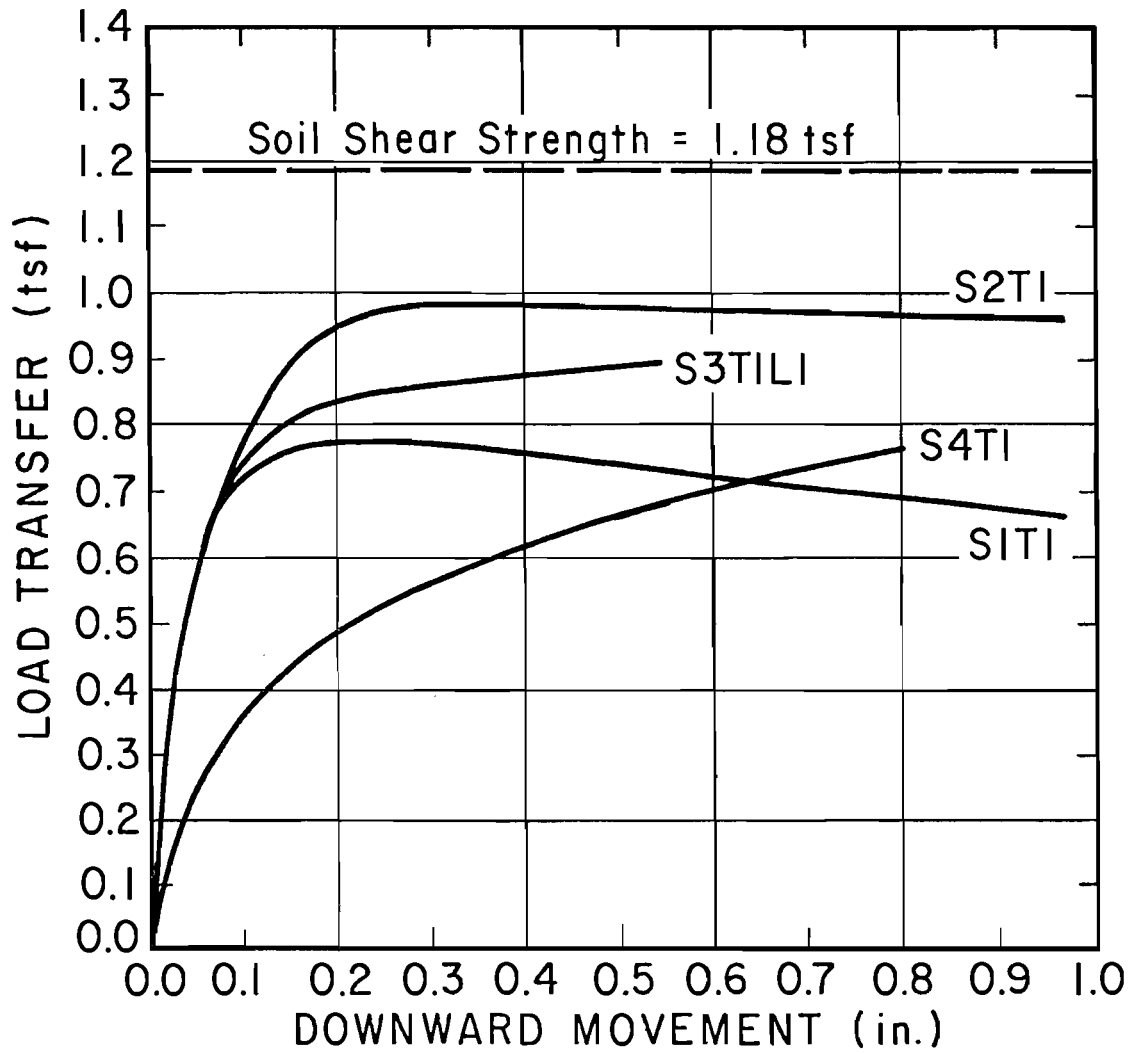


Fig. 12.62. Load Transfer Curves for Initial Load Tests, Depth: 8.3 Feet

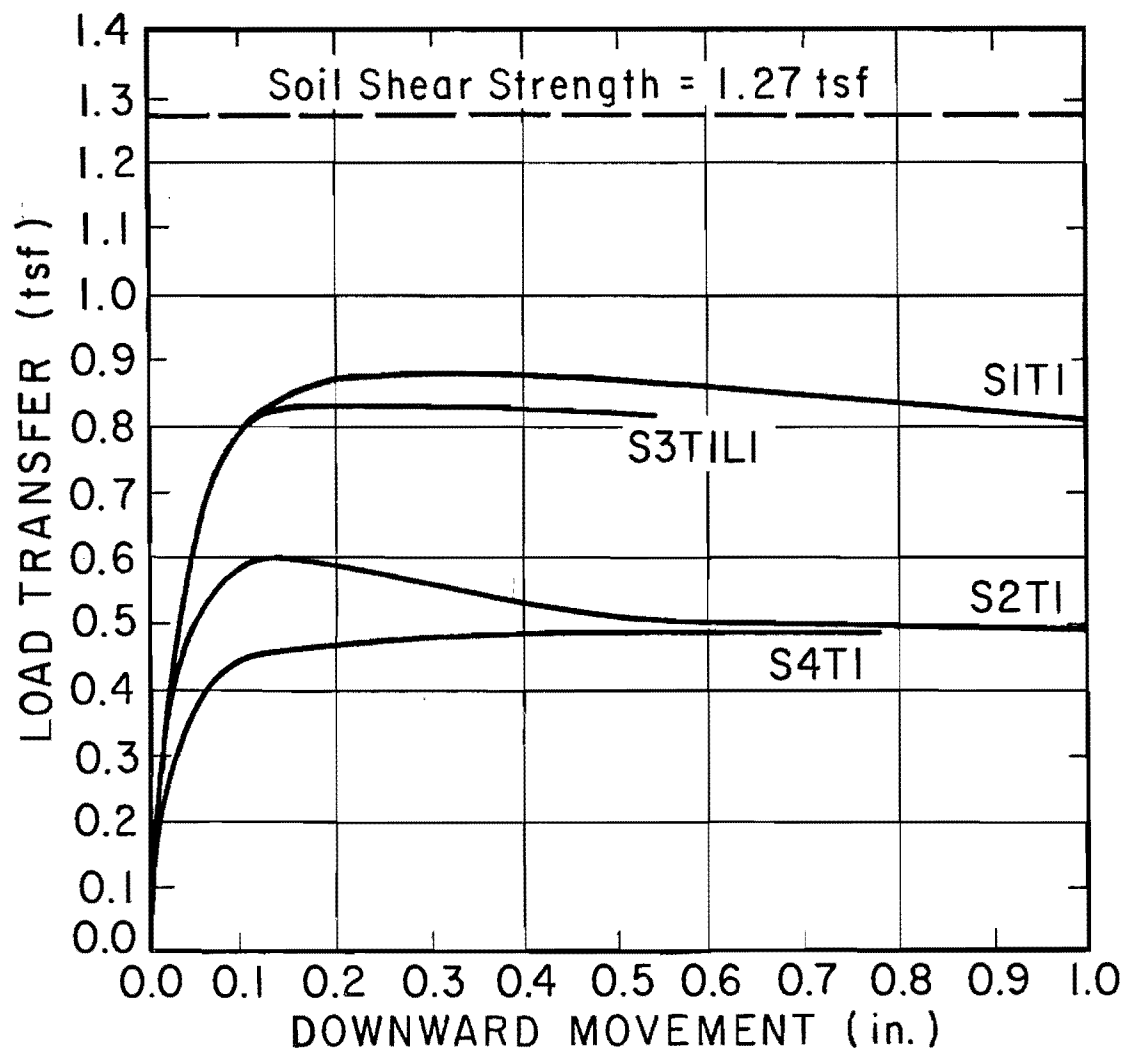


Fig. 12.63. Load Transfer Curves for Initial Load Tests, Depth: 14.6 Feet

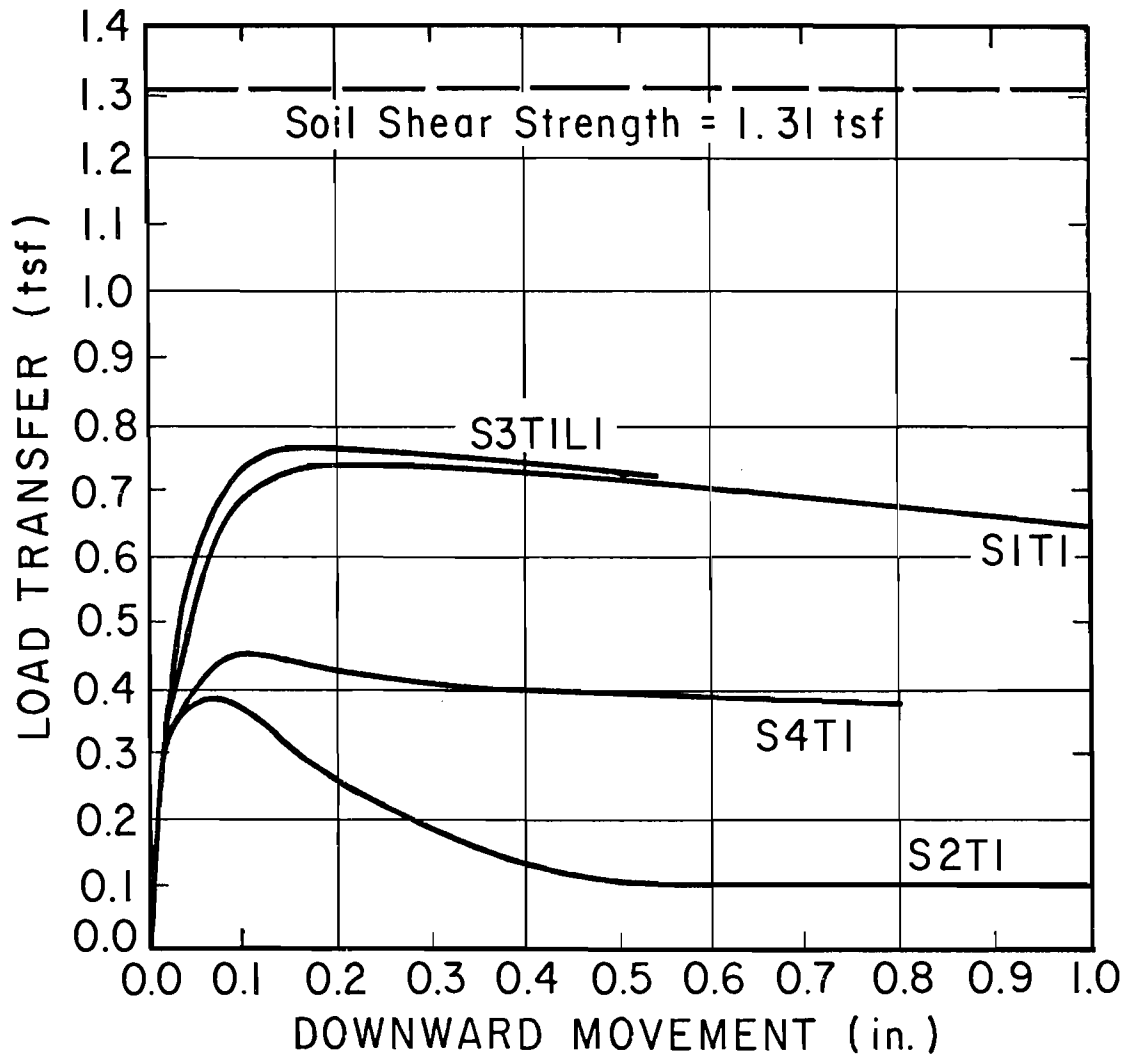


Fig. 12.64. Load Transfer Curves for Initial Load Tests, Depth: 16.7 Feet

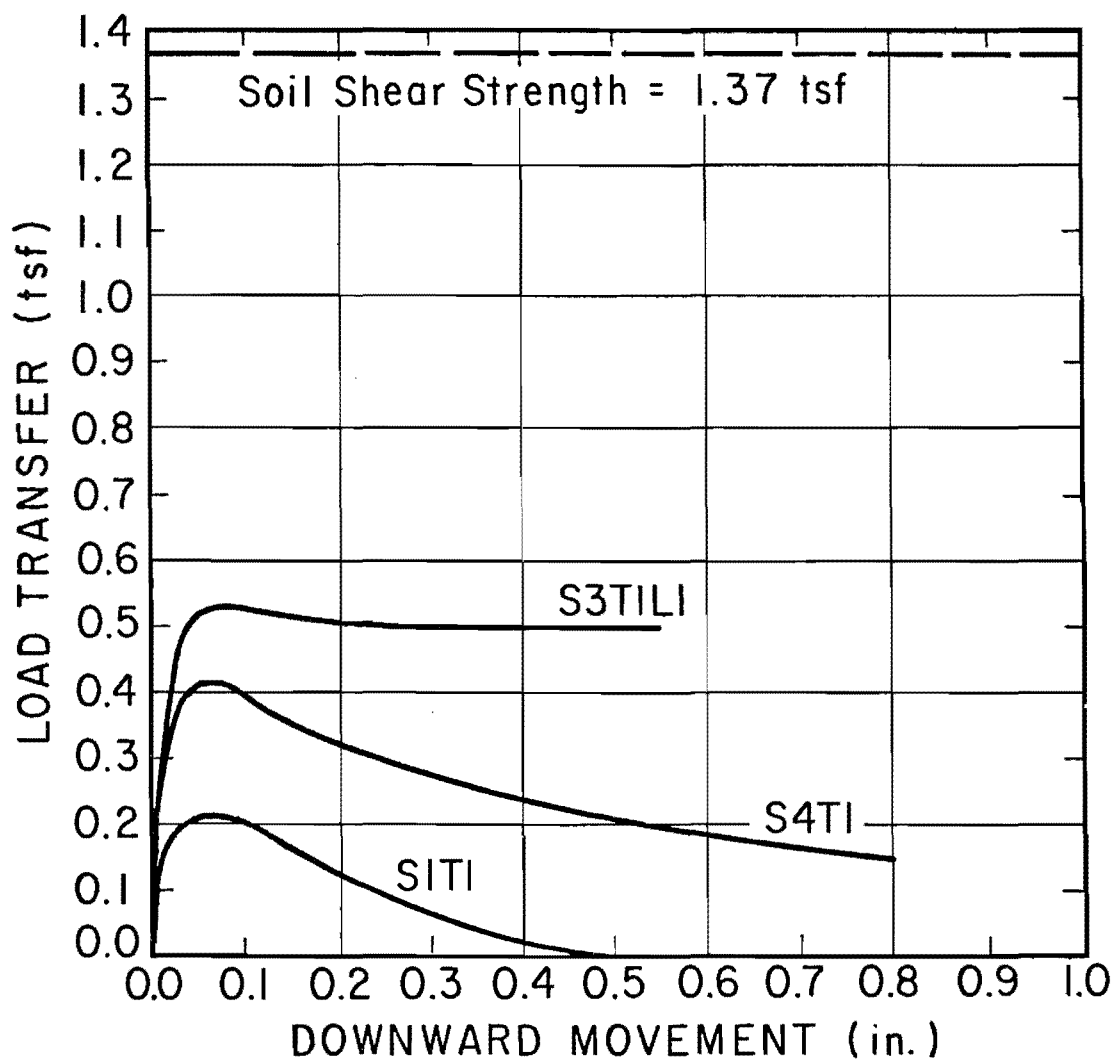


Fig. 12.65. Load Transfer Curves for Initial Load Tests, Depth: 20.8 Feet

S3, possibly because of side-base interference produced by the presence of the bell.

6. The displacement required to produce maximum load transfer in S1 and S3 was about 0.30 inches near the surface (8.3'), 0.20 inches near the middle of the shaft (14.6' and 16.7'), and 0.07 inches near the base (20.8'). Shaft 2 developed maximum load transfer at generally smaller displacements. Displacements required to mobilize maximum shear in S4 were extremely variable.

Nondimensional side and base load settlement curves, similar to those developed by Whitaker and Cooke (1966) for shafts in London Clay (Fig. 4.4), are shown in Figs. 12.66 through 12.69. The relationships given in Figs. 12.66 and 12.68 are for initial loadings, while those in Figs. 12.67 and 12.69 are for the second loadings. The average side load-settlement relationship published by Whitaker and Cooke for tests on five shafts with a 30.75-inch stem diameter at the Wembley test site is superimposed on the curves obtained for the SH225 tests in Fig. 12.66. The curve developed by Whitaker and Cooke indicates that slightly more displacement was required to develop the same degree of mobilization as the SH225 test shafts, presumably due to the differences in soil properties and testing procedures employed.

The nondimensional side load-settlement curves are, in effect, average nondimensional load transfer curves for the shafts. They infer that overall average load transfer is developed at about the same rate regardless of shaft geometry or maximum side capacity.

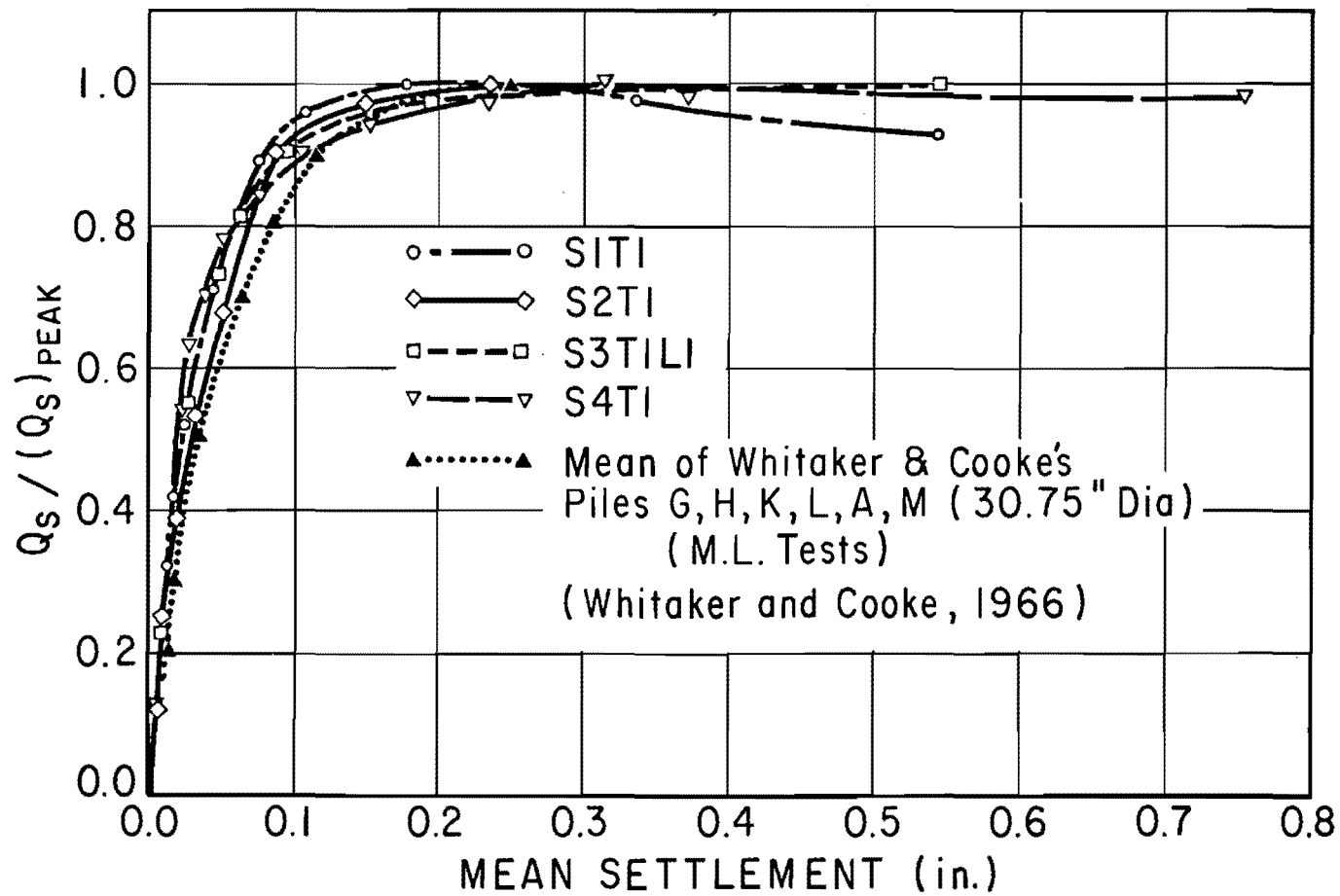


Fig. 12.66. Dimensionless Side Load-Settlement Relationships for Initial Load Tests

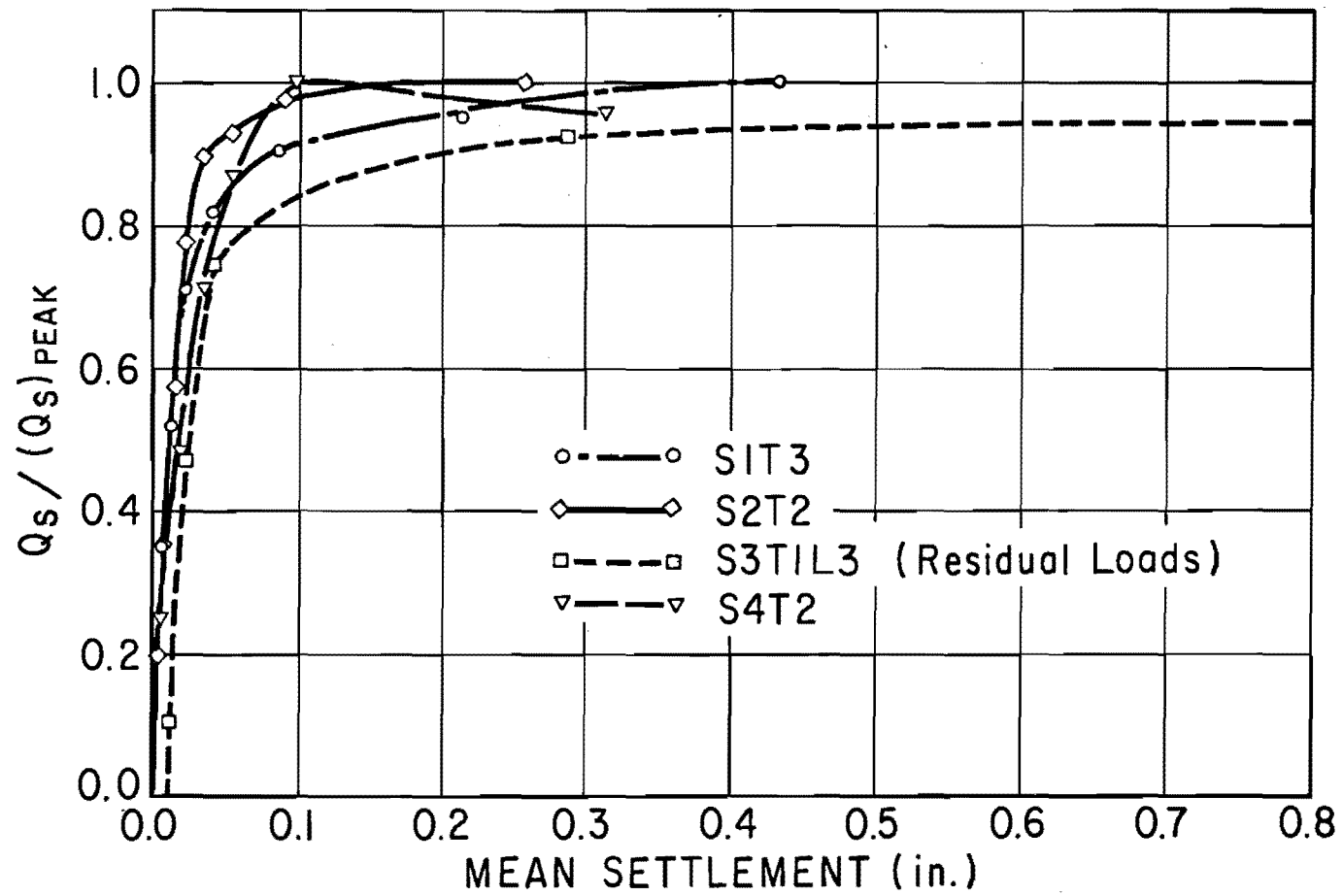


Fig. 12.67. Dimensionless Side Load-Settlement Relationships for Reloading

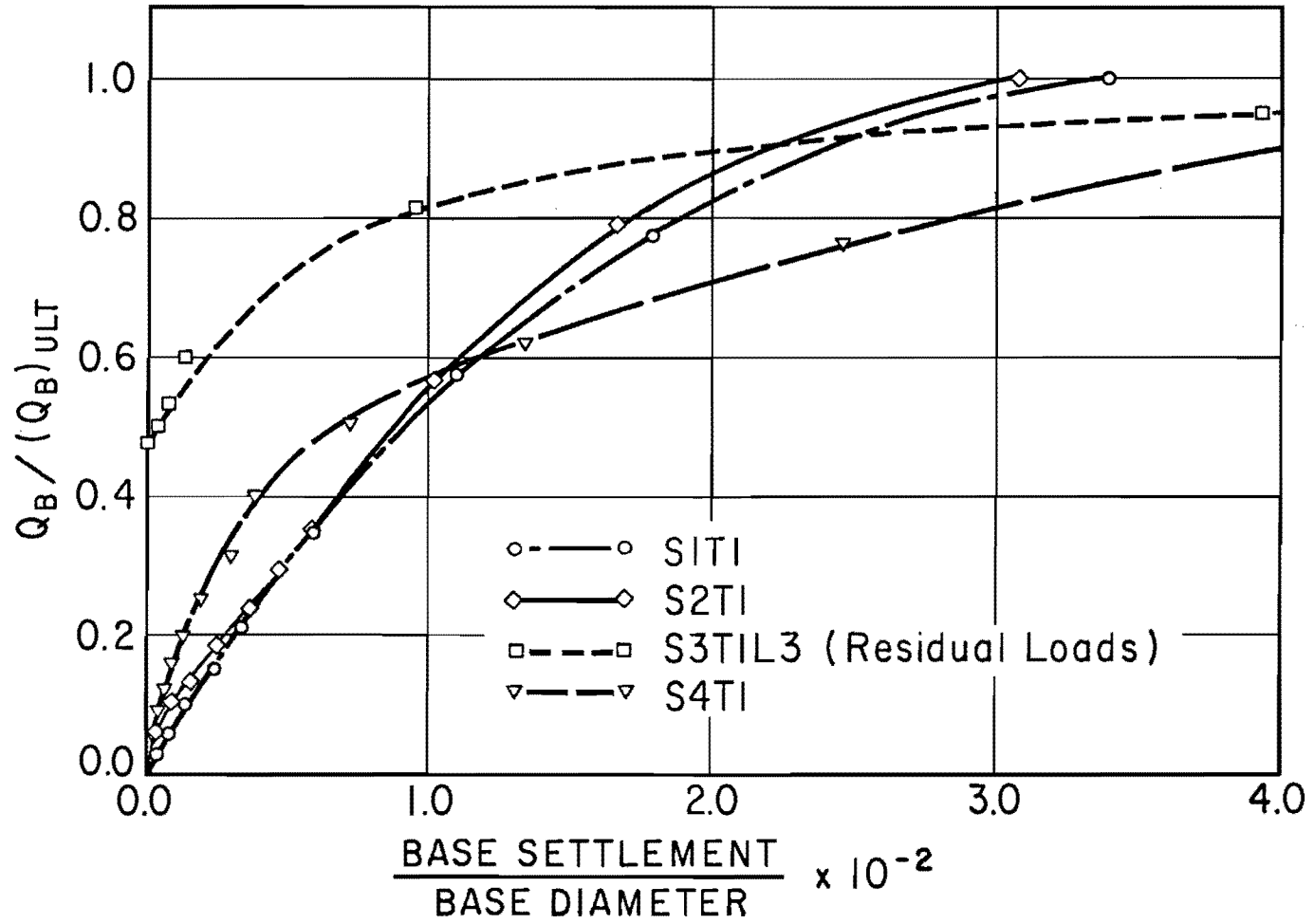


Fig. 12.68. Dimensionless Base Load-Settlement Relationships for Initial Load Tests

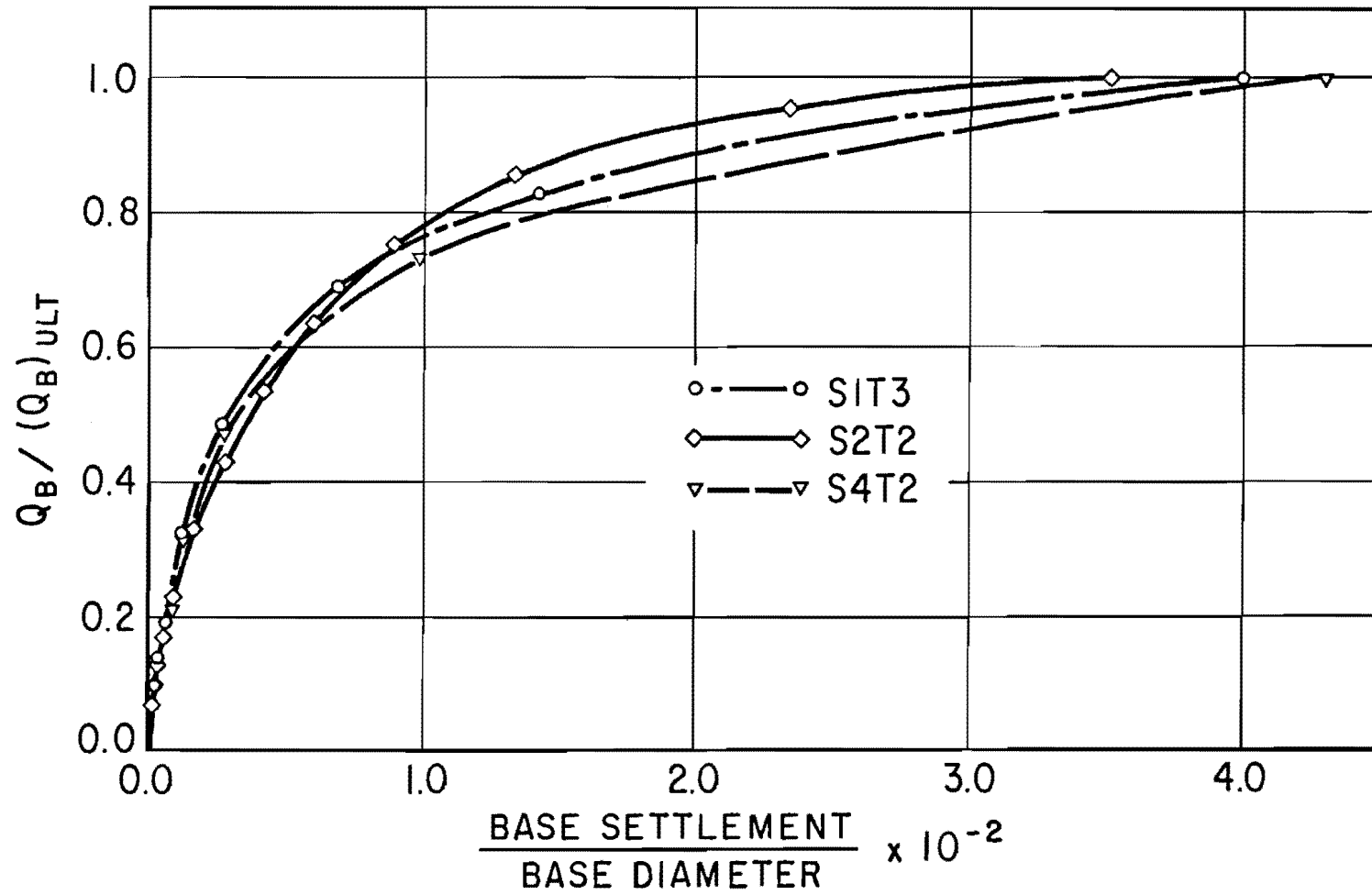


Fig. 12.69. Dimensionless Base Load-Settlement Relationships for Reloading

The peak side resistance was reached at a displacement of 0.20 to 0.25 inches for initial loading.

The nondimensional base load-settlement curves were not as consistent between shafts as those for the sides. The base curves for S1 and S2 were nearly identical, as seen in Fig. 12.68; however, the curve for S4, founded in Layer IV, was initially stiffer but required a larger displacement for full capacity mobilization. The load-displacement relationship for S3T1L3 is also included in Fig. 12.68 for completeness. Full base resistance was mobilized at a displacement of about 3 1/4 per cent of the base diameter in S1T1 and S2T1 and about 6 per cent for S4T1. The design of S3 did not allow an accurate estimate to be made for the displacement required to mobilize the soil supporting the base in S3T1L3. The offset in the curve is a result of the residual load present on the base after S3T1L2, during which the base was seated in the soil at the bottom of the cavity.

Figure 12.68 provides a means of checking Eq. 4.10c, which gives a formula for prediction of immediate base settlement in clay. For example, the dimensionless settlement of the bases of S1 and S2 at $\frac{Q_B}{(Q_B)_{ult}}$ of 0.5 was about 0.9 per cent. However, using the value of ϵ_{50} of 0.007 listed in Table 7.2 for the soil from Layer I, a corresponding dimensionless immediate settlement of 1.4 per cent is computed from Eq. 4.10c. Similarly, for S4, whose base was founded in Layer IV, the measured value of $\frac{\rho_B}{B}$ at $\frac{Q_B}{(Q_B)_{ult}}$ of 0.5 was about 0.7 per cent, while the value computed from Eq. 4.10c using ϵ_{50} of 0.012 from Table 7.2 is 2.4 per cent. (The soil stress-strain data from Layer IV were scarce,

and the tabulated value of ϵ_{50} may be in error.) Equation 4.10c, then, overestimates somewhat the base settlement for the SH225 tests.

An additional verification of the elasticity equations given in Chapter IV can be made by comparing base settlement at failure with that predicted from triaxial data in Eq. 4.10b. The triaxial failure strain for the soil from Layer I was about 3 1/2 per cent. Equation 4.10b, then, predicts that base failure in Layer I will occur at a settlement of about 7 per cent of the base diameter. Instead, Fig. 12.68 shows that failure occurred at about 3 1/4 per cent in S1T1 and S2T1. Neither the triaxial failure strain nor the load test base failure settlement was sharply defined, however, and the discrepancy is possibly largely one of determining exactly where "failure" occurred. The agreement for S4T1 was much better. Base failure occurred at a settlement of 6 per cent of the base diameter, while the triaxial failure strain for the soil from Layer IV was about 3 1/2 per cent.

Extrapolation of the initial tangent to the dimensionless base load-settlement curve for S3T1L3 to zero load should provide an approximation to the complete base load-settlement curve that would have existed had the base been cast directly against the soil.

The difference in shape between the dimensionless base load-settlement curve for S4T1 and those for S1T1 and S2T1 is surprising. The higher initial slope for S4T1 may be due to the fact that the base of S4 was embedded in a different soil than the others or to the effect of the depth at which the base is located. During reloading, however, the dimensionless base load-settlement curves for S1, S2, and S4 were nearly

identical, as shown in Fig. 12.69. All curves obtained upon reloading showed a higher initial slope.

The relative base and side factors of safety for S1T1 and S2T1 corresponding to various total factors of safety on the butt are shown in Fig. 12.70. The total factor of safety has been determined by dividing the applied load by the plunging load for the shaft. Corresponding side and base loads were then found and divided by the peak side resistance and ultimate base load, respectively. The difference in behavior between the cylindrical and belled shafts is easily seen. For example, for a total factor of safety of 3 against plunging failure, the cylindrical shaft (S1) had factors of safety of about 2.5 for the sides and about 14 for the base, indicating that the applied load was supported primarily by side resistance at that level of applied load. On the other hand, the belled shaft (S2) had corresponding factors of safety of less than one and 5.2. The factor of safety of less than one for the sides is a consequence of the fact that the soil supporting the sides of the stem is already in a post-failure condition, even though the total factor of safety is still 3.

Of fundamental interest for potential design application are the average shear strength reduction factors and bearing capacity factors that were measured in this study. Table 12.2 summarizes the average α factors obtained at both peak and ultimate side loads in the various tests. The available load from the soil is the value of peak side resistance that would have been measured had α been equal to unity. The average peak α factor for initial loading for the three shafts

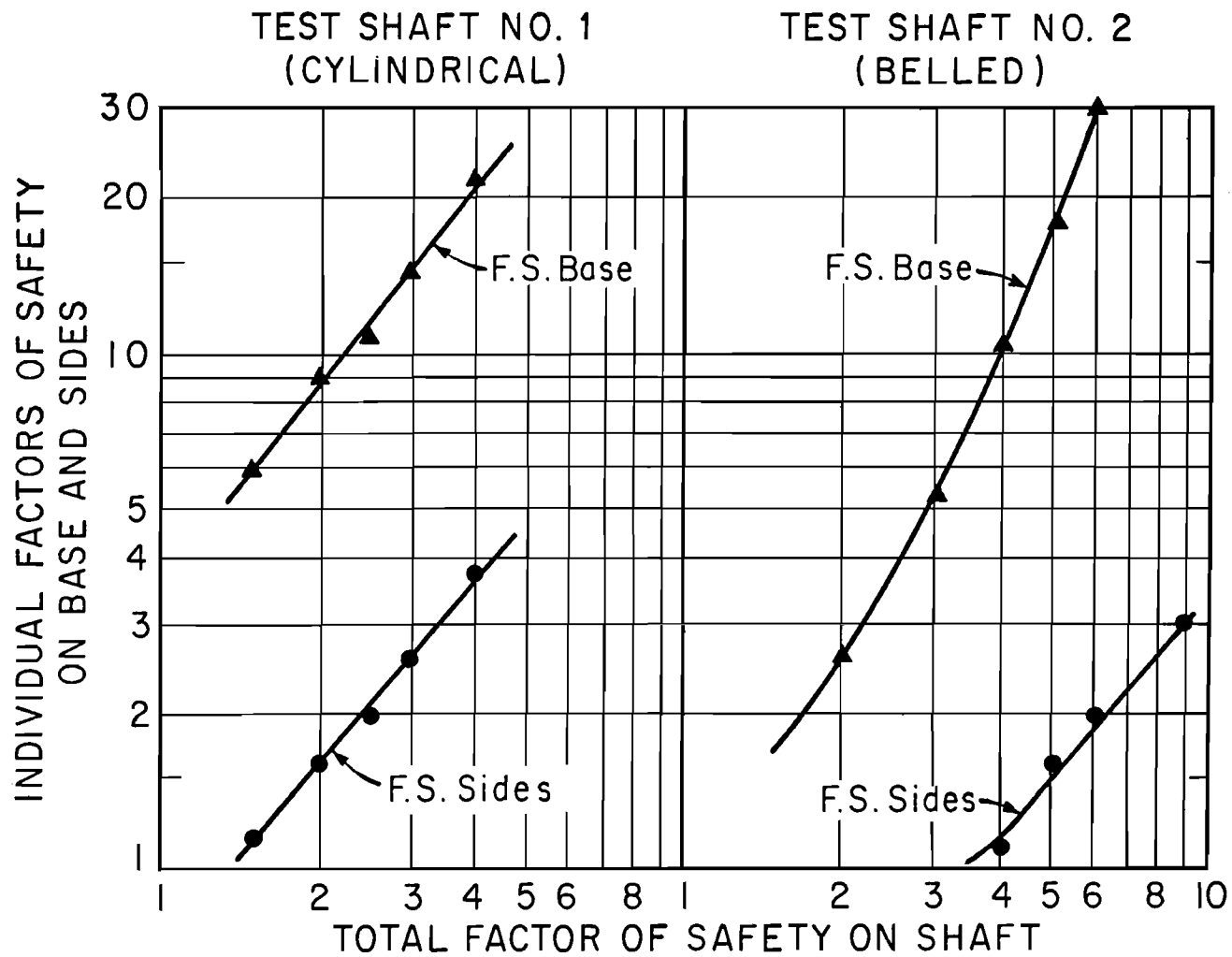


Fig. 12.70. Differentiation of Factor of Safety Into Base and Side Components, S1T1 and S2T1

TABLE 12.2. AVERAGE α FACTORS FOR ALL TESTS

Shaft /Test	Peak Load* Transferred (tons)	Ultimate Load Transferred (tons)	Peak α_{avg}	Ultimate α_{avg}
S1T1	96.7	88.0	0.44	0.40
S1T3	75.1	74.6	0.34	0.34
S2T1	91.6	90.4	0.53	0.52
S2T2	42.9	42.9	0.25	0.25
S3T1L1	120.9	63.7**	0.54	0.29
S3T1L3	54.0	52.4	0.24	0.24
S4T1	194.0	179.0	0.38	0.35
S4T2	180.0	165.0	0.35	0.32

* 222 tons maximum available from soil in side friction for Shafts 1 and 3.
 174 tons maximum available from soil in side friction for Shaft 2.
 516 tons maximum available from soil in side friction for Shaft 4.
 (assuming 32" diameter shaft)

** CRP at 5 1/2 inches displacement.

installed in the dry was 0.50, while the peak α factor for the shaft installed in a processed hole (S4) was 0.38. This reduction in side shear mobilization due to installing a shaft using the wet method is contrary to the observations of Barker and Reese (1970), who measured a rather high average α factor of about 0.6 for a test shaft at the HB&T site.

One possible parameter affecting the load transfer behavior of drilled shafts is the location of the water table (depth of 15 feet in the present study). The average α factors from the depth intervals 5 to 15 feet and 15 feet to bottom of stem have been computed for S1 through S3. The results are tabulated in Table 12.3. The average α factors were higher above the water table. However, other factors, including base-side interference may have had considerable influence on the tabulated α factors below 15 feet. The inference from Table 12.3 that higher α factors are developed above the water table, therefore, may be invalid.

An interesting comparison between the measured values of the average shear strength reduction factors for Layers I, II, III, and IV from S4T1 and the corresponding values predicted from the laboratory mortar migration study is given in Table 12.4. The field results from S4T1 clearly are not in agreement with the values predicted by the laboratory tests, except in Layer IV, where the borehole was not processed. Table 12.4 infers that processing may have a significant influence on the shear strength reduction factor. The best such comparison for Layer I for shafts installed dry is from S3T1L1, in which α_{peak} was 0.54, compared to 0.83 predicted from the laboratory tests. The subject of comparison

TABLE 12.3. SEPARATION OF α FACTORS INTO COMPONENTS ACTING
ABOVE AND BELOW WATER TABLE (DEPTH OF 15 FEET)

Shaft /Test	Ultimate Load Transferred 5'-15' Depth (tons)*	Ultimate Load Transferred Below 15' Depth (tons)**	α avg 5'-15'	α avg Below 15'
S1T1	58	20	0.61	0.24
S1T3	53	22	0.56	0.26
S2T1	60	16	0.63	0.44
S2T2	42	1	0.44	0.03
S3T1L1***	67	37	0.71	0.44
S3T1L1****	30	16	0.32	0.19
S3T1L3	17	30	0.18	0.32

* 95 tons maximum available from soil in side friction.

** 36 tons maximum available from soil in side friction for Shaft 2.

84 tons maximum available from soil in side friction for Shafts 1 and 3.

*** Peak values.

**** CRP at 5 1/2" displacement.

TABLE 12.4. PEAK α FACTORS FOR LAYERS I-IV AS INDICATED BY S4T1

Layer	Average α_{peak} from S4T1	Average α_{peak} from Laboratory Mortar Migration Study
I	0.35 (large variations)	0.83
II	0.40	1.00
III	0.35	0.96
IV	0.64	0.74

of field tests with laboratory mortar migration studies will be treated again later in this chapter.

Since the field study shows that the amount of load transferred both near the top and near the bottom of a drilled shaft can be quite small, designers may wish to disregard side resistance in those two regions. The field study indicates that each of the two regions extends for a distance equal to about twice the stem diameter. The shear strength reduction factors in the remaining parts of the shafts (as determined from the load distribution curves), therefore, have been tabulated in Table 12.5 for S1T1, S2T1, S2T2, S3T1L1, and S4T1. That table indicates an average shear strength reduction factor in the central zone of about 0.65 for the shafts installed dry and a factor of 0.33 for the shaft installed in a processed hole. As with other results, the values reported in Table 12.5 are somewhat dependent on the type of curve fitting procedure employed, but they are believed to be accurate estimations of the true values.

Another important result with possible design implications is the correlation of average developed side shear stresses at ultimate (plunging) load with the results of T.H.D. penetrometer soundings. A tabulation of average ultimate side shear stress along the full length of the stem, average number of penetrometer blows per foot along the stem, and the correlation factor between the two, p , is given for the initial test on each shaft in Table 12.6. Values of p ranging from 28 to 40 were obtained for the shafts installed in the dry, while a value of 56 was obtained for Test Shaft No. 4. By comparison, Vijayvergiya, Hudson,

TABLE 12.5. AVERAGE SHEAR STRENGTH REDUCTION FACTORS IN STEMS
EXCLUDING TOP AND BOTTOM TWO STEM DIAMETERS, $\bar{\alpha}$

Shaft /Test	$\bar{\alpha}$
S1T1	0.60 (peak)
S2T1	0.71 (peak)
S2T2	0.50 (ultimate)
S3T1L1	0.65 (peak)
S4T1	0.33 (peak)

TABLE 12.6. CORRELATION OF PEAK SIDE RESISTANCE WITH T.H.D. CONE PENETROMETER SOUNDINGS

Shaft	Peripheral Area (sq. ft.)	Ultimate Side Resistance (tons)	Average Ultimate Shear Stress Developed, $(q_s)_{ult}$ (tsf)	Average Number of Penetrometer Blows per Foot Along Length of Stem, N	$P_{avg\ side}^*$
1	181	88.0	0.48	19	40
2	145	90.4	0.62	17	28
3	181	120.9**	0.67	19	28
4	377	179.0	0.48	27	56

*Using Equation: $(q_s)_{ult} = \frac{N}{p}$; in tsf.

**Loading No. 1, at 0.5" Gross Settlement.

and Reese (1969) obtained a value of p equal to 35 for an instrumented shaft installed in the dry in a clay-shale in San Antonio. It appears that 35 is a reasonably good value for shafts installed in clay in the dry, but that a value of 55 to 60 may better apply to shafts installed wet in the event some drilling mud becomes entrapped between the concrete and soil, as occurred during the construction of Test Shaft No. 4.

Valid predictions of base bearing capacity for the shafts at the SH225 site are assumed to be given by Eq. 4.7. Since the shear strength profiles and net ultimate base capacities are known, values of N_c can be computed for each shaft. A set of N_c values for the initial loading on each shaft (except for S3, where the third loading was used) is tabulated in Table 12.7. The appropriate value of undrained cohesion, c_u , to be used in Eq. 4.7 is taken first to be the shear strength at one base diameter beneath the base and second to be the average shear strength for a distance of two base diameters beneath the base. Corresponding values of N_c are shown. It appears that the soil in Layers I, II, and III was mobilized by the base of S2, since the bearing capacity factor N_c is near 9 when the two-diameter average is used. On this basis, it is apparent that the value of the bearing capacity factor based upon the two-diameter average is more reliable.

No dependence of N_c on base geometry was observed, although S4 exhibited a slightly high base bearing capacity factor, possibly because the shear strength of the soil was underestimated slightly for Layer IV or because the base of S4 was situated at a greater depth. The bearing capacity factor was slightly low for S3 because the soil around the cavity had evidently been softened by the water that had collected in

TABLE 12.7. BEARING CAPACITY FACTORS, N_c

Shaft	Base Diameter (ft.)	Base Area (sq. ft.)	Base Depth (ft.)	Net Ultimate Base Load (tons)	Net Ultimate Base Load Divided By Base Area (tsf)	Shear Strength at One Base Diameter Below Base (tsf)	N_c Based Upon Shear Strength at One Base Diameter Below Base	Average Shear Strength for Two Base Diameters Below Base (tsf)	N_c Based Upon Average Shear Strength for Two Diameters Below Base
1	2.42*	4.59	23	52.0	11.3	1.20	9.4	1.20	9.4
2	7.5	44.2	23	446.6	10.1	0.70	14.4	1.13	8.9
3	2.5	4.91	24**	47.6	9.71	1.12	8.7	1.12	8.7
4	2.5***	4.91	45	142.0	29.7	2.30	12.6	2.30	12.6

*Diameter of steel plates in bottomhole load cell.

**Bottom of borehole at depth of 24 feet. Values obtained for Loading 3 used.

***Nominal diameter.

the cavity and possibly because the soil near the base had experienced some structural weakening due to opening of fissures.

Based on the overall field test results, it appears that the value of 9 for the bearing capacity factor with respect to the average UU triaxial test shear strength profile is valid for drilled shafts in Beaumont Clay.

The bearing capacity factors given in Table 12.7 are correlated with the results of T.H.D. cone penetrometer soundings in Table 12.8. The correlation factor, p' , divides the number of penetrometer blows per foot to yield net ultimate unit base capacity. Using the average number of blows per foot for a distance of two base diameters beneath the base as a reference, the average p' factor for S1, S2, and S3 was 2.8. That value appears to be a valid ultimate design factor for drilled shafts in Beaumont Clay, although a lower p' factor of 1.9 was obtained for S4.

By comparison, Vijayvergiya, Hudson, and Reese (1969) measured a p' factor of about 4 for a test on a shaft in clay-shale. The base in that test, however, was not fully plunged; hence, the true ultimate p' factor was undoubtedly less than 4.

One point of interest to the foundation designer is the comparison of the behavior of drilled shafts with that of driven piles. Although no driven pile tests were executed at the SH225 site, a meaningful comparison of drilled shaft and driven pile side resistance capacities is made in Fig. 12.71. Tomlinson (1969) has plotted values of the ratio of shear strength mobilized in skin friction to the average undisturbed shear strength of clay soils versus the shear strength for numerous pile

TABLE 12.8. CORRELATION OF BASE BEARING CAPACITY WITH T.H.D. CONE PENETROMETER SOUNDINGS*

Shaft	Net Ultimate Contact Pressure, $(q_B)_{ult, net}$ (tsf)	Number of Blows per Foot One Diameter Below Base	Average Number of Blows for Two Diameters Below Base	p'_{1D} **	$p'_{avg\ 2D}$ ***
1	11.3	32	32	2.8	2.8
2	10.1	16	25	1.6	2.5
3	9.7	33	31	3.4	3.2
4	29.7	55	55	1.9	1.9

*Using Equation: $(q_B)_{ult, net} = \frac{N}{p'}$; in tsf.

**Using Number of Blows per Foot at One Base Diameter Below Base.

***Using Average Number of Blows per Foot for Two Base Diameters Below Base.

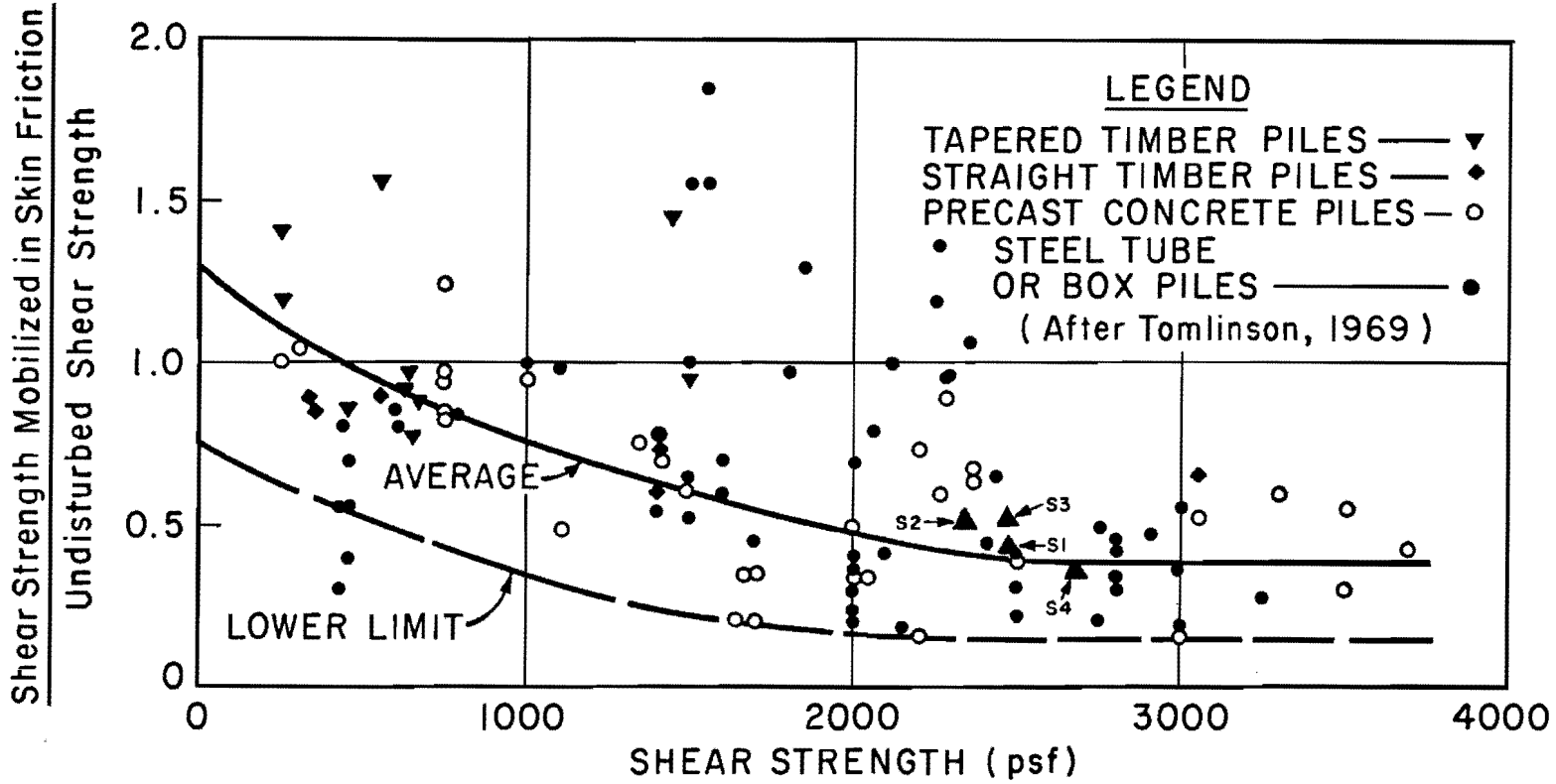


Fig. 12.71. Average Shear Strength Reduction Factors Versus Shear Strength for Driven Piles and Drilled Shafts in Clay

tests conducted in a variety of soils. That plot is reproduced in Fig. 12.71, and the corresponding overall average values from the initial tests of the shafts at the SH225 site are superimposed. It is evident that the ratios of mobilized shear stress to undisturbed shear strength for the three shafts installed dry fall slightly above Tomlinson's average for driven piles, while that of the shaft installed in a processed hole is slightly below the line of averages. Thus, it appears that, in the soil strength range tested, drilled shafts develop about the same average ultimate side resistance as do driven piles.

Field Inspection and Moisture Migration Studies

Visual Inspection of Test Shafts. Test Shaft Nos. 1 and 4 were inspected after testing was completed. Test Shaft No. 1 was actually removed from the ground on September 4, 1969, by augering a series of holes around the periphery of the shaft and picking the shaft up with a crawler crane, as shown in Fig. 12.72. Very little soil adhered to the sides of the shaft because the soil had been broken loose by the auger.

The entire shaft is pictured in Fig. 12.73. It was well-formed and was almost perfectly cylindrical. A slight bow in the axial alignment was noted, corresponding to an offset of about one inch in twenty feet. A minor enlargement is visible in Fig. 12.73 at the 15-foot depth, at which the silty stratum of soil was encountered.

The circumference of the shaft was measured at several locations along the stem, primarily as a check on the validity of the in-shaft calibration procedure, which assumes a constant cross section throughout the length of the stem. The results of the measurements, given in Table 12.9, provide a numerical indication of the uniformity of Sl.



Fig. 12.72. Extraction of S1



Fig. 12.73. View of S1 After Extraction

TABLE 12.9. MEASURED CIRCUMFERENCES OF TEST SHAFT NO. 1
AFTER EXTRACTION

Distance Below Ground (ft.)	Circumference of Concrete Shaft (in.) *
1 (protruding portion)	93 3/4
0 (calibration level)	95
5	96
10	96 1/2
14	97
15	100 3/4
16	97 3/4
20	96
22	96 1/4
22 1/2	96 1/4

* Nominal circumference = 94 1/4 inches.

Close-up photographs of two sections of S1 are shown in Figs. 12.74 and 12.75. Figure 12.74 shows a typical section. The surface of the shaft was quite smooth and contained a thin film (perhaps 1/16 inch thick) of reddish-colored soil. Figure 12.75 shows an atypical portion of the shaft, about 5 feet below the ground surface, in which the concrete, because of insufficient head, failed to penetrate fully the space between the cage and the borehole wall. This problem was aggravated by the fact that a considerable number of instrumentation tubes was present along that section of cage, blocking the free flow of concrete. The soil taken from the voids shown in Fig. 12.75 was about 10 per cent wetter than the natural soil. This poorly-formed section was small. Voids were no more than two inches deep, and no instrumentation was affected. The formation of surface voids similar to those pictured in Fig. 12.75 may be quite general in shafts installed with inadequate spacing between the cage and the borehole wall or with low-slump or improperly compacted concrete. Extensive formations of voids of this nature can adversely affect the load transfer capabilities of a drilled shaft.

The top 24 feet of S4 was exposed prior to S4T3 by excavating around the stem in a manner similar to that described for S1. A view of the freestanding section of the stem is given in Fig. 12.76. The large collar and the necked section below the collar are clearly visible. The largest part of the collar is located at a depth of about six feet. The circumference of the shaft at a depth of three feet was 108 inches. The nonuniform shape of S4 is in marked contrast to the well-formed, cylindrical shape of S1. Figure 12.76 demonstrates graphically the reason

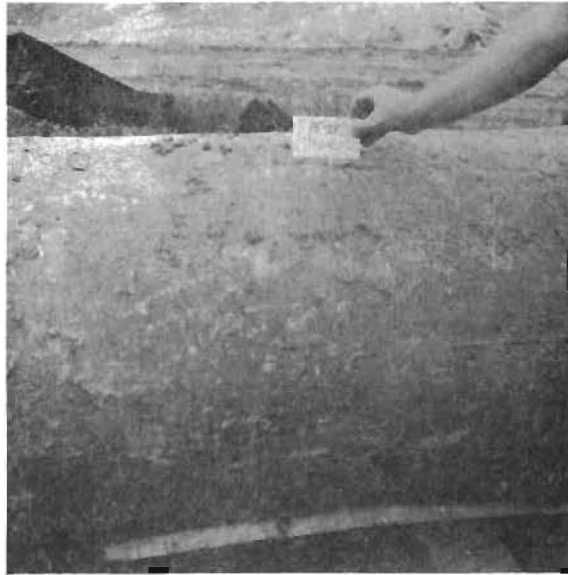


Fig. 12.74. Typical View of
Periphery of Sl



Fig. 12.75. View of Honeycombed Section
of Periphery of Sl



Fig. 12.76. View of Exposed Section of S4



Fig. 12.77. Taking Radial Samples in Access Borehole Adjacent to S3

for performing post-test calibration of instrumented shafts with stems installed using the wet method described in Chapter II.

Field Moisture Migration Study. In addition to inspecting visually the two exposed shafts, access holes were bored immediately adjacent to Test Shaft Nos. 1, 3, and 4 (prior to exposing the stems of S1 and S4) to allow recovery of undisturbed samples of soil adjacent to the walls of the shaft. Technicians entered each borehole immediately after boring was accomplished and drove thin-walled sampling tubes into the walls of the borehole until the cutting edge of each sampling tube struck the surface of the test shaft. The tube was then extracted. In this way, radial soil samples, extending from the surface of the test shaft to a distance of four to six inches away, were obtained. The sampling operation is pictured in Fig. 12.77, which also shows a typical dry borehole in Beaumont Clay.

The samples were allowed to remain in the tubes, which were immediately wrapped in aluminum foil, marked, and waxed. They were returned to the laboratory in Austin, where the soil was extruded from the tubes, and moisture contents were taken at one-quarter-inch intervals. In this way, moisture content profiles were obtained. An end view of a typical specimen, taken against S3 at a depth of 9 feet, is shown in Fig. 12.78. A light-colored concrete-soil mixture from the interface is visible in the lower left part of the specimen. Some of the interface soil has been removed near the center, revealing a well-defined, shiny shear plane at a distance of about one-eighth inch from the interface. It is believed that this shear plane was produced by the large-displacement load test

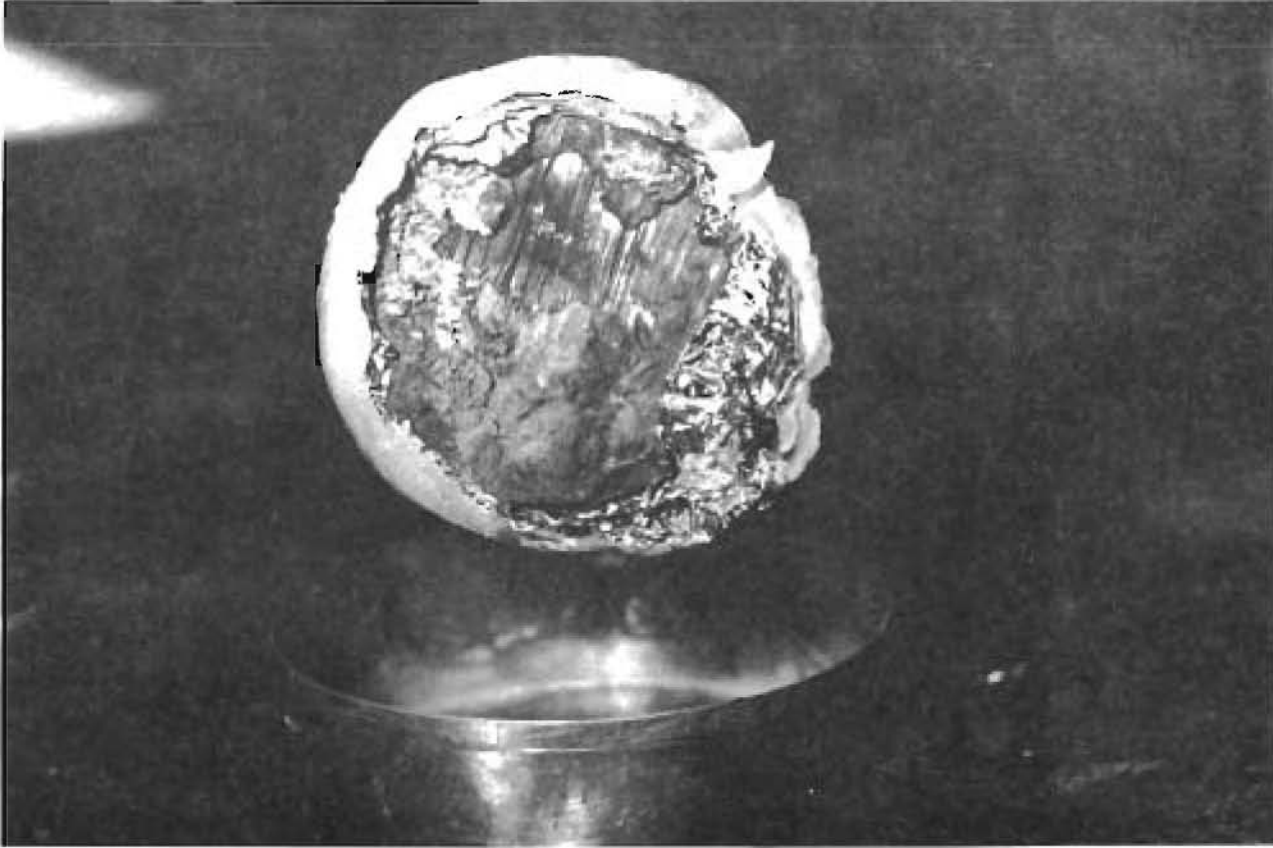


Fig. 12.78. View of End of Radial Sample Taken Adjacent to S3 at Depth of 9 Feet

on S3. The appearance of the specimen infers, then, that shearing along the stem occurred in the soil and not at the interface.

The moisture gradients obtained from the radial samples at the various depths indicated are given in Figs. 12.79 through 12.86. Samples from S1 were taken in September, 1969. Individual gradients are shown for S1 in Fig. 12.79. It is immediately evident that considerable variation in behavior occurred. The sample taken at a depth of 3 feet indicates that drying had occurred at that depth in the soil at the concrete-soil interface, suggesting that a shrinkage crack had penetrated to that depth. The samples taken at 15 feet and above generally indicate a slight drying of the soil as the interface is approached. The samples taken from below 15 feet generally indicate the opposite effect, particularly near the base, where an increase of six to eight per cent was measured (depth of 22 feet). The depth of greatest moisture content increase corresponds closely to the depth at which minimum load transfer was measured. Two samples were taken at a depth of 18 feet. One was taken from inside the access borehole, while the other was obtained from soil adhering to the shaft after extraction.

The average moisture content gradient for all S1 samples is given in Fig. 12.80. A very small average moisture gradient is indicated. However, the separate averages for the samples at 15 feet and above and for the samples below 15 feet, also shown in Fig. 12.80, clearly show that the soil adjacent to the interface was drier than the natural moisture content in the upper 15 feet (moisture content at a distance of 2 1/2 inches from the interface) and wetter below 15 feet, which was the

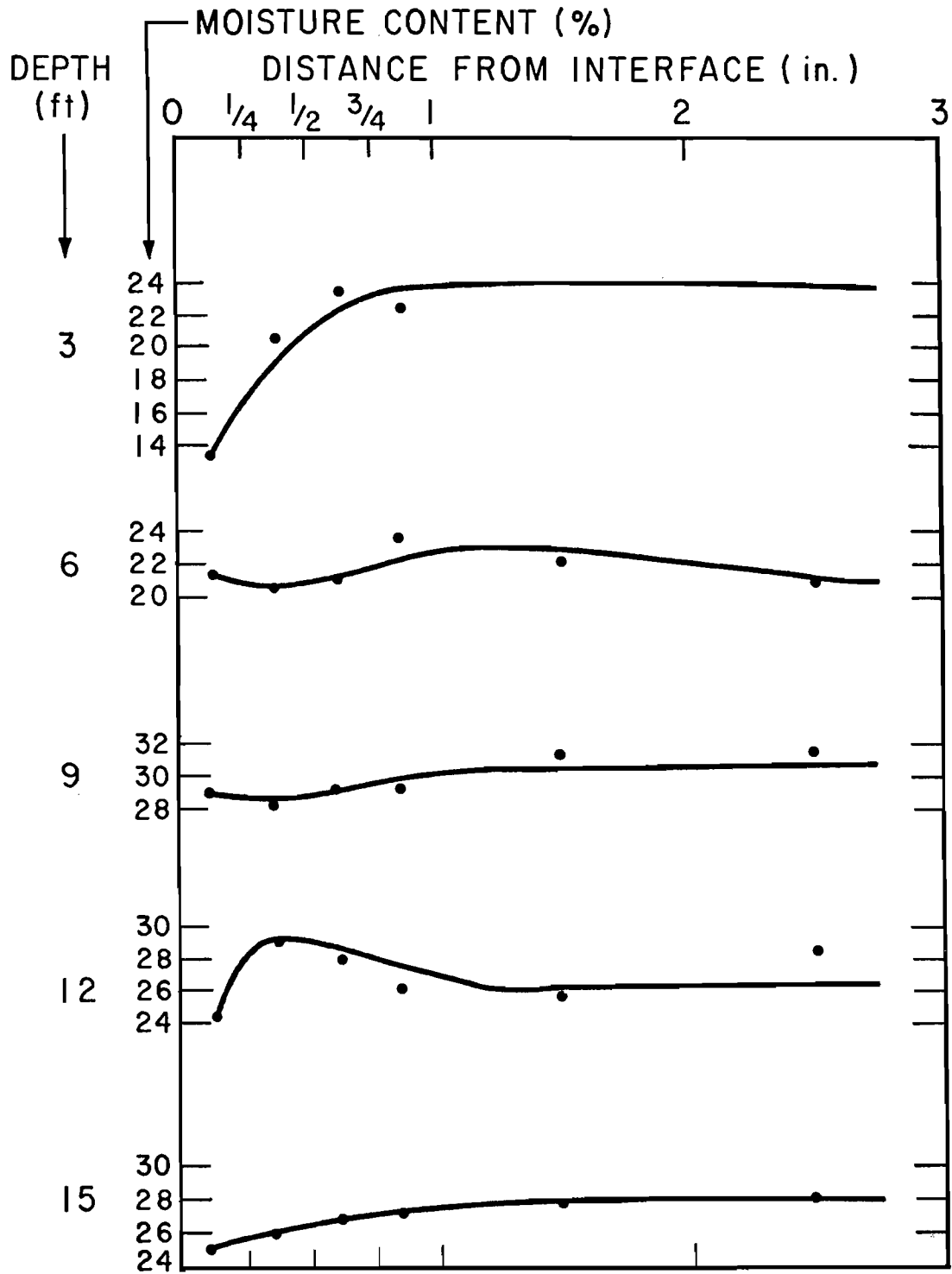


Fig. 12.79. Individual Radial Moisture Profiles Adjacent to S1

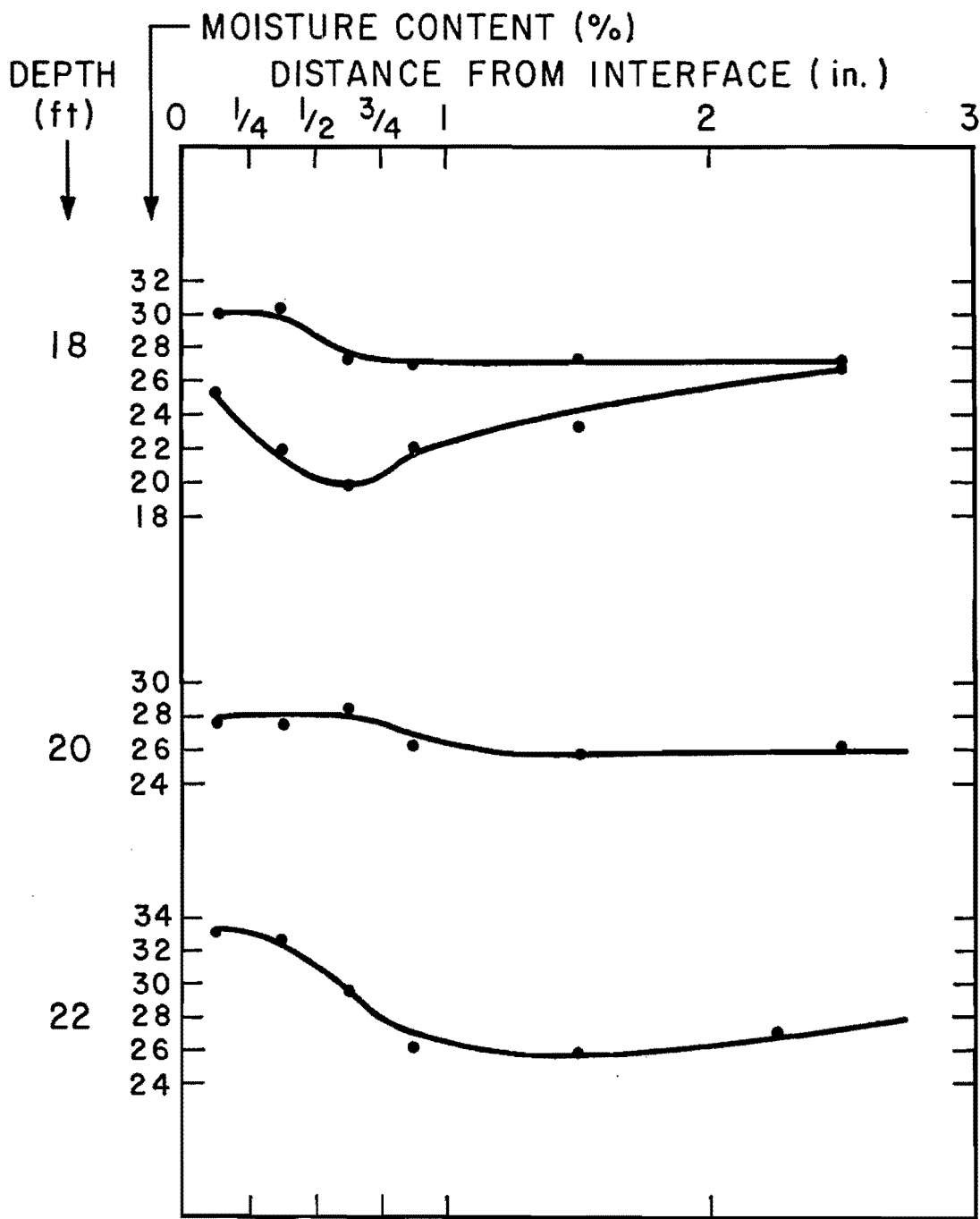


Fig. 12.79. Continued

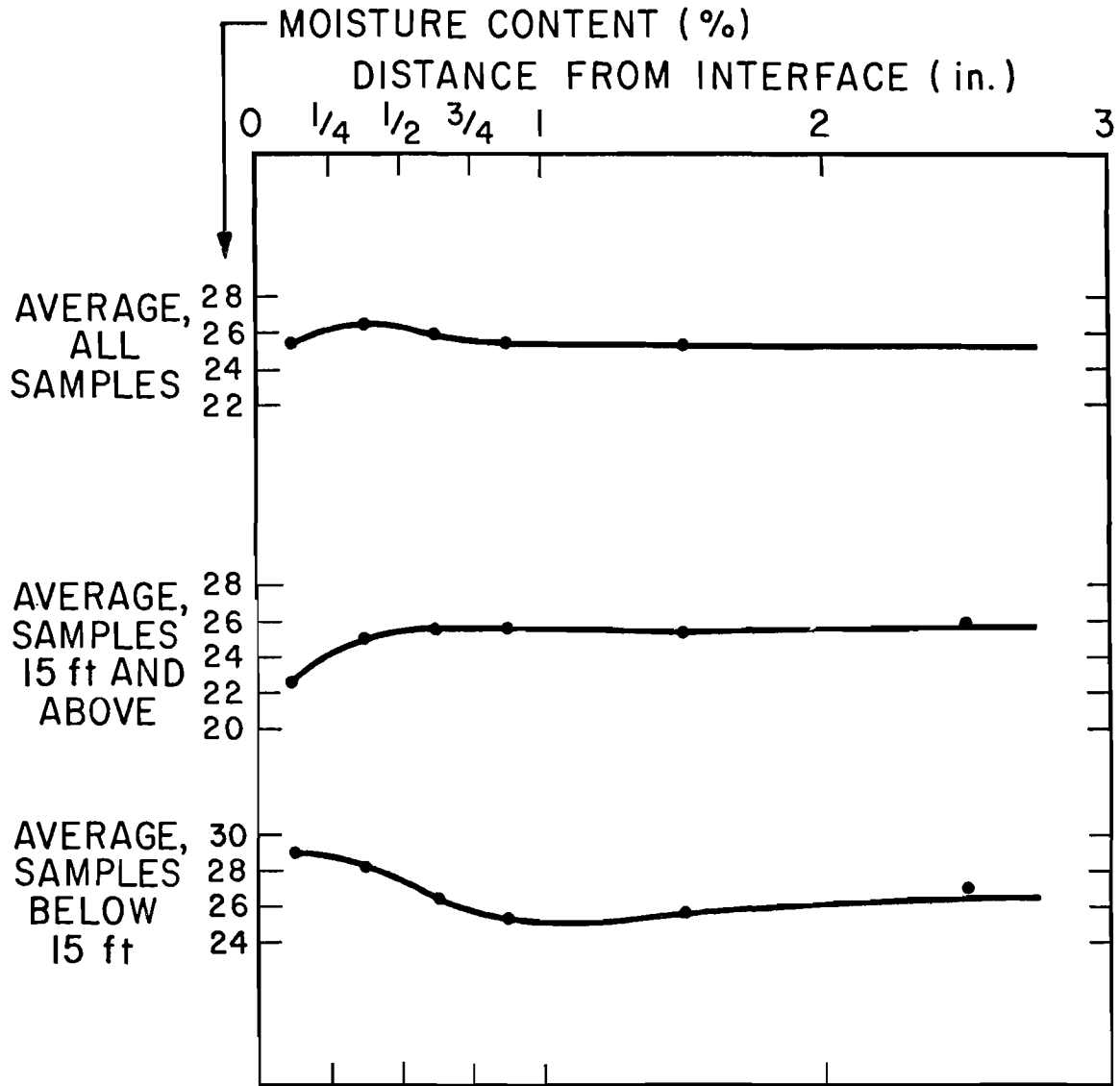


Fig. 12.80. Average Radial Moisture Profiles Adjacent to S1

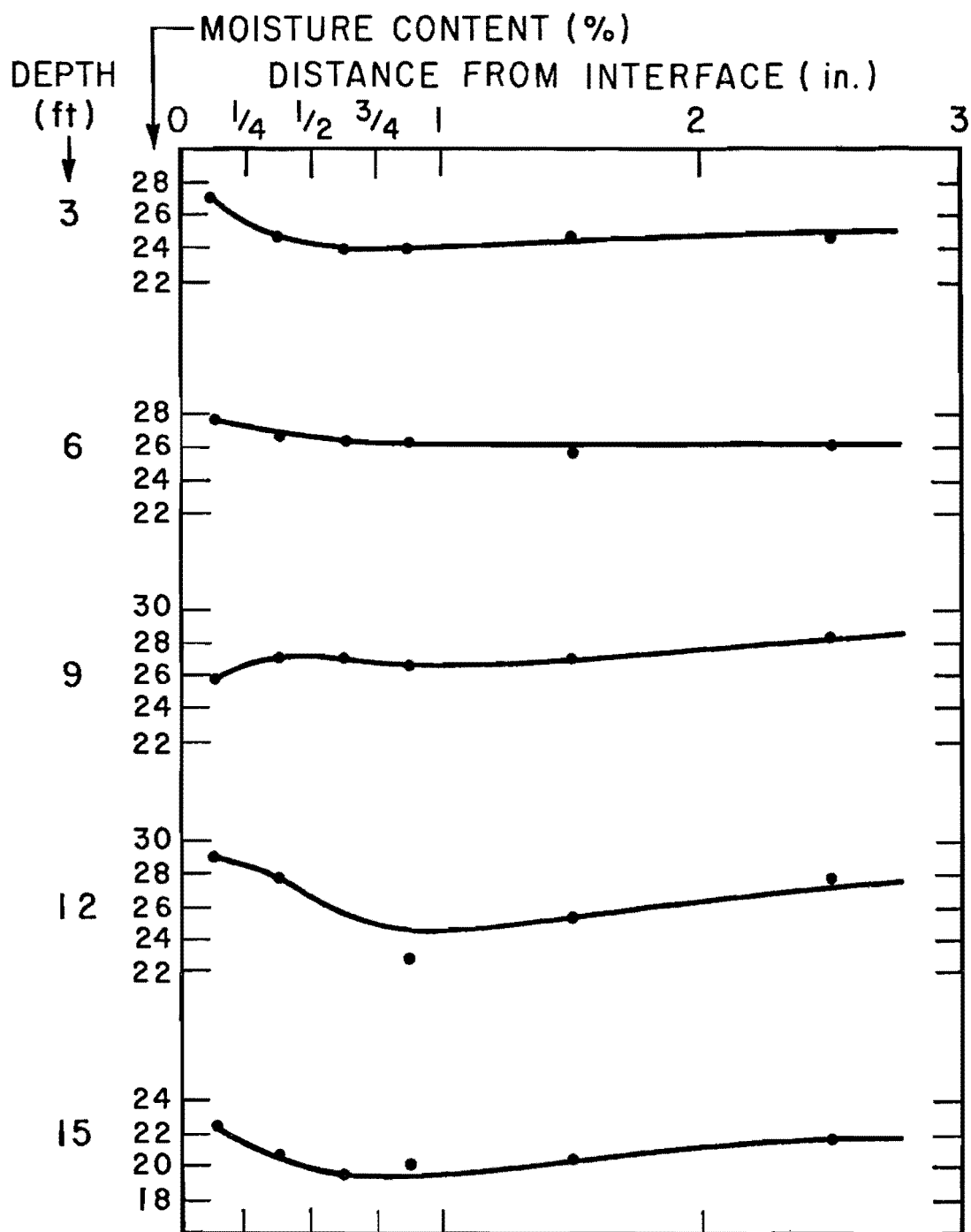


Fig. 12.81. Individual Radial Moisture Profiles Adjacent to S3

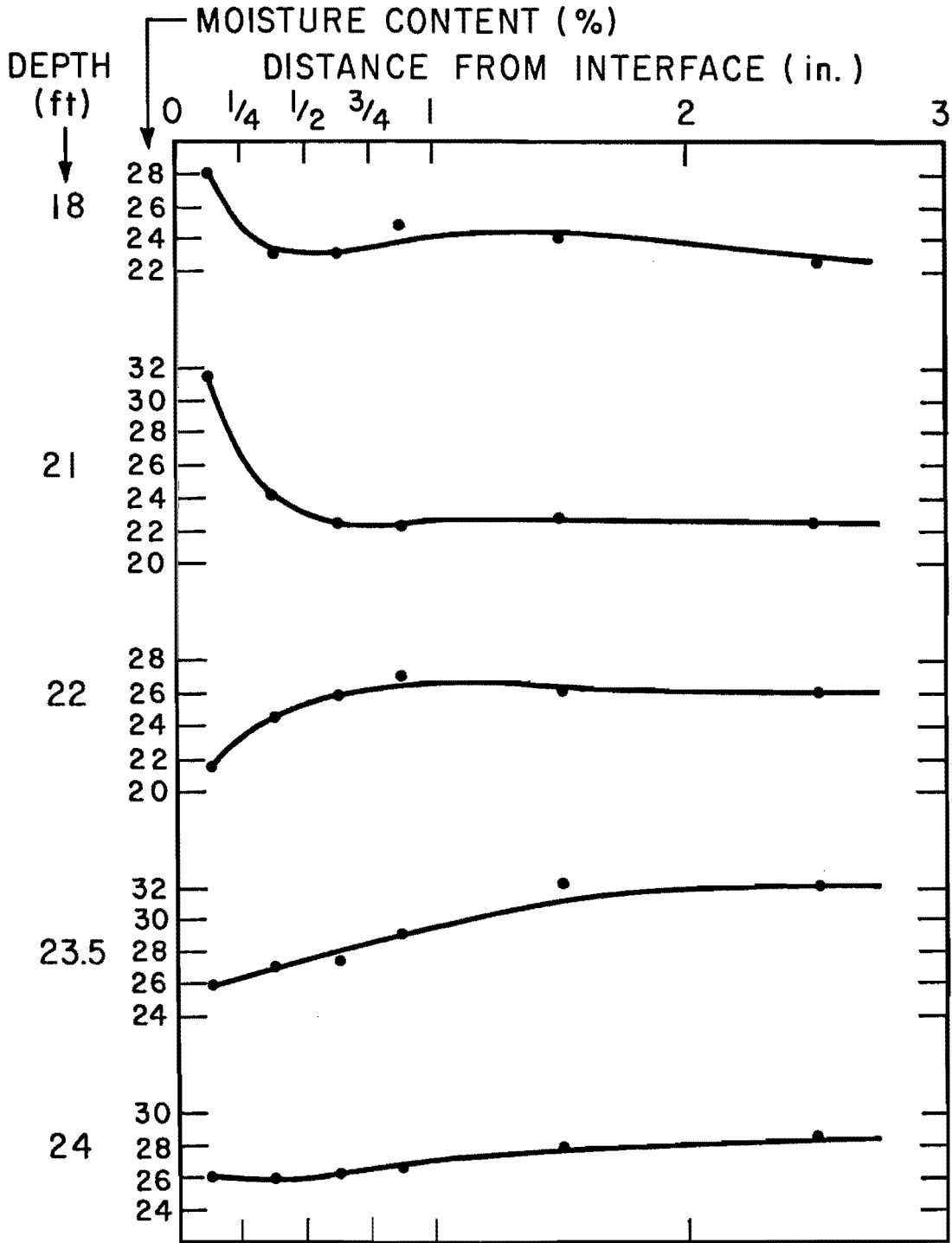


Fig. 12.81. Continued

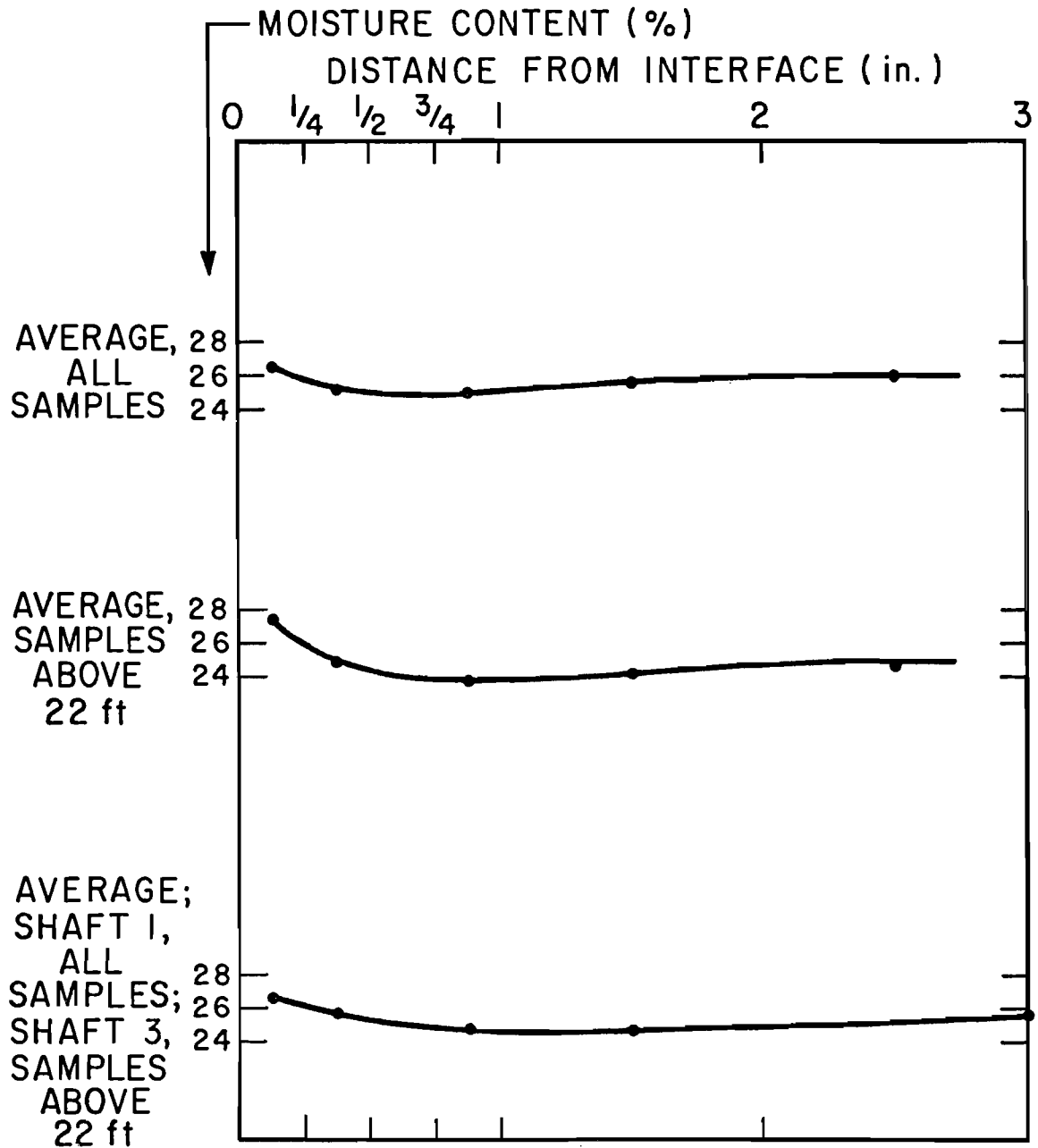


Fig. 12.82. Average Radial Moisture Profiles for S3 and Combined Average Gradient for S1 and S3

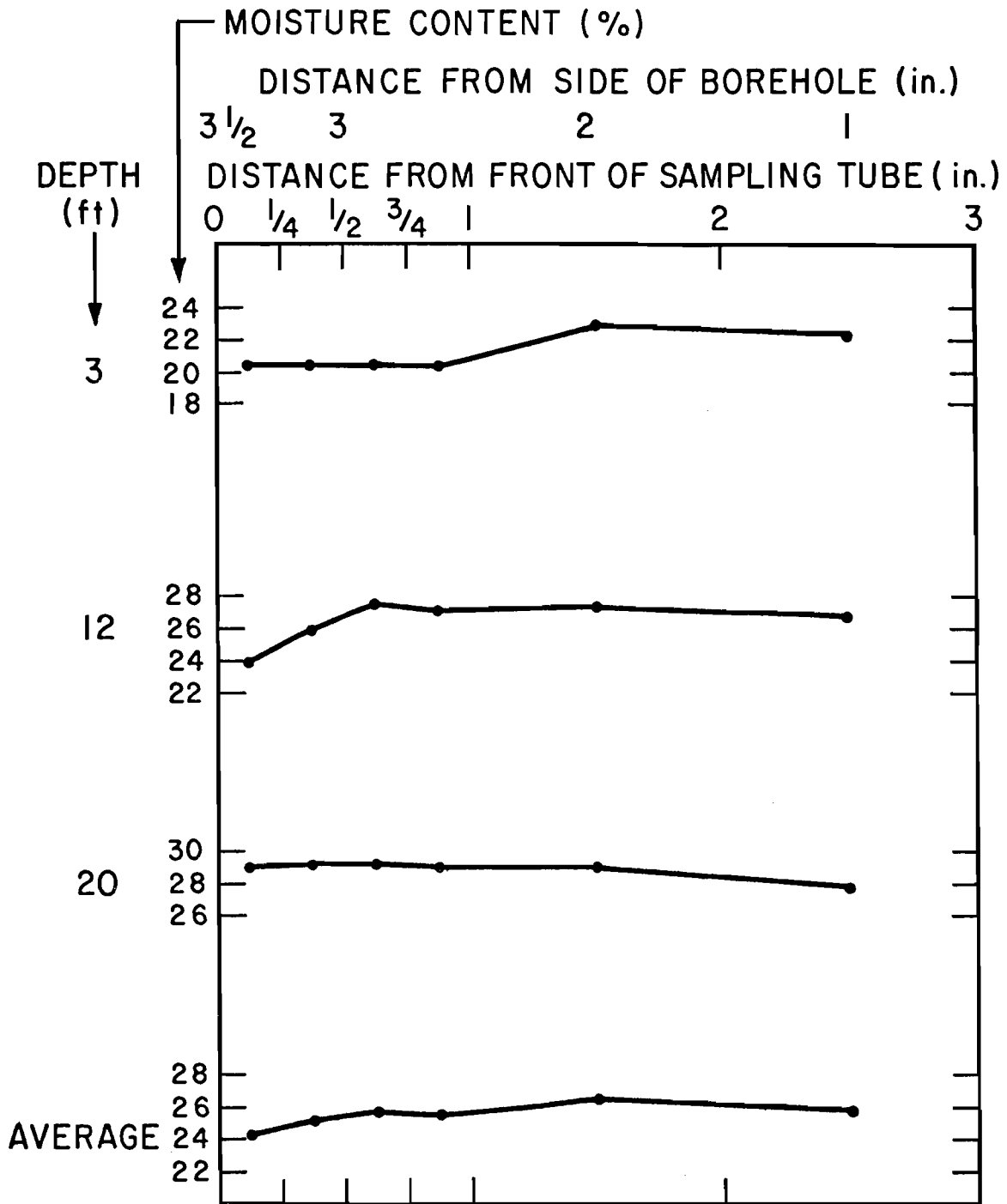


Fig. 12.83. Control Specimen Moisture Profiles for S3

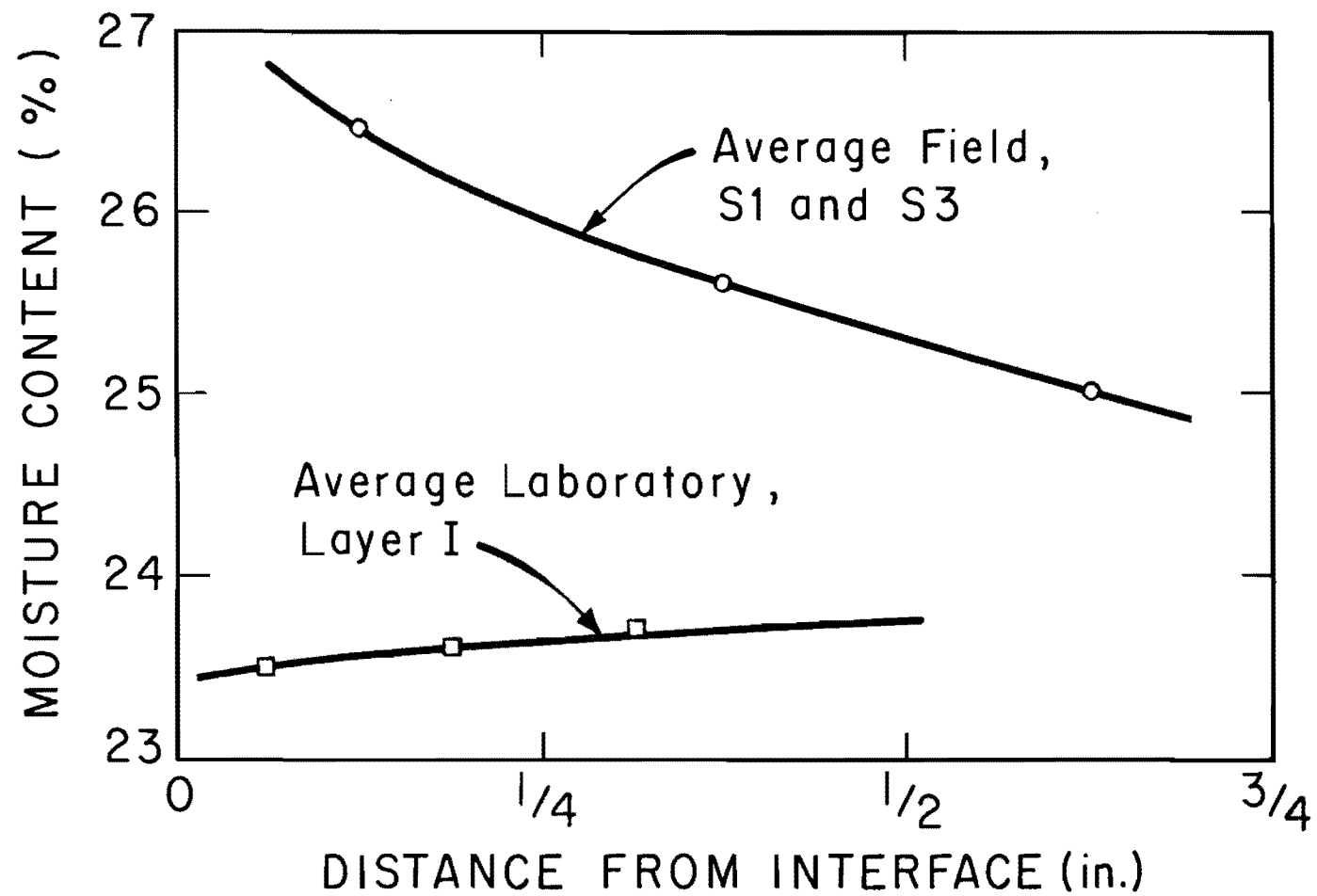


Fig. 12.84. Comparison of Field and Laboratory Radial Moisture Profiles for S1 and S3

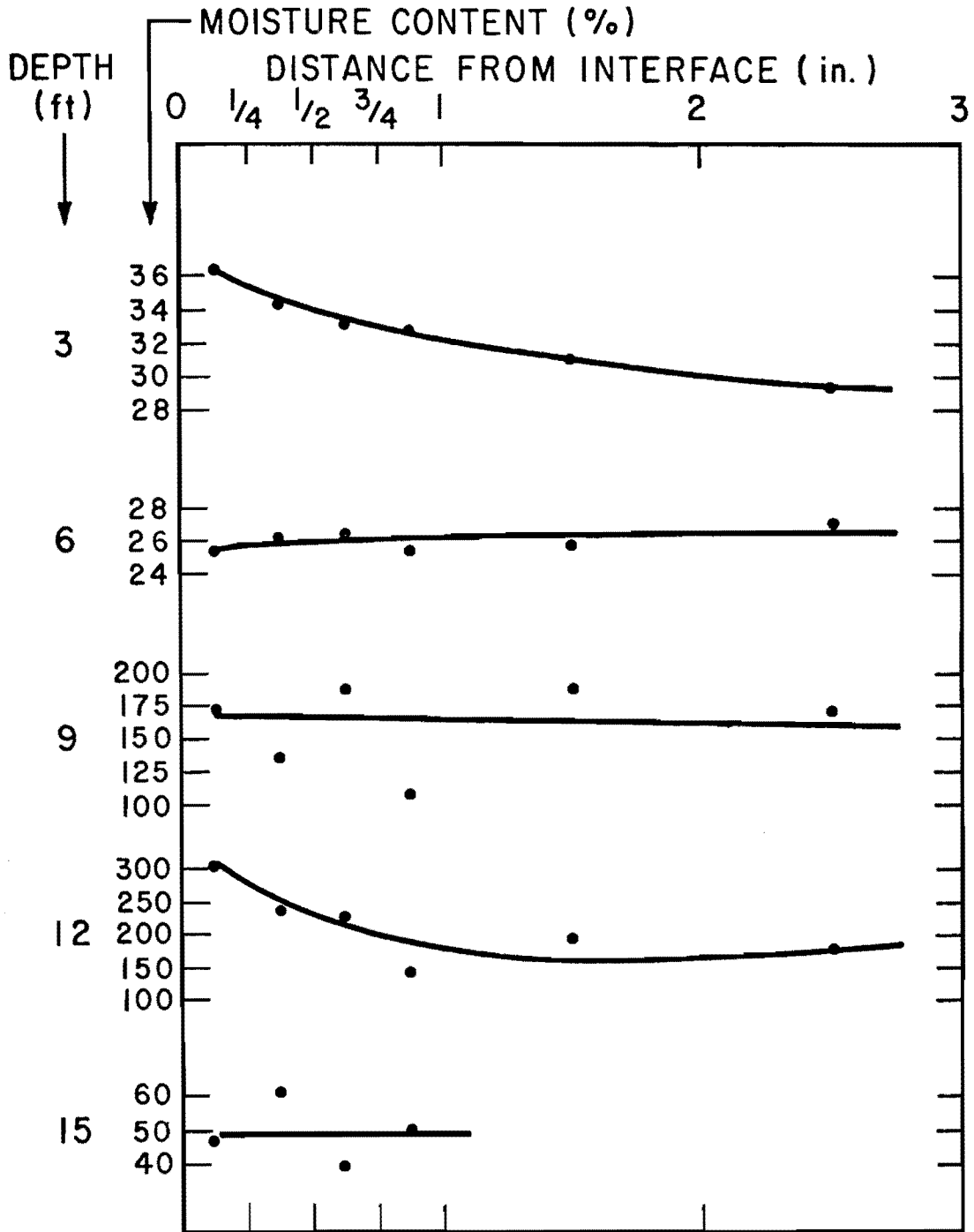


Fig. 12.85. Individual Radial Moisture Profiles for S4

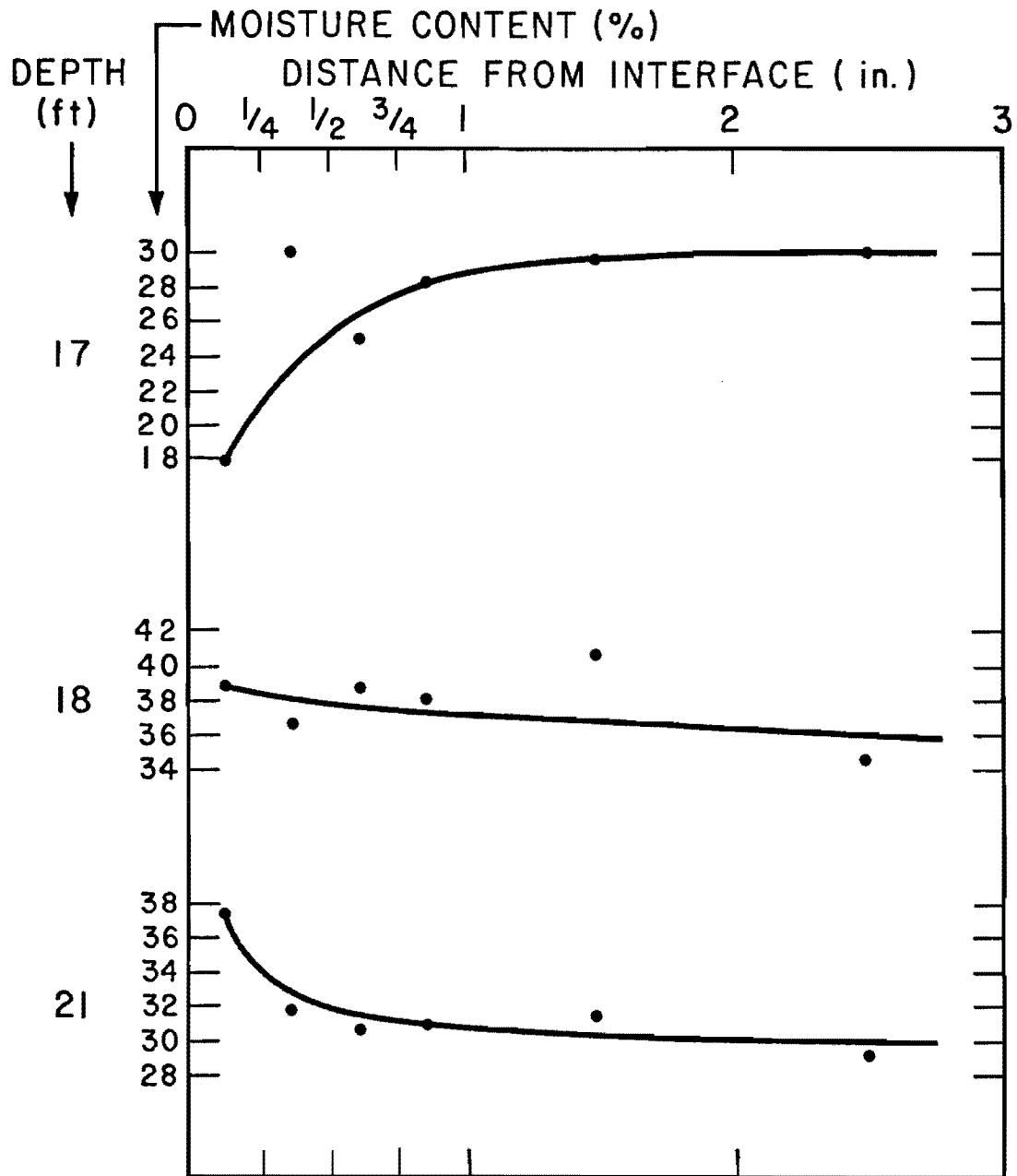


Fig. 12.85. Continued

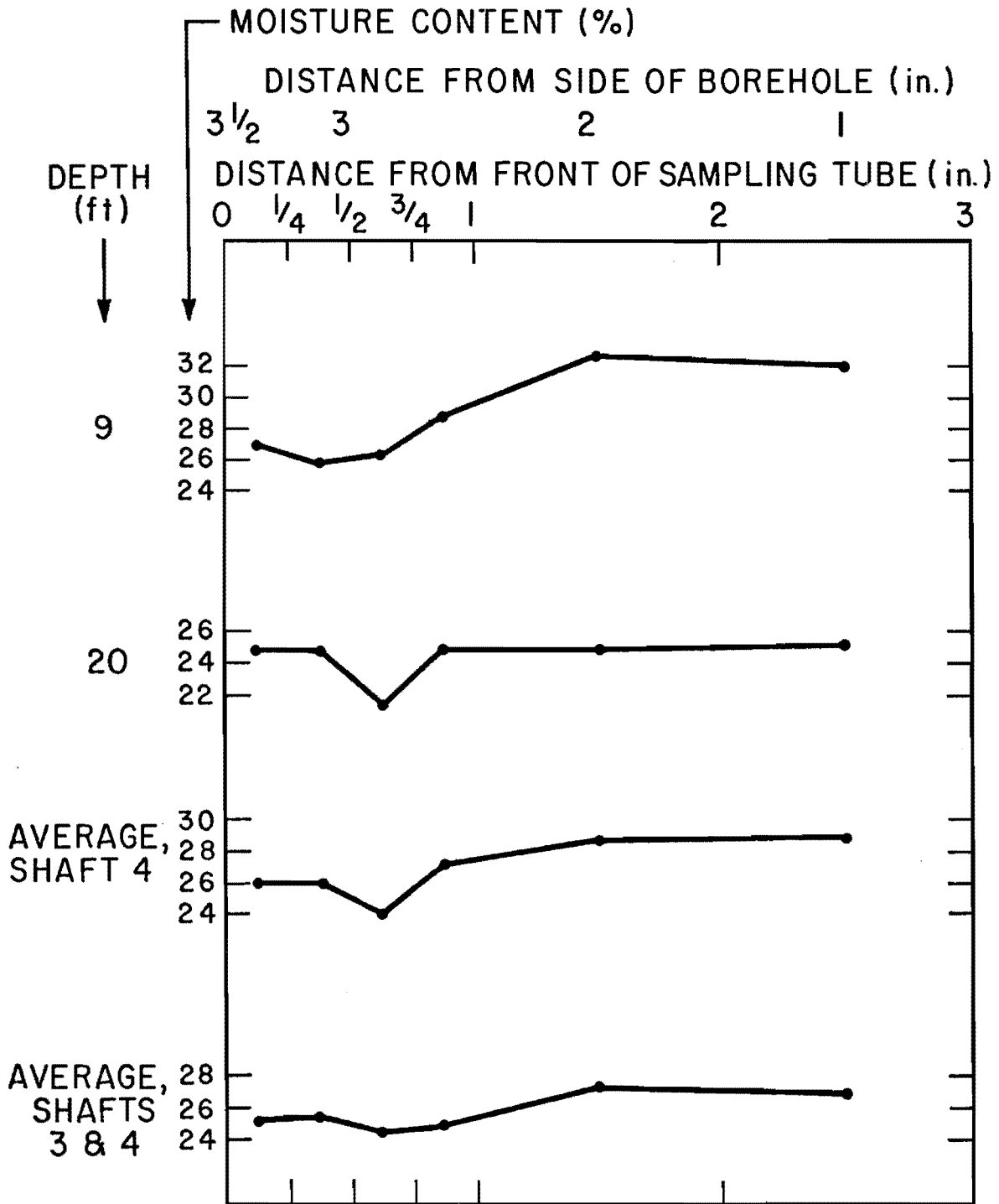


Fig. 12.86. Control Specimen Moisture Profiles for S4

approximate depth of the water table. The reason for the differences in behavior above and below 15 feet is not clear. However, it is assumed that the increase in moisture content in the soil adjacent to the shaft below 15 feet is at least partially a consequence of the fact that the bottom of the borehole contained water at the time of casting.

Similar moisture gradient curves were developed for S3 from samples taken in April, 1970, as shown in Figs. 12.81 through 12.83. Again, the individual relationships were variable. Unlike the samples for S1, however, the samples for S3 showed a consistent moisture gradient, with a higher moisture content adjacent to the shaft. Only the samples for the 9-foot, 22-foot, and 22.5-foot depths showed the opposite trend. The latter two specimens contained considerable acetone, and it is felt that the results of the moisture content determinations are largely invalid. The samples for the 18-foot and 21-foot depths showed significant moisture content increases in the half inch of soil adjacent to the test shaft. As in S1, the depths at which the maximum moisture content increase adjacent to the shaft occurred correspond to the depths at which measured load transfer was the smallest.

The average radial moisture gradient for S3 is given in Fig. 12.82. Also shown in the same figure is the average gradient excluding the samples from 22 and 22.5 feet. The latter curve indicates an average increase in moisture content of about three per cent for the soil adjacent to the walls of the shaft. The average for S1 and all samples from S3 above a depth of 22 feet is also given in Fig. 12.82. An overall average moisture content increase of about two per cent is indicated for the two shafts.

Figure 12.87 shows the changes in moisture content in the soil immediately adjacent to the shaft with depth for S1 and S3. The figure clearly indicates the effect of increased wetting with proximity to the base.

According to Eq. 7.1, an increase in moisture content of two per cent decreases the remolded shear strength by 17 per cent. Presumably the change in undisturbed shear strength would be even less. Therefore, the results of the field moisture migration studies indicate that, if moisture migration is the only cause of shear strength reduction, an average peak α factor of no less than 0.83 should have been measured, instead of the average value of 0.5 obtained in the field tests on S1 and S3. Clearly, then, other factors, including those enumerated in Chapter V, contribute significantly to the reduction of load transfer along the stems of drilled shafts.

Three tube samples were taken from the side of the access borehole situated opposite S3, at which it was thought that the moisture content would be essentially constant throughout the specimen. The moisture content gradients obtained from these control samples are plotted in Fig. 12.83. The average gradient indicates a variation of about ± 1 per cent in the controls. That variation is thought to be a reflection of real moisture content variations in the soil and not primarily due to sampling and testing procedures. Figure 12.83 implies that the moisture contents plotted for the average gradients developed for S1 and S3 may be in error by ± 1 per cent.

At this point it is appropriate to compare the results of the laboratory mortar-moisture migration study with the moisture content gradients

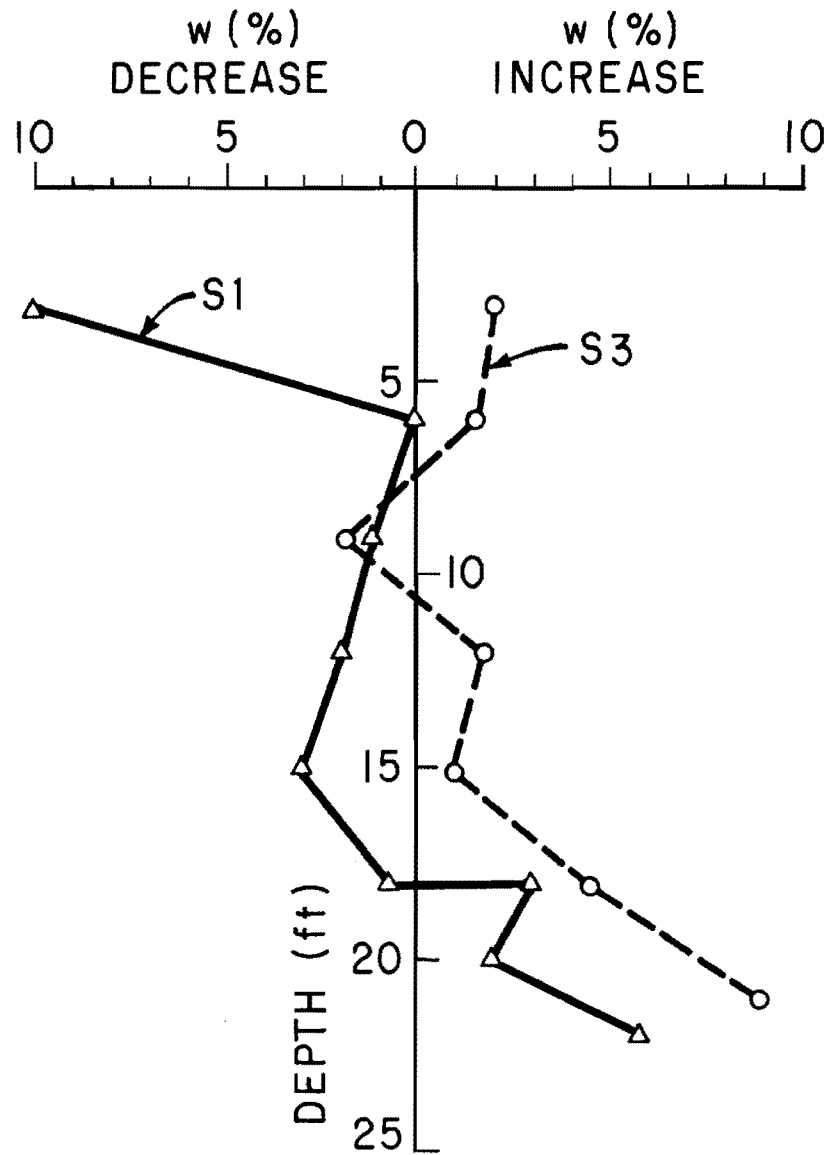


Fig. 12.87. Change in Moisture Content in Soil Immediately Adjacent to Shaft

obtained in the field. The best comparison can be made by superimposing the average moisture gradient for Layer I from the laboratory study on the average moisture gradient for S1 and S2 (given in the lower plot in Fig. 12.82), as shown in Fig. 12.84. The behavior of the soil in the field was clearly different from that in the laboratory. The field samples showed, on the average, a definite increase in moisture content with proximity to the interface, while the laboratory specimens did not. Perhaps this discrepancy is due to the relatively larger amount of free water available from the concrete in the field.

The laboratory studies indicated an average α factor of 0.83 in Layer I without an accompanying increase in moisture content. The initial field tests on S1 and S3 yielded average α values of 0.63, excluding the top and bottom two diameters of the stem, where surface and base effects not directly related to soil shear strength changes occurred. The difference in the two factors, 0.20, is presumably mainly due to softening of the soil because of moisture migration alone, assuming that disturbance due to trimming laboratory specimens and due to augering the borehole produced comparable effects on the shear strength. The value of 0.20 corresponds closely to the 17 per cent reduction in remolded shear strength due to moisture content changes predicted by Eq. 7.1. (Another possible cause of the differences is the change in orientation of the failure plane between laboratory and field tests and experimental effects, as discussed in Chapter VII. It is felt that the effect of shearing the soil along planes of different orientation would not change the α factor by as great an amount as is indicated.)

The side shear failure evidently occurred in the soil from the appearance of the bonding between the exposed shafts and soil and from the

observation of shear planes in the soil, such as shown in Fig. 12.78. This fact is consistent with the laboratory mortar migration study, which indicates that failure will occur at some distance from the interface. The reason for the shear strength reduction without water migration measured in Layer I by the mortar migration tests is unclear. Perhaps it is due to trimming disturbances, opening of surface fissures near the interface, or perhaps to experimental effects. It appears, however, that a similar non-moisture-dependent shear strength reduction, possibly caused by remolding or opening of fissures near the borehole wall, occurs in the field, which accounts partly for the magnitude of the shear strength reduction factor.

On the basis of comparison of field and laboratory tests, it seems appropriate to extend Eq. 5.2 tentatively to

$$\alpha = \alpha_1 \alpha_2 = (\alpha_{11} \alpha_{12} \alpha_{13}) \alpha_2 \dots \dots \dots (12.1)$$

for shafts installed in the dry, in which

- α = average shear strength reduction coefficient for entire length of shaft
- α_1 = ratio of shear strength of soil around shaft after placing concrete to that existing before placing concrete
- α_{11} = that part of α_1 due to softening because of migration of water from concrete into soil
- α_{12} = that part of α_1 due to the shear strength reduction not accompanied by moisture migration (remolding, opening of surface fissures)

α_{13} = that part of α_1 due to ground surface effects and base-side mechanical interference

α_2 = adhesion coefficient.

Based on the observation that good bond was observed between the soil and concrete on S1 during extraction, it is assumed that α_2 is unity. It appears that α_{11} , α_{12} , and α_{13} were all near 0.8 for S1T1, and that those factors were about the same for S3T1L1, except that α_{13} was about 0.9 because no base-side interference existed.

In summarizing results from S1 and S3, it appears that the laboratory mortar migration tests measure only a part of the total phenomenon of shear strength reduction and that such tests, although valuable, produce only an upper bound for the value of α in Beaumont Clay.

The results of moisture gradient tests for S4 are shown in Figs. 12.85 and 12.86. No significance can be attached to the average moisture gradient, since pockets of drilling mud adjacent to the walls of the shaft made the individual gradients vary considerably. Therefore, no average relationship is given.

In general, however, it is obvious that the soil adjacent to the borehole walls was much wetter than the soil adjacent to the stems of S1 and S3. The samples from the 9- to 15-foot levels were essentially nothing but drilling mud. Those samples contained a mixture of bentonite and the gray-colored soil from Layer II and contrasted both in color and consistency with the natural red-colored soil present from 1 to 6 inches from the walls of the shaft. The samples from 9 and 12 feet appeared to be near the liquid limit.

Samples from below the 15-foot level contained less evidence of entrapped drilling mud but did contain pieces of loosely bonded concrete

which had spalled or had been chipped off the wall of the shaft. The concrete composing the stem walls from depths of 15 to 21 feet was of very poor quality, containing only a small amount of cement mortar. The poor concrete was perhaps one-inch thick. It could be easily broken away from the shaft, exposing good-quality concrete beneath.

Apparently, the wet process described in Chapter II, by which S4 was installed, can significantly change the characteristics of the shaft-soil interface. The consequence of this change is reduced load transfer, as described earlier in this chapter. It is obvious that incomplete displacement of drilling mud occurred in the top portion of the shaft as the temporary casing was withdrawn, even though the construction procedure was quite good and was closely controlled. The extent and distribution of the pockets of mud could not be determined. No opportunity existed to inspect the lower half of the shaft. On the basis of examination of the load transfer curves, however, it appears that the adverse effect of drilling mud entrapment decreased with depth. Reiterating, that part of the shaft drilled in the dry gave much higher load transfer than did the portion drilled with mud.

It is appropriate to restate the fact that the test shaft at the HB&T site, constructed by the same procedure and with the same consistency concrete as S4, did not give evidence of load transfer reduction due to the presence of drilling mud (Barker and Reese, 1970). The implication, then, is that drilling mud entrapment may be a random result of the construction procedure, occurring in some shafts but not in others.

Equation 12.1 can be expanded to the following form for shafts installed in a processed hole:

$$\alpha = (\alpha_{11} \alpha_{12} \alpha_{13}) \alpha_2 \psi \dots \dots \dots (12.1a)$$

in which all factors are as defined previously except ψ , which is an additional reduction factor for shafts installed in a processed hole. The factor ψ was about 1.0 for the HB&T shaft and was about 0.6 for Shaft No. 4 at the SH225 test site.

Control moisture gradient specimens were taken in the access hole for S4. The gradients obtained from those specimens are shown in Fig. 12.86. The wide variation in moisture content for the 8-foot sample was due to heterogeneity in the soil. The low moisture content between one-half and three-fourths inches from the interface for the 20-foot sample is believed to be due to an erroneous moisture content determination.

Significance of Test Results

The field test program verified the fact that drilled shafts installed in Beaumont Clay can carry appreciable load in side resistance under short-term loading. The magnitudes of the average shear strength reduction factors were near those measured by other investigators in other clay formations with properties similar to Beaumont Clay (see Chapter V).

Significant information concerning the six parameters enumerated in Chapter VI, which the test shafts were designed to investigate, was acquired. No specific conclusions could be made concerning the effect of shaft length, however, because the only shaft that was not 23 feet

long had to be installed with mud, thereby invalidating direct comparisons of load transfer development patterns with the other shafts. Considerable knowledge was obtained about the other five parameters.

In summary, the testing program revealed that a fairly consistent average short-term peak shear strength reduction factor of about 0.5 can be expected from shafts installed in the dry in stiff clay, with a relatively minor dependence on the base geometry. The test results from S2 and S3 infer that the larger displacements required to mobilize a fixed percentage of the base capacity in a belled shaft corresponding to a reasonable design load may cause the soil along the sides of the stem to be in a failed condition, which, over a period of time, may result in a significant reduction in side capacity of belled shafts.

Drilled shafts installed by the wet method described in Chapter II may have significantly lower side capacities than identical shafts installed in the dry, principally because of the entrapment of drilling mud between the sides of the stem and the walls of the borehole. Such entrapment apparently does not occur consistently. If it does not occur, the side capacity of the shaft may be nearly equal to that of an identical shaft installed in the dry. Until a more consistent construction technique is developed, however, designers of drilled shafts in Beaumont Clay would not be justified in using shear strength reduction factors of greater than about one-third for computing the side capacity of that portion of a stem which had been exposed to drilling mud. The implication of this statement is, of course, that the use of mud should be restricted to only that portion of the stem in which it is required, and that as much of the hole as possible be drilled in the dry.

The value of unit load transfer was found to depend on several factors, as enumerated below.

1. Displacement: Unit load transfer increases linearly with downward displacement of the shaft up to about one-half of the peak load transfer. In shafts installed in the dry, peak load transfer appeared to occur at a displacement of about 0.2 inches in that part of the stem which was not influenced greatly by surface or base effects (more than two stem diameters from base or surface). A reduction in load transfer with displacements exceeding about 0.2 inches was observed.
2. Position on Shaft: As mentioned in the preceding item, load transfer behavior is considerably different in roughly the top and bottom two stem diameters than in the rest of the stem. The difference in behavior near the surface is due to a number of factors, including lack of adequate lateral pressure between the soil and the concrete, the presence of the free surface, and the typically irregular shape of the shaft in the top few feet. The reduction of both the magnitude of maximum unit load transfer and the displacement at which maximum load transfer occurs in the vicinity of the base is apparently brought about by a combination of increased softening of the soil near the base, due to water migration from the concrete, and to mechanical interference between the base and the soil along the sides of the shaft.

3. Type of Soil: There was no opportunity in the field to check the validity of the conclusion of the laboratory mortar migration tests that soil type was an important parameter governing the value of the shear strength reduction factor, since the only shaft installed in soil other than Layer I (CH) was cast in a processed hole. Based on the laboratory studies, however, shear strength reduction factors can be expected to be higher for ML and CL soils than for CH soils in a dry borehole.
4. Reloading: Peak load transfer is reduced when the applied load is removed and the shaft is reloaded to plunging failure again after a lapse of time.
5. Method of Installation: The presence of entrapped drilling mud can alter the load transfer characteristics of the shaft, decreasing the shear strength reduction factor by as much as 40 to 50 per cent over that of a shaft installed in the dry.
6. Other Factors Not Explicitly Investigated: Several other factors not investigated in the SH225 tests may have some effect on load transfer. They are:
 - a. Shear Strength of Clay. The concept of the α factor is probably valid only up to a limiting value of soil shear strength. No test shaft was installed through clay soil having a shear strength greater than about 2.2 tsf. Up to that strength, the value of α of 0.5

for dry-constructed shafts appears to be valid. Since the value of α corresponding to shear strengths in excess of 2.2 tsf has not been established, it is prudent to assume that Skempton's suggestion of placing an upper limit on maximum developed shear stress for design purposes for clays having greater shear strengths should be followed (Skempton, 1959). The various sets of load transfer curves indicate that a reasonable limiting design value for side resistance of dry shafts in Beaumont Clay is 0.9 tsf.

- b. Diameter of the Stem. The diameter of the stem is not likely to influence greatly the magnitude of maximum load transfer; however, shafts having stem diameters appreciably different from 30 inches may require different magnitudes of displacement than reported herein to mobilize peak load transfer.
- c. Location of Water Table. It is possible that load transfer characteristics may be somewhat different above and below the water table. No conclusions concerning whether presence of the water table above the base of the shaft will reduce peak load transfer can be drawn from any of the field studies of drilled shafts described in Chapter V, except when the existence of silt seams or fissures allows free water to leak into the borehole before concrete can be placed, as occurred during the construction of S1.

The field tests have provided some insight into the elements of the mechanism of shear strength reduction along the sides of the stem of a shaft installed in the dry. Those elements appear to be:

1. Softening of soil along borehole wall because of migration of water from the concrete. This effect was more pronounced near the bases of S1 and S3, from which radial moisture gradients were obtained.
2. Surface and base effects.
3. An additional reduction effect not due to either of the first two items. This effect may be caused by remolding the soil along the sides or opening of fissures along the surface of the borehole during drilling.

The laboratory mortar migration tests did not provide any reliable quantitative measure of the first two effects, but they did provide a means of modeling the third effect. Hence, the laboratory tests appear to provide only an upper bound for α .

The value of ultimate base resistance can be predicted reliably from Eq. 4.7 by using N_c equal to 9 and the average shear strength from UU triaxial compression tests, conducted in the manner described in Chapter VII, for a vertical distance of two base diameters beneath the base. The bearing capacity factor of 9 apparently applied to both belled and cylindrical shafts.